
Flame Spread Modelling Using FDS4 CFD model

by

Kwok Yan (Daniel) Ho

Supervised by

Dr. Charley Fleischmann

and

Dr Michael Spearpoint

June 2007

A thesis submitted in partial fulfilment of the requirements for the degree of
Master of Engineering in Fire Engineering

Department of Civil Engineering
University of Canterbury
Private Bag 4800
Christchurch, New Zealand

For a full list of reports please visit:

http://www.civil.canterbury.ac.nz/fire/fe_resrch_reps.html

ABSTRACT

This thesis examines the prediction of opposed flow flame spread in the Fire Dynamics Simulator version 4 (FDS4) Computational Fluid Dynamics (CFD) model by adapting the Lateral Ignition Flame Transport (LIFT) test procedure. It should be noted that FDS4 was all that was available at the time of the analysis despite FDS5 is now available for beta testing. This research follows on from previous work where LIFT experiments were conducted for various New Zealand timber and timber based products; those materials include Beech, Macrocarpa, Radiata Pine, Rimu, Hardboard, Medium Density Fibreboard (MDF), Melteca faced MDF, Plywood and Particle Board. The objective of this research is to investigate the accuracy of flame spread modelling in FDS4; where the prediction of opposed flow flame spread parameters from FDS4 were directly compared with the experimental results that were obtained experimentally.

The standardised procedure for determining the material ignition and flame spread properties was followed and applied to simulate the LIFT test. The LIFT test apparatus was set up in FDS4 with a domain size of 0.9 x 0.3 x 0.3 metres in the x, y and z directions respectively. From the heat flux distribution along the calibration specimen, it indicated that calibration of the LIFT apparatus can be executed in FDS4 where the percentage error is within 1.2%.

This report also provides the thermal transport properties (i.e. thermal conductivity and specific heat capacity) of the tested New Zealand timber and timber based products. These were determined using a transient plane source technique and subsequently these properties were entered as the surface identifications in FDS4. The ignition tests were not performed as part of the simulated LIFT test since a direct comparison with the results was required to give a more meaningful assessment. For this reason, the ignition parameters that were obtained from the previous experiments were employed to carry out the flame spread test.

Due to the concept of a preheat time required by the standard test method and FDS4 being not able to preheat specimens, the temperature immediately after the preheat time was calculated and implemented for the specimens. The heat transfer problem was solved using an explicit method; where specimens were divided into 11 different nodes.

Different scenarios were investigated to see the effect that the selected combustion model has on modelling flame spread. The two analytical models tested were (1) thermoplastic fuels and (2) charring fuels model. Furthermore, the flame spread was visualised using either the Mixture Fraction or the HRRPUV model in Smokeview; where the rate of flame spread for each specimen was obtained. And lastly, three different absorption coefficients (0.6, 0.7 and 0.8) for each specimen were examined; this parameter contributed significantly to the rate of flame spread as it determines the amount of heat flux being absorbed by the specimen during the time of preheating. A study of the grid size was also performed to investigate the accuracy of the FDS4 simulations with the grid size selected. It has been found that increasing the size of the grid cell does not greatly affect the flame spread results.

Moisture content and heat of vaporisation input variables were also examined. From the flame spread data, moisture content does not have a significant role in modelling flame spread. However, it was indicated that the heat of vaporisation has an effect on the output of the flame spread parameters.

It was determined from the sensitivity analysis that the most appropriate solid boundary condition to be used in predicting the flame spread would be thermoplastic fuels model with an absorption coefficient of 0.8. By using this scenario as the basis, the plot of the arrival time against the distance along the specimen exhibits a similar trend of flame spread with the experimental results at first, but later on, the extinction of flame front actually occurred at a much earlier stage than the experimental results showed.

In general, the analyses showed that FDS4 cannot perform the LIFT test where the prediction of flame heating parameter and minimum heat flux for spread were out by more than 20% shown by the direct comparison between experimental results. However, the prediction of minimum heat flux required for ignition seems to agree with the experimental results where the percentage error is within 20%.

Acknowledgements

I would like to thank the following people who have contributed to this research in various ways:

- I wish to sincerely thank both my supervisor Dr. Charley Fleischmann and my co-supervisor Dr Mike Spearpoint for giving me the opportunity to work with them and their dedication, support and encouragement given to this project.
 - Geoffrey Merryweather for his help in providing the LIFT results; without those results this research is not possible.
 - Grant Dunlop and Bob Smith in the fire lab on the use of the cone calorimeter.
 - Philip Park for the assistance on the hot disk test, without him the Hot Disk experiments would have not be carried out as smoothly as I would have liked.
 - My fellow classmates who have made my time during postgraduate experience memorable and worthwhile.
 - The New Zealand Fire Service Commission for their continued support of the Fire Engineering program at the University of Canterbury.
 - My friend Jeremy Rees helping me to proof read various chapters of my report.
 - Finally, to my parents, Ping-Yi, brothers and sisters for their love, support and encouragement.
-

Table of Contents

1	INTRODUCTION	1
1.1	Previous studies of ignition time and flame spread at the University of Canterbury....	2
1.2	Impetus for Research	3
1.3	Research Objectives	4
1.4	Report Outline	5
2	LITERATURE REVIEW	7
2.1	Pioneering Work on Flame Spread theory	7
2.1.1	The flame spread models of deRis	7
2.1.2	Experimental and theoretical work of McAlevy et al.....	9
2.1.3	The fire-spread model of Williams.....	9
2.1.4	The Fernandez-Pello Williams model	10
2.1.5	Frey and T'ien model	11
2.1.6	Quintiere	12
2.2	Surface Flame Spread	13
2.2.1	Introduction	13
2.2.2	Velocity for opposed flow flame spread over solid.....	15
2.2.3	Velocity for wind aided flame spread over solid.....	21
2.3	Factors affecting flame spread.....	24
2.3.1	Opposed flow velocity and oxygen concentration	24
2.3.2	Flow turbulence	25
2.3.3	CO concentration	27
2.3.4	External radiation	27
2.3.5	Gravity	28
2.3.6	Size of the material	29
2.3.7	Grain Orientation	29
2.3.8	Density.....	30
2.3.9	Moisture Content	30

2.3.10	Charred material	31
2.4	Technique of measuring ignition properties and flame spread.....	32
2.4.1	LIFT test	32
2.4.2	RIFT test.....	33
2.5	Published data for the LIFT test	34
2.5.1	Quintiere and Harkleroad (1984).....	34
2.5.2	Nisted (1991)	35
2.5.3	Dietenberger (1996 a), (1996b) and (2004).....	38
2.5.4	Babrauskas and Wetterlund (1999)	40
2.5.5	Merryweather (2006).....	41
3	FIRE DYNAMICS SIMULATOR VERSION 4 (FDS4).....	43
3.1	Introduction	43
3.2	Numerical Grid.....	43
3.3	Hydrodynamic Model.....	44
3.3.1	Fundamental Conservation Equations	45
3.4	Combustion Model	47
3.4.1	Mixture Fraction Combustion Model	47
3.4.2	Enhancements to the Mixture Fraction Model	50
3.5	Thermal Radiation Model.....	53
3.6	Thermal Boundary Conditions	54
3.6.1	Convection heat flux.....	54
3.6.2	Thermoplastic Fuels	55
3.6.3	Charring Fuels	56
4	THEORY OF THE LIFT TEST	59
4.1	Introduction	59
4.2	Ignition Test.....	60

4.2.1	Ignition Theory	61
4.2.2	Calculation for Ignition Test.....	65
4.3	Flame Spread Test	66
4.3.1	Flame Spread Theory.....	67
4.3.2	Calculation for Flame Spread Test	69
5	EXPERIMENTAL SETUP ON THE CHARRING OF TIMBER	72
5.1	Cone Calorimeter.....	72
5.2	Test Specimens	75
5.3	Calibration of the cone element heater	76
5.4	Specimen Mounting.....	76
5.5	Experimental Procedure	77
5.6	Analysis of Char Density and Ignition Temperature.....	78
6	THERMAL PROPERTIES OF TIMBER AND TIMBER BASED PRODUCTS	82
6.1	Introduction	82
6.2	Theory of the transient plane source technique.....	85
6.3	Sample preparation	88
6.4	Density measurements	89
6.5	Experimental Procedure of the Hot Disk Test.....	93
6.6	Results from the Hot Disk Test	96
6.6.1	Virgin Materials.....	98
6.6.2	Charred Materials	101
7	SETTING UP AND CALIBRATION OF THE LIFT APPARATUS IN FDS4	103
7.1	Geometries of the LIFT apparatus.....	103
7.2	Calibration of Flux to the Specimen.....	104

7.3	LIFT apparatus in FDS4	104
7.4	Other Input Variables for the LIFT apparatus in FDS4.....	108
7.5	Calibration results from FDS4.....	110
7.6	Summary for the calibration of the LIFT apparatus	120
8	FLAME SPREAD TEST IN FDS4.....	125
8.1	Ignition Test Procedure	125
8.2	Flame Spread Test Procedure	125
8.2.1	Calibration results from FDS4.....	126
8.2.2	Preheat Time.....	126
8.2.3	Other Input Variables for the flame spread test in FDS4	137
8.3	Analysis method of flame spread	142
8.4	Flame spread results from FDS4	143
8.4.1	Flame spread for Beech	144
8.4.2	Flame spread for Hardboard	144
8.4.3	Flame spread for Macrocarpa	145
8.4.4	Flame spread for MDF	145
8.4.5	Flame spread for Melteca faced MDF	146
8.4.6	Flame spread for Radiata Pine.....	146
8.4.7	Flame spread for Plywood.....	147
8.4.8	Flame spread for Pynefloor	147
8.4.9	Flame spread for Rimu	148
8.5	Flame spread correlations parameters	148
8.5.1	Flame heating correlations for Beech.....	149
8.5.2	Flame heating correlations for Hardboard.....	149
8.5.3	Flame heating correlations for Macrocarpa.....	150
8.5.4	Flame heating correlations for MDF	150
8.5.5	Flame heating correlations for Melteca faced MDF.....	151
8.5.6	Flame heating correlations for Radiata Pine.....	151
8.5.7	Flame heating correlations for Plywood.....	152

8.5.8	Flame heating correlations for Pynefloor	152
8.5.9	Flame heating correlations for Rimu	153
8.5.10	Summary of the flame spread parameters	153
9	SENSITIVITY ANALYSIS	156
9.1	Grid Sizing.....	156
9.1.1	Calibration of the LIFT apparatus for different grid sizes.....	156
9.1.2	Flame spread results for different grid sizes.....	161
9.1.3	Discussion on the effect of the grid size on flame spread	162
9.2	Sensitivity on the pyrolysis model.....	164
9.2.1	FDS4 input for the pyrolysis models.....	164
9.2.2	Flame spread results for the pyrolysis models.....	165
9.2.3	Discussion on the technique of analysing the flame spread	167
9.3	Sensitivity on the FDS4 inputs	168
9.3.1	Heat of vaporisation.....	168
9.3.2	Moisture Content	170
10	DISCUSSION.....	173
10.1	Comparison of thermal properties	173
10.1.1	Thermal conductivity and specific heat capacity	173
10.2	Comparison of ignition temperature.....	175
10.3	Comparison of density of virgin wood and char material	176
10.4	Flame Spread data	179
10.4.1	Arrival time versus distance along specimen	179
10.5	Flame spread correlations parameters	180
10.5.1	Flame heating parameter, Φ	182
10.5.2	Critical heat flux for ignition, $\dot{q}_{o,ig}''$	186
10.5.3	Critical heat flux for flame spread, $\dot{q}_{o,s}''$	189

11	CONCLUSIONS	193
12	FURTHER WORK AND RECOMMENDATIONS	195
13	REFERENCES	196
	APPENDIX A – LIFT CALIBRATION DATA	202
	APPENDIX B – CALCULATION FOR DENSITY.....	204
	APPENDIX C – HOT DISK TEST RESULTS.....	211
	APPENDIX D – IGNITION TEST RESULTS FROM MERRYWEATHER (2006)	223
	APPENDIX E – CALIBRATION FDS4 INPUT FILES.....	229
	APPENDIX F – PREHEAT TEMPERATURE PROFILES.....	233
	APPENDIX G – FLAME SPREAD TEST FDS4 INPUT FILES	244
	APPENDIX H – FLAME SPREAD TEST CALCULATIONS.....	277
	APPENDIX I – FLAME SPREAD RESULTS USING HRRPUV	280

List of Figures

Figure 2-1: The shape of the spreading flame postulated by deRis (deRis 1968).....	8
Figure 2-2: Flame spread model (Quintiere 1981)	12
Figure 2-3: Flame spread for natural and forced flow (Quintiere 1998).....	14
Figure 2-4: Energy conservation analysis in opposed flow flame spread (Quintiere 2002) ...	16
Figure 2-5: Qualitative dependence of opposed flow flame speed with Damkohler number, D (Quintiere 2002)	18
Figure 2-6: Energy conservation analysis in wind-aided flame spread (Quintiere 2002).....	22
Figure 2-7: Flame spread rate over thick PMMA sheets as a function of the opposed forced flow velocity for several flow oxygen mass fractions (Fernandez-Pello et al. 1981)	25
Figure 2-8: Flame spread rate over thin PMMA sheets as a function of the opposed forced flow velocity for several flow oxygen mass fractions (Fernandez-Pello et al. 1981)	25
Figure 2-9: Variation of the opposed flow flame spread rate over thick PMMA sheets with the turbulence intensity for several air flow velocities.....	26
Figure 2-10: Variation of the CO concentration with oxygen mass fraction for ceiling flame spread at different turbulence intensities. Flow velocity of 2ms^{-1} (Chao and Fernandez-Pello 1996).....	27
Figure 2-11: Pyrolysis front and flame tip upward spread rates over wood sheets as a function of the external radiant flux (Saito et al. 1985).....	28
Figure 2-12: Incident flux and grain orientation scenarios (Spearpoint 1999).....	29
Figure 2-13: Relationship between density and rate of combustion (Kollmann and Cote 1968)	30
Figure 2-14: Effect of moisture content on the ignition of wood (reproduced from (Cholin 2003)).....	31
Figure 2-15: Degradation zones in a wood section (White 2002).....	31
Figure 2-16: Reduced scale Ignition and flame spread attachment (RIFT) (Azhakesan et al. 1998).....	34
Figure 3-1: State relations for propane (McGrattan 2004)	50
Figure 3-2: Oxygen-temperature phase space showing where combustion (McGrattan 2004)	53
Figure 4-1: LIFT showing angled gas radiant panel (left) and sample holder (right) (Merryweather 2006).....	60

Figure 4-2: A perspective view of the ignition test using the LIFT (Merryweather 2006).....	61
Figure 4-3: Specimen for the ignition test.....	61
Figure 4-4: Model for ignition study (ASTM Committee E-5 on Fire Standards. 2004b).....	62
Figure 4-5: Pilot ignition results under radiative heating.....	65
Figure 4-6: A plot of ignition time as a function of external irradiance.....	66
Figure 4-7: A perspective view of the flame spread test using the LIFT (Merryweather 2006)	67
Figure 4-8: Correlations of Lateral Flame Spread.....	71
Figure 5-1: Cone calorimeter at the University of Canterbury.....	72
Figure 5-2: Schematic view of the cone calorimeter (Babrauskas 2002).....	73
Figure 5-3: Cross sectional view of the cone heater (Babrauskas 2002).....	73
Figure 5-4: All timber and timber based products specimens for testing.....	75
Figure 5-5: Thermocouple bead placed in the wood specimen and its temperature reading ..	76
Figure 5-6: Distance between the cone heater and specimen.....	77
Figure 5-7: Measuring the temperature of ignition.....	78
Figure 5-8: Charring of the Rimu specimen.....	78
Figure 5-9: Char specimens after burning.....	79
Figure 5-10: A plot of the ignition temperature for different types of timber and timber based products.....	81
Figure 6-1: Principal electrical circuit for the modified bridge arrangement (Anis-ur-Rehman and Maqsood 2003).....	85
Figure 6-2: Transient recording of the thermal transport properties of the material surrounding the sensor (Gustafsson 1998).....	86
Figure 6-3: Temperature increase of the sensor (Gustafsson 1998).....	87
Figure 6-4: Minimum distance from sensor to boundary surface.....	89
Figure 6-5: Measured average density for the timber and timber based products.....	90
Figure 6-6: Charred specimens used for the Hot Disk test.....	91
Figure 6-7: Measured char density for the timber and timber based products.....	92
Figure 6-8: Sample for measuring char density.....	93
Figure 6-9: Hot Disk test setup in a temperature control room.....	94
Figure 6-10: Schematic of experimental configuration for measuring the thermal properties of a pair of specimens.....	94

Figure 6-11: Testing of calcium silicate specimen using the Hot Disk test	96
Figure 6-12: Thermal conductivity (average) for each timber and timber based product.....	98
Figure 6-13: Specific heat capacity (average) for each timber and timber based product	99
Figure 6-14: Comparison between the measured thermal conductivity and literature values	100
Figure 6-15: Comparison between the measured specific heat capacity and literature values	100
Figure 6-16: Thermal conductivity (average) for charred materials	101
Figure 6-17: Specific heat capacity (average) for charred materials.....	102
Figure 7-1: Arrangement of the specimen and radiant panel in LIFT (not to scale).....	103
Figure 7-2: An overview of the layout of the LIFT apparatus in FDS4.....	105
Figure 7-3: Positions of fluxmeters along the dummy specimen	107
Figure 7-4: A snap view of the LIFT apparatus setup from Smokeview	108
Figure 7-5: Snapshot of the heat flux along the specimen in Smokeview	113
Figure 7-6: Heat flux over the dummy specimen for scenarios with constant temperature (i.e. Scenario 1 to 4).....	114
Figure 7-7: Heat flux over the dummy specimen for scenarios with varying temperatures (i.e. Scenario 5 to 8).....	114
Figure 7-8: Heat flux along the dummy specimen for different scenarios.....	115
Figure 7-9: Heat flux changes with time along the specimen for 10mm grid size.....	116
Figure 7-10: Percentage difference compared with the standards required against time for 10mm grid size	117
Figure 7-11: Variation from standard for LIFT calibration conducted by Merryweather (Merryweather 2006).....	118
Figure 7-12: Heat flux changes with time at 50mm along the dummy specimen for 10mm grid size.....	119
Figure 7-13: Heat flux changes with time at 350mm along the dummy specimen for 10mm grid size.....	119
Figure 7-14: Comparison of the heat flux over the dummy specimen	120
Figure 7-15: Comparison of the flux distribution on New Zealand native timber	122
Figure 7-16: Comparison of the flux distribution on timber based products	123
Figure 7-17: Comparison of the flux distribution on timber based product (Pynefloor)	124

Figure 8-1: Actual surface temperature profile along the specimen and temperature varies with depth	127
Figure 8-2: Schematic sketch of the heat transfer problem	128
Figure 8-3: Heat transfer model for the interior nodes	131
Figure 8-4: Heat transfer model for the other surface node	133
Figure 8-5: Heat transfer model for the exposed surface node.....	134
Figure 8-6: Temperature profile along Beech specimen after preheating	136
Figure 8-7: Preheat temperature modelled in FDS4	136
Figure 8-8: A snapshot of flame spread test setup from Smokeview	137
Figure 8-9: Reaction identification for wood	138
Figure 8-10: State relationship of mass fraction as a function of mixture fraction for wood	138
Figure 8-11: Example of the FDS4 input for the thermoplastic fuels model	139
Figure 8-12: Example of the FDS4 input for the charring fuels model.....	140
Figure 8-13: A perspective view of the flame spread test in Smokeview	143
Figure 8-14: Front view of the flame spread test in Smokeview.....	143
Figure 8-15: Arrival time versus flame front position for Beech (using Mixture Fraction) .	144
Figure 8-16: Arrival time versus flame front position for Hardboard (using Mixture Fraction)	144
Figure 8-17: Arrival time versus flame front position for Macrocarpa (using Mixture Fraction).....	145
Figure 8-18: Arrival time versus flame front position for MDF (using Mixture Fraction)...	145
Figure 8-19: Arrival time versus flame front position for Melteca faced MDF (using Mixture Fraction).....	146
Figure 8-20: Arrival time versus flame front position for Radiata Pine (using Mixture Fraction).....	146
Figure 8-21: Arrival time versus flame front position for Plywood (using Mixture Fraction)	147
Figure 8-22: Arrival time versus flame front position for Pynefloor (using Mixture Fraction)	147
Figure 8-23: Arrival time versus flame front position for Rimu (using Mixture Fraction)...	148
Figure 8-24: Correlations of lateral flame spread for Beech (using Mixture Fraction)	149
Figure 8-25: Correlations of lateral flame spread for Hardboard (using Mixture Fraction) .	149

Figure 8-26: Correlations of lateral flame spread for Macrocarpa (using Mixture Fraction)	150
Figure 8-27: Correlations of lateral flame spread for MDF (using Mixture Fraction)	150
Figure 8-28: Correlations of lateral flame spread for Melteca faced MDF (using Mixture Fraction)	151
Figure 8-29: Correlations of lateral flame spread for Radiata Pine (using Mixture Fraction)	151
Figure 8-30: Correlations of lateral flame spread for Plywood (using Mixture Fraction)	152
Figure 8-31: Correlations of lateral flame spread for Pynefloor (using Mixture Fraction)	152
Figure 8-32: Correlations of lateral flame spread for Rimu (using Mixture Fraction)	153
Figure 9-1: FDS4 input for a grid size of 15mm	156
Figure 9-2: FDS4 input for a grid size of 20mm	157
Figure 9-3: FDS4 input for a grid size of 25mm	157
Figure 9-4: LIFT test setup in FDS4 using a grid size of 15mm (a view from Smokeview)	157
Figure 9-5: LIFT test setup in FDS4 using a grid size of 20mm (a view from Smokeview)	158
Figure 9-6: LIFT test setup in FDS4 using a grid size of 25mm (a view from Smokeview)	158
Figure 9-7: Arrival Time versus Flame Front Position for Beech with different grid sizes (using Mixture Fraction)	161
Figure 9-8: Correlations of Lateral Flame Spread for Beech with different grid sizes (using Mixture Fraction)	162
Figure 9-9: Comparison of flame heating parameter between the results from Merryweather (2006) and FDS4 using different FDS4 model and absorption coefficient	165
Figure 9-10: Comparison of critical flux for ignition between the results from Merryweather (2006) and FDS4 using different FDS4 model and absorption coefficient	166
Figure 9-11: Comparison of critical flux for spread between the results from Merryweather (2006) and FDS4 using different FDS4 model and absorption coefficient	166
Figure 9-12: Arrival Time versus Flame Front Position for Beech with different heat of vaporisation (using Mixture Fraction)	169
Figure 9-13: Correlations of Lateral Flame Spread for Beech with different heat of vaporisations (using Mixture Fraction)	169
Figure 9-14: Arrival Time versus Flame Front Position for Beech with different moisture contents (using Mixture Fraction)	171

Figure 9-15: Correlations of Lateral Flame Spread for Beech with different moisture contents (using Mixture Fraction).....	172
Figure 10-1: Comparison between the thermal conductivity for charred and virgin wood ..	174
Figure 10-2: Comparison between the specific heat capacity for charred and virgin wood .	174
Figure 10-3: Comparison of ignition temperature	176
Figure 10-4: Comparison of wood density between measured and Merryweather (2006) ...	177
Figure 10-5: Comparison between the wood and char density	178
Figure 10-6: Comparison between the prediction of flame front's arrival time for Beech in FDS4 and the results from Merryweather (2006) using Mixture Fraction.....	179
Figure 10-7: Comparison of the correlations of lateral flame spread for Beech specimen ...	181
Figure 10-8: Comparison of flame heating parameter between the results from Merryweather (2006) and FDS4 (Thermoplastic fuels $\epsilon=0.6$ Mixture Fraction).....	183
Figure 10-9: Comparison of flame heating parameter between the results from Merryweather (2006) and FDS4 (Thermoplastic fuels $\epsilon=0.7$ Mixture Fraction).....	183
Figure 10-10: Comparison of flame heating parameter between the results from Merryweather (2006) and FDS4 (Thermoplastic fuels $\epsilon=0.8$ Mixture Fraction)	184
Figure 10-11: Comparison of critical flux for ignition between the results from Merryweather (2006) and FDS4 (Thermoplastic fuels $\epsilon=0.6$ Mixture Fraction).....	187
Figure 10-12: Comparison of critical flux for ignition between the results from Merryweather (2006) and FDS4 (Thermoplastic fuels $\epsilon=0.7$ Mixture Fraction).....	187
Figure 10-13: Comparison of critical flux for ignition between the results from Merryweather (2006) and FDS4 (Thermoplastic fuels $\epsilon=0.8$ Mixture Fraction).....	188
Figure 10-14: Comparison of critical flux for spread between the results from Merryweather (2006) and FDS4 (Thermoplastic fuels $\epsilon=0.6$ Mixture Fraction).....	190
Figure 10-15: Comparison of critical flux for spread between the results from Merryweather (2006) and FDS4 (Thermoplastic fuels $\epsilon=0.7$ Mixture Fraction).....	191
Figure 10-16: Comparison of critical flux for spread between the results from Merryweather (2006) and FDS4 (Thermoplastic fuels $\epsilon=0.8$ Mixture Fraction).....	191

List of Tables

Table 1-1: Materials tested by Merryweather (Merryweather 2006)	3
Table 2-1: Relative flame spread rates (Quintiere and Harkleroad 1984).....	15
Table 2-2: Flame spread data for typical aircraft and construction materials (Quintiere and Harkleroad 1984).....	35
Table 2-3: Summary of flame spread test results (Nisted 1991)	37
Table 2-4: Derived thermophysical constants for siding materials (Dietenberger 1996a).....	39
Table 2-5: Derived thermophysical parameters of ignitability (Dietenberger 2004)	40
Table 5-1: Calculated char density	80
Table 5-2: Measured ignition temperature	81
Table 6-1: Thermal transport properties for virgin and charred materials	97
Table 7-1: Calibration of Flux to the Specimen (ASTM Committee E-5 on Fire Standards. 2004b).....	104
Table 7-2: Description of calibration scenarios.....	112
Table 7-3: Temperature required on the radiant panel	121
Table 8-1: Emissivity of various wood species (Anon 2006)	131
Table 8-2: Flame heating parameters for the selected timber and timber based products	154
Table 8-3: Minimum heat flux for ignition for the selected timber and timber based products	154
Table 8-4: Critical heat flux for spread for the selected timber and timber based products .	155
Table 9-1: Summary for the calibration of the LIFT apparatus in FDS4	159
Table 9-2: Summary of the flame spread parameters from Merryweather (2006) and FDS4 using different grid sizes.....	163
Table 9-3: Summary of the flame spread parameters using different heat of vaporisation...	170
Table 9-4: Summary of the flame spread parameters using different moisture content.....	172
Table 10-1: Char properties for various wood species (Tran and White 1992)	178
Table 10-2: Comparison of the flame spread parameter using thermoplastic fuels model $\epsilon=0.7$	185

Nomenclature

Symbol	Description
a	overall radius of the sensor
A	pre-exponential factor
b	ignition correlation parameter
C	coefficient for natural convection (1.52 for a horizontal surface and 1.31 for a
c_s	specific heat of the material
D^*	characteristic fire diameter
$D(\tau)$	dimensionless time dependent function
E_A	activation energy
\mathbf{f}	volumetric body force, which is the drag exerted by water droplets emanating from other external forces sprinklers
$F(t)$	time to reach equilibrium or steady state in the material; is ratio of the minimum heat flux for ignition and the external heat flux imposed
\mathbf{g}	gravity
h	heat-transfer coefficient at ignition
h_i	heat of reaction of the species i
I_b	radiation intensity
k	thermal conductivity of the gas
k_c	temperature-dependent conductivity of the material
L	characteristic length related to the size of the physical obstruction
\dot{m}''	mass loss rate of fuel
\dot{m}_O'''	oxygen mass consumption
M_F	fuel molecular weights

M_o	oxygen molecular weights
P_0	total output of power from the sensor
Pr	Prandtl number
\dot{q}'''	heat release rate per unit volume
\dot{q}_c''	convective heat flux
\dot{q}_e''	external heat flux
$\dot{q}_{o,ig}''$	minimum heat flux required for ignition
\dot{q}_r''	(net) radiative heat flux at the surface
\dot{Q}''	energy release per unit area
r	stoichiometric mass ratio of oxygen to fuel
R	universal gas constant
Re	Reynolds number
R_0	resistance of the sensor just before it is being heated or at time $t=0$
T_f	thermal enthalpy of the flame
T_v	thermal enthalpy of the fuel
T_∞	thermal enthalpy of the ambient
t	piloted ignition time.
T_f	flame temperature
T_{ig}	ignition temperature of the solid surface
T_s	surface temperature
\mathbf{u}	velocity unit vector in the u, v and w directions
	flame spread velocity
V_p	

V_g	opposed flow velocity
Y_F^l	fraction of fuel in the fuel stream
Y_O	oxygen mass fraction
Y_O^∞	oxygen mass fraction in ambient condition
Z	mixture fraction
Z_f	flame surface
Δ	solid fuel thickness
ΔH_{ev}	heat of water vaporisation
ΔH_{pyr}	heat of pyrolysis
ΔH_O	heat release rate per unit mass of oxygen consumed
ΔH_v	heat of vaporisation.
ΔT	difference between the surface of the object and the gas temperature
ΔT_i	constant temperature difference that develops almost instantly over the thin
$\Delta T_{ave}(\tau)$	temperature increase of the sample surface on the other side of the insulating layer and facing the Hot Disk sensor representing perfect “thermal contact” closely realised by a deposited film or an electrically insulating sample (PVD)
$\nabla \cdot k \nabla T$	product of the rate of the conductivity change and the rate of the temperature
$\nabla \rho$	force acting on the fluid due to the pressure difference
$\nabla \cdot \mathbf{q}_r$	radiative energy flux
$\nabla \cdot \tau$	viscous stress tensor (τ) acting on the fluid within the control volume, which is the product between the viscosity and the velocities of the fluid volume is subjected to in a turbulent environment

Greek symbol	Description
α	Temperature Coefficient of the Resistivity (TCR)
α_s	thermal diffusivity of the solid fuel
ε	emissivity
Λ	thermal conductivity of the sample
$k\rho c$	effective thermal properties
κ	thermal diffusivity of the specimen; or local (grey or band-mean) absorption coefficient as a function of the mixture fraction and temperature and is determined by a sub model implemented in FDS4 called RADCAL
λ_s	thermal conductivity of the solid
λ_g	thermal conductivity of the gas
ϕ	flame heating parameter
δ	thickness of the material
δx	nominal size of a grid cell
ρ_m	moisture density
ρ_s	total density of the solid
ρC_v	heat capacity per unit volume
$\frac{\partial \rho}{\partial t} + u \cdot \nabla \rho$	material derivative
σ	Stefan-Boltzmann constant
Θ	characteristic time
χ_r	local fraction of that energy emitted as thermal radiation

1 Introduction

Flame spread over a combustible solid surface is one of the issues in fire safety that needs to be taken into consideration since it influences the initial development of fire and the heat release rate. Hence, regulatory authorities only allow certain materials, which are specified in the building code, to be used in the construction of buildings. This is to ensure that all occupants are able to escape safely in the event of a fire. The most commonly used parameters for comparing flame spread of different materials are known as the flame spread correlation parameters, which is determined using the flame spread velocities of materials in conjunction with the corresponding incident heat flux. There are several flame spread tests available that can be carried out to measure the flame spread of materials. One of the methods is called the Lateral Ignition and Flame Test (LIFT) which is a standard test given in the ASTM fire standards. Another method is a reduced scale version of the LIFT test known as the Reduced Ignition and Flame spread Technique (RIFT).

There have been a number of reported studies investigating the flame spread of different materials by adapting the ignition test from the cone calorimeter or ISO 5657 ignition apparatus (Anon 1986) or RIFT apparatus. Subsequently, using the results from the ignition tests and correlating the results to the flame spread tests either using the LIFT or RIFT method.

Fire Dynamics Simulator version 4 (FDS4) is a computational fluid dynamics (CFD) model for fire-driven fluid flow, which is developed by National Institute of Standards and Technology (NIST) (McGrattan and Forney 2004). It should be noted that FDS4 was all that was available at the time of the analysis despite FDS5 is now available for beta testing. FDS4 is able to simulate fire behaviour as it develops in a given space i.e. in a building or open space, and the FDS4 software currently used is the fourth version. Over the years as computer processor's speed increases, CFD model such as FDS4 have been increasingly employed by fire engineers as a tool to model fires. As FDS4 is becoming more popular in use, the accuracy of FDS4 also needs to be improved in order to simulate a more realistic fire; therefore, there is a need to determine whether the flame spread modelling used in FDS4 matches with experimental data.

1.1 Previous studies of ignition time and flame spread at the University of Canterbury

Ngu (2001) studied the ignition properties of some New Zealand timbers and timber products using simple thermal models. Ignition times were obtained for six different types of timber and timber based products. British Standard BS 476: Part 13 also known as the ISO Ignitability Test (Anon 1986) is adapted to carry out the ignition test. The timber tested were Radiata Pine, Rimu, Beech, Macrocarpa, while the timber based products were medium density fibreboard (MDF) and plywood. Additionally, seven different thermal correlations developed by various researchers (as listed below) were used to determine the best way to predict the ignition time.

1. Mikkola and Wichman
2. Tewarson
3. Quintiere and Harkleroad
4. Janssens
5. Toal, Silcock and Shields
6. Delichatsios, Panagiotou and Kiley
7. Spearpoint and Quintiere

Both Huynh (2003) and Merryweather (2006) collected flame spread data on various New Zealand native timbers and timber based products. A description of their research is provided to give an overview of the work that was carried out at the University of Canterbury.

Huynh (2003) studied the flame spread of indigenous New Zealand timber and timber products using the RIFT. The flame spread tests were conducted on eight different wood types, these being: Radiata Pine, Rimu, Beech, Macrocarpa, Medium Density Fibreboard (MDF), Plywood, Particle board and Laminated Veneer Lumber (LVL).

Meanwhile, Merryweather (2006) continued investigating the properties of ignition and flame spread using the standard LIFT test for nine different New Zealand timbers and timber based products; a list of the materials used is shown in Table 1-1. In addition, flame spread tests were conducted using the RIFT method. Ignition and flame spread data from the LIFT and RIFT were obtained. The main focus in this research is used the flame spread results

from the LIFT test that was conducted by Merryweather to carry out a direct comparison between the experimental results and the results from FDS4.

Table 1-1: Materials tested by Merryweather (Merryweather 2006)

Material	Manufacturer and trade name	Description	Density of tested samples kg/m ³
Plywood	IPL “Tuffply”	C/D grade untreated radiata pine, 17mm	487
Particle board (chipboard)	Laminex Corp (Fletcher Wood Panels) “Pynefloor”	Radiata Pine based flooring particle board	745
	Laminex Corp (Fletcher Wood Panels) “Superflake”	Radiata Pine based particle board	673
Medium density fibreboard (MDF)	Fletcher Wood Panels “Customwood”	18mm Radiata Pine based standard MDF	620
Melteca faced medium density fibreboard	Laminex Corp (Fletcher Wood Panels) Melteca	White Melamine faced MDF	681
Melteca faced particle board	“Regal” pre finished shelving, 18mm	White Prefinished and clashed shelving from builders merchants	661
Hardboard	Unbranded	Hardboard fibreboard 5mm	683
Radiata Pine (Monterey pine)		Clear grade, 16mm thickness	425
Macrocarpa		Clear grade, 16mm thickness	514
Rimu		Heart grade 16mm thickness	660
Beech		16mm thickness	489

1.2 Impetus for Research

Due to the rapid growth of computer power, the more traditional zone model is slowly being replaced by computer modelling such as Computation Fluid Dynamics (CFD) model. Fire Dynamics Simulator version 4 (FDS4) is one of the CFD models commonly used in the fire

engineering industry. Improvements are continually being made to FDS4 since it has been on public release by the National Institute of Science and Technology (NIST) in 2000.

While FDS4 has developed so much in the past years, an attempt to model the LIFT test in FDS4 is necessarily to examine how FDS4 predicts opposed flow flame spread. This report only focuses on the LIFT test conducted by Merryweather on the nine different timbers and timber based products for comparison.

Potentially, if FDS4 can predict flame spread for New Zealand timbers and timber based products, it also has the capability to predict flame spread for other materials. There are many advantages in running simulation in FDS4 to model flame spread over the LIFT test. Not only would it save time and effort by not actually doing the experiments, but also cost savings will be made in terms not contracting out to a laboratory for testing the material's flame spread characteristics. But most importantly, it means performing a LIFT test can be done anywhere as long as a computer is available to carry out the simulation. This is important as the number of LIFT test apparatuses available in laboratories worldwide is limited; where an estimate of 20 has been made by Babrauskas (Babrauskas and Wetterlund 1999).

1.3 Research Objectives

The aim of this research is to determine how well FDS4 predicts opposed flow flame spread of timber and timber based products. This is carried out by comparing the flame spread results predicted from FDS4 to the LIFT tests conducted by Merryweather at the University of Canterbury. As a result, this will enable us to determine whether or not FDS4 can replace the LIFT apparatus to predict opposed flow flame spread. The objectives of this research can be summarised into the following seven stages:

- To conduct a literature review on the methods of measuring opposed flow flame spread.
- To set up the geometry of the LIFT test apparatus in FDS4.
- To calibrate the simulated LIFT test apparatus in FDS4.

- To measure the thermal properties of the timber based products used by Merryweather.
- To simulate flame spread tests in FDS4 for the 9 different timber based products.
- To determine the flame spread parameters for each material.
- To verify the prediction of flame spread in FDS4 by comparing with the experiments conducted by Merryweather.

The following outputs will be compared directly with the results from the experiments by Merryweather:

- The flame (pyrolysis front) velocity, V
- The critical flux for ignition, $\dot{q}_{o,ig}''$
- The critical flux for spread, $\dot{q}_{o,s}''$
- The flame heating parameter, Φ

1.4 Report Outline

There are a total of 11 chapters in this report. The content of each chapter is summarised below to give the reader an idea of the process involved in this research.

Chapter 2 presents the background information on flame spread in general. A review of the historical development of the LIFT test apparatus is also presented. In addition, the work on modelling flame spread is discussed.

Chapter 3 outlines the main assumptions and governing equations behind the FDS4 to give a general overview and broad understanding of the concepts behind the model. This chapter is

mainly referenced from the Technical Reference Guide of FDS4 (McGrattan (editor) July 2004) and Combustion Fundamentals of Fire (Cox 1995a).

Chapter 4 describes the LIFT apparatus in detail based on the ASTM fire standard. The flame spread theory behind the LIFT test by Quintiere and Harkleroad is also presented.

Chapter 5 demonstrates the procedure for obtaining charred specimens in order to determine both their physical and thermal properties so that it can be applied in the FDS4 model. In particular, the thermal properties of the virgin and charred materials are measured using a transient plane source (TPS) technique.

Chapter 6 describes the theory of the Hot Disk test, based on TPS technique, which is applied to determine the thermal properties of the timber and timber based products. In addition, the results from the Hot Disk test are discussed.

Chapter 7 describes the process of setting up the LIFT test apparatus in FDS4. Calibration of the LIFT test is performed in FDS4 to ensure the required heat fluxes specified by the ASTM fire standard are met.

Chapter 8 describes the flame spread test procedure in FDS4 and shows FDS4 input file that is used to model the test. An outline of the heat transfer model to account for the preheat time required is also described.

Chapter 9 presents the sensitivity analysis based on the grid sizes analysed in FDS4, the type of the pyrolysis model and both the heat of vaporisation and moisture content of the specimen.

Chapter 10 reports on how well FDS4 predicts the flame spread by comparing the flame spread parameters and the critical flux required for both the ignition and flame spread from FDS4 with the experimental values obtained by Merryweather.

Chapter 11 concludes the report and summarises the major findings as well as a list of recommendations for future research on the predicting flame spread using FDS4.

2 Literature Review

This chapter presents a literature review and background information on surface flame spread. The history of flame spread theory will be briefly discussed. In addition, some of the flame spread data relating to the LIFT and RIFT test conducted by various researchers will be presented. Other published flame spread models are also reviewed.

2.1 Pioneering Work on Flame Spread theory

The earliest researchers in flame spread quickly understood that certain polymeric materials possessed nearly ideal burning behaviours which rendered them suitable for repeatable scientific testing (Wichman 1992). For example, PMMA (polymethylmethacrylate) has been described as an "ideal vaporizing solid" whose decomposition in a fire can accurately be explained by simple and accurate models. As a result, many researchers studied and conducted experiments on flame spread on this material. This section provides a brief insight on the development of the flame spread theory. More information can be found in the literature reviews by Fernandez-Pello and Hirano (1983), Wichman (1992), Quintiere (2002) and Huynh (2002).

2.1.1 The flame spread models of deRis

Flame spread research started in 1968 PhD thesis of deRis (1968), where the flame spread theory was developed and is still used today. Two dimensional conservation equations were solved to develop a basic understanding of the propagation mechanism. deRis did this by applying first principles in conjunction with physical assumptions. By doing so, the relevant two dimensional conservation equations and its boundary conditions are derived. Subsequently, the techniques of modern applied mathematics are applied to solve the equations. This method is considered to be the key development in the theory of flame spread. The following physical assumptions were used in his studies:

- Gravitational effects are ignored.
- All solids are vaporising (i.e. no solids were to melt or pyrolyse).
- The flame front has a "triple-flame" structure.

- The flame spread is independent of the opposing flow.

Figure 2-1 shows the “triple-flame” structure postulated by deRis. The “secondary flame fronts” are actually premixed flames; the lower is fuel rich; the upper fuel lean. The reason for assuming the flame spread is independent of the opposing flow is because deRis recognised that there was no “quiescent” environment in normal gravity flame spread. If the environment is quiescent initially, the hot flaming zone would induce an opposing flow in which the average velocity is usually many times greater than the flame spread velocity. Since deRis employed the Oseen-flow assumption, where $v = 0, u = U_\infty, p = \text{constant}$ (Exact solution of the Navier-Stokes equations), the equations do not matter whether the opposing flow is induced or forced.

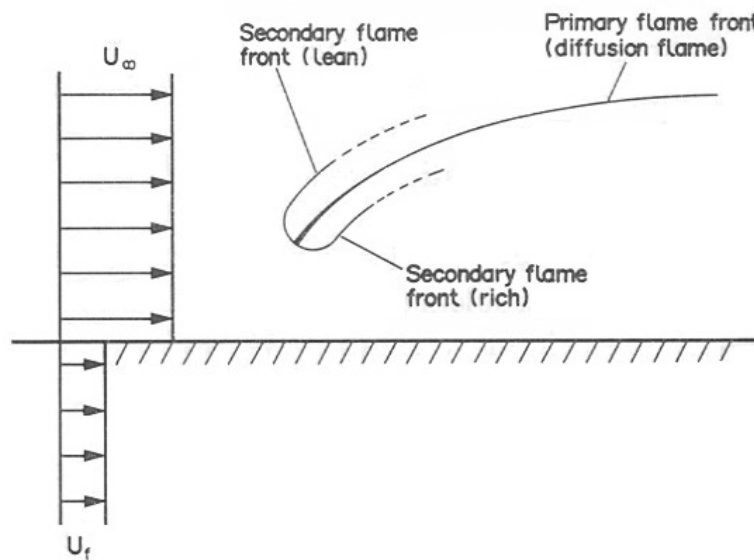


Figure 2-1: The shape of the spreading flame postulated by deRis (deRis 1968)

One of the main features in his thesis was to distinguish the materials as either thermally thin or thermally thick. From his research, the flame spread equations for both the cases were presented as shown below:

For the thermally thin case:

$$U_f = \sqrt{2} \frac{\alpha_s \lambda_s}{\Delta \lambda_g} \left[\left(\frac{r_g}{r_s} \right) \frac{(T_f - T_v)}{(T_v - T_\infty)} \right] \tag{Equation 2-1}$$

For the thermally thick case:

$$U_f = U_\infty \left[\left(\frac{r_{gy}}{r_{sy}} \right) \frac{(T_f - T_v)}{(T_v - T_\infty)} \right]^2 \quad \text{Equation 2-2}$$

where $r_g = [\rho_g c_{pg} \lambda_g]^{1/2}$ is the thermal responsivities of the gas; $r_s = [\rho_s c_s \lambda_s]^{1/2}$ is the thermal responsivities of the solid.

2.1.2 Experimental and theoretical work of McAlevy et al

The work by McAlevy et al (McAlevy and Magee 1969) was carried out around the same time as the work by deRis. The flame spread problem was approached using propellants, which means they relied principally on their experiments for analysing flame spread. They hypothesised that the rate of flame spread is an “intrinsic combustion quantity”. This assumption is the opposite of the theory of deRis, where the flame spread rate actually depends on flow velocity. In addition, the thickness of the specimen was not considered in their experiments as a factor that will have an impact on the flame spread.

As mentioned in the literature reviewed by Wichman (1992), ad hoc assumptions were necessary due to their ad hoc elimination of streamwise diffusion. Despite of this, their observations and experimental techniques are still valid and widely used today. For example, a wind tunnel was used in their experiments which air is forced at a specified rate. In addition, they were the first researchers to use PMMA as a propellant binder due to the uniform burning properties of PMMA. McAlevy et al found that for low opposed flow velocities, the flame spread rate over PMMA increased. However, the flame spread rate starts to decreased when the opposed flow velocity reaches to a certain critical value.

2.1.3 The fire-spread model of Williams

The article by Williams (Williams 1976) examined the mechanisms of fire spread, where an equation for the heat balance across the surface of fire inception is proposed and examined. As a result, it leads to flame spread formulas for various special cases such as downward spread (opposed flow spread). This heat balance leads to the derivation of a ‘universal’ flame spread equation as shown in Equation 2-3.

$$q = \rho_s U_f \Delta h$$

Equation 2-3

where q is the energy per second transported across the separation line S (the line between no flame and flame); ρ_s is the fuel density; Δh is the thermal enthalpy difference between the fuel at ignition and ambient temperatures.

The q changes accordingly depending on the mode of heat transfer across S. For gas-phase conduction, both the thermally thin and thick fuels equates to Equation 2-1 and Equation 2-2 respectively; which are the fundamental flame spread formulas developed by deRis (deRis 1968). However, there seems to be an element of symmetry missing in Equation 2-2 to deduce a flame spread formula for solid-phase conduction. Consequently, the heat equation described by Williams is only applicable when the gas-phase process dominates flame spread over solid-phase process. In addition, Williams also examined flame spread over non-simple materials like matchstick arrays and materials that drip or run during spread.

2.1.4 The Fernandez-Pello Williams model

A flame spread theory (Fernandez-Pello and Williams 1977) was proposed for predicting the steady rate of spread of a flame over the surface of a solid in directions ranging from downward to horizontal. This theory was based on the following 4 aspects:

1. A thorough analysis of the gas-phase equations, including the equations for conservation of linear momentum
2. A way of dealing the solid-phase problem based partly on previous observations from the work on solid fuel degradation kinetics
3. A detailed analysis of the gas-phase chemistry, using the method of high activation energy analysis for the gasification and ignition reactions
4. The experimental measurements obtained by Fernandez-Pello

Fernandez-Pello and Williams hypothesized on the basis of their experiments that the bulk of the heat transfer ahead of the flame front occurred through the solid phase period. This assumption was supported from their observations where the solid phase dominates the

forward heat transfer when the solid-to-gas Peclet ratio is small. Wichman and Williams suggested that this condition is valid only for low free stream oxidizer concentrations such as air (Wichman 1992).

Their theory was primarily based on the foundation provided from the experiments observations and data available. This evidence was later questioned by other researchers; where they found that solid phase does not dominate the forward heat transfer as suggested by Fernandez-Pello and Williams. In fact, the heat flux from the gas phase is many times larger than solid phase heat flux. This implies that the Fernandez-Pello and Williams theory actually underestimated the heat transfer from the gas phase, hence the calculated heat flux required for flame spread is less than the actual heat flux required in the experiment (Quintiere 1981)

In addition, The Fernandez-Pello and Williams model examines small-scale downward spread over an ‘ideal’ solid in a gravitational field. Thus, it is one of the few studies of flame spread that explicitly includes gravitational effects. It shows that the predictions of the model can be made to agree well with many experimental observations.

2.1.5 Frey and T’ien model

The article by Frey and T’ien presents a theory for opposed flow flame spread over a thermally thin solid fuel. The Frey and T’ien model (Frey and T’ien 1979) was considered to be the first successful numerical study of flame spread (Wichman 1992).

This model retained the Oseen flow and constant gas property assumptions; however, it ignored infinite chemistry, linearised the mass flux boundary condition and the constant vaporisation temperature in the gasification zone. In order to investigate extinction limits and near extinction flame behaviour, species equations with one-step overall chemical reaction and second-order, finite rate Arrhenius kinetics were used. An ad hoc volume heat sink term arises in their two dimensional energy equation, which enables them to examine the influences heat losses may have on the flame-extinction behaviour.

Parameters such as pressure, oxygen mass fraction, and magnitude of opposed flow velocity were investigated which enabled them to observe the effects it has on the flame spread. They

found that as pressure decreases the flame extends further due to the increase of characteristic thermal length; for the case without heat losses, flame extinction occurs due to the changes in the opposed flow velocity induced by decreasing the pressure. They also kept the opposed flow velocity constant and found that no extinction limit occurs. On the other hand, the flame spread rate is dependent on pressure if the heat losses are included.

2.1.6 Quintiere

Quintiere suggested a simplified theory for generalizing results from a radiant panel rate of flame spread apparatus (Quintiere 1981). This theory was developed based on the experimental results of the lateral flame spread rate and piloted ignition time under an externally imposed radiant heat flux. The radiant panel was designed to produce a flux distribution on the wall mounted sample of 5 W.cm^{-2} at the ignited end and 0.2 W.cm^{-2} at the other end.

Quintiere illustrated his theoretical flame spread model in a diagram as shown in Figure 2-2; where the solid is considered thermally thick and both the initial and ambient temperature is constant. The derivation of the rate of flame spread over a solid with an imposed external radiant flux of arbitrary space and time variation can be found in Appendix 1 of Quintiere (1981), while the relationship between material surface temperature and imposed external radiant flux at thermal equilibrium is given in Appendix 2 of Quintiere (1981).

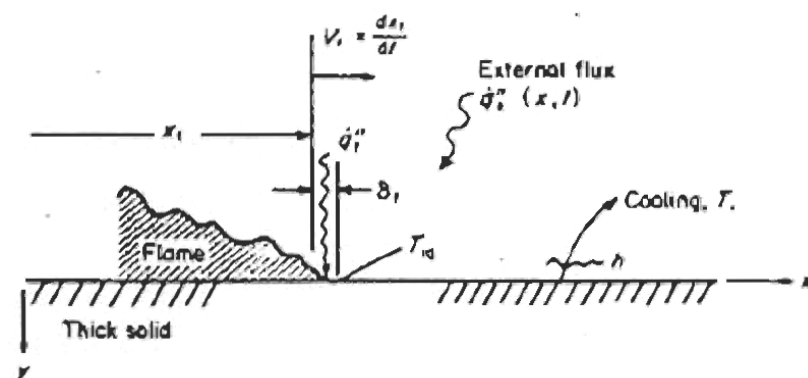


Figure 2-2: Flame spread model (Quintiere 1981)

The flame spread experiments conducted by Quintiere have shown that an appropriate preheating time, which is the exposure time before sample is ignited, is needed in order to correlate the flame spread rate represented by Equation 2-4 below.

$$\frac{1}{V} = C(\dot{q}''_{o,ig} - \dot{q}''_e) \quad \text{Equation 2-4}$$

where V is the flame spread rate; C is the material constant; $\dot{q}''_{o,ig}$ is the minimum flux for piloted ignition; \dot{q}''_e is the flux distribution.

This simple theoretical model leads to the development of a flame spread apparatus and has since been modified to the standard flame spread test known as the Lateral Ignition Flame Transport (LIFT) test. The theory and experimental procedure for the LIFT test will be further discussed in Chapter 4.

2.2 Surface Flame Spread

2.2.1 Introduction

Flame spread is the process in which the perimeter of the fire grows (Quintiere 1998). It is quite different to fire spread, which is the process of advancing a combustion front comprising surface flame spread, smouldering growth and the fire ball in premixed flame propagation. There are two types of burning surface: normal burning perpendicular to the surface and spread along the surface. The flame spread problem is defined when the normal burning perpendicular to the surface is smaller than the spread along the surfaces. In this case, the normal burning calculation is expected to be insignificant when compared with the spread calculation (Wichman 1992). It is important to note that surface flame spread as described in this section is not the flame propagation in premixed fuel and air systems, but rather the moving flame phenomenon in close proximity to the source of its fuel originating from a solid or liquid phase. As in the premixed case, the flame front propagates differently compared to solids or liquids; due to a lower flammability limit (Quintiere and Harkleroad 1984).

Quintiere (2002) stated that the process of growth is unstable depending on the time for flame spread and the time for burning. If the spread time is small compared to the burn time, fire growth is likely to accelerate. Meanwhile, fire growth could decelerate and stop if the spread time is large compared to the burn time. This leads to the flame spread velocity. The rate of flame spread is different depending on materials. For example the spread of solids

will be different compared with spread through porous solid arrays (forest brush and debris). Again the spread of liquids propagate differently compared to the spread of gases, as discussed for the premixed gases above.

The mechanism of flame spread such as the flame velocity depends on the direction of the wind. Either (1) wind-aided flame spread where the flame spread in the same direction as the air flow or (2) opposed flow flame spread which refers the flame spread in the opposite direction as the air flow. Natural and forced flow can be applied to demonstrate both the wind-aided and opposed flow flame spread scenario as shown in Figure 2-3. Natural flow is the air flow caused by the buoyancy, while forced flow is the air generated by other medium such as meteorological wind or a mechanical fan. In this research, only opposed flow flame spread is considered.

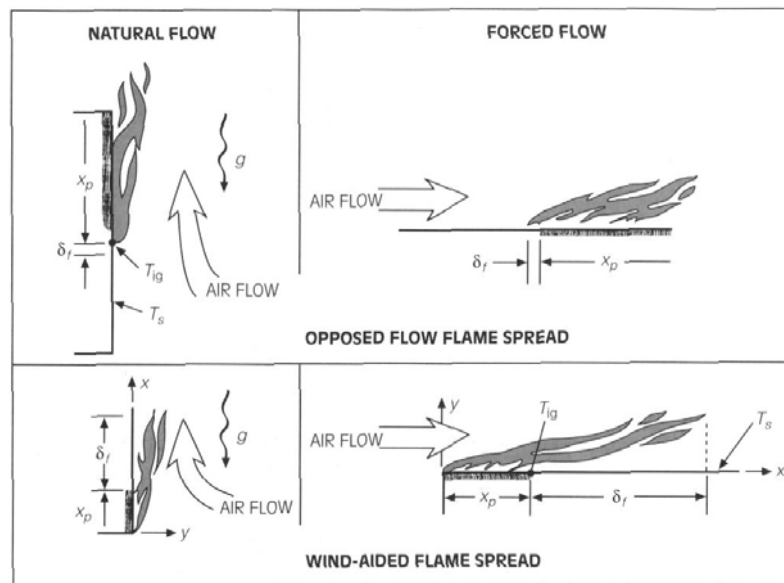


Figure 2-3: Flame spread for natural and forced flow (Quintiere 1998)

Table 2-1 demonstrates how the flame spread rate changes dramatically depending on the fire, state condition of the fuel and direction of the wind i.e. a smouldering fire or a flaming fire, flame travelling upward or downward, fuel orientation and fuel type i.e. a solid or liquid or gas phase (premixed). As expected, the flame spread for premixed gases travels more rapidly than solids. While upward (wind aided) flame spread propagates faster than opposed

flow flame spread. Only flame spread over solids is discussed in this research as the materials used for the testing is wood.

Table 2-1: Relative flame spread rates (Quintiere and Harkleroad 1984)

Phenomenon	Rate (cm/s)
Smouldering	10^{-3} to 10^{-2}
Lateral or downward spread on thick solids	$\sim 10^{-1}$
Upward spread on thick solids	1 to 10^2
Horizontal spread on liquids	1 to 10^2
Forest and urban fire spread	1 to 10^2
Pre-mixed flame speeds	
<i>Laminar deflagration</i>	10 to 10^2
<i>Detonation</i>	$\sim 3 \times 10^5$

Pyrolysis is the process of breaking up a substance into other molecules as a result of heating; also known as thermal decomposition (Quintiere 1998). The combustion of the pyrolysis area and the rate of pyrolysis are associated with the burning rate. The burning rate is an essential parameter as it is related to the temperature, visibility, toxicity and corrosivity of the fire which are the main criteria in determining the life safety in fire. Therefore, flame spread rate plays an important role in assessing the hazard in fire.

The following sections detail the flame spread over solids for both the opposed flow and wind-aided flame spread, which is based on the energy conservation principle described in Quintiere (2002). This is intended to give the underlying theory used in predicting the surface flame spread.

2.2.2 Velocity for opposed flow flame spread over solid

Opposed flow flame spread depends on the thickness of the solid, whether it is thermally thin or thermally thick. For thicknesses that are between thermally thin and thermally thick, the term thermally intermediate is applied; however no flame spread equations are available for the thermally immediate case. In this section, the flame spread velocity calculation for the thermally thin and thick case will be described.

It is important to know the meaning of the term thermally thin and thermally thick before going into detail about the flame spread concept; thermally thin means the heat penetrates the whole thickness of the material; while in the case for thermally thick material the heat does not completely penetrate through the solid. A schematic sketch of the energy conservation analysis in opposed flow flame spread is illustrated in Figure 2-4. In all cases, the assumption of a steady flame spread rate and the reference frame is fixed to the pyrolysis front is applied.

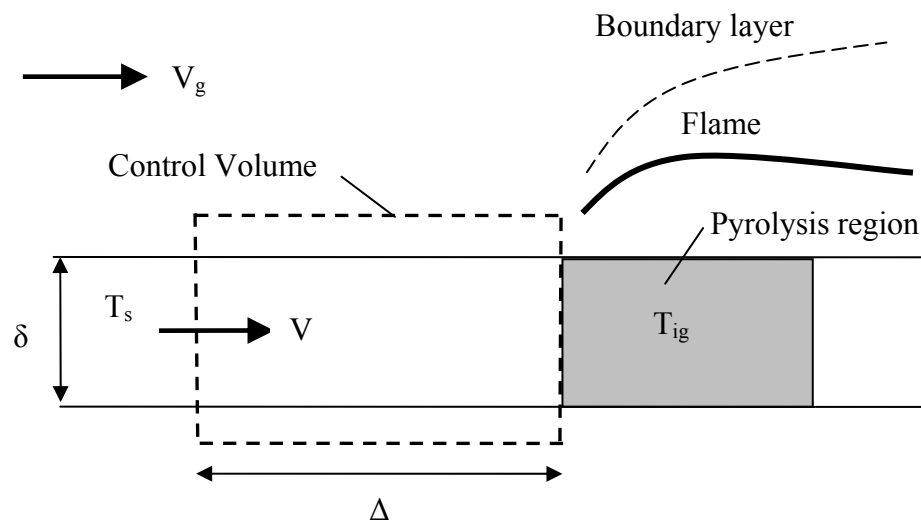


Figure 2-4: Energy conservation analysis in opposed flow flame spread (Quintiere 2002)

Flame spread velocity for the thermally thin case

Based on the energy conservation analysis as shown in Figure 2-4, an energy equation for the control volume is developed. The control volume covers the area from the unaffected region by the flame to the region where pyrolysis begins as indicated in Figure 2-4. If a constant heat flux (\dot{q}'') is assumed over the length Δ of the control volume, the rate of flame spread can be represented by Equation 2-5; where ρ is the density of the solid, c is the specific heat capacity, δ is the physical thickness, T_{ig} and T_s is the temperature of both ignition and surface respectively.

$$\rho c \delta (T_{ig} - T_s) V = \dot{q}'' \Delta \quad \text{Equation 2-5}$$

The net forward flame heat flux characterised as conduction in the gas phase is given as follows:

$$\dot{q}'' \approx k_g \left(\frac{T_f - T_r}{\Delta} \right) \quad \text{Equation 2-6}$$

where k_g is the gas phase conductivity; T_f is the flame temperature and T_r is the reference temperature for the solid (either the ignition or surface temperature).

Equation 2-7 is obtained by combining Equation 2-5 and Equation 2-6 above. Interestingly, this equation is almost identical to the flame spread equation for thermally thin solids as indicated in Equation 2-1 developed by deRis.

$$V = \frac{\sqrt{2} k_g (T_f - T_s)}{\rho c \delta (T_{ig} - T_s)} \quad \text{Equation 2-7}$$

The flame temperature of a combustible solid is extremely difficult to measure in nature as the flame fluctuates significantly during combustion. Equation 2-8 illustrates the equation used to determine flame temperature in an idealised condition (adiabatic stoichiometric combustion) as mentioned in Quintiere (2002). The approximation of an ideal condition is somewhat different to a real scenario, where the heat losses and chemical kinetic effects the flame temperature.

$$T_f - T_{ig} = \frac{(T_{\infty} - T_{ig}) + (Y_{ox,\infty} / r c_g) (\Delta H - L)}{1 - Y_{ox,\infty} / r} \quad \text{Equation 2-8}$$

Because ΔH and $Y_{ox,\infty} / r$ are relatively large, and $\Delta H_{ox} = \Delta H / r$ is nearly a constant for most hydrocarbons (13kJ/g). As a result, a relationship is identified for Equation 2-8; it is found that the flame temperature and the ambient oxygen concentration are strongly dependent on each other, as indicated in Equation 2-9. In addition, it is interesting to note that when Equation 2-9 is substituted back into Equation 2-7, a flame spread equation is yielded which is identical to the equation derived by McAlevy et al (1969).

$$T_f - T_{ig} \sim Y_{ox,\infty} \Delta H_{ox} / c_g$$

Equation 2-9

The parameter used to express the effect of the chemical kinetic effect is the Damkohler number (D). The relationship between D and opposed flow velocity V_g is indicated in Equation 2-10; where t_{chem} is the time for chemical reactions to be completed in the flame and t_{flow} is the fluid flow transit time through the flame.

$$D \sim \frac{t_{flow}}{t_{chem}} \sim \frac{1}{V_g^2}$$

Equation 2-10

Figure 2-5 represents the results given with the measured spread velocity normalised with the ideal theoretical velocity Figure 2-5 plotted against D . The results from Figure 2-5 show that as the flame spread velocity decreases D also decreases.

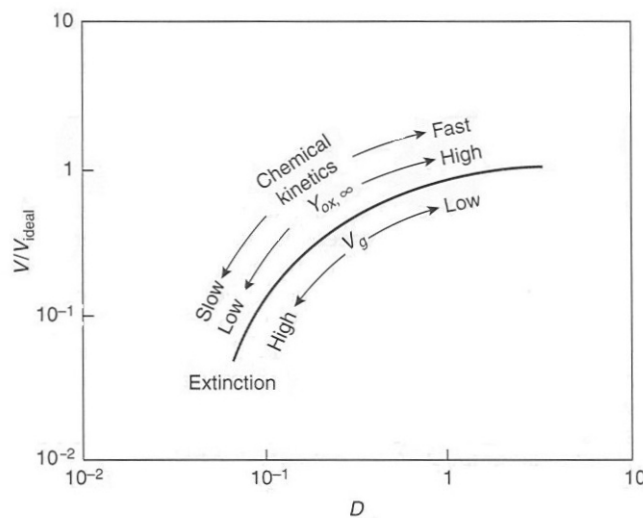


Figure 2-5: Qualitative dependence of opposed flow flame speed with Damkohler number, D (Quintiere 2002)

For opposed flow flame in pure natural convection, the ambient flow velocity is calculated as follows:

$$(V_g)_{\text{natural convection}} \sim \left(\frac{v_g g \Delta H Y_{ox,\infty}}{c_g r T_\infty} \right)^{1/3} \quad \text{Equation 2-11}$$

where v_g is the gas phase kinematic viscosity. However, V_g induced by buoyancy is basically a function of $Y_{ox,\infty}$ to the power of 1/3.

For thermally thin solids, the opposed flow flame spread velocity with an ambient oxygen concentration ($Y_{ox,\infty}$) is given as follows:

$$V = V_{ideal} f(D) \quad \text{Equation 2-12}$$

where V_{ideal} is the ideal velocity and $f(D)$ is the function of Damkohler number to account for the chemical kinetics effect. It should be noted that at some critical value of D there would be extinction of the flame.

From all of the considerations stated, the opposed flow flame spread on thermally thin materials can therefore be represented by Equation 2-13. It is understood that for a common combustible if the solid has a thickness of less than 1 mm ($\delta < 1mm$) it is considered to be a thermally thin material and Equation 2-13 is applicable.

$$V = \frac{\phi(V_g, Y_{ox,\infty}, \text{material properties})}{\rho c \delta (T_{ig} - T_s)} \quad \text{Equation 2-13}$$

where the function flame heating parameter ϕ depends on the opposed flow velocity, the ambient oxygen concentration and the material properties.

Flame spread velocity for the thermally thick case

Similar to the case of thermally thin material, the energy conservation analysis as shown in Figure 2-4 is used to determine the flame spread velocity for thermally thick material. In this case, the thermal penetration depth (δ) must be considered to be dependent of time where temperature across the solid depth varies with time. From heat conduction theory, the relationship between δ and thermal properties $k\rho c$ of the solid corresponds to Equation

2-14; where t is the time for the flame's pyrolysis front to transverse the heating length (Δ) of the control volume and is represented in Equation 2-15.

$$\delta \approx \sqrt{\frac{k}{\rho c} t} \quad \text{Equation 2-14}$$

$$t = \frac{\Delta}{V} \quad \text{Equation 2-15}$$

By substituting both Equation 2-14 and Equation 2-15 back into Equation 2-5, the rate of flame spread can be represented as follows:

$$V = \frac{(\dot{q}''_f)^2 \Delta}{k \rho c (T_{ig} - T_s)^2} \quad \text{Equation 2-16}$$

The heating length Δ is dependent on the forward heat transfer. In opposed flow flame spread, the dominant mode of heat transfer is the conduction in the gas phase. Therefore, forward conduction must be balanced with convection as represented in Equation 2-17 below. The relationship between Δ and both the material properties and velocity of ambient air is correlated as presented in Equation 2-18.

In addition, the equation of opposed flow flame spread for the thermally thick case is produced (Equation 2-19) by combining Equation 2-16 and Equation 2-18 with Equation 2-6. Quintere (2002) indicated that the flame spread velocity expression is identical to the equation (Equation 2-2) derived by deRis (1969).

$$\rho c V_g \frac{\partial T}{\partial x} \sim k \frac{\partial^2 T}{\partial x^2} \quad \text{Equation 2-17}$$

$$\Delta \sim \left(\frac{k}{\rho c} \right)_g / V_g \quad \text{Equation 2-18}$$

$$V = \frac{V_g (k \rho c)_g (T_f - T_{ig})^2}{k \rho c (T_{ig} - T_s)^2} \quad \text{Equation 2-19}$$

It should be noted that the opposed flow flame spread velocity calculated from Equation 2-19 is an ideal value due to the flame temperature being assumed as an adiabatic stoichiometric value. Due to the heat losses and chemical kinetics effect that will influence the flame spread rate as discussed early; the Damkohler number is used to take into the account of the

chemical kinetic effects. The actual flame spread velocity is similar to the thermally thin case as indicated in Equation 2-12 where the actual velocity is $V = V_{ideal} f(D)$; the product of the ideal velocity (V_{ideal}) and the function of the Damkohler number D .

Quintiere and Harkleroad developed a practical test (LIFT test) procedure to describe essentially the behaviour of opposed flow flame spread on thermally thick materials burning under ambient conditions. More information on the LIFT test is covered in Chapter 4. The equation used for determining the opposed flow flame spread for thermally thick materials in LIFT test is as follows:

$$V = \frac{\phi}{k\rho c(T_{ig} - T_s)^2} \quad \text{Equation 2-20}$$

where Φ is the flame heating parameter and similarly for the thermally thin case, it depends on both the opposed flow velocity and ambient oxygen concentration.

2.2.3 Velocity for wind aided flame spread over solid

As mentioned previously, wind aided flame spread is not considered in this research since the LIFT test only operates under an opposed flow condition. However, wind aided flame spread velocity is reviewed in this section to recognize the difference between opposed flow and wind aided flame spread. The condition for wind aided flame spread results from either external wind or buoyancy induced flow created as flame spreads up a wall or under a ceiling. In general, wind aided flame spread can be acceleratory and appears more rapid than opposed flow flame spread.

A schematic sketch of the energy conservation analysis in wind-aided flame spread is illustrated in Figure 2-6; where the length of the control volume is selected downstream of the pyrolysis zone starting from the edge of the pyrolysis region to a distance Δ along the solid. Δ is dependent of the flame length which varies from 0.1 to 10 m for wind aided flame spread; In addition, the distance Δ is relatively longer when compared to the opposed flow flame spread of 1 to 3 mm.

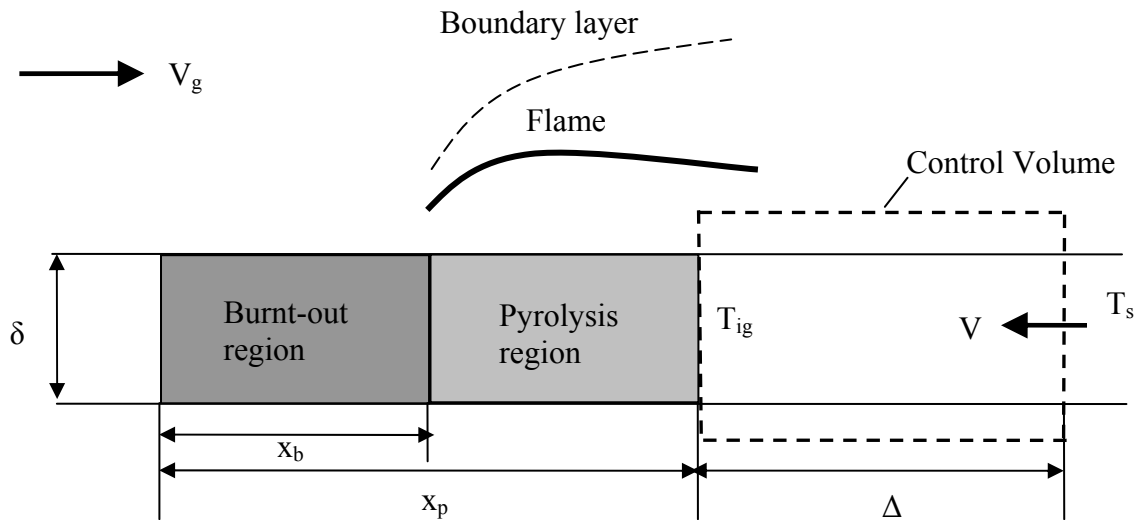


Figure 2-6: Energy conservation analysis in wind-aided flame spread (Quintiere 2002)

The same equations are derived when an energy balance is carried out for the control volume. As a result, the flame spread velocity for both the case of thermally thin and thick is represented respectively in Equation 2-21 and Equation 2-22 below.

Flame spread velocity for the thermally thin case

$$V = \frac{dx_p}{dt} = \frac{\dot{q}'' \Delta}{\rho c \delta (T_{ig} - T_s)} \quad \text{Equation 2-21}$$

Flame spread velocity for the thermally thick case

$$V = \frac{dx_p}{dt} = \frac{(\dot{q}'')^2 \Delta}{k \rho c (T_{ig} - T_s)^2} \quad \text{Equation 2-22}$$

Alternatively, the flame spread velocity equation can be written in the form of Equation 2-23.

$$V = \frac{dx_p}{dt} = \frac{x_f - x_p}{\tau} \quad \text{Equation 2-23}$$

where τ is an ignition time associated with the flame heat flux and x_f is the flame length measured from $x = 0$, while a constant flame heat flux over the region Δ is assumed and x_p

$$x_p = x_p(0) + \int_0^t V(s) ds \quad \text{Equation 2-24}$$

It is proposed that x_f is directly related to energy released per unit width \dot{Q}' where \dot{Q}' is calculated as shown in Equation 2-26. Quintiere (2002) mentioned that the cone calorimeter can potentially provide information to obtain \dot{Q}'' .

$$x_f - x_b = K[\dot{Q}']^n \quad \text{Equation 2-25}$$

$$\dot{Q}' = \int_{x_b}^{x_p} \dot{Q}''(\xi) d\xi \quad \text{Equation 2-26}$$

The energy released per unit width for upward spread on a flat wall under conditions $K = 0.067 m^{5/3} kW^{-2/3}$ and $n = 2/3$ can be shown as follows.

$$\dot{Q}' = x_p(0)\dot{Q}''(t) + \int_0^t \dot{Q}''(t-s)V(s) ds \quad \text{Equation 2-27}$$

As mentioned previously, the extent of heating Δ is related to flame length and this has shown to depend on the energy release rate to some power n ; where n is approximately 0.5 to 1 for upward turbulent spread. Due to the energy release rate being dependent on the extent of the pyrolysing region ($x_p - x_b$), it implies that the flame spread velocity for flames to travel up to the pyrolysis region is proportional to $(x_p - x_b)$ with n power as indicated in Equation 2-28. Again, this equation is only applicable for a constant heat flux over the solid.

$$V = \frac{dx_p}{dt} \propto (x_p - x_b)^n \quad \text{Equation 2-28}$$

Many researchers have studied the relationship of n for different materials the wind aided flame spread. A review on the factor n can be found in Quintiere (2002). Similar to opposed flow flame spread, there is a standard test known as the ASTM E84 Steiner tunnel test method for measuring wind-aided flame spread; this test measures wind-aided flame spread on a ceiling mounted material in a duct under forced flow conditions.

2.3 Factors affecting flame spread

The prediction of flame spread rate is considered to be very difficult to solve despite basic assumptions and empirical correlations that are applied in flame spread equations such as Equation 2-13 and Equation 2-21 for opposed-flow and wind aided flame spread respectively.

As the materials for the flame spread tests are timber and timber based products, wood is considered to be important variable and hence it is in the context of this research to discuss the effect it has on flame spread. Not only environmental factors such as oxygen concentration, external radiation and flow turbulence can have an influence on the rate of flame spread but physical parameters such as geometry of the material, charring characteristics, density and grain orientation can also have an effect on flame spread. These factors must be accounted for in order to determine the rate of flame spread more accurately. This section provides a brief summary of these factors and addressing the effect wood has on flame spread.

2.3.1 Opposed flow velocity and oxygen concentration

Due to the scope of this research, only opposed flow velocity will be considered in this section. The effect of wind-aided velocity can be found in literature such as in Cox 1995 and Quintiere 2002. The chemical kinetic effects determine whether or not the opposed flow velocity has an impact on the rate of flame spread.

When chemical kinetic effects are insignificant, the rate of the flame spread is independent of the opposed flow velocity. However, when chemical kinetic effects become important the independence between flame spread velocity and opposed flow velocity is no longer valid. The chemical kinetic effects is considered to be important when the time for chemical reactions to be completed in the flame (t_{chem}) becomes long compared to the fluid flow transit time (t_{flow}) through the flame (Quintiere 2002).

The effects of opposed flow velocity and oxygen concentration of a gas flow for thick PMMA sheets is shown in Figure 2-7 and

Figure 2-8 respectively. From this figures, it indicated that as the oxygen concentration increases, the flame spread rate also increases.

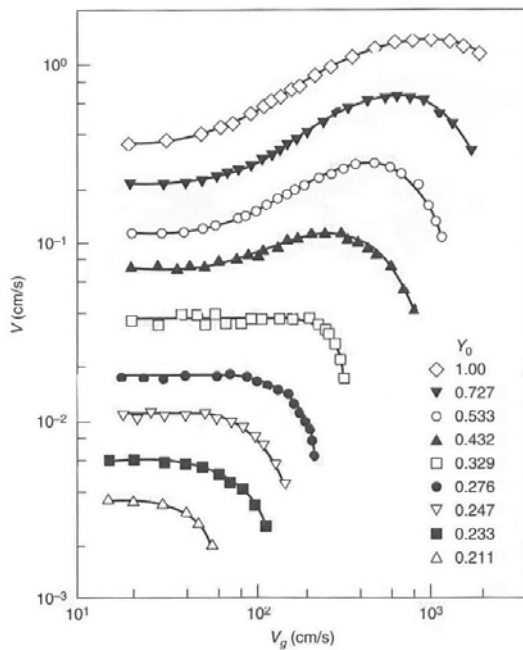


Figure 2-7: Flame spread rate over thick PMMA sheets as a function of the opposed forced flow velocity for several flow oxygen mass fractions (Fernandez-Pello et al. 1981)

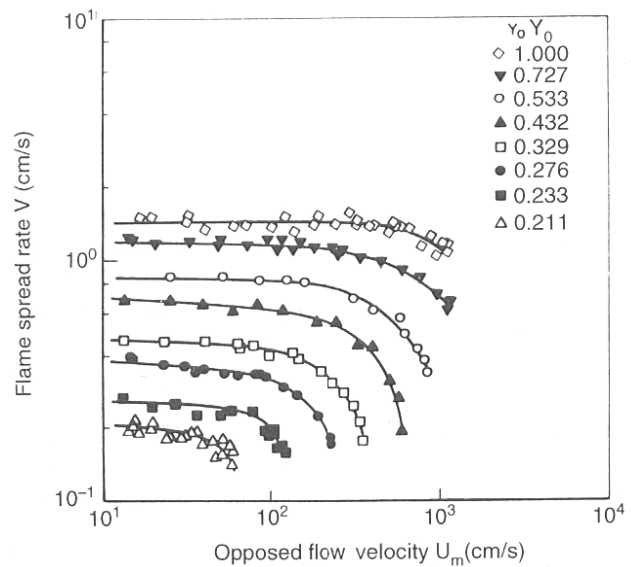


Figure 2-8: Flame spread rate over thin PMMA sheets as a function of the opposed forced flow velocity for several flow oxygen mass fractions (Fernandez-Pello et al. 1981)

2.3.2 Flow turbulence

The effect of flow turbulence has a direct impact on the solid heating; where the surface heat flux may actually enhance the heat transfer from the flame to the solid or the convective cooling of the solid. As for the gas phase reaction, turbulence will not only enhance the fuel vapour/oxidiser mixing but also cool the reacting gas by entrainment of ambient gas.

In opposed flow flame spread, since the ignition reaction occurs under a fuel lean condition, the dominant effect caused by turbulence is considered to be mixture dilution and convective cooling while the enhanced mixing is the secondary effect. The result would be a decrease in the Damkohler number and consequently an increase in the gas induction time. Therefore it can be seen that the increasing flow turbulence should increase the flame spread in the solid heating dominated regime and decrease the spread rate in the chemical kinetics dominated regime (Cox 1995b). It should be noted that a Damkohler number is used to account for the

chemical kinetics effect; which is adapted (Equation 2-12) in the theory of surface flame spread by Quintiere (2002).

Zhou et al (1990) studied the effects of flow velocity and turbulence on the opposed flow flame spread for thick PMMA sheets. The plot of variation of the opposed flow flame spread rate over thick PMMA sheets with the turbulence intensity for several air flow velocities is shown in Figure 2-9. It indicates that the spread rate first increases and then decrease as the turbulence intensity is increased. This experiment clearly demonstrated that the prediction of the effect of turbulence have on the opposed flow flame spread is correct.

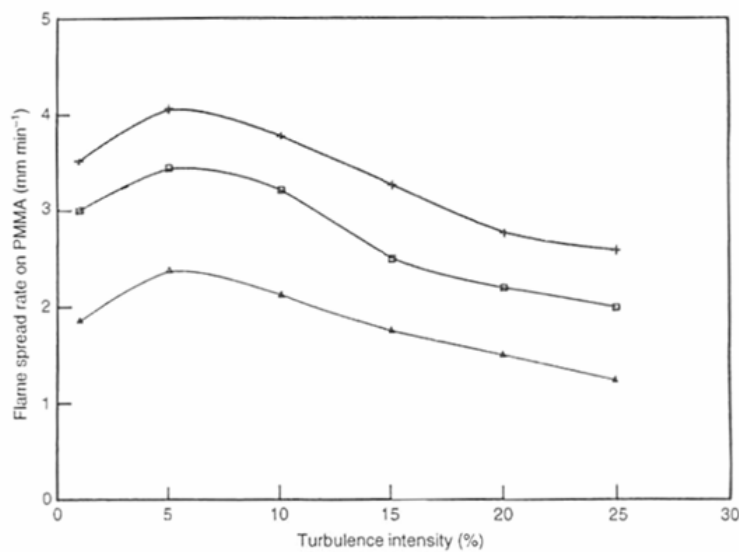


Figure 2-9: Variation of the opposed flow flame spread rate over thick PMMA sheets with the turbulence intensity for several air flow velocities (Zhou et al. 1990) +, 0.75 ; ■, 1.00; ▲, 1.25.

2.3.3 CO concentration

The concentration of carbon monoxide (CO) affects the combustion completeness and consequently the flame temperature. Measurements of the CO and unburnt hydrocarbon concentrations show that there is relatively high level of combustion incompleteness at oxygen mass fractions below 25% and that in general the flow velocity and turbulence intensity tend to increase the combustion incompleteness (Cox 1995b). Figure 2-10 is the experimental results of the variation of the CO concentration with the oxygen mass fraction for ceiling flame spread at different turbulence intensities. The results also indicated that as

the turbulence intensity increases, the level of incomplete combustion also increases and ultimately lowers the flame temperature.

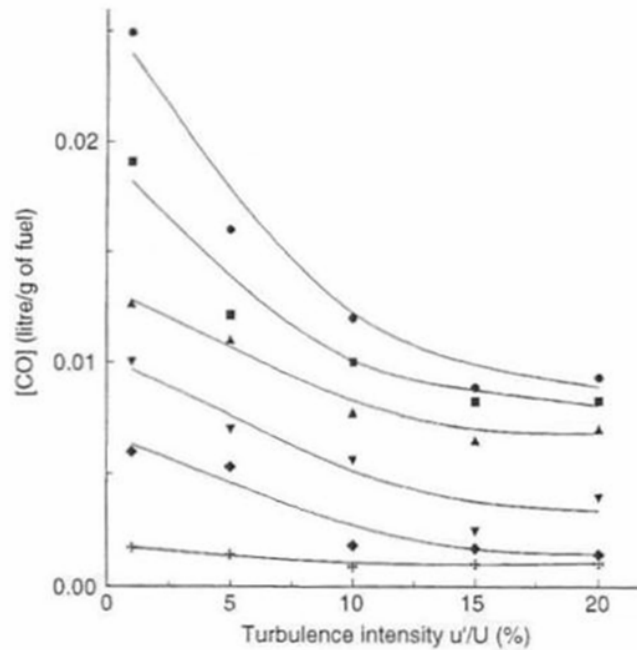


Figure 2-10: Variation of the CO concentration with oxygen mass fraction for ceiling flame spread at different turbulence intensities. Flow velocity of 2ms^{-1} (Chao and Fernandez-Pello 1996). Y_o : ●, 0.19; ■, 0.21; ▲, 0.23; ▼, 0.30; ◆, 0.40; +, 0.50.

2.3.4 External radiation

The effect of the external radiation on the flame spread rate appears through the surface heat flux, which in turn affects the fuel heating and pyrolysis rates and flame length, and the initial temperature of the solid. Figure 2-11 shows the pyrolysis front and flame tip upward spread rates over wood sheets as a function of the external radiant flux and are named “flammability diagrams” by Quintiere 1981. This graph is used to obtain the ignition and flame spread properties of the material; which is the part of the ignition test in LIFT test. As expected, it indicated that the flame spread velocity increases as the external heat flux increases.

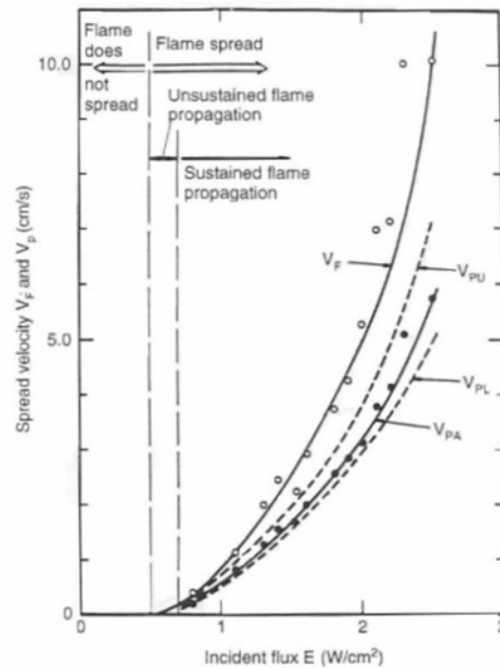


Figure 2-11: Pyrolysis front and flame tip upward spread rates over wood sheets as a function of the external radiant flux (Saito et al. 1985)

2.3.5 Gravity

Gravity influences the flame spread through the buoyant flow that is created by the density difference in the flame vicinity. Natural convection flame spread is similar to forced flow flame spread but with the gas velocity induced by buoyancy. It has been determined by researchers (Cox 1995b) that increasing or decreasing gravity is equivalent to increasing or decreasing the flow velocity.

In addition, the influence of micro gravity on flame spread has been extensively studied by Olson. The study (Olson et al. 1988) had suggested that at low flow velocities, a micro gravity environment may be more dangerous than a normal gravity one from the point of view of material flammability. More information on the effect of micro gravity can be found in the literature review by Fernandez-Pello (Cox 1995b).

2.3.6 Size of the material

The form, surface, shape and the size of the cross section of combustible materials play a major role in the overall fire behaviour. The term surface/volume ratio is used to classify the combustibility of the material. As this ratio increases, both the ignitability and the rate of

flame spread of the material increases. On the other hand, sharp corners and uneven surfaces enlarge the surface/volume ratio and thus give a less favourable fire behaviour (Blass 1995).

2.3.7 Grain Orientation

In the study by Spearpoint (2000), it was found that the ignition and burning rate of wood depends on the grain orientation. When volatiles in wood are able to escape the surface of the wood, it starts to ignite and burn. Spearpoint (2000) stated that ignition of wood is more easily achieved when the wood is exposed with incident flux parallel to grain compared to grain being perpendicular to the incident heat flux. The configuration of the grain orientation with respect to the incident flux is illustrated in Figure 2-12 below.

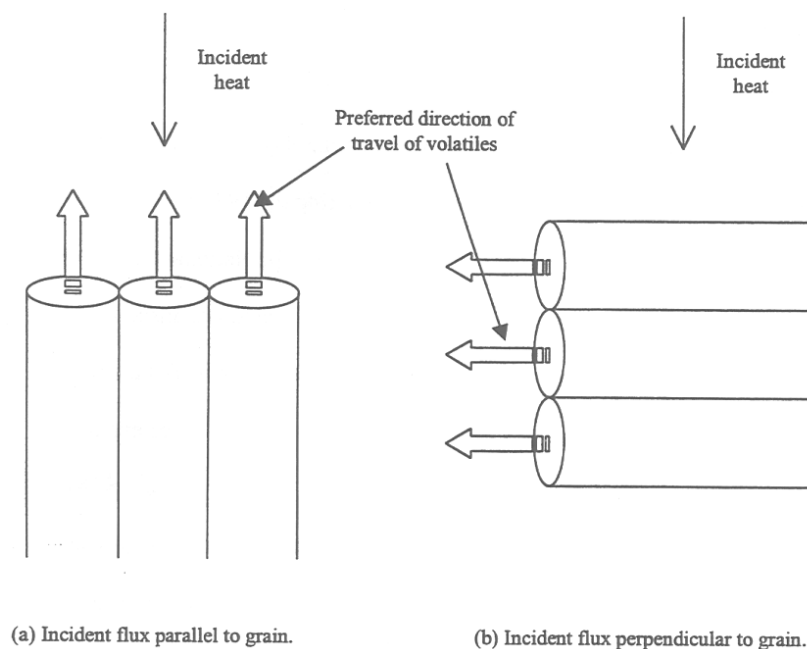


Figure 2-12: Incident flux and grain orientation scenarios (Spearpoint 1999)

For the case where incident heat flux is perpendicular to the grain, the flow of volatiles to the exposed surface is impeded by the cell walls. Furthermore, the walls have to decompose in order for ignition to occur. By doing so, the mass flux level of fuel is sufficient to achieve the lower flammable limit to ignite the wood. Spearpoint (2000) found that for low heat fluxes, the decomposition process requires additional energy. As a consequence, a longer time is needed for the ignition of the wood under the same condition.

Therefore volatiles generated just below the surface of the unaffected wood can travel more easily along the grain compared to perpendicular to the grain. It should be noted that the samples used in this research are based on the incident heat flux is perpendicular to the grain.

2.3.8 Density

The study of the relationship between density of wood and the rate of combustion was conducted by Kollmann and Cote (1968); which is illustrated in Figure 2-13. As expected, the higher the wood density the longer it will take for the wood to ignite. Similar findings were concluded by Quintiere (2002) where it was found that the flame spread speed will increase as the fuel density decreases for a given flame heat flux.

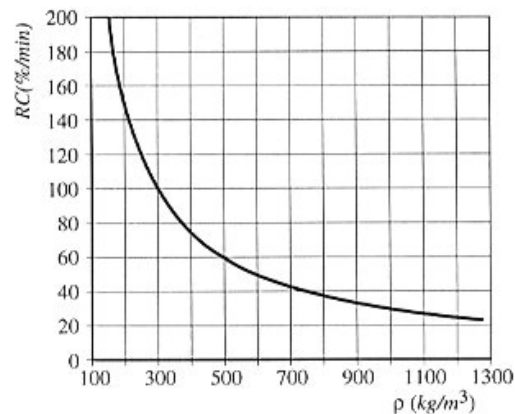


Figure 2-13: Relationship between density and rate of combustion (Kollmann and Cote 1968)

2.3.9 Moisture Content

It is interesting to note that the moisture content of wood also has an effect on fire behaviours. This is because it directly affects both the thermal conductivity and specific heat capacity of materials and thus the ignition and burning rate of materials. This is demonstrated by the study of Cholin (2003) where it found that as the moisture content of wood increases, the ignition time for a given incident heat flux also increases. The plot of the effect of moisture content on the ignition of wood is shown in Figure 2-14; where oak and western red cedar are used as the wood species.

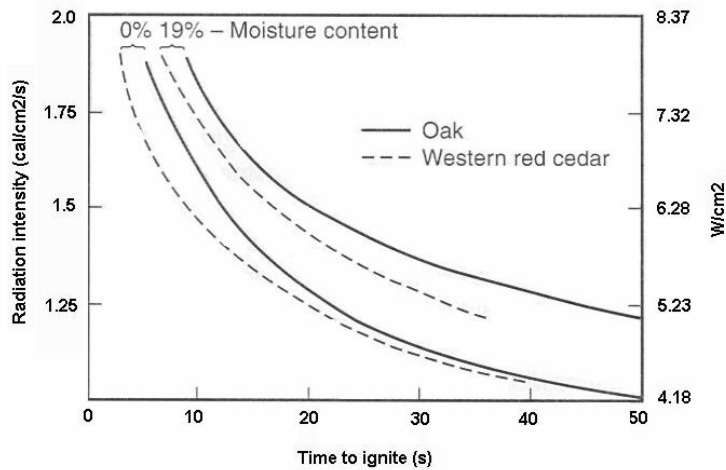


Figure 2-14: Effect of moisture content on the ignition of wood (reproduced from (Cholin 2003))

2.3.10 Charred material

When any material is exposed to their minimum heat flux for ignition, they will ignite. In particular, woods pyrolyses and forms a char layer to protect its virgin material underneath. The effect of charring on flame spread seems to be mainly due to the fuel pyrolysis rate (Cox 1995a). As the layer of char builds up, the fuel pyrolysis rate decreases and it may even reach a point where flame spread cannot be sustained. Figure 2-15 shows the degradation zones in a wood section.

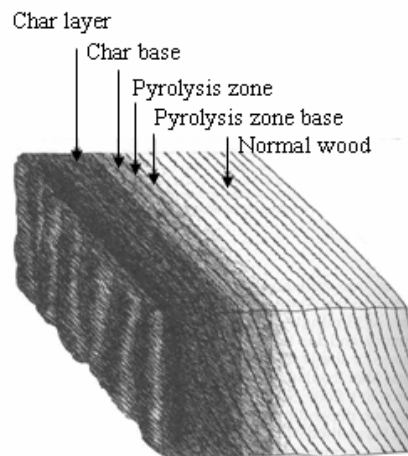


Figure 2-15: Degradation zones in a wood section (White 2002)

The formation of char at the pyrolysing surface acts as an insulator reducing the heat transfer to the pyrolysis zone, consequently reducing the pyrolysis rate. As the pyrolysis rate

decreases, both the fuel vapour concentration in the gas phase and the flame length is greatly reduced. If the char builds up to a level where no fuel pyrolysis occurs, there will be no flame spread at all.

For flames to spread over charring materials, it is generally necessary to apply an external radiant flux above a certain value (Drysdale 1999). This is because the additional energy allows the heat to transfer through the insulation layer generated by charring material. Thus increasing the pyrolysis rate and causing flame spread. Due to the charring process, a time dependent function is introduced in the flame spread problem and is considered to be very difficult to solve.

2.4 Technique of measuring ignition properties and flame spread

There are two methods currently available to measure opposed flow flame spread. First is the “Lateral Ignition Flame Transport” (LIFT) test listed in ASTM E1321 (ASTM Committee E-5 on Fire Standards. 2004b) which is the standard method for obtaining opposed flow flame spread parameter. The other method is the known as the “Reduced scale Ignition and Flame spread Technique” (RIFT) test and it is not a standard test.

2.4.1 LIFT test

In general, the LIFT test comprises of two parts; the first part is the ignition test, where the minimum heat flux required for ignition and the effective thermal properties ($k\rho c$) are obtained. The second part of the LIFT test is the flame spread test, where it is used to determine the flame spread properties. This test employs a radiant panel inclined at an acute angle to the sample surface, where ignition vents and flame spread rates are measured as functions of incident radiation and exposure time.

The sample in the LIFT apparatus is mounted vertically as opposed to the typical horizontal setup in a cone calorimeter or ISO ignitability apparatus. In terms of ignition test, it has been shown that vertical samples are slightly more difficult to ignite due to the difference in the convective boundary layer (Atreya et al. 1985).

In the flame spread test, flame may spread both laterally and upward. However, the rate of lateral flame spread is considered to be slower than the rate of upward flame spread. This is due to the air flow velocity where the former is opposed flow velocity and the latter is concurrent flow.

The flame spread parameters are determined by correlating different exposure conditions where the inverse square root of the flame spread rate over thick materials against a product of the heat flux and a time function is plotted. The theory behind the LIFT test originates from Quintiere (1981) and the underlying theory and equations that are used to determine the ignition and flame spread parameters can be found in Chapter 4.

2.4.2 RIFT test

As mentioned earlier, Reduced scale Ignition and Flame spread Technique (RIFT) is the alternative method that can be used to measure opposed flow flame spread and was developed recently by Azhakesan, Shields and Silcock (1998). The apparatus for the RIFT is basically a cone calorimeter in a vertical orientation as illustrated in Figure 2-16 below. It should be noted that the RIFT is not a standard test method; however the cone calorimeter is a standard test method with a designation number of E1354-04a oxygen consumption calorimeter in the ASTM fire standards.

Azhakesan et al first published the paper on the RIFT method in 1998. In their experiments four materials were tested: plywood, hardboard, fibreboard and melamine faced particle board. Their flame spread results were compared with both the results from the LIFT test and the surface spread of flame test (BS476 part 6) found in literature. They have found that the flame heating parameters being slightly higher than those obtained from the LIFT test. Other than that the flame spread results obtained from the RIFT method in general were similar to the other methods.

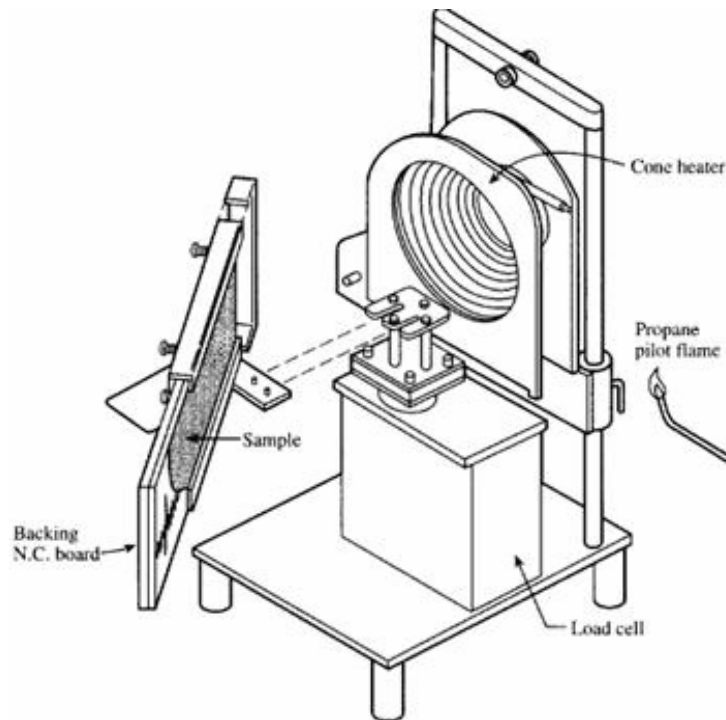


Figure 2-16: Reduced scale Ignition and flame spread attachment (RIFT) (Azhakesan et al. 1998)

In this research, the setup of the LIFT test method is applied in FDS4 to predict the flame spread parameters for all the selected timber and timber based products. Therefore the RIFT is not further investigated in this research.

2.5 Published data for the LIFT test

This section provides a selection of LIFT data that is taken from notable literature. A summary of other literature on ignition and flame spread tests can be found in Ngu (1998), Huynh (2002), and Merryweather (2006).

2.5.1 Quintiere and Harkleroad (1984)

In 1984 Quintiere and Harkleroad published a paper titled “New Concepts for Measuring Flame Spread Properties”. This paper discusses further improvements in the measuring technique of the flame spread theory developed by Quintiere (1981); the results of this leads to the current ASTM standards for the LIFT apparatus and procedure. One of the major improvements of the theory was to include a preheating time which can be calculated using

the ignition parameter. In their studies, the material that was used in the experiment was particle board.

In addition, the LIFT apparatus was also modified to give more consistent results. The modifications include the location of the pilot flame and the addition of a flange on the top of the sample holder. This was to improve the consistency of the ignition time and reduce the effect of the heat flux from pilot flame on the material.

By adapting the new experimental procedure, Quintiere and Harkleroad (1984) carried out more tests to determine the flame spread parameters for six materials representative of aircraft (interior panels, carpeting, seat cushions) and buildings (plywood, PMMA, rigid foam). Table 2-2 shows the lateral flame spread data for typical aircraft and construction materials.

Table 2-2: Flame spread data for typical aircraft and construction materials (Quintiere and Harkleroad 1984)

Material	Tig (°C)	kpc (kW/m ² K) ² s	Φ (kW ² /m ³)	Ts, min (°C)
Wood fiber board	355	0.46	2.3	210
Wood hardboard	365	0.88	11.0	40
Plywood	390	0.54	13.0	120
PMMA	380	1.00	14.4	<90
Flexible foam plastic	390	0.32	11.7	120
Rigid foam plastic	435	0.03	4.1	215
Acrylic carpet	300	0.42	9.9	165
Wallpaper on plasterboard	412	0.57	0.8	240
Asphalt shingle	378	0.70	5.4	140
Glass reinforced plastic	390	0.32	10.0	80

2.5.2 Nisted (1991)

The research by Nisted (1991) was a part of the work carried out within the Nordic research programme known as the European REaction to FIRE Classification (EUREFIC) programme,

where the focus of the studies was based on project 5 “Models for flame spread and application of test data”. The method used for testing the flame spread behaviour was the ASTM E 1321 – 90 “Standard Test Method for Determining Material Ignition and Flame Spread Properties”, which is now superseded by the ASTM E 1321 -97a (ASTM Committee E-5 on Fire Standards. 2004b). The materials selected were in accordance with the EUREFIC programme; which had a total of 11 materials include plaster boards, plywood, Melamine faced high density non combustible board, mineral wool, fire rated particle boards, rockwool, polyurethane foam, PVC wall carpet on plaster board and fire rated polystyrene. These materials were tested using the LIFT test. A summary of the flame spread results for each material is tabulated in Table 2-3. However, flame spread properties for the two particle board materials were not obtained since the material was not ignited.

Table 2-3: Summary of flame spread test results (Nisted 1991)

Material	Flame spread parameter	Minimum heat flux for ignition	Minimum heat flux for ignition	Minimum temperature for spread	Flame heating parameter
	C_s' (s/mm) ^{1/2} (m ² /kW)	$q''_{o,ig}$ (kW/m ²)	$q''_{o,s}$ (kW/m ²)	$T_{s,min}$ (°C)	Φ
Painted gypsum paper plaster board (13mm)	0.0435	42.8	26.02	429	94.14
Ordinary plywood (12mm)	0.1208	18.8	3.94	110	64.07
Textile wallcovering on gypsum paper plaster board (13mm)	0.1545	16.8	4.22	117	43.56
Melamine faced high density non combustible board (13mm)	0.0114	77.7	30.74	422	399.56
Plastic faced Steel sheet on mineral wool (25mm)	0.0083	87.4	25.67	413	1927.26
FR particle board type B1 (16mm)	Material did not ignite				
Faced rockwool (30mm)	0.0751	18.3	8.47	231	8.98
FR particle board (12mm)	Material did not ignite				
Polyurethane foam covered with steel sheet (80mm)	0.0293	29.4	11.36	224	306.95
PVC-wall carpet on gypsum paper plaster board (13mm)	0.1299	18.5	15.64	378	47.84
FR polystyrene (25mm)	0.0219	43.9	15.65	268	1708.76

2.5.3 Dietenberger (1996 a), (1996b) and (2004)

In 1996, Dietenberger developed a new protocol for calibration of the LIFT and suggested ways of improving the calibration so that the radiant panel can be aligned to match the required flux profile. In addition, a high level of irradiance was also recommended to minimise the error due to the time taken to insert the sample into place.

The heat transfer coefficient in the ASTM E 1321-97a (2002) standards has a value of $0.015\text{kW/m}^2\text{K}$ specified at points closer than 650 mm from the hot end of the sample. However, the convection heat transfer coefficient actually varies along the sample. As a result, a higher ignition temperature will be calculated using the equation in the ASTM E 1321-97a (2002) standards. From the study carried out by Dietenberger, the actual heat transfer coefficient along the material was determined and is shown in Equation 2-29 below; where x is the distance along the sample from the hot end, in metres.

$$h = (13.9 - 0.0138x)(q''_{e,50mm}) \text{ kW/m}^2\text{K}, \quad \text{Equation 2-29}$$

By using the corrected heat transfer coefficient calculated from Equation 2-29, the ignition temperatures was found to be approximately 70°C less than that predicted for the same materials using the value from the ASTM E 1321-97a (2002) standards.

In addition, the LIFT apparatus was adapted in this study to test various siding materials (plywoods, softwoods, and vinyl), some of which were painted, humidified, or sawn. By following the newly developed procedure useful, accurate information about the thermophysical properties were obtained. Full consistency was achieved with independent literature values of these properties and can be used directly in the database of fire growth models. Table 2-4 shows the results of the thermophysical constants for the siding materials tested by Dietenberger (1996b). It provides the minimum heat flux for ignition, ignition temperature, moisture content, thermal conductivity, and thermal diffusivity.

Table 2-4: Derived thermophysical constants for siding materials (Dietenberger 1996a)

Material/condition	q_{ig} (kWm^{-2})	λ Factor	T_{ig} (K)	M (%)	$\lambda \times 10^{-3}$ ($\text{kWm}^{-1}\text{K}^{-1}$)	$\alpha \times 10^{-6}$ (m^2s^{-1})
Cedar/oven-dried	15.3	1.0	587	7.6	0.134	0.178
Cedar/50%RH/thin	20.1	1.0	635	9.9	0.144	0.172
Redwood/oven-dried	13.3	1.0	560	3.4	0.152	0.181
Redwood/30%RH	16.7	1.0	600	8.7	0.171	0.166
Redwood/50%RH	19.2	1.0	631	9.4	0.179	0.165
Pine/oven-dried	14.3	1.0	561	4.7	0.158	0.176
Pine/30%RH	18.8	1.0	621	5.6	0.169	0.174
Pine/50%RH	20.8	1.0	640	9.2	0.183	0.164
Rustic plywood/50%RH	18.8	1.0	634	10.6 ^a	0.217	0.157
Painted plywood/50%RH	19.5	1.0	629	9.5 ^a	0.211	0.159
Hardboard/oven-dried	14.7	1.84	572	0.0	0.237	0.176
Hardboard/30%RH	14.7	1.84	578	5.0 ^a	0.257	0.163
Hardboard/50%RH/thin	14.5	1.84	581	7.9 ^a	0.273	0.156
Vinyl + polystyrene foam	N/A	N/A	700	N/A	0.145	0.087

The piloted ignition behaviour of wood products using the LIFT test and cone calorimeter has also been studied by Dietenberger. This was carried out due to the difficulties in analysing the test data obtained, which was then used for deriving fundamental physical properties. These properties include surface emissivity, surface ignition temperature, thermal conductivity and thermal diffusivity. They are considered to be important parameters especially when modelling the fire growth rate using computer software. Because there are differences in the piloted ignitability for each test method, the convective heat transfer coefficient between the two apparatus was investigated by (Dietenberger 1996b). The material that was used in this study was Redwood and other materials were tested later.

Table 2-5 shows the derived thermophysical parameters of ignitability, showing the effective thermal properties, ignition temperature and thermal diffusivity. The types of materials include building materials such as timber, gypsum board and polyurethane foam.

Table 2-5: Derived thermophysical parameters of ignitability (Dietenberger 2004)

Material	Test no.	$k\rho c$ (MJ) [$\text{kJ}^2/\text{m}^2\text{K}^2\text{s}$]	T_{ig} (MJ) [K]	$r_w =$ k / k_w	T_{ig} (MD) [K]	$k/\rho c$ (m^2/s) $\times 10^7$	$k\rho c$ (MD) [$\text{kJ}^2/\text{m}^2\text{K}^2\text{s}$]
Gypsumboard, Type X	1, 7, 15	0.519	603	N/A	608.5	3.74	0.451
FRT Douglas-fir plywood	2	0.515	623	0.86	646.8	1.37	0.261
Oak veneer plywood	3	1.103	577	1.11	563	1.77	0.413
FRT plywood (Forintek)	4	0.412	649	0.86	650	1.31	0.346
Douglas-fir plywood (ASTM)	5	0.282	608	0.863	604.6	1.37	0.221
FRT polyurethane foam***	6	0.033	545	N/A	689	4.91	0.0284
FRT Southem Pine plywood	8	1.209	615	1.43	672	2.26	0.547
Douglas-fir plywood (MB)	9	0.231	634	0.86	619	1.38	0.233
Southern Pine plywood	10	0.256	640	0.86	620	1.38	0.29
Particleboard	11	1.195	524	1.72	563	2.72	0.763
Oriented strandboard	12	0.244	621	0.985	599	1.54	0.342
Hardboard	13	0.4	624	0.604	593	0.904	0.504
Redwood lumber	14	0.165	653	1.0	638	1.67	0.173
White spruce lumber	16	0.286	615	1.0	621	1.67	0.201
Southern Pine boards	17	0.328	627	1.0	644	1.63	0.26
Waferboard	18	0.793	509	1.62	563	2.69	0.442

The results from Dietenberger showed a basic agreement in the derived values of ignition temperatures, thermal diffusivities, and thermal conductivities between LIFT and cone calorimeter ignitability tests. Due to the large differences in convective cooling of the specimen in different testing apparatus, the minimum heat flux for ignition was found not to be a viable ignition parameter.

2.5.4 Babrauskas and Wetterlund (1999)

A review of the literature was carried out by Babrauskas to determine how much is known about the heat fluxes from flame to surface in opposed-flow spread (Babrauskas 1995). From the review, there were only a few reported studies found. The heat fluxes varied significantly among the reported data; despite the fact that similar materials were used under similar flame spread conditions. Interestingly, no data were found for the geometry of the LIFT test although the LIFT test is a standard test of measuring flame spread. There is an empirical formula for the "driving force" for flame spread in the flame spread theory of the LIFT test but it does not explicitly quantify the heat flux. As a result, Babrauskas and Wetterlund found that there was a need to experimentally measure the heat fluxes from flame to surface of the specimen in the LIFT test.

Experiments were conducted at Swedish National Testing and Research Institute (SP) in Sweden on 6 materials with both the LIFT and cone calorimeter. Materials included particle board, fire retardant polyurethane foam, black PMMA, insulating fibreboard, cotton fabric with a Kevlar liner over polyurethane foam and acrylic pile fabric over polyurethane foam.

Apart from the flame spread data that were obtained for different materials, the effect of preheating the material was also discussed; where the material properties were found to be affected by preheating the material. Importantly it concluded that the flame heat flux was essentially constant between the materials tested, and therefore is not considered to be a major variant in flame spread modelling (Babrauskas and Wetterlund 1999).

2.5.5 Merryweather (2006)

Merryweather conducted a series of LIFT and RIFT tests using different types of timber based panels. The materials tested include manufactured products such as Medium Density Fibreboard (MDF), hardboard, plywood, particle boards (Trade name: Pynefloor and Superflake), Melteca faced MDF, Melteca faced particle board and New Zealand native species: Beech, Macrocarpa, Radiata Pine, Rimu. It should be note that Superflake and Melteca faced particle board were only tested with RIFT since other similar materials were being tested. The results from the LIFT tests were then compared with the results from the RIFT. In addition, the flame spread test with RIFT was carried out using the ignition test results from the ISO 5657 ignitability apparatus.

Merryweather reported that inconsistent flame spread data was obtained if using the RIFT for the ignition tests; “due to the design of the apparatus, which disrupts the airflow over the face of the sample” and recommended not to use the RIFT ignition method. However, better flame spread results were achieved when combined the ignition test results from the ISO 5657 ignitability apparatus with the RIFT. In general, a faster ignition time in the ignition test was obtained in the ISO 5657 ignitability apparatus than the LIFT test using the same material, with a 4% difference.

The effect of sample preheating was also investigated in the study by Merryweather, where it was found that the flame heating parameters are lower for half preheated samples than fully

preheated samples. It has been concluded that preheating the sample is essential in order to model the flame spread accurately, which is required in the ASTM fire standards.

The research in this report mainly uses the results from the LIFT tests that were obtained by Merryweather and directly compares them with the results that are predicted from the numerical simulation, which is FDS4 in this case.

3 Fire Dynamics Simulator version 4 (FDS4)

This chapter outlines the theoretical basis, main assumptions and governing equations behind FDS4 to give a general overview and broad understanding of the concepts behind the model. In addition, the theory that is used in FDS4 to predict the fire growth and flame spread will be discussed. The details covered in this chapter are referenced from Cox (1995) and McGrattan (2004).

3.1 Introduction

Fire Dynamics Simulator version 4 (FDS4) is a Computational Fluid Dynamics (CFD) model of fire-driven fluid flow. This software is developed by Building and Fire Research Laboratory (BFRL) at National Institute of Standards and Technology (NIST) in cooperation with VTT Building and Transport, Finland. The FDS4 program can simulate fire behaviour as it develops in a building and the FDS4 software is currently up to its fourth edition; therefore FDS4 version 4 is implied when the term “FDS4” is used throughout this research report.

Smokeview is a software tool design to visualise numerical calculations generated by FDS4. This is an important tool as it provides an excellent visualisation of the FDS4 results. FDS4 and Smokeview are typically used conjointly to simulate and visualise the flame spread induced by a fire, respectively (Forney and McGrattan 2004).

3.2 Numerical Grid

All FDS4 calculations must be performed within a domain that is made up of rectangular meshes, each with its own rectilinear grid. All objects in FDS4 are forced to conform within the numerical grid(s).

Firstly, a grid is specified to establish the overall physical dimensions of the rectangular grid by the PDIM namelist group; where the origin of the domain is the point (XBAR0,YBAR0,ZBAR0), and the opposite corner of the domain is at the point (XBAR,YBAR,ZBAR).

Secondly, the number of grid cells spanning each coordinate direction is specified to establish the dimensions of the computational grid by the GRID namelist group. The grid consists of IBAR cells, JBAR cells and KBAR cells in the x, y and z direction respectively. The longer horizontal dimension should be taken as the x-direction. It should be noted that calculations perform the best if the grid cells are close to cubes. Furthermore, because an important part of the calculation uses a Poisson solver based on Fast Fourier Transforms, the dimensions of the grid should each be of the form $2^l 3^m 5^n$, where l , m and n are integers.

Finally, the grid cells can also be stretched or shrunk in two of three coordinate directions using the TRNX, TRNY, and/or TRNZ groups if desired.

3.3 Hydrodynamic Model

FDS4 solves numerically a form of the Navier-Stokes equations appropriate for low speed, thermally-driven flow with an emphasis on smoke and heat transport from fires. The core algorithm is an explicit predictor-corrector scheme, 2nd order accurate in space and time (McGrattan 2004).

There are three main techniques to simulate turbulence, which are Large Eddy Simulation (LES), Direct Numerical Simulation (DNS) and Reynolds-Averaged Navier-Stokes (RANS). However, FDS4 only has an option of either LES or DNS. LES is a technique used to model the processes of dissipation in relation to viscosity (μ), thermal conductivity (k) and material diffusivity (α); which occur at length scales smaller than those that are explicitly resolved on the numerical grid. In other words, the parameters μ , k and α in the turbulence equations cannot be used directly in most practical simulations. There are some flow scenarios where it is possible to use the diffusive parameters μ , k and α directly. Usually this means that the numerical grid cells are in the order of 1 mm or less, and the simulation is regarded as a Direct Numerical Simulation (DNS).

By default in FDS4, turbulence is treated using the LES technique. Nevertheless, a DNS can be performed if the underlying numerical grid is fine enough. This research will follow the LES approach due to practical reasons.

3.3.1 Fundamental Conservation Equations

The conservation equations for mass, momentum and energy for a Newtonian fluid are stated in this section. These are the basic equations which are commonly used in fluid dynamics models. These equations basically say that for a particular quantity the inflow, outflow and the rate of storage, in conjunction with production or destruction, within a specified control volume must be balanced. The description of the equations, the notation used, and the various assumptions employed are extracted from elsewhere (Tannehill et al. 1997).

Conservation of mass

In general, the conservation of mass equation, describes the overall mass continuity within a control volume. It implies that the rate of mass storage within the control volume, due to changes in density, is balanced by the net rate of inflow, by convection, of mass across the control volume boundaries (Cox 1995a). In a steady flow situation i.e. no changes in density, this simply means that what flows in must flow out.

The equation for the conservation of mass is written as shown below (Equation 3-1); where the first term defines the change in density with respect to time while the second term describes the rate of mass change due to convection.

$$\frac{\partial \rho}{\partial t} + \nabla \cdot \rho \mathbf{u} = 0 \qquad \text{Equation 3-1}$$

Conservation of species

To ensure that the species across each control volume boundary is preserved, the concept of conservation of species is applied in FDS4. The equation for conservation of species states that the time rate of storage of the species l is balanced by its net rate of flow into the control volume of the species due to effects of both convection and diffusion together with its production or destruction (of the species) within the volume due to chemical reactions (Cox 1995a).

The equation used in FDS4 is reproduced below (Equation 3-2); where the first and second term on the left hand side (LHS) represents the rate of change species due to density changes and the inflow or outflow of species due to convection, respectively. Meanwhile, on the right hand side (RHS) of the equation describes the inflow or outflow of species due to diffusion and the production or destruction of species during the reaction.

$$\frac{\partial}{\partial t}(\rho Y_i) + \nabla \cdot \rho Y_i \mathbf{u} = \nabla \cdot \rho D_i \nabla Y_i + \dot{m}_i^m \quad \text{Equation 3-2}$$

Conservation of momentum

The equation describing the conservation of momentum is derived by applying Newton's second law of motion, which states the rate of change of momentum of a fluid element is equal to the sum of forces acting on it (Cox 1995a). In FDS4, this equation is written as follows:

$$\rho \left(\frac{\partial \mathbf{u}}{\partial t} + (\mathbf{u} \cdot \nabla) \mathbf{u} \right) = \rho \mathbf{g} + \mathbf{f} + \nabla \cdot \boldsymbol{\tau} - \nabla \rho \quad \text{Equation 3-3}$$

The terms on the LHS of Equation 3-3 represent the rate of change of momentum of a travelling fluid in a control volume, while, the forces acting upon the travelling fluid are indicated on the RHS of the equation; where the first term is associated with gravity force acting on the fluid within the control volume.

Conservation of energy

The conservation of energy describes a balance between the rate of accumulation within the control volume of both internal and kinetic energies, and energy influx due to convection, conduction, thermal radiation, the interdiffusion of species together with the net rate of work done on the gases by viscous stresses and body forces (Cox 1995a). There are many ways to illustrate the concept of conservation of energy depending on the primary variables such as temperature, enthalpy or internal energy. The way FDS4 deals with this principle is shown in Equation 3-4 below.

$$\frac{\partial}{\partial t}(\rho h) + \nabla \cdot \rho h \mathbf{u} = \frac{\partial \rho}{\partial t} + u \cdot \nabla \rho - \nabla \cdot \mathbf{q}_r + \nabla \cdot k \nabla T + \sum_l \nabla \cdot h_l \rho D_l \nabla Y_l \quad \text{Equation 3-4}$$

The LHS of the equation describes the net rate of energy accumulation; whereas on the RHS, consists of the rate of energy that is lost or gained within the control volume.

Equation of State

In FDS4, the equation of state is approximated as shown in Equation 3-5. This equation contributes to the overall conservation equations as it relates to the thermodynamic quantities section within the control volume.

$$p_0 = \rho T R \sum \left(\frac{Y_i}{M_i} \right) = \rho T \frac{R}{M} \quad \text{Equation 3-5}$$

3.4 Combustion Model

Two types of combustion model can be employed in FDS4 and the choice depends on the method of analysing the turbulence. For a LES calculation, where the grid size is not fine enough to resolve the diffusion of fuel and oxygen, it uses a mixture fraction-based combustion model. Meanwhile, for a DNS calculation, where the grid size is fine enough to model the diffusion of fuel and oxygen, a global one-step, finite-rate chemical reaction is most appropriate (McGrattan 2004).

The required computation time for DNS calculations is usually long due to the fine grid cells; because of this reason LES calculation is preferred for most applications. As for this research, a LES calculation will be used for the FDS4 model; therefore the theory of the finite rate reaction used in DNS calculations will not be presented.

3.4.1 Mixture Fraction Combustion Model

The mixture fraction combustion model is based on the assumption that large-scale convective and radiative transport phenomena can be simulated directly, but physical

processes occurring at small length and time scales must be represented in an approximate manner (McGrattan 2004). It is a conserved scalar quantity which is defined as the fraction of gas at a given point in the flow field that originated as fuel.

In FDS4, the mass fraction of most concern is the oxygen mass fraction as it provides the information required to determine the local oxygen mass consumption rate. This ultimately enables FDS4 to determine the local heat release rate from the principle of oxygen calorimetry (Janssens 2002), where it is stated that the local heat release rate is directly proportional to the oxygen consumption rate (independent of the fuel source). The most general form of the combustion reaction is used in FDS4 as shown in Equation 3-6.



where the variables v_i are the stoichiometric coefficients for the overall combustion process that reacts fuel 'F' with oxygen ' O_2 ' to produce a number of products 'P'.

The FDS4 model is based on the assumptions that the combustion is mixing-controlled and the reaction of fuel and oxygen is infinitely fast. This simply implies that the term mixture fraction $Z(x, t)$ can be used to describe all species of interest within the control volume; where all of the major species (reactants and products) which make up the mass fractions can be derived from the mixture fraction by means of "state relations". The state relations are empirical expressions which are determined by a combination of simplified analysis and measurements taken in the laboratory. The mixture fraction Z is defined as:

$$Z = \frac{sY_F - (Y_O - Y_O^\infty)}{sY_F^l + Y_O^\infty}, \quad s = \frac{v_O M_O}{v_F M_F} \quad \text{Equation 3-7}$$

By design, Z varies from one ($Z=1$) in a region containing only fuel, to zero ($Z=0$) where the oxygen mass fraction equals its ambient value Y_O^∞ (usually 21% oxygen in the air).

The main assumption FDS4 has made in the mixture fraction model is that the chemical reactions are so fast that consumption of fuel and oxidizer occur so rapidly that the fuel and oxidizer cannot coexist. As a result, the fuel and oxidizer vanish simultaneously and a flame surface (Z_f) will be formed; Equation 3-8 defines the flame surface.

$$Z_f = \frac{Y_o^\infty}{sY_F^l + Y_o^\infty} \quad \text{Equation 3-8}$$

In addition, the assumption that fuel and oxidizer cannot co-exist leads to the state relation between the oxygen mass fraction Y_o and the mixture fraction Z ; this relationship is represented in Equation 3-9 below.

$$Y_o(Z) = \begin{cases} Y_o^\infty(1 - Z/Z_f) & Z < Z_f \\ 0 & Z > Z_f \end{cases} \quad \text{Equation 3-9}$$

As mentioned earlier, the state relation of a particular fuel is an empirical expression derived from the stoichiometric reaction of the fuel in terms of mass fractions. Therefore, different fuels have different state relations. As an example, Figure 3-1 shows the state relations of various species for propane. From this figure, the intersection between the fuel and oxygen is the point where the flame surface occurs; therefore for the fuel of propane FDS4 predicts flame surface occurs when the mixture fraction Z equals to 0.05.

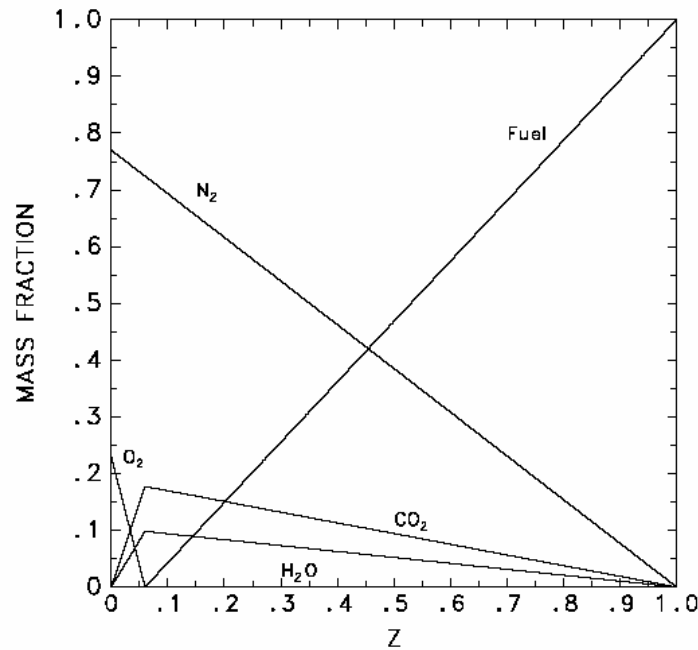


Figure 3-1: State relations for propane (McGrattan 2004)

The local heat release rate is approximated in FDS4 based on the conservation equations and the state relation for oxygen. Hence the heat release rate (\dot{q}''') is a function of the heat release rate per unit mass of oxygen consumed (ΔH_o) and the oxygen mass consumption \dot{m}_o''' as shown in Equation 3-10. It should be noted that ΔH_o for most fuels is approximately 13.1 MJ/kg. More details on this concept can be found in the technical reference guide of FDS4 (McGrattan 2004).

$$\dot{q}''' = \Delta H_o \dot{m}_o''' \quad \text{Equation 3-10}$$

3.4.2 Enhancements to the Mixture Fraction Model

There are several limitations (both numerical and physical) in the mixture fraction model described in the previous section. The numerical limitations are related to the resolution of the underlying numerical grid. As for coarse grids, the accuracy of the fuel transport and combustion processes is diminished by the high levels of numerical diffusion (bigger grid cells). In addition, the procedure shown above for determining the local heat release rate works well for calculations in which the fire is adequately resolved (McGrattan 2004). A

measure of how well the fire is resolved is given by the non-dimensional expression $D^*/\delta x$; where D^* is a characteristic fire diameter and δx is the nominal size of a grid cell.

$$D^* = \left(\frac{\dot{Q}}{\rho_\infty c_p T_\infty \sqrt{g}} \right)^{\frac{2}{5}} \quad \text{Equation 3-11}$$

The term $D^*/\delta x$ can be thought of as the number of computational cells spanning the characteristic diameter of the fire, which is not necessarily the physical diameter. Obviously, the more cells spanning the fire, the better the resolution of the FDS4 calculation would be. This means that for fire scenarios, where D^* is small compared to the physical diameter of the fire, and/or the numerical grid is relatively coarse, the stoichiometric surface $Z = Z_f$ will underestimate the observed flame height. It has been found empirically that a good estimate of flame height can be found for crude grids if a different value of Z is used to define the combustion region as indicated in Equation 3-12 (McGrattan 2004).

$$\frac{Z_{f,eff}}{Z_f} = \min\left(1, C \frac{D^*}{\delta x}\right) \quad \text{Equation 3-12}$$

The term C in Equation 3-12 is an empirical constant equal to 0.6 to be used for all fire scenarios. As the resolution of the calculation increases (i.e. $D^*/\delta x$ increases), the $Z_{f,eff}$ approaches the ideal value Z_f at which point the approximation of Z is no longer required. The advantage of having this ratio is that it provides a quantifiable measure of the grid resolution by considering both the size of the grid cells and the fire.

Another problem that results from a coarse numerical grid is that a disproportionate amount of the combustion energy is released near the edges of the fire source. The heat release rate per unit area of the flame sheet is proportional to the local gradient of the mixture fraction and the local value of the material diffusivity. The gradient of the mixture fraction is large at

the base of the fire because there is a stream of pure fuel meets surrounding air. The diffusivity is large on a coarse grid because it is related to the Smagorinsky viscosity (McGrattan 2004). Therefore, a large amount of combustion energy is discharged close to the edges of the burner. To prevent too much of the energy from being released too close to the burner when a coarse grid is used, there is a maximum bound imposed on the local heat release rate per unit area of flame sheet (McGrattan 2004). This upper bound is based on a simple analysis in which the fire is assumed to be conical in shape with surface area (A) and a flame height (H) given by Heskestad's correlation (Heskestad 2002).

$$\frac{H}{D} = 3.7Q^{*2/5} - 1.02; \quad A = \pi\sqrt{r^2 + h^2} \quad \text{Equation 3-13}$$

The actual surface area of a real flame is larger than that of a cone assumed. Consequently, when a coarse grid is used the upper bound estimate (mentioned above) will prevent too much energy from being released too close to the fire. On the other hand, the combustion energy will be high enough without impeding the calculation when the grid is well-resolved. It should be noted that any energy “clipped” off in the calculation due to the upper bound is redistributed over the entire flame volume.

The physical limitation of the mixture fraction method is that it is assumed that fuel and oxygen burn instantaneously when mixed. This is a good assumption in the case of large-scale, well-ventilated fires. However, it is a poor assumption in some cases, such as under-ventilated compartment fires or when a suppression agent like water mist or carbon dioxide (CO₂) is introduced, where the fuel and oxygen may mix but may not burn at all.

FDS4 has employed a simple model for flame extinction; where the surrounding volume is assessed to determine if the volume supports combustion. This concept is illustrated in Figure 3-2, where it shows the values of temperature and oxygen concentration for which burning can and cannot take place. Once the gas environment in the model falls into the “No Burn” zone, the state relations as indicated in Figure 3-1 are no longer valid for a mixture fraction Z below stoichiometric; this is due to the fact that some fuels maybe mixed with the other combustion products.

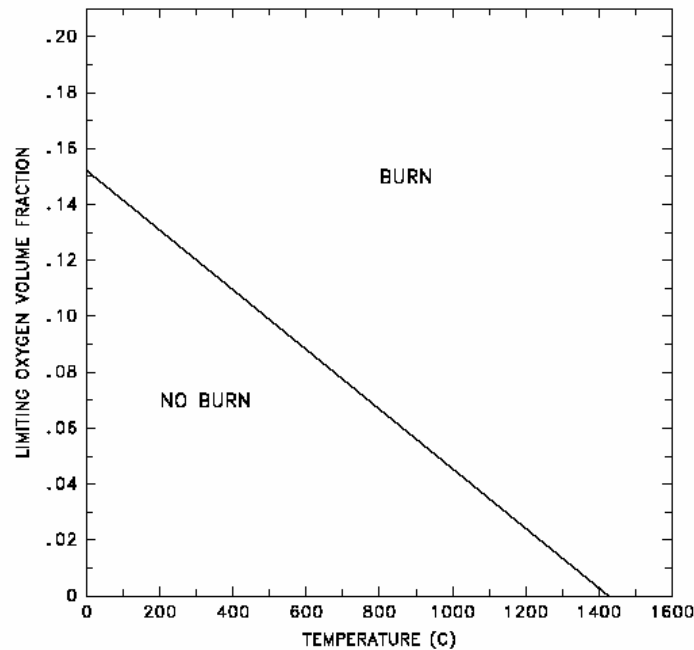


Figure 3-2: Oxygen-temperature phase space showing where combustion (McGrattan 2004)

3.5 Thermal Radiation Model

Radiative heat transfer is computed in the FDS4 model using the solution of the Radiation Transport Equation (RTE) for a non-scattering grey gas and in seldom cases, a wide band model can be used instead of the grey gas model (McGrattan 2004). The radiation equation is solved using a technique called Finite Volume Method (FVM) which is similar to the convective transport.

In a limited spatial resolution, there is a drawback in using the FVM to determine the source term radiation intensity (I_b). This occurs at the flame sheet where the temperatures are distributed over a grid cell which is much lower than expected to be for a diffusion flame. However, the source term must be modelled in those grid cells cut by the flame sheet simply because it is highly dependent on the temperature term (raised to the fourth power). As for area outside the flame zone, there is better confidence in the computed temperature and the source term can assume to be an ideal value.

To overcome this problem, FDS4 has implemented Equation 3-14 in the model as shown below: (McGrattan 2004).

$$\kappa I_b = \begin{cases} \kappa \sigma T^4 / \pi & \text{Outside flame zone} \\ \max(\chi_r \dot{q}''' / 4\pi, \kappa \sigma T^4 / \pi) & \text{Inside flame zone} \end{cases} \quad \text{Equation 3-14}$$

3.6 Thermal Boundary Conditions

All solid surfaces need to be assigned with a thermal boundary condition and information such as thermal properties or burning behaviour of the material. Commonly used material properties are stored in a database and invoked by name. The type of thermal boundary condition applied at any given surface depends on whether that surface is to heat up and burn (combustible surface), whether the burning rate will simply be prescribed (heat of vaporisation), or whether there is to be any burning at all (inert surface). Both the thermoplastic and charring fuels boundary condition is adapted on the solid surface in this research

3.6.1 Convection heat flux

The heat fluxes to a solid surface comprise of both convection and radiation. The radiative flux at the surface is obtained from the boundary condition for the radiation equation, in section on Thermal Radiation Model discussed previously. The calculation of the convective heat flux depends on the selected technique in modelling the turbulence; whether it is a DNS or LES calculation. In a DNS calculation, the convective heat flux to a solid surface \dot{q}_c'' is obtained directly from the gas temperature gradient at the boundary. On the other hand in a LES calculation, the convective heat flux to the surface is obtained from a combination of natural and forced convection correlations defined in the following equations:

$$\dot{q}_c'' = h \Delta T \quad \text{Equation 3-15}$$

$$h = \max \left[C |\Delta T|^{\frac{1}{3}}, \frac{k}{L} 0.037 \text{Re}^{\frac{4}{5}} \text{Pr}^{\frac{1}{3}} \right] \quad \text{Equation 3-16}$$

where ΔT is the difference between the surface of the object and the gas temperature, C is the coefficient for natural convection (1.52 for a horizontal surface and 1.31 for a vertical surface), L is the characteristic length related to the size of the physical obstruction, k is the thermal conductivity of the gas, Re and Pr is the Reynolds number and Prandtl number, respectively.

3.6.2 Thermoplastic Fuels

This boundary condition is assigned when pyrolysis of the solid material is assumed to occur at the surface, or if no pyrolysis occurs at all. It does not mean the material of the solid surface must be a thermoplastic; despite the name “thermoplastic fuels” indicated. But rather this boundary condition implies that the combustion of the solid surface is based on either the heat of vaporisation (ΔH_v) or the heat release rate per unit of the surface area (HRRPUA) of the fuel. One important parameter that is needed in this boundary condition is the ignition temperature (T_{ig}) of the solid surface. The solid surface ignites when it reaches to the T_{ig} assigned.

If the solid surface is assumed to be thermally-thick, a one-dimensional heat conduction equation for the material temperature ($T_s(0, t)$) is applied in the direction x pointing into the solid; where the point $x=0$ represents the surface. The conduction equation is indicated in Equation 3-17 below.

$$\rho_s c_s \frac{\partial T_s}{\partial t} = \frac{\partial}{\partial x} \left(k_s \frac{\partial T_s}{\partial x} \right) ; -k_s \frac{\partial T_s}{\partial x}(0, t) = \dot{q}_c + \dot{q}_r - \dot{m} \Delta H_v \quad \text{Equation 3-17}$$

It is assumed that fuel pyrolysis takes place at the surface, thus the heat required to vaporize fuel is extracted from the incoming energy flux. The equation for the pyrolysis rate is indicated in Equation 3-19; which is approximated using a single first order Arrhenius reaction.

$$\dot{m}'' = A \rho_s e^{-E_A/RT}$$

Equation 3-18

R is the universal gas constant. The value of the pre-exponential factor A and the activation energy (E_A) can be selected so that the solid surface ignites close to the ignition temperature prescribed. In addition, the actual burning rate is governed by the overall energy balance in the solid. It should be noted that these parameters are often difficult to obtain for real fuels. It is stated in the FDS4 user guide (McGrattan and Forney 2004): if the terms A and E_A are not known, the critical mass flux and T_{ig} must be prescribed. This directs the code to choose A and E_A so that the fuel burns at the rate of critical mass flux when its surface reaches the T_{ig} .

If the surface material is assumed to be thermally-thin, $T_s(t)$ is affected by gains and losses due to convection, radiation and pyrolysis. The thermal lag of the material is a function of the product of its density, specific heat and thickness (δ); the equation representing the thermal lag is defined as follows:

$$\frac{\partial T_s}{\partial t} = \frac{\dot{q}_c'' + \dot{q}_r'' - \dot{m}'' \Delta H_v}{\rho_s c_s \delta}$$

Equation 3-19

3.6.3 Charring Fuels

Charring fuels is another thermal boundary condition that could be prescribed on the surface boundary in FDS4. The purpose of having this condition is to model the effect of char material when it is formed during the ignition of the solid; the most commonly known char material is wood. The heat transfer and pyrolysis of charring materials are described using a one-dimensional model. The pyrolysis is assumed to take place over an infinitesimally thin front in order to simplify the original model. The model includes the conduction of heat inside the material, the evaporation of moisture and the degradation of the virgin material to gaseous fuel and char. The volatile gases are instantaneously transported to the surface. The

governing equation for energy and the boundary condition on the surface is shown in Equation 3-20 and Equation 3-21 respectively. It should be noted that the energy required to pyrolyse the fuel does not come from the incoming heat flux (which applies to thermoplastic fuels) but rather the energy that is coming out from the inside of the material at the pyrolysis surface.

$$\bar{\rho} c \frac{\partial T_s}{\partial t} = \frac{\partial}{\partial x} k_s \frac{\partial T_s}{\partial x} + \frac{\partial \rho_s}{\partial t} [\Delta H_{pyr} - C(T - T_0)] + \frac{\partial \rho_m}{\partial t} [\Delta H_{ev} - D(T - T_0)] \quad \text{Equation 3-20}$$

$$-k_s \frac{\partial T_s}{\partial x}(0, t) = \dot{q}_c + \dot{q}_r \quad \text{Equation 3-21}$$

where ρ_s is the total density of the solid and ρ_m is the moisture density. ΔH_{pyr} and ΔH_{ev} are the heats of pyrolysis and water vaporisation, respectively. In addition, the C and D coefficients are defined as follows:

$$C = \frac{\rho_{s0} c_{p,s0} - \rho_{char} c_{p,char}}{\rho_{s0} - \rho_{char}} - \bar{c}_{p,g} \quad \text{Equation 3-22}$$

$$D = \bar{c}_{p,m} - \bar{c}_{p,g}$$

where the subscripts s0 and char refer to the virgin material and char, and the subscripts g and m refer to the gaseous products of pyrolysis and the moisture. An overbar denotes the average value for the quantity between the temperature (T) and ambient temperature (T_0).

Again, the pyrolysis rate of the material is modelled similar to the thermoplastic fuels where a single first order Arrhenius reaction is assumed (Equation 3-18). However, in the charring fuels model the value of A and E_A are chosen in relation to the pyrolysis temperature. The pyrolysis is assumed to take place over a thin front moving inside the material, where the velocity of the front is given by Equation 3-23: This is to reduce the uncertainty related to the coefficients of the pyrolysis rate so that the burning rate is controlled by the heat of pyrolysis and the heat transfer inside of the material (McGrattan 2004).

$$v = \frac{\dot{m}''}{\rho_{s0} - \rho_{char}} \quad \text{Equation 3-23}$$

To calculate the thermal properties of the material during the drying and charring processes, the following equations are implemented in FDS4; where the thermal properties of the virgin material and char may be temperature dependent.

$$\overline{\rho c} = \rho_a c_{p,s0} + \rho_c c_{p,char} + p_m c_{p,m} \quad ; \quad k_s = k_{s0} \frac{\rho_s}{\rho_{s0}} + k_{char} \frac{\rho_c}{\rho_{char}} \quad \text{Equation 3-24}$$

$$\rho_a = \rho_{s0} \frac{\rho_s - \rho_{char}}{\rho_{s0} - \rho_{char}} \quad ; \quad \rho_c = \rho_s - \rho \quad \text{Equation 3-25}$$

4 Theory of the LIFT test

4.1 Introduction

The Lateral Ignition Flame Transport (LIFT) test is a standard test method for determining material ignition and flame spread properties, which can be found in the ASTM Fire Standards (ASTM Committee E-5 on Fire Standards. 2004b) with a designation number of E 1321-97a (2002). As suggested by the title of the ASTM E 1321 97a (2002) standards, this test is used to determine the material ignition properties such as the minimum heat flux for ignition; and ultimately a correlation with flame spread, which can be compared between different materials, namely called the flame heating parameter (Φ).

The mathematical model of ignition and flame spread that are implemented in the ASTM E 1321-97a (2002) standards comes from the work by both Quintiere (1981) and Quintiere and Harkleroad (1982) as mentioned in Chapter 2.

It is interesting to note that the LIFT test actually originated from the standard test method for flammability of marine surface finishes (ASTM E 1317-97a (2002)). The major difference between the two standards tests are that the location and direction of the piloted flame. In the ASTM E 1321 standards, a horizontal piloted flame is situated at the top of the sample holder where a 180mm long flange is used to ensure that the piloted flame reaches to 180mm in length. This is to ensure that the radiation from the burner flame has no effect on the test of both the ignition and flame spread. Meanwhile, the ASTM-E1317 standards use a vertical piloted flame at the hot end of the sample; which is approximately 10mm away from the sample and a flame length of roughly 230mm. In addition, the ASTM E1317 standards use a thermopile in the hood to give information about the heat release, and this is not used in the ASTM E1321 standards.

The LIFT test comprises of two parts; the first part is the ignition test, where the minimum heat flux required for ignition and the effective thermal properties ($k\rho c$) are obtained. The other part of the LIFT test is the flame spread test, where it is used to determine the flame spread properties. This is done by setting the minimum heat flux required for ignition that is found in the ignition test on the specimen. The theory for both the ignition and flame spread test are described in the following sections. A picture of the LIFT apparatus required in the

ASTM E 1321-97a (2002) is shown in Figure 4-1; where the main components of the LIFT equipment are labelled.

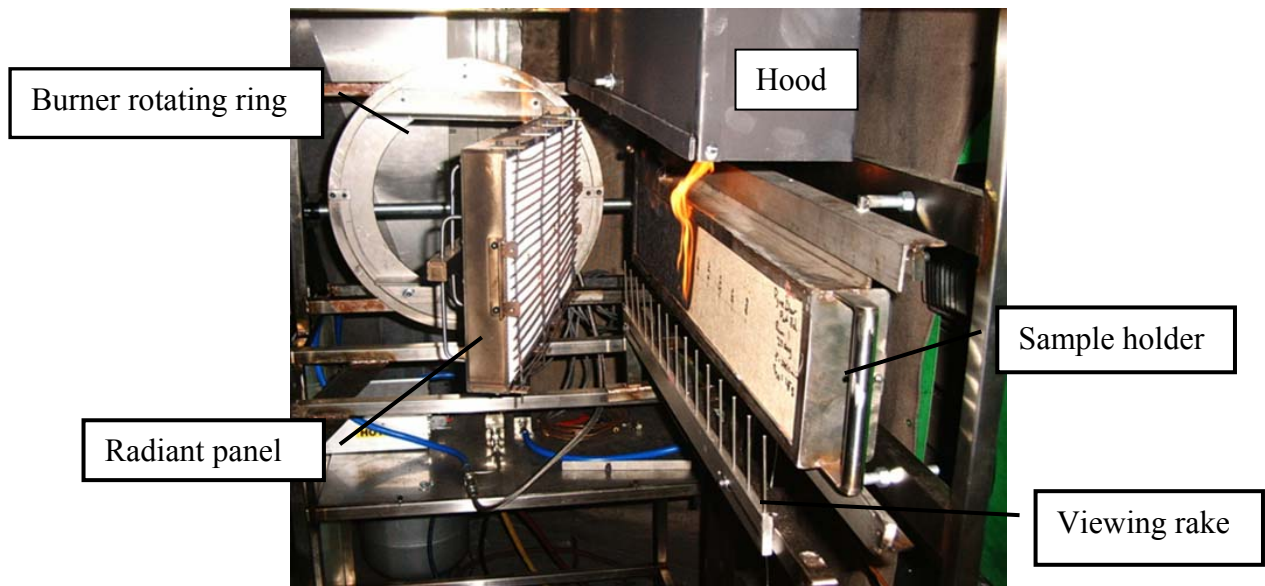


Figure 4-1: LIFT showing angled gas radiant panel (left) and sample holder (right) (Merryweather 2006)

4.2 Ignition Test

As mentioned previously, the ignition test is part of the LIFT test and is used to determine the minimum heat flux ($\dot{q}_{o,ig}''$) required for ignition. Figure 4-2 shows the LIFT apparatus setup for the ignition test. As can be seen in the figure, the dimension of the sample in the specimen holder must be $155\text{mm} \times 155\text{mm}$ as shown in Figure 4-3.



Figure 4-2: A perspective view of the ignition test using the LIFT (Merryweather 2006)

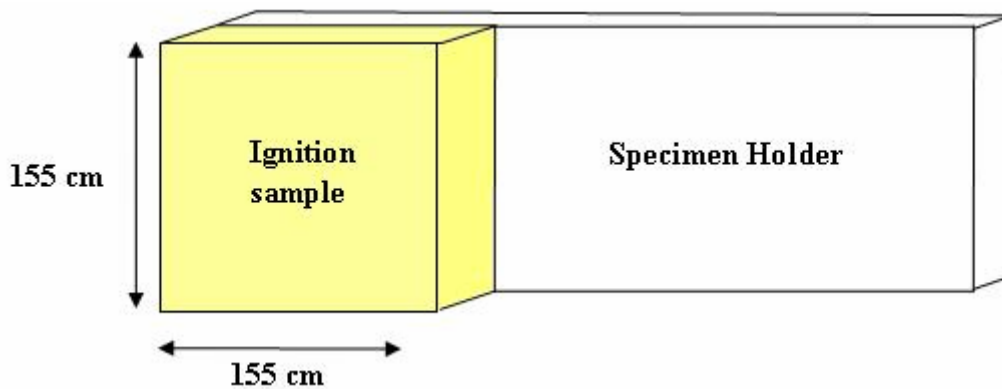


Figure 4-3: Specimen for the ignition test

4.2.1 Ignition Theory

The ignition theory used in the test is based on two reasonable assumptions. The first assumption is that the material is considered to be a semi-infinite solid. This is because the depth of heating under a piloted ignition is normally 2 to 5 mm for the most common organic solids that is used in the construction industry; where their thermal diffusivity ($k/\rho c$) is in between 0 to $10^{-7} m^2 / s$. The other assumption made in the ignition theory is that the ignition temperature of materials is independent to the external radiant flux. This means that when a material is subjected to an external heat flux from an ambient temperature, it will ignite with a piloted flame when the surface temperature of the material reaches to its ignition temperature; regardless of the external radiant flux.

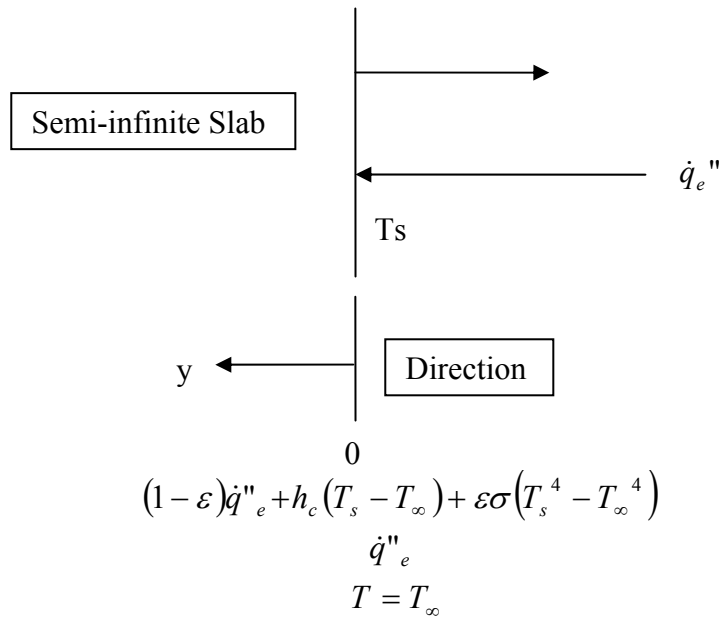


Figure 4-4: Model for ignition study (ASTM Committee E-5 on Fire Standards. 2004b)

Consequently, the ignition theory is a one dimensional heat transfer problem; where a semi-infinite slab is subjected to an external heat flux (\dot{q}_e'') and it will ignite when the surface temperature reaches to the ignition temperature. Figure 4-4 illustrates the ignition model that is considered in the ignition theory; where ε is the emissivity and σ is the Stefan-Boltzmann constant.

The heat transfer problem for ignition is first simplified by assuming the surface emissivity is one ($\varepsilon = 1$) as follows:

$$\dot{q}_e'' - h_c(T - T_\infty) - \sigma(T^4 - T_\infty^4) = 0 \tag{Equation 4-1}$$

The change in temperature can be written as a function of time as shown in Equation 4-2.

$$\frac{\partial T}{\partial t} = \frac{k}{\rho c} \frac{\partial^2 T}{\partial y^2} \tag{Equation 4-2}$$

At the surface boundary where $y = 0$: $-\frac{\partial T}{\partial y}$, the heat transfer problem is further simplified;

$$\text{where } \dot{q}''_e - h_c(T - T_\infty) - \sigma(T^4 - T_\infty^4) \cong \dot{q}''_e - h(T - T_\infty)$$

The following are the other boundary conditions applicable for the ignition problem:

$$\begin{aligned} y \rightarrow \infty: T &= T_\infty \\ t = 0: T &= T_\infty \end{aligned} \quad \text{Equation 4-3}$$

Therefore the temperature at $y = 0$ can be written as follows:

$$T_s - T_\infty = \frac{\dot{q}''_e}{h} \left(1 - \exp(-\tau) \operatorname{erfc}(\sqrt{\tau})\right) \quad \text{Equation 4-4}$$

where $\tau = \frac{h^2 t}{k\rho c}$, h is the heat-transfer coefficient at ignition and t being the piloted ignition time.

The minimum heat flux for piloted ignition in theory implies that ignition occurs for $t \rightarrow \infty$ when conductive losses into the material is zero and heat losses from the surface is equal to the external flux as indicated in Equation 4-5.

$$\dot{q}''_{o,ig} = h(T_{ig} - T_\infty) \quad \text{Equation 4-5}$$

In the case of $t = t_{ig}$ and $T = T_{ig}$, Equation 4-6 is a result of back substituting Equation 4-5 into Equation 4-4.

$$\frac{\dot{q}''_{o,ig}}{\dot{q}''_e} = \left(1 - \exp(-\tau) \operatorname{erfc}(\sqrt{\tau})\right) \quad \text{Equation 4-6}$$

It is difficult to measure the surface temperature at ignition; however, it is possible to correlate the surface temperature with the external heat flux. Therefore if the critical heat flux for ignition is determined, the ignition temperature can also be found. The critical radiative heat flux for piloted ignition can be represented by Equation 4-7.

$$\dot{q}''_{o,ig} = h_c(T - T_\infty) + \sigma(T^4 - T_\infty^4) \equiv h(T_{ig} - T_\infty) \quad \text{Equation 4-7}$$

From experimental ignitions tests, a correlation of the critical flux for ignition has been determined; where ignition times were measured at a range of heat flux levels. It has found the following relationship (Equation 4-8); where the function $F(t)$ is the empirically determined counterpart to $(1 - \exp(-\tau) \operatorname{erfc}(\sqrt{\tau}))$ of Equation 4-4 and Equation 4-6.

$$\frac{\dot{q}''_{o,ig}}{\dot{q}''_e} = F(t) = \begin{cases} b\sqrt{t}, & t \leq t^* \\ 1, & t \geq t^* \end{cases} \quad \text{Equation 4-8}$$

As t or $\tau \rightarrow \infty$, the term $1 - \exp(-\tau) \operatorname{erfc}(\sqrt{\tau})$ approaches to 1 so that the preheat time t^* in the function $F(t)$ is regarded as a time to reach equilibrium or steady state in the material. On the other hand, as t or $\tau \rightarrow 0$, the term $1 - \exp(-\tau) \operatorname{erfc}(\sqrt{\tau})$ approaches $k\rho c$. Due to the behaviour of $F(t)$ for $t \leq t^*$, it has been found that the ignition correlation parameter (b) is defined as follows:

$$b = \frac{2h}{\sqrt{\pi k\rho c}} \quad \text{Equation 4-9}$$

As for the effective thermal property ($k\rho c$), it is calculated as follows:

$$k\rho c = \frac{4}{\pi} \left(\frac{h}{b} \right)^2 \quad \text{Equation 4-10}$$

4.2.2 Calculation for Ignition Test

A series of experiments are required where ignition times are measured for different external fluxes. Subsequently, a plot of the test-data results for $\frac{\dot{q}''_{o,ig}}{\dot{q}''_e}$ versus \sqrt{t} is necessary to determine the ignition correlation parameter (b) and the required preheat time for the material (t^*). This graph should look similar to the one shown in Equation 4-5; where the slope of the plot is the ignition correlation parameter and the intercept between the slope line and the straight line equals to the square root of the required preheat time.

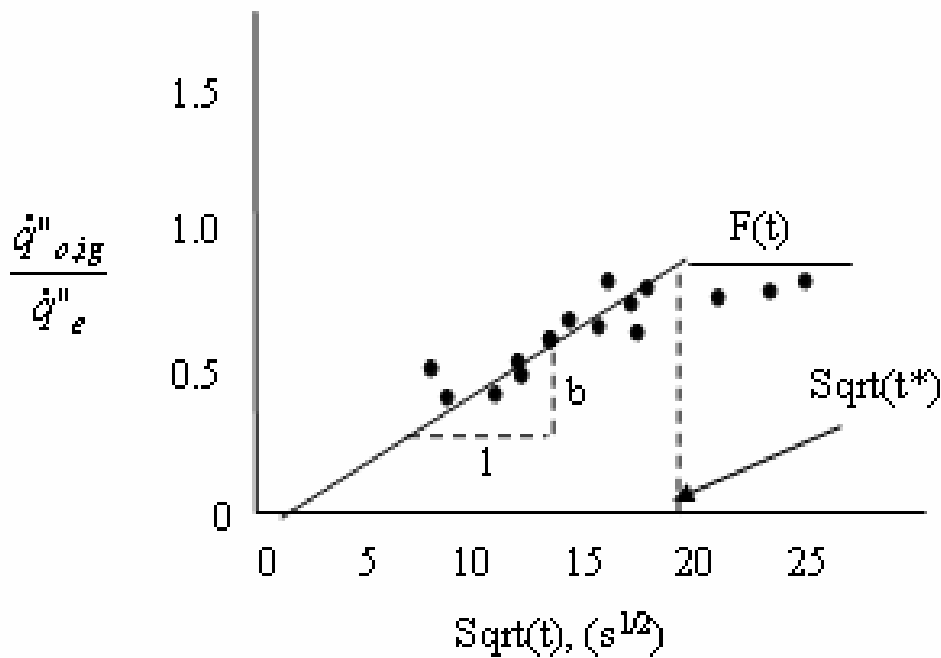


Figure 4-5: Pilot ignition results under radiative heating

In addition, the critical heat flux for ignition is also obtained from the ignition test performed where different external heat fluxes are used to measure its ignition time. An example of the plot of the ignition time against the external heat flux is illustrated in Figure 4-6 and the minimum heat flux required for ignition is indicated by the dotted line.

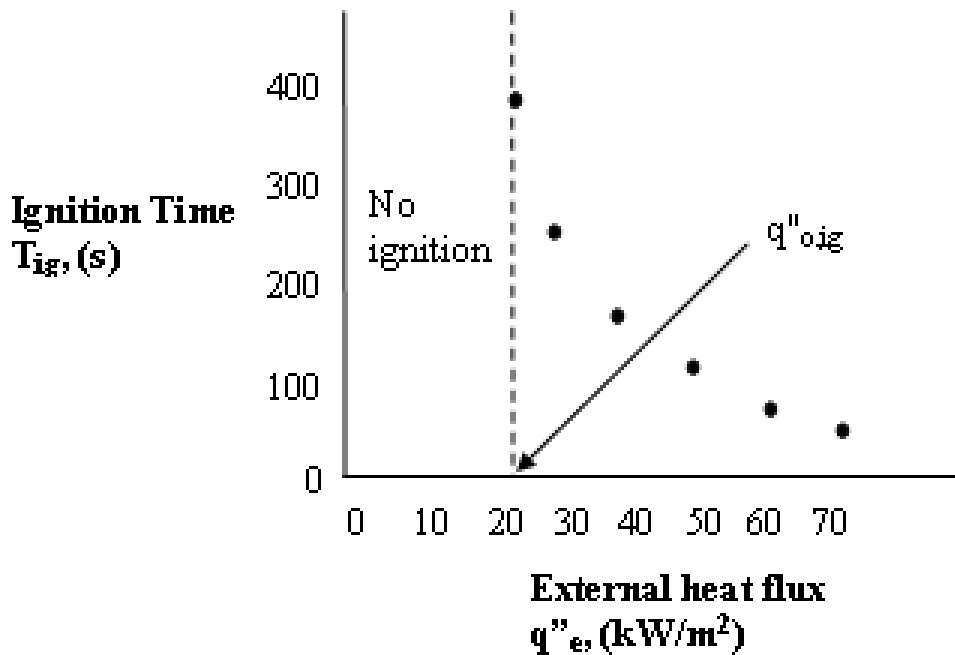


Figure 4-6: A plot of ignition time as a function of external irradiance

By assuming a surface emissivity of one and steady conditions, the convective coefficient (h_c) depends on the LIFT apparatus and operating levels. The theoretical and measured data linking specimen-surface temperature to imposed heat flux is plotted shown in the ASTM E 1321-97a (2002) standards. This curve is used to determine the ignition temperature at surface by correlating the minimum heat flux for ignition. Consequently, the effective thermal property ($k\rho c$) can be determined using Equation 3-2 where the heat transfer coefficient at ignition (h) is calculated using Equation 4-5.

4.3 Flame Spread Test

The flame spread test is the second part of the LIFT test. In this test, the heat flux measured at 50mm along the specimen is set at approximately 5kW/m^2 above the minimum heat flux for ignition; which is determined in the ignition test. The dimension of the specimen must be $155\text{mm} \times 800\text{mm}$ as shown in Figure 4-7, where the flame spread test is illustrated. Note that the flame spreads from the left hand side to the right hand side (along the specimen length).



Figure 4-7: A perspective view of the flame spread test using the LIFT (Merryweather 2006)

4.3.1 Flame Spread Theory

The theory behind the flame spread test comes from the work by Quintiere (1981), where he found the mathematical solution for the flame spread velocity (V_p) as shown in Equation 4-11:

$$V_p = \frac{(\dot{q}''_f)^2 (x_f - x_p)}{\frac{\pi}{4} k \rho c (T_{ig} - T_s)^2} \quad \text{Equation 4-11}$$

where $T_s - T_\infty = \frac{\dot{q}''_e}{h} (1 - \exp(\tau) \operatorname{erfc}(\sqrt{\tau}))$ as indicated in Equation 4-4.

Additionally, deRis (1969) derived an opposed flow flame spread equation in a steady condition; this is solved by making an assumption that both the gas and solid fuel phase is in two dimensions.

$$V_p = V_g \frac{(k\rho c)_g}{k\rho c} \left(\frac{T_f - T_{ig}}{T_{ig} - T_s} \right)^2 \quad \text{Equation 4-12}$$

where V_g is the opposed flow velocity and T_f is the flame temperature.

As mentioned in the literature review, the opposed flow velocity depends on the chemical kinetic effects. Therefore, a Damkohler number is introduced to act as kinetic data for the fuel to account for the kinetic changes. If kinetics is important and the Damkohler number is not used then the actual flame spread velocity calculated is lower than that given by Equation 4-12. However, if chemical kinetic effects are not significant, Equation 4-12 is considered to be acceptable.

The major problem in using Equation 4-12 to determine the flame velocity is the difficulty in obtaining the flame temperature. Nevertheless, it is observed that the numerator in both the flame velocity equations by Quintiere and deRis (Equation 4-11 and Equation 4-12) suggest another property. The flame spread data can ultimately be correlated by applying a variable in the denominator as given in Equation 4-13. This variable is the material flame spread property which is known as the flame heating parameter (ϕ). In addition, it should be a constant for a particular material under a fixed V_g and ambient oxygen concentration.

$$V = \frac{\phi}{k\rho c (T_{ig} - T_s)^2} \quad \text{Equation 4-13}$$

Here $k\rho c$ is the effective thermal property, T_{ig} and T_s is the ignition temperature and surface temperature respectively.

The actual flame temperature can be calculated using Equation 4-14; this formula is rearranged by substituting the flame heating parameter ϕ back into Equation 4-12.

$$T_f = T_{ig} + \left(\frac{\phi}{V_g (k\rho c)_g} \right)^{-1/2} \quad \text{Equation 4-14}$$

where $(k\rho c)$ is taken for air at normal temperature to be $3.3 \times 10^{-5} \left(\frac{\text{kW}}{\text{m}^2 \text{K}} \right)^2 \text{ s}$.

Equation 4-13 can be rewritten as Equation 4-15 by making the use of other equations.

$$V(t)^{-1/2} = \left(\frac{h^2 \phi}{k\rho c} \right)^{-1/2} (\dot{q}''_{o,ig} - \dot{q}''_e(x)F(t)) \quad \text{Equation 4-15}$$

Here t denotes the time the pyrolysis front is at position x and is the time over which the external heat flux \dot{q}''_e has been imposed.

The flame spread correlation parameter is calculated as follows:

$$\phi = \frac{4}{\pi} \frac{1}{(Cb)^2} \quad \text{Equation 4-16}$$

where C is the slope of the line through the data points and is a constant term related to

$\left(\frac{h^2 \phi}{k\rho c} \right)^{-1/2}$; while b is the ignition correlation parameter.

4.3.2 Calculation for Flame Spread Test

The flux-distribution values for the specimen (Appendix A) are used to compute $F(x)$ at the x -positions corresponding to the flame front arrival times; which is represented by Equation 4-17 below.

$$F(x) = \frac{\dot{q}_e''(x)}{\dot{q}_e''(50)} \quad \text{Equation 4-17}$$

The external heat flux imposed on the specimen can be calculated by rearranging the equation above to the following form.

$$\dot{q}_e''(x) = F(x) \times \dot{q}_e''(50) \quad \text{Equation 4-18}$$

The flame-front velocity is calculated by taking the running three-point least square fit as given in Equation 4-19; where t is the flame front arrival time and its position x .

$$V = \frac{\sum tx - \frac{\sum t \sum x}{3}}{\sum t^2 - \frac{(\sum t)^2}{3}} \quad \text{Equation 4-19}$$

The analysis of the flame spread data is carried out by plotting a graph for $V^{-1/2}$ against $\dot{q}_e(x)F(t)$; where $F(t)$ is ratio of the minimum heat flux for ignition and the external heat flux imposed (Equation 4-8) and is reproduced below for convenience. Here t^* is the time for specimen to reach thermal equilibrium or also known as the preheating time.

$$F(t) = \begin{cases} b\sqrt{t}, & t \leq t^* \\ 1, & t \geq t^* \end{cases} \quad \text{Equation 4-20}$$

Figure 4-8 below shows an exemplar plot of $V^{-1/2}$ versus $\dot{q}_e(x)F(t)$, this graph illustrates the correlation of lateral flame spread for a material. The slope of the straight line fitted to correlated flame spread data, which is indicated in the figure, is the flame spread parameter (C).

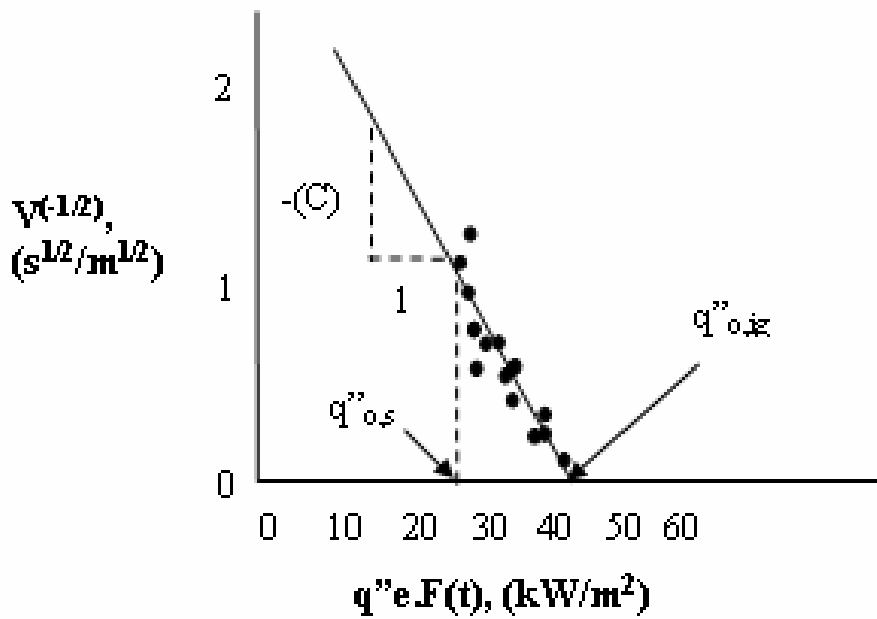


Figure 4-8: Correlations of Lateral Flame Spread

From the graph of the correlations of lateral flame spread, the minimum heat flux for both the ignition and spread can be obtained. It should be noted that the correlated minimum heat flux for ignition is different to the one found in the ignition test; nevertheless, these values should be similar. In addition, the flame heating parameter (ϕ) is computed using Equation 4-16 in conjunction with the b (in the ignition test) and C (in the flame spread test) parameter that is determined previously.

5 Experimental setup on the charring of timber

This chapter briefly describes the cone calorimeter apparatus that is used to burn all of the timber and timber based products in order to obtain charred samples; hence the thermal properties for the charred timber based products are measured and applied in the FDS4 charring fuels model. It should be noted that only the cone element heater portion of the cone calorimeter test is employed to obtain char specimens. For this reason, any information (i.e. the mass loss rate, heat release rate and effective heat of combustion) which would have normally been recorded from the cone calorimeter test is not measured in this test.

5.1 Cone Calorimeter

The cone calorimeter is an apparatus for assessing materials reaction to fire and was developed by Babrauskas in the early 1980's and even today it is still considered to play a dominant role in bench scale fire testing of various products. The concept behind this test is based on the oxygen consumption calorimetry (Janssens 2002). Standard procedures for the cone calorimeter are shown in both the ASTM E 1354-04a of the ASTM fire standards and the ISO 5660-1: 1993(E) standards; it is important to follow those standards when this test is performed. The function of the cone calorimeter test includes determining the effective heat of combustion, mass loss rate, ignitability, smoke and toxic gases production. Figure 5-1 shows the cone calorimeter used in the laboratory to burn the timber and timber based products into charred specimens. For more details on the cone calorimeter can be found in the SFPE Handbook (Babrauskas 2002).



Figure 5-1: Cone calorimeter at the University of Canterbury

Figure 5-2 shows the main components of the cone calorimeter which includes the cone element heater, the spark igniter, the load cell and the exhaust hood. The details of the cone element heater are illustrated in Figure 5-3.

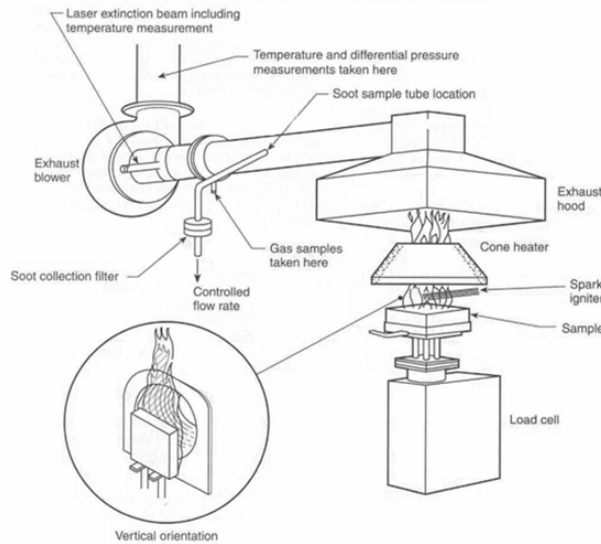


Figure 5-2: Schematic view of the cone calorimeter (Babrauskas 2002)

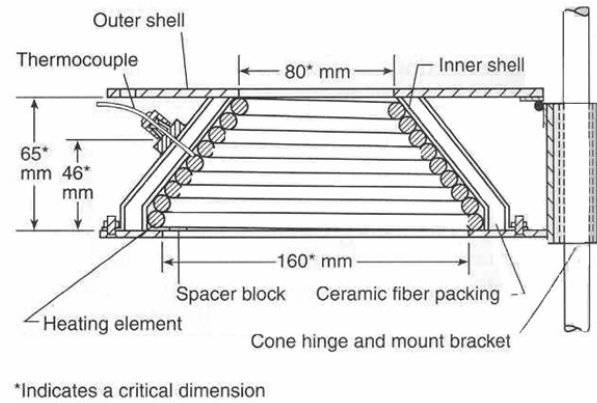


Figure 5-3: Cross sectional view of the cone heater (Babrauskas 2002)

The size of the test specimen is 100 mm by 100 mm (± 5 mm) with a maximum thickness of 50 mm. The surface of test specimen should be flat and a complete test requires that at least 12 specimens are available.

During a cone calorimeter test, the surface of the test specimen (shown in Figure 5-2) is exposed to a constant level of heat irradiance, within the range of 0 to 100 kW/m², from a cone element heater. An electrical spark igniter is used for igniting the volatile gases from the heated specimen. Combustion gases coming off from the heated specimens are collected by an exhaust hood for further analysis; where heat release rate is determined using the principles of oxygen consumption calorimetry and the production of toxic gases such as CO, CO₂ (or HCN when applicable) is assessed by gas analysers. Smoke production is assessed by using a flow through smoke measuring system; where a helium-neon laser beam is used to measure the attenuation of smoke in the exhaust duct. As attenuation is related to the actual volume flow rate, smoke density is also measured where the variable smoke extinction area [m²/s] is determined.

The test specimen is mounted on a load cell as shown in Figure 5-2. The load cell records the mass loss rate of the specimen during combustion. For a full analysis of the material, it requires a range of heat fluxes for testing. The typical levels of irradiance are 25, 35, 50 and 75 kW/m². In addition, three specimens shall be tested at each heat flux level according to ISO 5660-1:1993(E).

There are a number of outputs that can be extracted from the cone calorimeter test which are listed as follows:

- Time to ignition [s]
- Total heat released [MJ/m²]
- Maximum heat release rate [kW/m²]
- Mass loss rate [g/s]
- Average heat release rate after a time (i.e. after 180 s or 300 s) [kW/m²]
- Effective heat of combustion [MJ/kg]
- Average smoke production [m²/s]
- Production of CO (carbon monoxide) [g]
- Production of other gas components such as HCN (cyanic acid) [g]

Again, all of the outputs above were not obtained with the exception for time to ignition, as they are outside the scope of this research; where the objective of using the cone calorimeter is to turn the timber and timber based product to charred specimens. The use of the charred specimens allows the thermal properties to be measured using a hot disk thermal constants analyser (Gustafsson 1998). By doing so, it enables the charring fuels model in FDS4 to model flame spread.

5.2 Test Specimens

A standard specimen size of the cone calorimeter test has a dimension of 100mm x 100mm; however, in this test not all of the specimens are in the standard size due to the limited number of unused specimens available since the research carried out by Merryweather (2006). Both the specimen's breadth and width ranges from 94 to 100mm while the thickness varies from 5mm to 24mm. A summary of all specimens dimension is tabulated in Appendix B. Although the size of the specimen varies from the standard, it does not have any effect on the main objective of the experiment which is to get a charred layer on the timber for measuring the thermal properties.

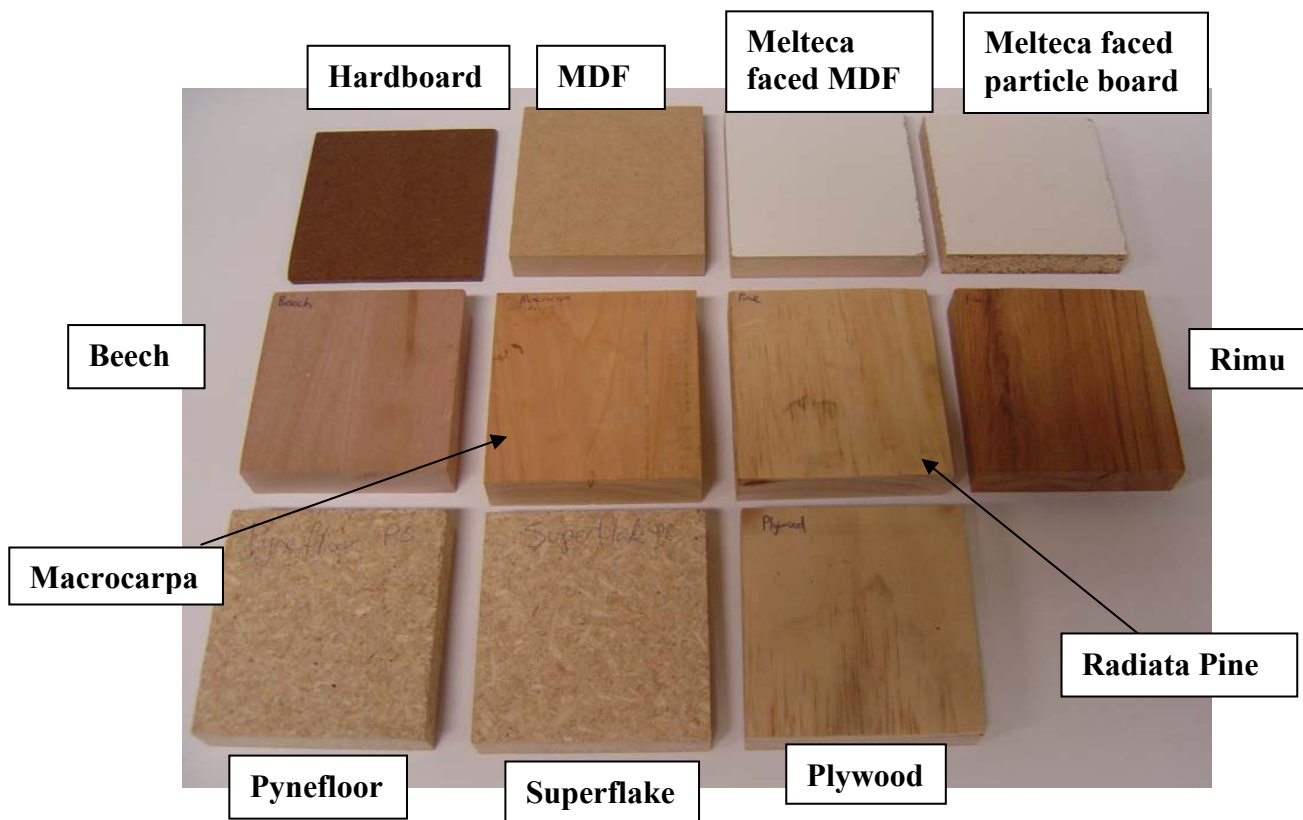


Figure 5-4: All timber and timber based products specimens for testing

Each timber and timber based product requires two samples for the cone calorimeter test; simply because two samples are needed to determine the thermal properties in the hot disk test. A thin thermocouple bead was carefully placed on the surface (at the centre of the specimen) for all specimens before testing. This enables the temperature of ignition to be measured, which is used for comparison with the results obtained by Merryweather (2006)

later on. Figure 5-5 shows the thermocouple bead on the sample with a temperature reading from the multimeter.



Figure 5-5: Thermocouple bead placed in the wood specimen and its temperature reading

5.3 Calibration of the cone element heater

As mentioned earlier, the typical levels of irradiance that is required on the surface of the specimens are 25, 35, 50 and 75 kW/m². In this test, however, the radiant heat flux from the cone element heater on the specimen surface was set to 35kW/m². The reason for selecting a heat flux of 35kW/m² is because a flame heat flux of 33kW/m² is likely to be on wall materials when the wall lining flaming is not significantly affected by large smoke particles from a fire (Azhakesan et al. 2000).

The cone element heater was calibrated using a heat fluxmeter to ensure that the radiant heat flux on the surface of the specimen is the same as what has been specified. It was found that the corresponding heat flux on the surface of the specimen is 35kW/m² when the temperature controller was at a temperature of 665°C.

5.4 Specimen Mounting

The distance between the bottom surface of the cone heater and the top of the specimen is set at 25mm as required by the fire standards. The configuration of the test is illustrated in Figure 5-6.

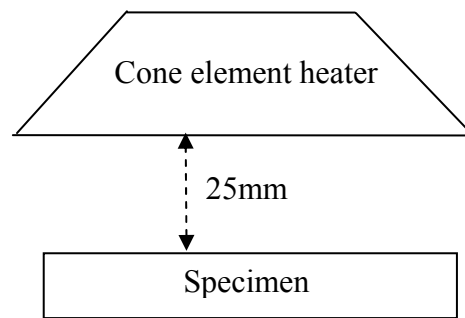


Figure 5-6: Distance between the cone heater and specimen

5.5 Experimental Procedure

After the cone heater was calibrated to a temperature of 665°C, which is equivalent to an irradiance level of 35kW/m², the radiation shield was inserted and then the specimen was positioned in a specimen holder correctly (25mm below the cone heater). The radiation shield is a component of the cone heater which is made of ceramic fibreboard. The use of the shield prevented heating of the specimen before the actual test began. It was vital that the shield was not in place for more than 10 seconds as heat energy might penetrate through and affect the specimen. In addition, it should be noted that the specimen holder was at room temperature initially.

Once the specimen is in position, start the ignition timer and remove the radiation shield. The piloted ignition source, which is a spark plug, is set in place and the power turned on.

Both the ignition temperature and time of ignition for each specimen is recorded. Figure 5-7 illustrates the procedure of obtaining the ignition temperature. All specimens were heated to a sufficient depth of char layer is formed (more half of the thickness of the virgin material). Figure 5-8 shows the experiment carried out to burn the Rimu specimen to form a char layer on the surface.



Figure 5-7: Measuring the temperature of ignition



Figure 5-8: Charring of the Rimu specimen

5.6 Analysis of Char Density and Ignition Temperature

There is standard test method in the ASTM fire standards (Anon 2004) for determining the char density of ablative materials, such as the ASTM E471-96(2002). However, this method is not used in this research as no such machinery is available in the laboratory. Instead the char density of the timber and timber based products is calculated by using the mass and volume approach ($\rho = \frac{Mass}{Volume}$). The char mass is determined by subtracting the mass of the charred specimen from the mass of the virgin specimen. The volume of char is estimated due to the irregularity of the specimen as shown in Figure 5-9 which is calculated using the measured depth and area of the charred section in the specimen. It is interesting to observe that the shape of the specimen changes from a flat surface to a bow shape under combustion. This is particularly the case for the hardboard, as the thickness of the specimen is small (5mm).

The author of this research recognises the limitations in determining the density of char; as it is difficult to measure the char density due to the cracks in the specimen and the amount of char available is relatively small. Nevertheless, the char density is not considered to be an important variable in the FDS4 input when compared to other variables such as the thermal

properties (k and c) of char. Therefore an estimate of the char density is deemed to be adequate.

On the other hand, the ignition temperature is relatively easy to obtain; as it is read from the multimeter (as shown in Figure 5-7) once the specimen is ignited.

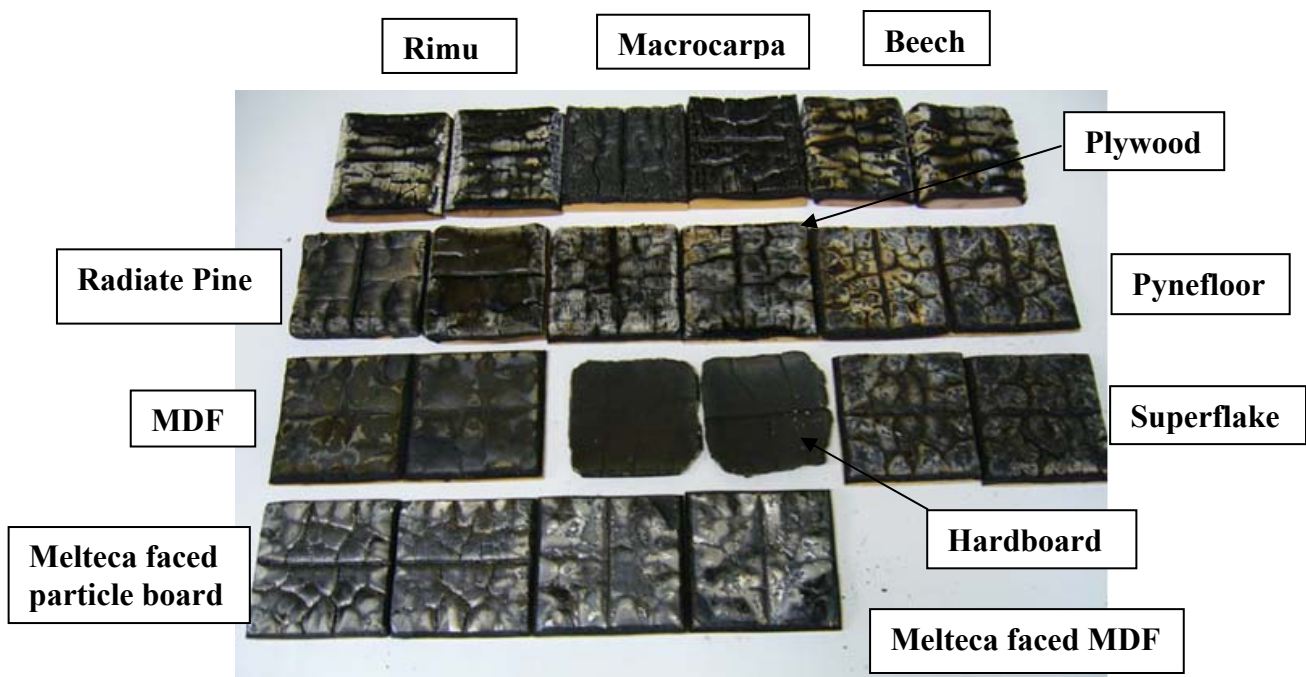


Figure 5-9: Char specimens after burning

Table 5-1 and

Table 5-2 show the calculated char density and ignition temperature for the different types of charred timber and timber based products. The average values are used for both the input of the charring fuels model in FDS4 and for comparison between the values from Merryweather (2006) later on. Figure 5-10 compares the ignition temperature for different types of timber and timber based products. It illustrates that the ignition temperature ranges from which compares well with the ignition temperature for wood. It also proves that the technique of using a thermocouple bead gives a consistent method in obtaining the ignition temperature for wood.

Table 5-1: Calculated char density

Material	Char density (kg/m ³)			
	Specimen 1	Specimen 2	Average	Standard Dev
Hardboard	494	526	510	22.4
Medium Density Fibreboard (MDF)	471	525	498	38.6
Melteca faced MDF	551	625	588	52.6
Melteca faced particle board	463	419	441	30.7
Beech	282	316	299	23.4
Macrocarpa	316	255	285	43.8
Radiata Pine (Monterey pine)	264	234	249	21.6
Rimu	415	428	422	9.0
Particle board (Pynefloor)	403	391	397	9.0
Particle board (Superflake)	582	586	584	2.6
Plywood	31	40	35	6.7

Table 5-2: Measured ignition temperature

Material	Ignition Temperature (°C)			
	Specimen 1	Specimen 2	Average	Standard Dev
Hardboard	398	386	392	8.5
Medium Density Fibreboard (MDF)	390	400	395	7.1
Melteca faced MDF	406	420	413	9.9
Melteca faced particle board	385	405	395	14.1
Beech	360	347	354	9.2
Macrocarpa	329	320	325	6.4
Radiata Pine (Monterey pine)	431	396	414	24.7
Rimu	338	361	350	16.3
Particle board (Pynefloor)	356	335	346	14.8
Particle board (Superflake)	358	368	363	7.1
Plywood	343	365	354	15.6

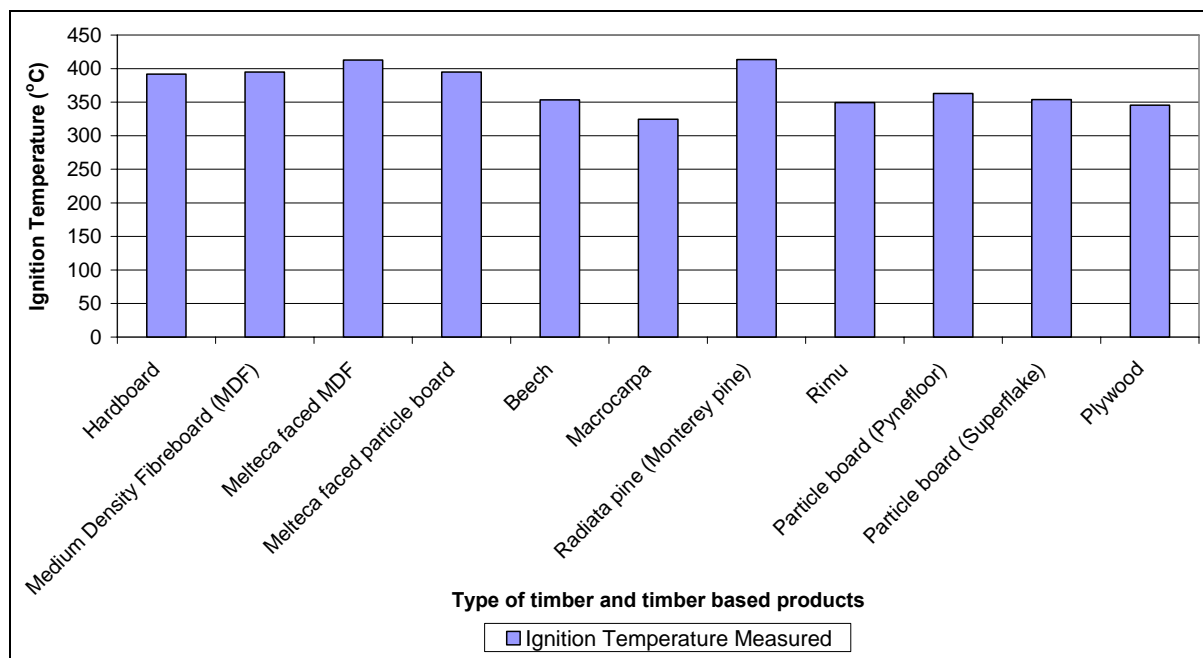


Figure 5-10: A plot of the ignition temperature for different types of timber and timber based products

6 Thermal Properties of timber and timber based products

This chapter outlines the theory of the Hot Disk test which is applied to determine the thermal properties of the timber and timber based products. It should be noted that this section is only intended to give an overview of the Hot Disk theory and more details on the transient plane source measurement technique are described in detail by Gustafsson (1991) and Log (1995). Meanwhile, the development of the theory can be found in the literature paper by Anis-ur Rehman and Maqsood (2003).

6.1 Introduction

Thermal transport properties such as thermal conductivity and specific heat capacity are important parameters in fire modelling as it determines how heat is transferred through solids (i.e. the rate of temperature changes). Therefore, these variables are essential for prediction of flame spread of solids.

There are various experimental methods for measuring the thermal transport properties. The main difference between each technique is the recording method of the temperature; where a steady state method is referred to when the temperature is recorded independent of time, whereas, a transient method is referred to when the temperature is recorded varying with time. In addition, the transient method can be further divided into two main categories; 1) methods for which it is not possible to determine the power delivered to the sample and with which the thermal diffusivity is measured. 2) methods for which it is possible to precisely determine the power delivered to the sample and with which thermal conductivity and in some cases also the thermal diffusivity can be precisely measured (Gustafsson 1998).

All of the methods assumed that initially the specimen is at thermal equilibrium (i.e. with the ambient temperature). The theoretical considerations have been summarised and can be found in the paper by He (2005). Below is a list of the current available methods for measuring thermal conductivity and are classified into either steady state method or non steady state (transient) method.

Steady State Methods:

1. One dimensional heat flow

- Guarded Hot Plate
- Unguarded Hot Plate
- Different arrangements for linear heat flow

2. Radial heat flow

- Cylindrical Method
- Spherical Method
- Ellipsoidal Method

Non Steady state (Transient) Methods:

1. Methods for measuring thermal diffusivity

- Angstrom Method
- Laser Flash Method
- (Laser) Step Method

2. Methods for measuring thermal conductivity

- Hot Wire Method

3. Methods for measuring thermal conductivity and thermal diffusivity

- Transient Hot Strip Method
- Transient Plane Source Method

Each method has its advantages and disadvantage. For example the Guarded Hot Plate is very often used for high insulating materials and is an ASTM standard test which gives an

accurate result. However, it requires large samples in most cases and is considered to be a time consuming experiment to perform.

Another example would be the Laser Flash methods, where a disk shaped sample is irradiated on one side for a short period with a laser pulse, creating a temperature increase in the sample. The change in temperature is then measured on the other side by using a thermocouple that is soldered to the sample surface or recorded by an infrared sensor placed at a certain distance from the sample. As a result, the thermal diffusivity is obtained. However, further experiments are needed in order to obtain the thermal conductivity and specific heat capacity. Despite the time required in obtaining the thermal diffusivity being considered as instant, this method is again considered to be time consuming as additional experiments are needed to get the other thermal transport properties. On the other hand, this method can work at high temperatures and in different atmospheres, but is only applicable to dense materials.

One of the most precise and convenient techniques for studying thermal transport properties is the transient plane source (TPS) technique. It is a modern technique, which gives information on thermal conductivity, thermal diffusivity as well as specific heat capacity of the material under study (Gustafsson 1998). This technique can be used over a broad range of temperatures, i.e., from 77 to 1073 K, while the thermal conductivity measurements can be carried out within the range of 0.005 to 500 W.m⁻¹.K⁻¹ (Anis-ur-Rehman and Maqsood 2003). The thermal transport properties are measured by monitoring the temperature changes in time for a given rate of heat flow.

In this research, only the thermal conductivity and specific heat capacity of the timber and timber based products are required for the input of FDS4 model. These properties are determined using an apparatus called the Hot Disk Thermal Constants Analyser which adapts the TPS technique. Figure 6-1 below shows the principle electric circuit setup of the Hot Disk system.

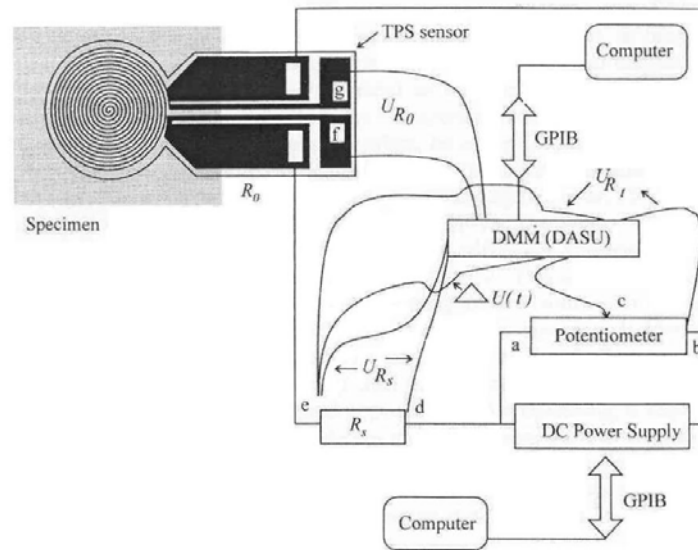


Figure 6-1: Principal electrical circuit for the modified bridge arrangement (Anis-ur-Rehman and Maqsood 2003)

6.2 Theory of the transient plane source technique

This section describes the theory underlying the Hot Disk Thermal Constants Analyser. The TPS method considers the three-dimensional heat flow inside the specimen; where the specimen is assumed to be an infinite medium. This device has a double spiral shaped sensor element (resistive element) known as the Hot Disk sensor. It acts both as a heat source for increasing the temperature of the sample and a “resistance thermometer” for recording the time dependent temperature increase. The sensor element is made of a 10 μm thick Nickel-metal double spiral and the insulation material protecting the spiral shape is made of either Kapton or Mica depending on the testing temperature. In this research, Kapton is used. Figure 6-2 below illustrates both the current through the sensor and the temperature increase of the sensor which are necessary to determine the thermal transport properties of the material surrounding the sensor.

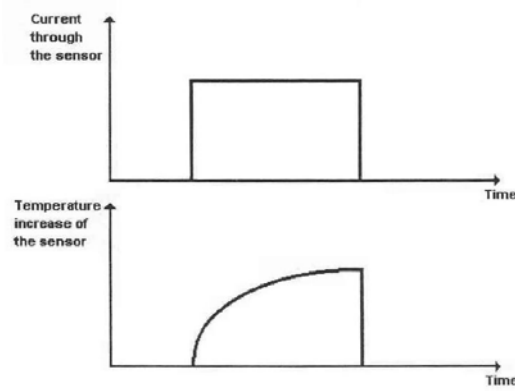


Figure 6-2: Transient recording of the thermal transport properties of the material surrounding the sensor (Gustafsson 1998)

If the Hot Disk is electrically heated, the change in electrical resistance $R(t)$ of the conducting pattern shown in Figure 6-1 can be express as a function of time as follows:

$$R(t) = R_0 \{1 + \alpha[\Delta T_i + \Delta T_{ave}(\tau)]\} \quad \text{Equation 6-1}$$

where R_0 is the resistance of the sensor just before it is being heated or at time $t=0$, α is the Temperature Coefficient of the Resistivity (TCR), ΔT_i is the constant temperature difference that develops almost instantly over the thin insulating layers, $\Delta T_{ave}(\tau)$ is the temperature increase of the sample surface on the other side of the insulating layer and facing the Hot Disk sensor.

By rearranging Equation 6-1, the temperature increase recorded by the sensor can be given as follows:

$$\Delta T_{ave}(\tau) + \Delta T_i = \frac{1}{\alpha} \left(\frac{R(t)}{R_0} - 1 \right) \quad \text{Equation 6-2}$$

where ΔT_i is the measure of the “thermal contact” between the sensor and the sample surface with $\Delta T_i=0$ representing perfect “thermal contact” closely realised by a deposited (PVD or

CVD) thin film or an electrically insulating sample. ΔT_i becomes constant after a very short time Δt_i as indicated in Figure 6-3; Δt_i can be estimated using Equation 6-3 below.

$$\Delta t_i = \frac{\delta^2}{\kappa_i} \quad \text{Equation 6-3}$$

where δ is the thickness of the insulating layer and κ is the thermal diffusivity of the layer material.

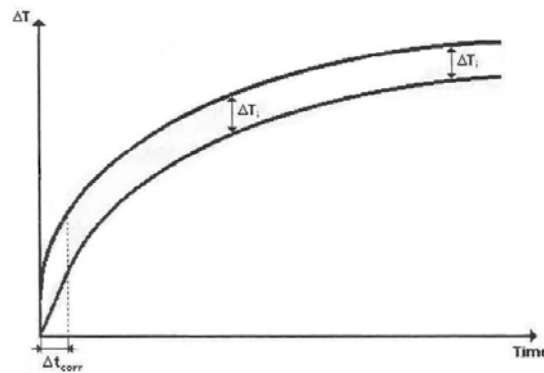


Figure 6-3: Temperature increase of the sensor (Gustafsson 1998)

The time dependent temperature increase of the sensor is given by the theory as:

$$\Delta T_{ave}(\tau) = \frac{P_0}{\pi^{3/2} a \Lambda} D(\tau) \quad \text{Equation 6-4}$$

where P_0 is the total output of power from the sensor, a is the overall radius of the sensor, Λ is the thermal conductivity of the sample that is being tested, $D(\tau)$ is a dimensionless time dependent function with Equation 6-5.

$$\tau = \sqrt{\frac{t}{\Theta}} \quad \text{Equation 6-5}$$

Here t is the time measured from the start of the transient recording, Θ is the characteristic time given in Equation 6-6 and κ is the thermal diffusivity of the specimen.

$$\Theta = \frac{a^2}{\kappa} \quad \text{Equation 6-6}$$

By making a plot of the recorded temperature increase versus $D(\tau)$, a straight line is obtained; where the intercept of graph is ΔT_i and the slope is $\frac{P_0}{\pi^{3/2} a \Lambda}$ using experimental times much longer than Δt_i .

Since κ and by that Θ are not known before the experiment, the final straight line from which the thermal conductivity is calculated is obtained through a process of iteration. In this way it is possible to determine both the thermal conductivity and the thermal diffusivity from one single transient recording (Gustafsson 1998). If all heat is transported via a solid specimen, the thermal conductivity (Λ), the thermal diffusivity (κ) and the heat capacity per unit volume (ρC_p) are expressed by:

$$\Lambda = \frac{\kappa}{\rho C_p} \quad \text{Equation 6-7}$$

6.3 Sample preparation

All specimens were conditioned in the temperature control room for at least 24 hours before testing; where the temperature and humidity inside the temperature control room was 21°C and 50%, respectively. Hot Disk tests were performed for the virgin and charred materials and calcium silicate specimen. The materials for the virgin and charred specimens are the timber and timber based products which include Hardboard, Medium Density Fibreboard (MDF), Melteca faced MDF, Melteca faced Particle Board, Beech, Macrocarpa, Radiata Pine, Rimu, Plywood, Pynefloor Particle Board and Superflake Particle Board. Note that Pynefloor and Superflake are the trade names of the Particle Board.

The specimen for the virgin materials is prepared according to the standard size for a cone calorimeter test, which is 100 mm x 100 mm. It should be noted that not all of the specimens have the exact size required by the standards (with the smallest specimen being 95 mm x 94 mm) due to the limited number of the specimens available. However, this is not a major issue as long as the requirements of the Hot Disk test are satisfied; where the thickness of a flat sample is not less than the diameter of the Hot Disk sensor and the minimum distance from sensor to boundary surface is greater than the probe depth as indicated in Figure 6-4. A list of the virgin wood specimen sizes is shown in Appendix B

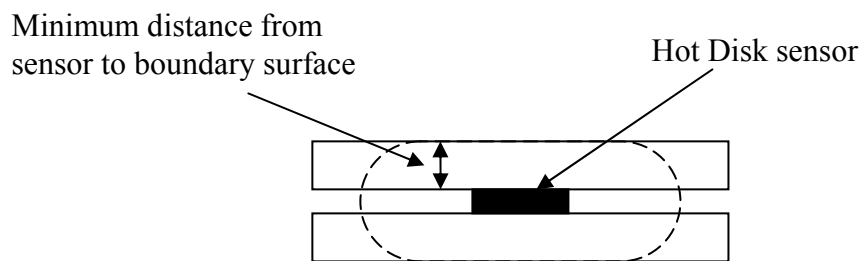


Figure 6-4: Minimum distance from sensor to boundary surface

As for the charred materials, the specimens are obtained by exposing the virgin materials to heat using a cone heating element, as described in Chapter 5. The dimension of the charred specimens is tabulated in Appendix B.

In addition, calcium silicate specimens are also prepared to determine its density and thermal transport. This is the material of the dummy specimen which is required for the calibration of the LIFT test; Afterwards, these properties are input into the FDS4 model for the calibration of the LIFT test in FDS4 as discussed in Chapter 7.

6.4 Density measurements

The density of the material is required due to the specific heat capacity calculated from the Hot Disk test being a function of the density of the particular material tested. Therefore, the specific heat capacity is obtained by having the heat capacity per unit volume divided by the density of the material.

Density of the virgin materials is calculated using the mass volume approach and the calculation can be found in Appendix B. Figure 6-5 shows the density measured for the timber and timber based products where the density of the specimens varies from 438 kg/m³ for Radiata Pine to 844 kg/m³ for Hardboard. The densities of melteca faced boards were similar to a plain board of that type. This is due to the facing being only a minor portion compared with the bulk of the product. It should be noted that the density shown in the figure represents the average density of the two specimens tested. Additionally, the density of ‘Spruce’ is obtained from the FDS4 database and is only used to compare with the experimental values.

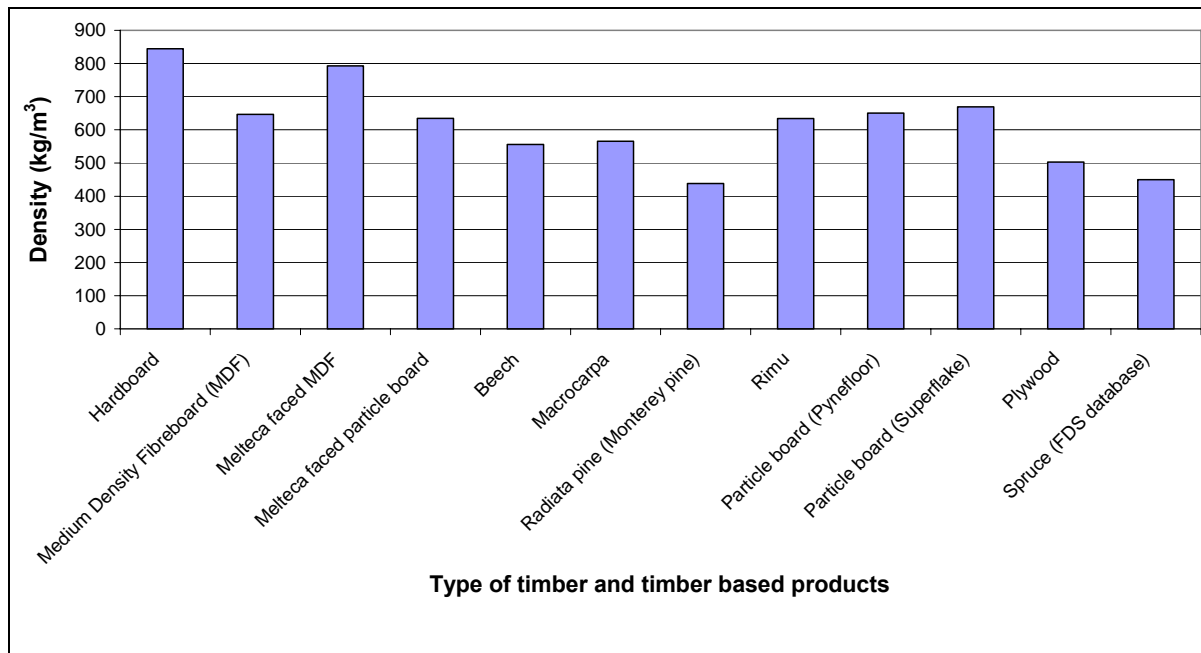


Figure 6-5: Measured average density for the timber and timber based products

As for the density of charred material, it is again calculated by using the mass volume technique. However, the volume of the char is approximated due to the non uniformity of the charred specimens as indicated in Figure 6-6.



Figure 6-6: Charred specimens used for the Hot Disk test

Figure 6-7 shows the calculated char density for each material. It indicated that the char density of the specimens ranges from 249 kg/m^3 for Radiata Pine to 588 kg/m^3 for Melteca faced MDF. With the exception of ‘Superflake’ particle board being an outlier and has a char density of 39 kg/m^3 which is significantly lower than all other materials. The reason for this is most likely due to the difficulties in obtaining the actual volume of the material. Further tests could not be performed due to the limited number of specimens available. However, no LIFT tests were carried out by Merryweather (2006) for the ‘Superflake’ particle board and therefore the char density measured for the ‘Superflake’ particle board is not modelled in FDS4. Again the char density of ‘Spruce’ is also presented to compare with the experimental values. In this case, the char density of ‘Spruce’ is quoted as 120 kg/m^3 .

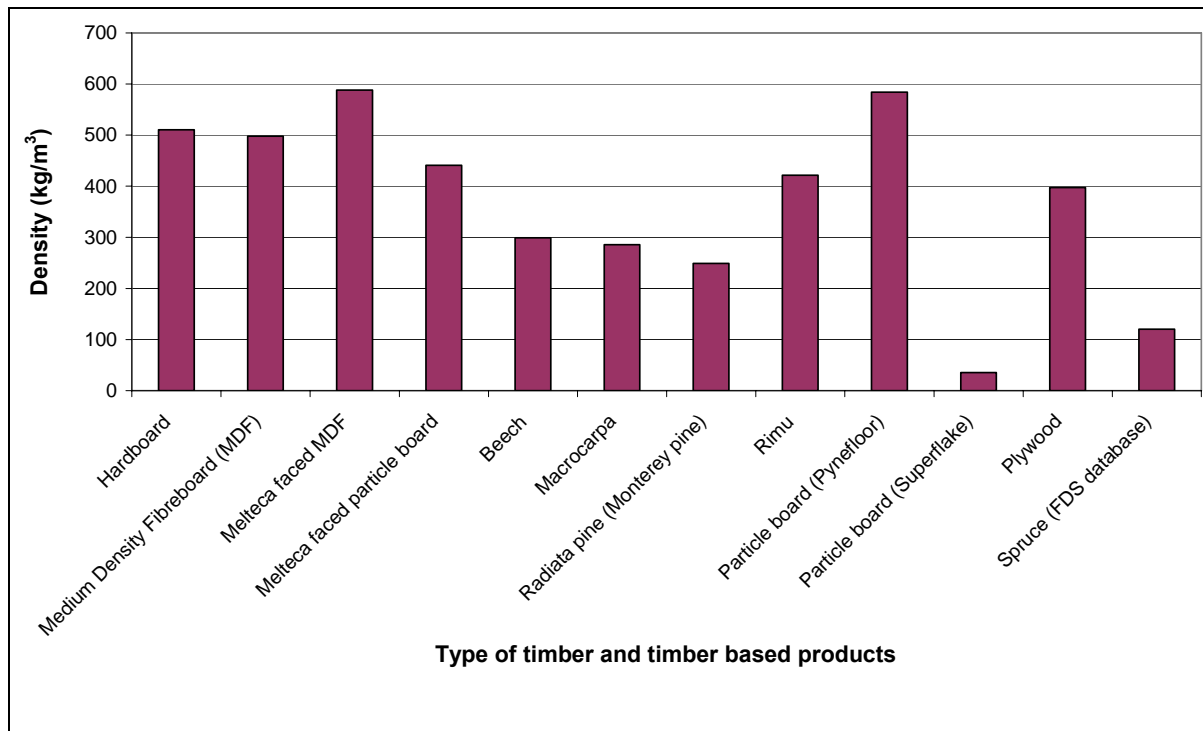


Figure 6-7: Measured char density for the timber and timber based products

The samples were burnt using the cone calorimeter until there is a predominant char depth layer. In another word, the samples were actually a combination of charred layer and uncharred layer (virgin material) as indicated in Figure 6-8. However, only the charred layer was used to measure the char density. A summary of the results is shown in Figure 6-7.

There are two reasons in selecting this technique to measure the char density of the samples:

- No equipments are available in the laboratory to measure char density and;
- Char will break into small pieces as it pyrolyses and becomes flakes. Hence it is very difficult to measure char density.

Therefore the samples were burnt until there is a predominant charred layer and the char densities were obtained using a mass volume approach; where the mass of the charred layer was measured by subtracting the mass of the virgin material to the total mass of the sample, while the volume is measured using digital callipers (i.e. multiplying the breadth, length and thickness to approximate the volume of char).

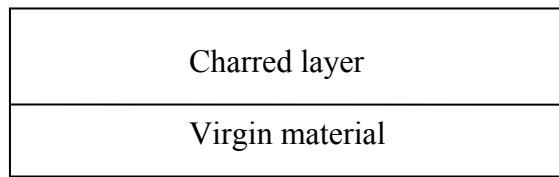


Figure 6-8: Sample for measuring char density

6.5 Experimental Procedure of the Hot Disk Test

All eleven timber and timber based products were tested to determine their thermal transport properties. This is carried out by using the Hot Disk Thermal Constants Analyser, which is also known as the Hot Disk test. It consists of a variety of transient plane source probes connected to a computerised control unit; where the main components are: Hot Disk sensor, Keithley 2400 Sourcemeter, PCMCIA/IEEE interface and computer with Hot Disk Thermal Constants Analyser Software installed. Figure 6-9 shows the basic setup of the Hot Disk test; where the main components are indicated.

All experiments are carried out in the temperature control room where the temperature is adjusted to 21°C with a humidity of 50%. The reason for conducting the experiments in a temperature control room is that it helps to minimise the influence of air currents during the Hot Disk test. Instructions for using the Hot Disk test can be found in the user manual (Gustafsson 1998). Temperature Coefficient of the Resistivity (TCR) is a variable that is required for the Hot Disk test and it depends on the temperature of testing. As the temperature is kept constant at 21°C in the control room, a value of 0.00470 [1/K] is selected. In addition, the available probing depth is chosen to be 8 mm because the thickness of the samples is approximately 18mm with the exception of hardboard.

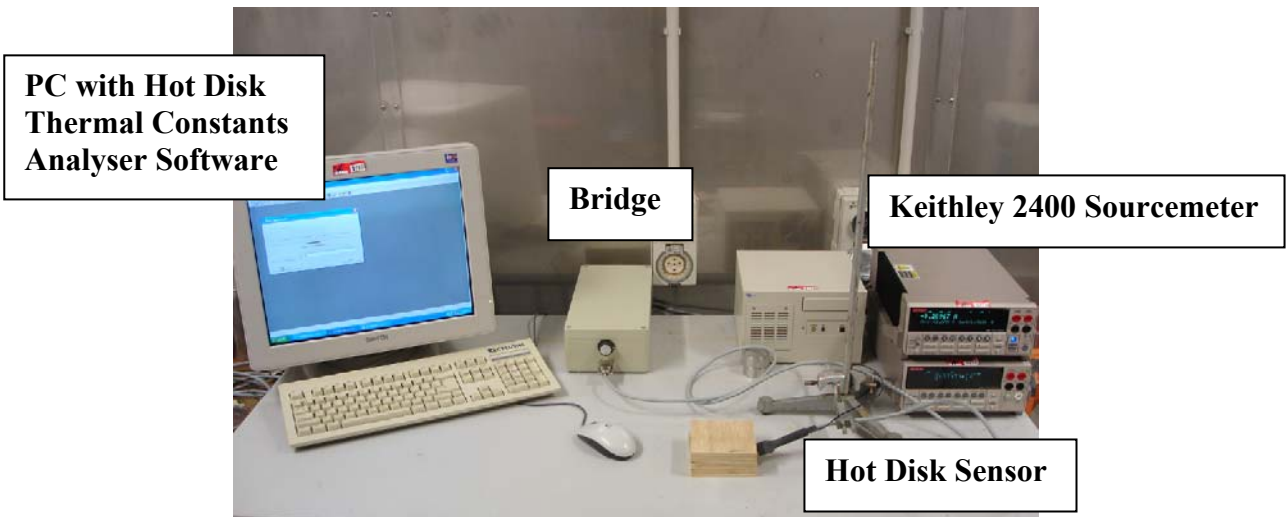


Figure 6-9: Hot Disk test setup in a temperature control room

Specimens of the timber and timber based products were placed directly into the Hot Disk Thermal Constants Analyser for evaluation of their thermal transport properties; where the Hot Disk sensor is sandwiched horizontally between the two identical specimens as indicated in Figure 6-10. For the current study, a designation number of “Spiral 4921” is selected for the Hot Disk sensor which has an equivalent length of 9.21 mm in radius. Measurements were obtained with the output of power as 0.2 W and the selected measuring time varied from 160s to 320s depending on the materials.

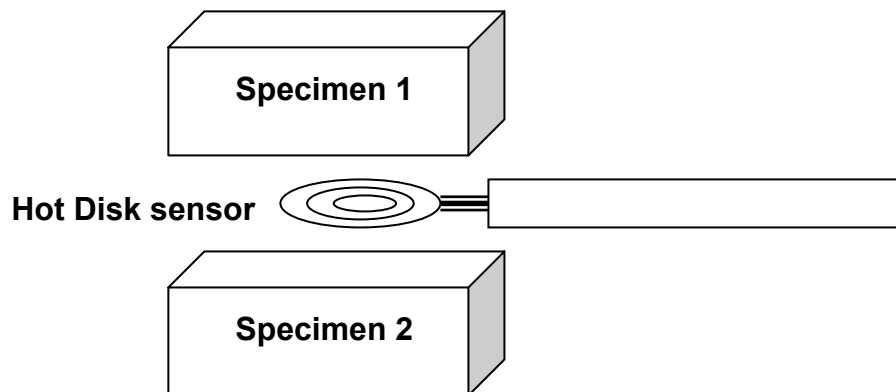


Figure 6-10: Schematic of experimental configuration for measuring the thermal properties of a pair of specimens

The Hot Disk analyser samples 200 points during the test and selected points for the quantitative analysis vary between 10 and 200. The starting and ending points are selected

accordingly to ensure the parameters “Temperature Increase” (TI) and “Total to Characteristic Time” (TCT) were satisfactory. A total of five Hot Disk tests are carried out for each specimen and an average value was used as the final input for FDS4.

Both TI and TCT are the most important variables in deciding whether the thermal conductivity and heat capacity per unit volume are accurate. The thermal transport properties are only acceptable if a green light bulb appears for TI and TCT. If a yellow light bulb appears, then either the measuring time or the output of power (or both) needs to be adjusted according to acquire a green light bulb for both the TI and TCT. The recommended value for the TI term is in between 3K and 5K, while the value for the TCT term ranges from 0.5 to 0.7.

After measuring both the thermal conductivity and specific heat capacity of all the materials, the virgin material was put in the cone calorimeter to burn until there is a predominant char depth layer as mentioned previously in Section 6.4. The procedure for the charring of the virgin wood is described in Chapter 5. The Hot Disk test procedure is again followed for these charred materials to obtain the thermal transport properties. It should be noted that this time the density of the charred material is used to calculate the specific heat capacity; instead of the density of the virgin material.

Unlike the flat surfaces specimen provided by the virgin material, a bow shaped is formed after the wood is burnt and charred as shown in Figure 6-6. This makes the measurement of the thermal transport properties in a Hot Disk test very difficult. Therefore, when the Hot Disk test is carried out for the charred specimens, a weight is put on top of the specimen to ensure that the two specimen’s surfaces are in contact with the Hot Disk sensor.



Figure 6-11: Testing of calcium silicate specimen using the Hot Disk test

In addition, the thermal transport properties for calcium silicate (dummy specimen for the calibration of the LIFT test) are determined. Figure 6-11 illustrates the Hot Disk test performed for calcium silicate specimens.

6.6 Results from the Hot Disk Test

The measured response of the Hot Disk sensor is analysed using the built-in software to determine both the thermal conductivity [W/m.K] and heat capacity per unit volume [MJ/m³.K] of the specimens. Note that the specific heat capacity [kJ/kgK] is not directly determined from the Hot Disk test. Therefore the specific heat capacity of the specimen is obtained by dividing the heat capacity per unit volume obtained with the density of the specimen. A summary of the thermal transport properties for both the virgin and charred materials is tabulated in Figure 6-1 below. All of the results from the Hot Disk test are given in Appendix C.

It should be noted that the calcium silicate which is the material used for the dummy specimen as required in the ASTM fire standards in the LIFT test is also included in the figures below for comparison. In addition, the thermal transport properties for ‘Spruce’ which is the found in the FDS4 database, is also included for reference. As wood species ‘Spruce’ is the only example provided on the use of the charring fuels model where limited information is given in the FDS4 technical guide; therefore it is also used for comparing with other timber and timber based products.

Table 6-1: Thermal transport properties for virgin and charred materials

Material	Average Density (kg/m ³)	Average Thermal Conductivity (W/mK)	Average Specific Heat Capacity (kJ/kgK)	Average Char Density (kg/m ³)	Char Average Thermal Conductivity (W/mK)	Char Average Specific Heat Capacity (kJ/kgK)
Hardboard	844	0.24	1.06	510	0.21	0.87
Medium Density Fibreboard (MDF)	647	0.18	0.77	498	0.10	0.51
Melteca faced MDF	793	0.22	1.2	588	0.14	0.96
Melteca faced particle board	635	0.20	1.2	441	N/A	N/A
Beech	556	0.19	0.72	299	0.10	0.74
Macrocarpa	566	0.20	0.61	285	0.08	0.56
Radiata pine (Monterey pine)	438	0.17	0.50	249	0.09	0.90
Rimu	634	0.22	0.75	422	0.10	0.43
Particle board (Pynefloor)	650	0.23	1.2	584	0.10	0.70
Particle board (Superflake)	670	0.22	1.3	35	N/A	N/A
Plywood	503	0.18	0.58	397	0.080	0.78
Spruce (from FDS database)	450	0.13	N/A	120	0.077	0.68
Calicum Silcate	1055	0.31	0.77	N/A	N/A	N/A

6.6.1 Virgin Materials

A summary of both the thermal conductivity and the specific heat capacity of the timber and timber based products are illustrated in Figure 6-12 and Figure 6-13 respectively. The thermal conductivity for the timber and timber based products ranges from 0.17 W/m.K for Radiata Pine to 0.24 W/m.K for Hardboard. In general, the thermal conductivity is similar for both the timber and timber based products, which is shown by the narrow range in the figure. Hence, there are little differences in the thermal conductivity for the timber and timber based products.

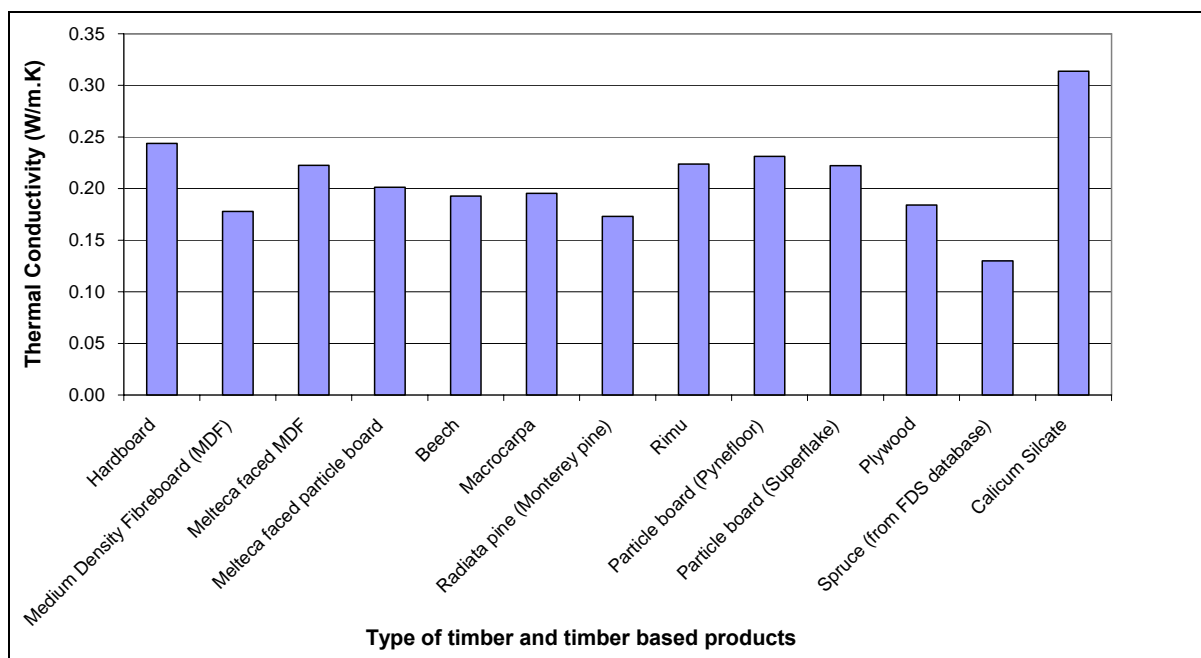


Figure 6-12: Thermal conductivity (average) for each timber and timber based product

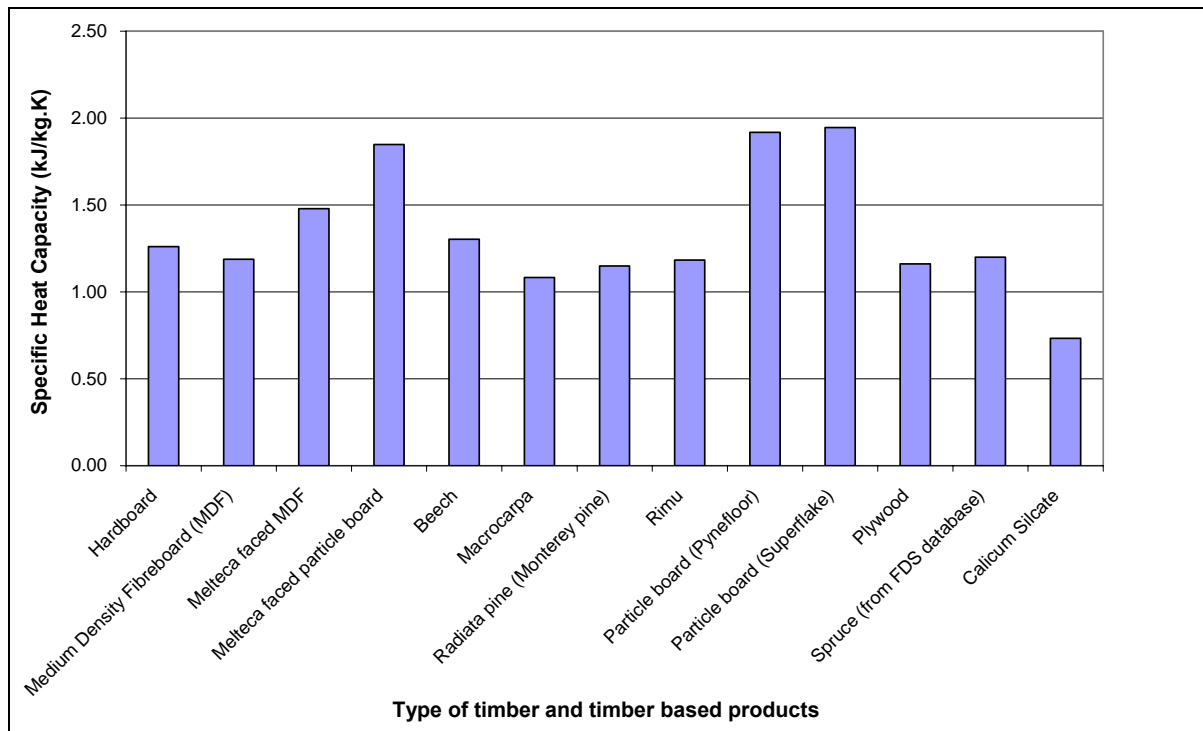


Figure 6-13: Specific heat capacity (average) for each timber and timber based product

As for the specific heat capacity of the timber and timber based products, it ranges from 1.08 kJ/kg.K for Macrocarpa to 1.92 kJ/kg.K for Pynefloor particle board.

The thermal conductivity and specific heat capacity for the calcium silicate is determined to be 0.31 W/m.K and 0.75 kJ/kg.K respectively. Calcium silicate has a higher thermal conductivity and lower specific heat capacity. This is expected as the characteristic of a calcium silicate is to dissipate heat energy as quickly as possible and minimise the heat energy stored within the material. As a result, an accurate heat flux reading can be obtained during the calibration of the LIFT test.

Both the measured thermal conductivity and specific heat capacity are compared to the values found from literature (Incropera and DeWitt 2001) as illustrated in Figure 6-14 and Figure 6-15 respectively. It indicated that the measured thermal conductivity is only slightly higher than the values from literature i.e. the measured thermal conductivity is no greater than 0.8 W/m.K of the literature value. On the other hand, the measured heat specific capacity is very similar to those found in literature.

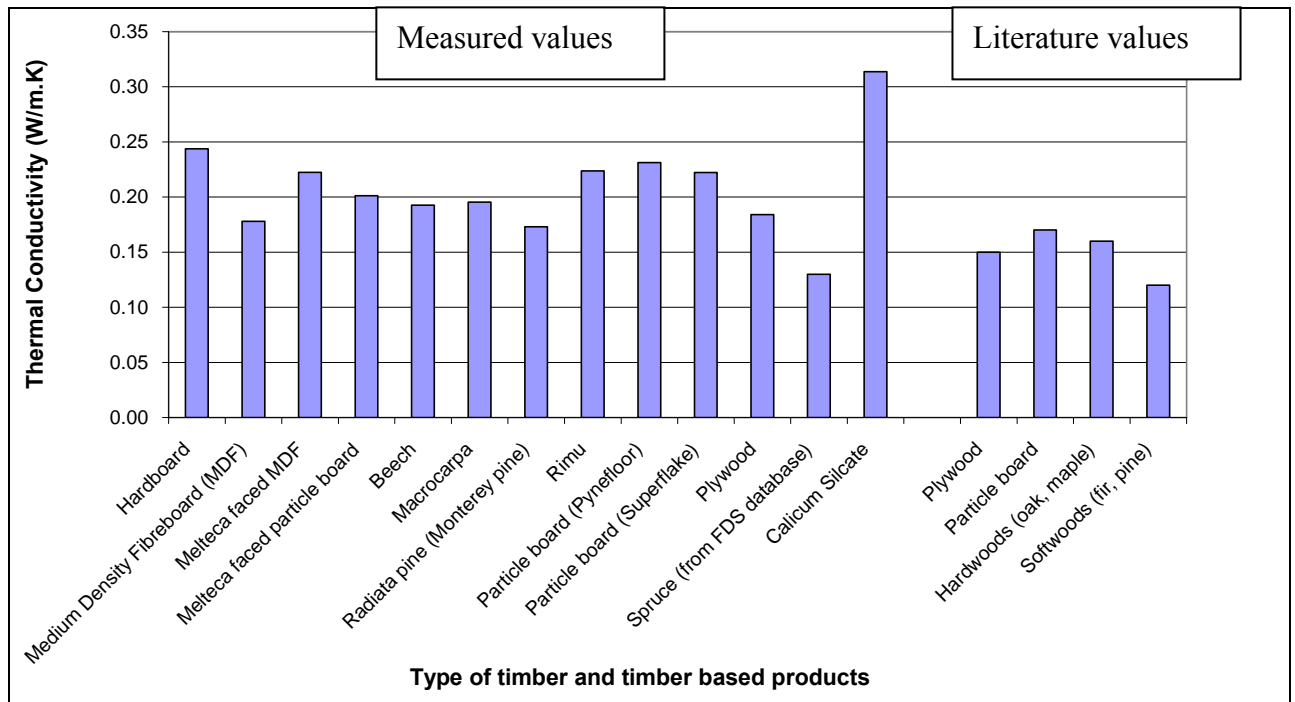


Figure 6-14: Comparison between the measured thermal conductivity and literature values

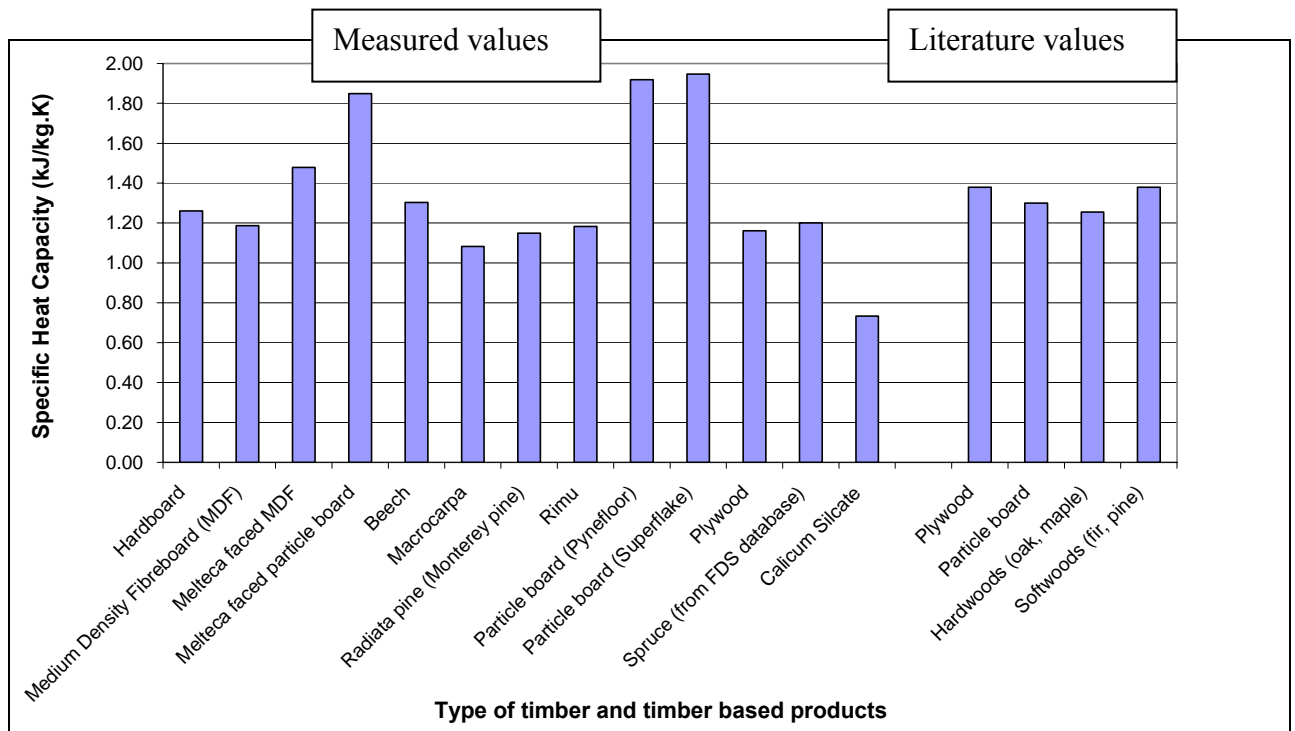


Figure 6-15: Comparison between the measured specific heat capacity and literature values

6.6.2 Charred Materials

Figure 6-16 and Figure 6-17 show the thermal conductivity and specific heat capacity for the charred materials. It indicates that the thermal conductivity for the charred materials varies from 0.08 W/m.K for Macrocarpa to 0.21 W/m.K for Hardboard. It is found that the thermal conductivity for most timber and timber based products is approximately 0.1 W/m.K with the exception of Hardboard where the thermal conductivity is over 0.2 W/m.K (twice as much as the other materials). This is most likely due to the very thin layer of the charred Hardboard specimen when compared to the other materials as it was outside the range for the Hot Disk Test method.

Meanwhile, the specific heat capacity of the charred materials ranges from 0.43 kJ/kg.K for Rimu to 0.96 kJ/kg.K for Melteca faced MDF. It should be noted that the char density plays an important role in calculating the specific heat capacity; where the char density is determined by estimating the volume of the charred material.

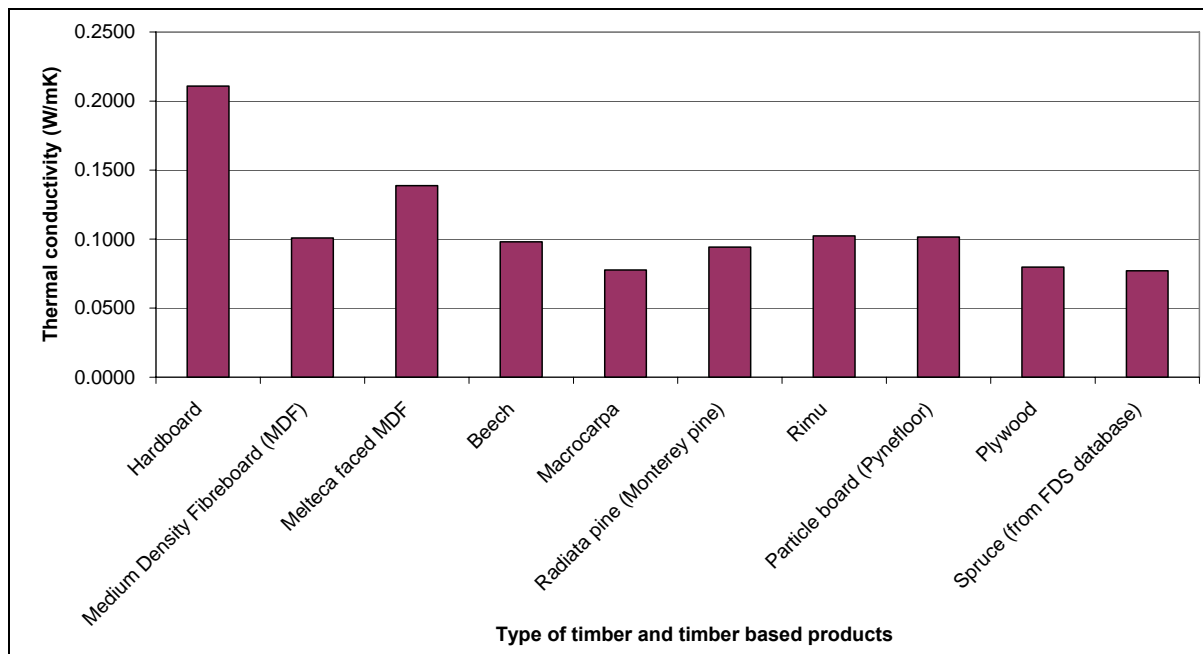


Figure 6-16: Thermal conductivity (average) for charred materials

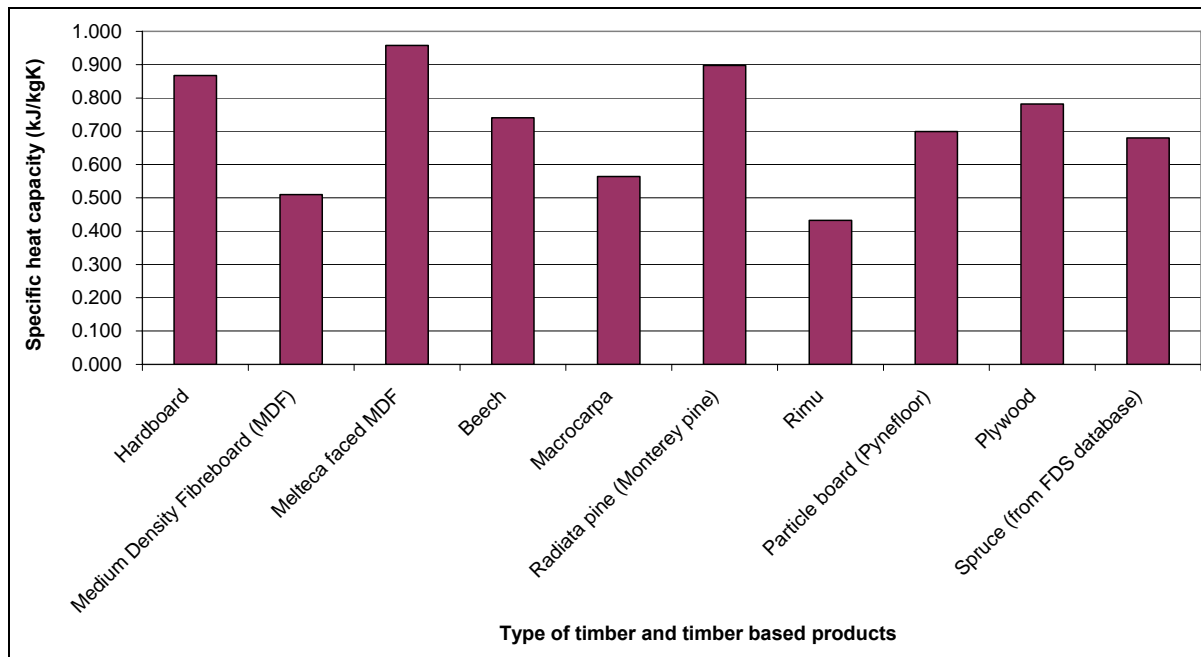


Figure 6-17: Specific heat capacity (average) for charred materials

In summary, the transient plane source method has been applied to measure the thermal conductivity and specific heat capacity of timber and timber based products for both virgin and charred material. The obtained results are in reasonable agreement with ‘Spruce’ as a Surface ID found in the FDS4 database and is adapted in modelling flame spread in FDS4.

7 Setting up and calibration of the LIFT apparatus in FDS4

This chapter describes the process of setting up the LIFT apparatus in FDS4; where the calibration of the LIFT test is performed in FDS4 to ensure that the heat flux profile along the specimen is adequate for testing flame spread. In addition, the actual heat flux distribution along each of the timber and timber based products specimens that is applied in FDS4 to carry out flame spread tests is determined.

7.1 Geometries of the LIFT apparatus

The layout of the LIFT test apparatus is given in the ASTM E 1321-97a (2002) standards as shown in Figure 7-1 below; it indicates the basic configuration of the LIFT with regard to the position of the radiant panel and the specimen. The specimen is 806mm long and the radiant panel is 483 mm long. The position of the radiant panel is inclined at an angle of 15° to the specimen. The geometry of the LIFT apparatus is considered to be important as it is determines the amount of heat flux being exposed on the specimen. Therefore, the actual measurement of the LIFT apparatus is adapted when the specimen and the radiant panel are entered in FDS4.

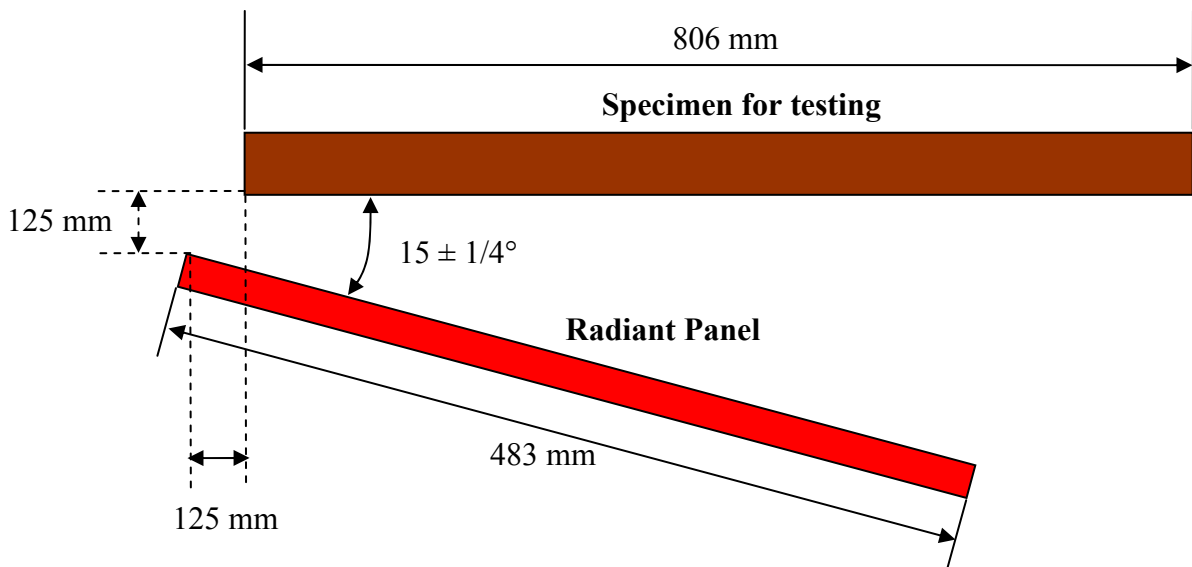


Figure 7-1: Arrangement of the specimen and radiant panel in LIFT (not to scale)

7.2 Calibration of Flux to the Specimen

The calibration of the LIFT apparatus is given in the “Standard Test Method for Determining in Material Ignition and Flame Spread Properties”, ASTM E 1321 – 97a (2002), where it consists of the required heat flux level at different locations along a dummy specimen. The dummy specimen is a non-combustible insulating board and its function is to stabilise the operating condition of the equipment, mounted in the apparatus in the position of the specimen and removed only when a test specimen is to be inserted.

The typical flux levels required for the specimens are reproduced in Table 7-1 below. The ASTM standards require that the heat flux to be as accurate as it can be, particularly at the 50 and 350 mm positions, while it must be within 10% of the typical values at other locations.

Table 7-1: Calibration of Flux to the Specimen (ASTM Committee E-5 on Fire Standards. 2004b)

Distance From Exposed End of the Specimen, mm	Typical Flux Levels at the Specimen, kW/m ²	Calibration Position to be Used, kW/m ² ^A
0	49.5	
50	50.5	50.5
100	49.5	
150	47.1	x
200	43.1	
250	37.8	x
300	30.9	
350	23.9	23.9
400	18.2	
450	13.2	x
500	9.2	
550	6.2	x
600	4.3	
650	3.1	x
700	2.2	
750	1.5	x

^A An x indicates the fluxes at the additional six measuring positions required by the standard. The seven empty spaces represent the fluxes at the additional measuring positions recommended by the standard.

7.3 LIFT apparatus in FDS4

The numerical grids in FDS4 are simplified to increase the efficiency the model where all grid cells are made of rectangular blocks. According to the diagram shown in Figure 7-1, the

geometries of the LIFT apparatus do not conform to the rectangular grid; consequently either the specimen or radiant panel needs to be in a non continuous form. As the objective of this research is to ultimately determine the flame spread parameters of the timber and timber based products, the specimen is considered to be the most important term and needs to be in a continuous form to predict flame spread as accurately as possible. As a result, the radiant panel is constructed in FDS4 using rectangular obstructions in which the process is sometimes called “stair stepping”; where a series of rectangular blocks in steps are used as indicated in Figure 7-2.

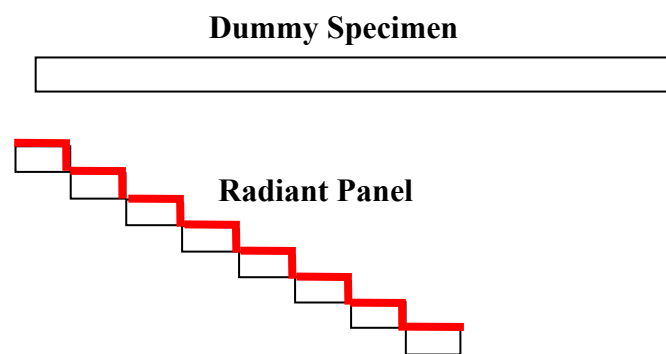


Figure 7-2: An overview of the layout of the LIFT apparatus in FDS4

Once the obstructions (radiant panel and dummy specimen) were created in FDS4 using the geometries indicated in Figure 7-1 each obstruction needs to be assigned with an appropriate surface identification to ensure that the obstruction behaves with the same function as specified in the ASTM E 1321-97a (2002) standards.

In calibrating the simulated LIFT apparatus, the radiant panel needs to provide adequate heat flux on the dummy specimen as indicated in Table 7-1. This is achieved by assigning a fixed temperature to the surface of the obstruction whose surfaces are exposed to the specimen. These surfaces are indicated by the thick dark lines as shown in Figure 7-2. The function “SURF_ID6” is used when specifying the surfaces with a fixed temperature.

As for the dummy specimen, it should be a non combustible insulating board having a thickness of roughly 20 +/- 5mm with a density of 750 +/- 100 kg/m³ as specified in the standard procedure. To simulate the type of material accurately in FDS4, the material properties need to be determined; these properties include the thermal conductivity, specific

heat capacity, density and thickness of the material. In the experiment carried out by Merryweather (2006), calcium silicate is used as the material of dummy specimen and again is used in the FDS4 simulation. From the Hot Disk test performed as discussed in Chapter 6, the properties of calcium silicate were measured and are indicated below and entered into the FDS4 model.

- Thermal conductivity of calcium silicate board = 0.3442 W/mK
- Specific heat capacity of calcium silicate board = 0.6697 kJ/kgK
- Density of calcium silicate board = 1080 kg/m³.
- Thickness of the calcium silicate board = 19 mm

The calibration of the simulated LIFT apparatus is performed by inserting a heat flux meter onto the surface of the dummy specimen in FDS4. This then enables the heat flux along the dummy specimen to be measured and compared with the requirements from the standard. The function “THCP” is used to record the incident heat flux on the specimen as a function of time. Consequently, QUANTITY value is selected to be “GAUGE HEAT FLUX”. This parameter is defined in FDS4 as the amount of energy that would be absorbed if the surface were cold and is more appropriate to use when comparing predictions with experimental measurements (McGrattan and Forney 2004).

Since FDS4 cannot locate the appropriate surface for taking measurements, the parameter IOR is used when designating a solid phase quantity. For the chosen geometries, the direction of measurements on the THCP is specified to be “IOR=-2”, where the orientation of the solid surface is in the negative direction. As a result, the heat flux from the radiant panel can be measured.

A total of 16 gauge heat fluxmeters were specified on the dummy specimen. This was to simulate the water based heat fluxmeters required in the ASTM E 1321 97a (2002). Figure 7-3 illustrates the position of the fluxmeters along the dummy specimen which is used for the calibration the LIFT apparatus.

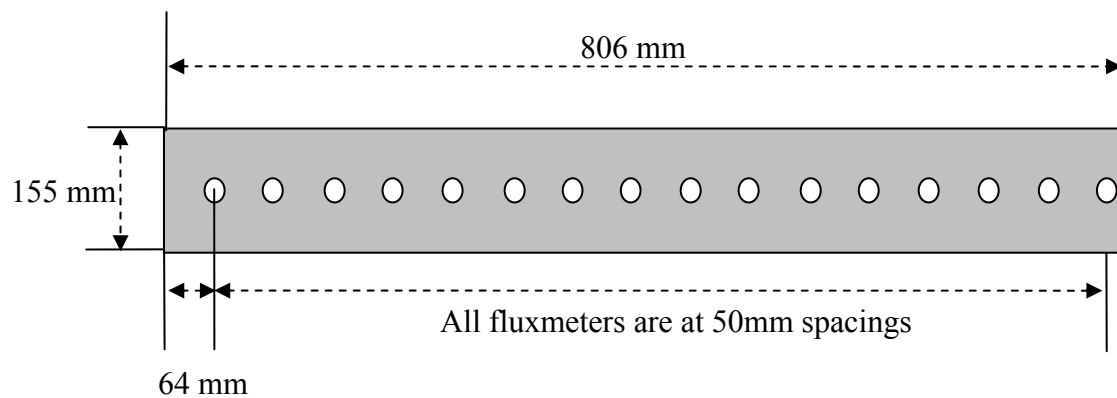


Figure 7-3: Positions of fluxmeters along the dummy specimen

Beside the thermocouples along the dummy specimen, a FDS4 boundary file for the gauge heat flux is also specified as a type of output in the FDS4 model. This allows FDS4 to record the gauge heat flux for all solid surfaces, which then is used to visualise the heat flux along the dummy specimen in Smokeview. However, the boundary file for the radiant panel is unnecessary since the only information that is required for calibration is the heat flux on the dummy specimen. Therefore, a term “BNDF_BLOCK =FALSE” is added on the obstruction line for the radiant panel.

In addition, a backing board is added to the back of the dummy specimen as required by the ASTM standards to satisfy the theoretical analysis assumption of no heat loss through the specimen. The thickness of the backing board is approximately 25 +/- 5mm. In this research, calcium silicate is also used as the material for the backing board; therefore, identical surface identification is employed to the backing board as it did for the dummy specimen.

Figure 7-4 shows the basic setup of the simulated LIFT apparatus in Smokeview; where it includes the radiant panel, the dummy specimen and the gauge heat flux meters for calibration.

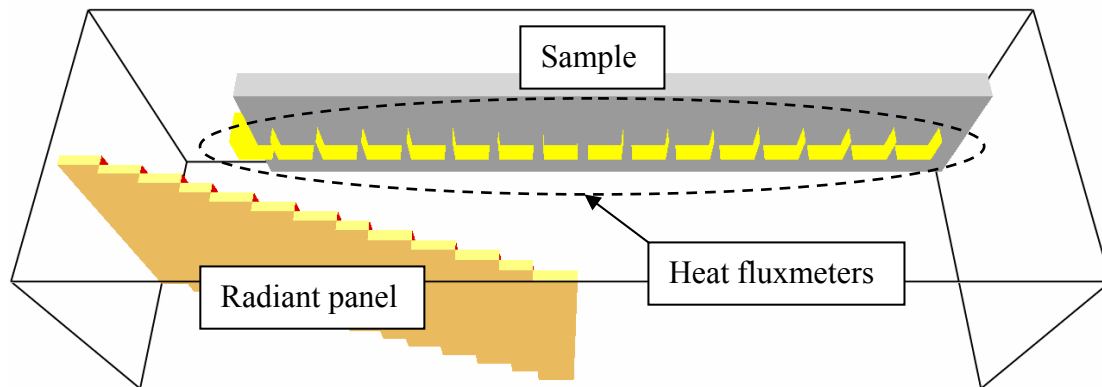


Figure 7-4: A snap view of the LIFT apparatus setup from Smokeview

The radiant panel was defined by 0.4 m by 0.1 m rectangular obstructions, where its incline angle to the dummy specimen is at 14° instead of 15° required by the standards. This is not considered to be an issue since the most important part in the calibration process is to have the correct heat flux distribution along the dummy specimen.

Two types of radiant panel setup are examined: (1) constant temperature and (2) different temperature along the radiant panel. This is to determine which type of setup can demonstrate a better heat flux distribution along the dummy specimen when compared to the requirements. Additionally, the radiant panel having a steeper angle (by changing the geometry of the rectangular obstructions) is also tested to determine whether this setting would correspond to a better the heat flux profile over the specimen.

It should be noted that the thermal properties of the dummy specimen are actually measured using the hot disk test as described in details in Chapter 6; where the thermal conductivity and the specific heat capacity of the specimen are determined.

7.4 Other Input Variables for the LIFT apparatus in FDS4

The LIFT test procedure set out in ASTM E 1321 97a (2002) describes the space for conducting tests. These details include the test area, the location of the apparatus inside the area, the surrounding temperature, room drafts and the fume exhaust system. By making use of this information, the FDS4 model is set to simulate the LIFT test as accurately as possible. The following sections will list all of the parameters that are entered into the FDS4 model.

From the geometries given in Figure 7-1, the domain size of the LIFT apparatus in FDS4 is selected to be 0.95m long, 0.3m width and 0.3 m high in the x, y and z direction, respectively. The ambient room temperature is required to remain at 25 +/- 5°C, therefore both the ambient temperature (TMPA) and temperature outside of the computational domain (TMPO) is set at 25°C.

As a trial model, a grid size of 10mm was selected in the x, y and z directions. Later on, the accuracy of the chosen grid sizes in the FDS4 will be examined; where different grid sizes are tested to assess the effect that the grid size has on predicting the flame spread in FDS4.

The length of simulation time (TWFIN) of the LIFT test is chosen to be 1000 seconds (~ 16 minutes), which is the time when modelling finishes. This is decided as it was found from the experimental results that no flame spread would occur after 1000 seconds.

All surface boundaries of the domain were open in FDS4; therefore, the term SURF_ID='OPEN' was entered on the &VENT CB= line for the surface boundaries 'XBAR0', 'XBAR', 'YBAR0', 'YBAR', 'ZBAR0' and 'ZBAR' to create vents.

The approach of selecting the corresponding temperature on the radiant panel was carried out using a trial and error method; where the temperature on the radiant panel wall (TMPWAL) was adjusted to match the heat flux distribution required by the standards.

Number of output dumps per calculation (NFRAMES) was selected to be 1000, which was the default value. This enabled 'thermocouple' data and boundary data to be saved every second (i.e. TWFIN/NFRAMES = 1000/1000).

Only one reaction can be specified in a FDS4 model; therefore, the reaction is chosen carefully to ensure the combustion characteristics of the material were captured. The REAC line in the FDS4 input comprises various parameters associated with the gas phase reaction of fuel and oxygen. For the calibration of the LIFT apparatus model, methane was selected as the reaction in the model. This was because the standards specified that the fuel gas used in the LIFT shall be either natural gas or methane. However, the reaction variable in FDS4 will not have a major impact on flame spread as it is more to do with the visibility and heat release rate.

As FDS4 only allows one reaction input in the model and samples in the simulated flame spread tests will ignite and burn as wood, the most appropriate reaction to choose for the model would be wood i.e. & REACTION='WOOD'. The heat flux profile along the dummy specimen obtained from using wood as the reaction has been verified; where it provides a very similar heat flux profile to the one using methane as the reaction. Therefore using wood as the reaction in FDS4 is considered to be more appropriate. The reaction identification for wood comes from the FDS4 database and is reproduced below:

```
&REAC ID='WOOD'  
  FYI='Ritchie, et al., 5th IAFSS, C_3.4 H_6.2 O_2.5'  
  SOOT_YIELD = 0.01  
  NU_O2     = 3.7  
  NU_CO2    = 3.4  
  NU_H2O    = 3.1  
  MW_FUEL   = 87.  
  EPUMO2    = 11020. /
```

Additionally, no restart function should be carried out for the flame spread test. This is because restarting the FDS4 model will cause the heat flux to fluctuate during the initial stage and affect the heat flux being exposed on the specimen as a result. The FDS4 input for the calibration of the LIFT apparatus can be found in Appendix E.

7.5 Calibration results from FDS4

There are basically three different types of scenario being modelled to examine the effect they have on the heat flux distribution: (1) constant temperature on the radiant panel wall; (2) different temperature on the radiant panel wall; (3) radiant panel having a steeper inclined angle to the dummy specimen with varying temperature on the element. A full description of each scenario is tabulated in

Table 7-2. Eventually, the scenario that meets the requirement in the standards will be used to carry out flame spread tests. This section shows the results of the calibration of the LIFT apparatus obtained from FDS4; where the heat flux measured against the distance along the dummy specimen are plotted.

Table 7-2: Description of calibration scenarios

Scenario	Name	Description
1	840 with dummy	A temperature of 840°C is set on the surfaces of the radiant panel which are exposed to the surface of the specimen
2	845 with dummy	A temperature of 845°C is set on the surfaces of the radiant panel which are exposed to the surface of the specimen
3	850 with dummy	A temperature of 850°C is set on the surfaces of the radiant panel which are exposed to the surface of the specimen
4	860 with dummy	A temperature of 860°C is set on the surfaces of the radiant panel which are exposed to the surface of the specimen
5	850 front with 860	A temperature of 850°C is set on the surfaces of the radiant panel which are exposed to the surface of the specimen with the exception for the following section: From 150 to 270mm along the radiant panel is set at 860°C
6	840 front with 850 and 860	A temperature of 850°C is set on the surfaces of the radiant panel which are exposed to the surface of the specimen with the exception for the following sections: From 0 to 80mm along the radiant panel is set at 840°C From 150 to 270mm along the radiant panel is set at 860°C
7	850 front with 820	A temperature of 850°C is set on the surfaces of the radiant panel which are exposed to the surface of the specimen with the exception for the following section: From 340 to 490mm along the radiant panel is set at 820°C
8	850 front with 800	A temperature of 850°C is set on the surfaces of the radiant panel which are exposed to the surface of the specimen with the exception for the following section: From 420 to 490mm along the radiant panel is set at 800°C
9	850 with Dummy steeper	A temperature of 850°C is set on the surfaces of the radiant panel which are exposed to the surface of the specimen similar to Scenario 3. However, the radiant panel has a steeper slope.

Figure 7-5 is a snapshot of the gauge heat flux distribution along the dummy specimen from Smokeview. From the figure, it provides a visual perspective of the heat flux on the dummy specimen. As indicated by the legend in the figure, the maximum heat flux is no more than 55 kW/m^2 which is comparable with the requirement of 50.5 kW/m^2 .

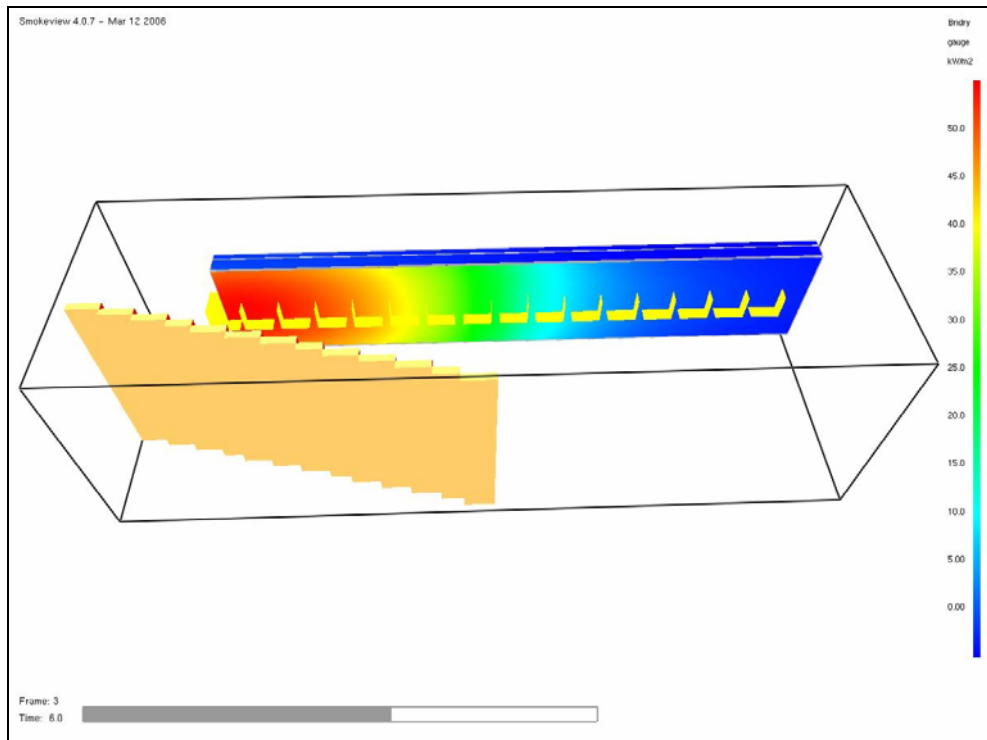


Figure 7-5: Snapshot of the heat flux along the specimen in Smokeview

Figure 7-6 and Figure 7-7 show the comparison of gauge heat flux profile along the dummy specimen with the requirements from the standards for different scenarios. It indicated that a similar heat flux pattern is obtained from the FDS4 model where the specified temperature on the radiant panel varied between 840°C and 860°C .

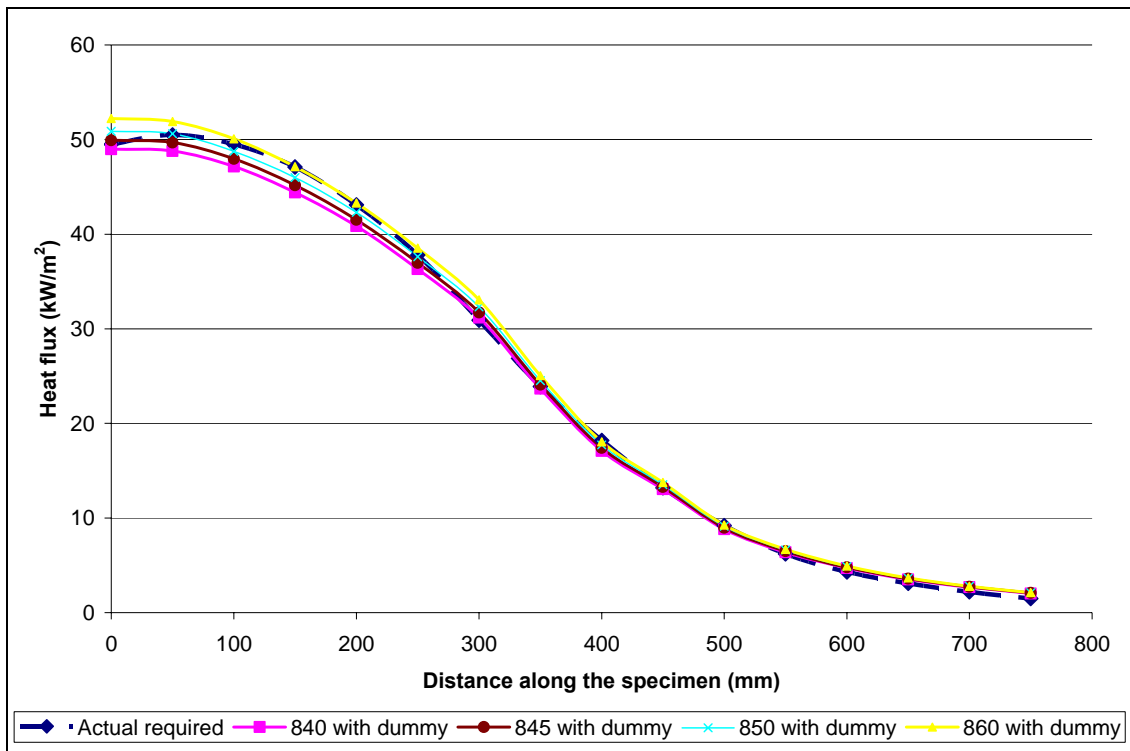


Figure 7-6: Heat flux over the dummy specimen for scenarios with constant temperature (i.e. Scenario 1 to 4)

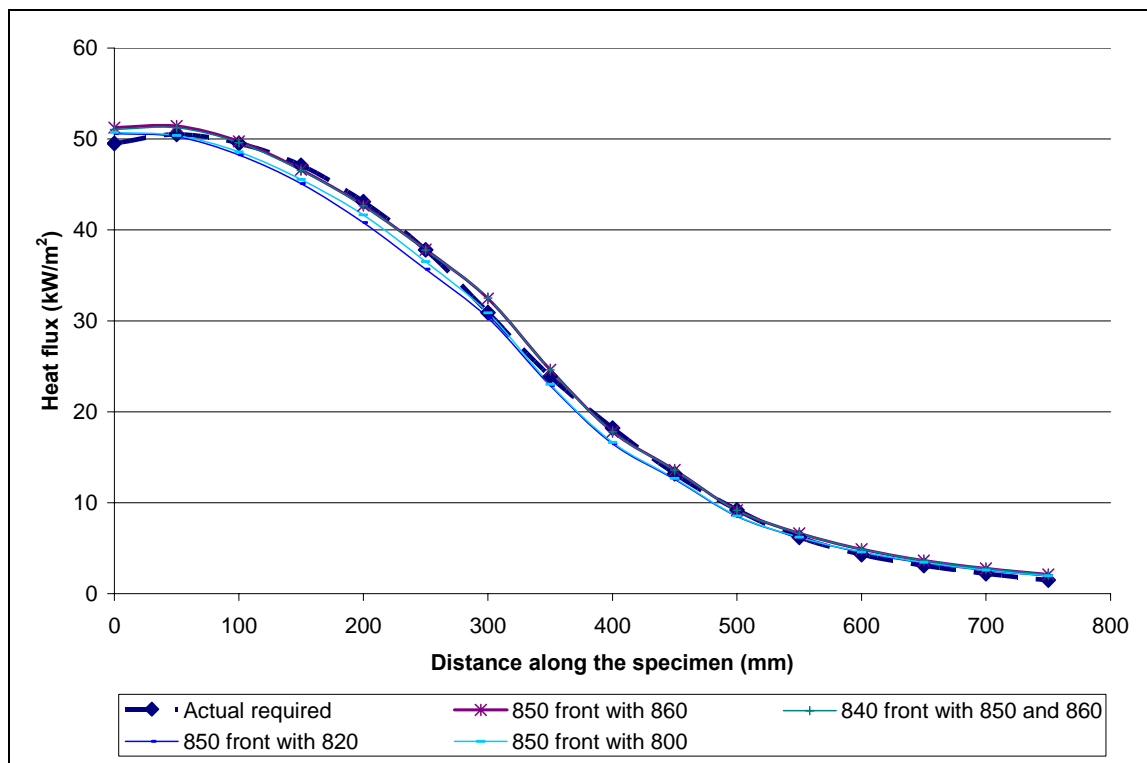


Figure 7-7: Heat flux over the dummy specimen for scenarios with varying temperatures (i.e. Scenario 5 to 8)

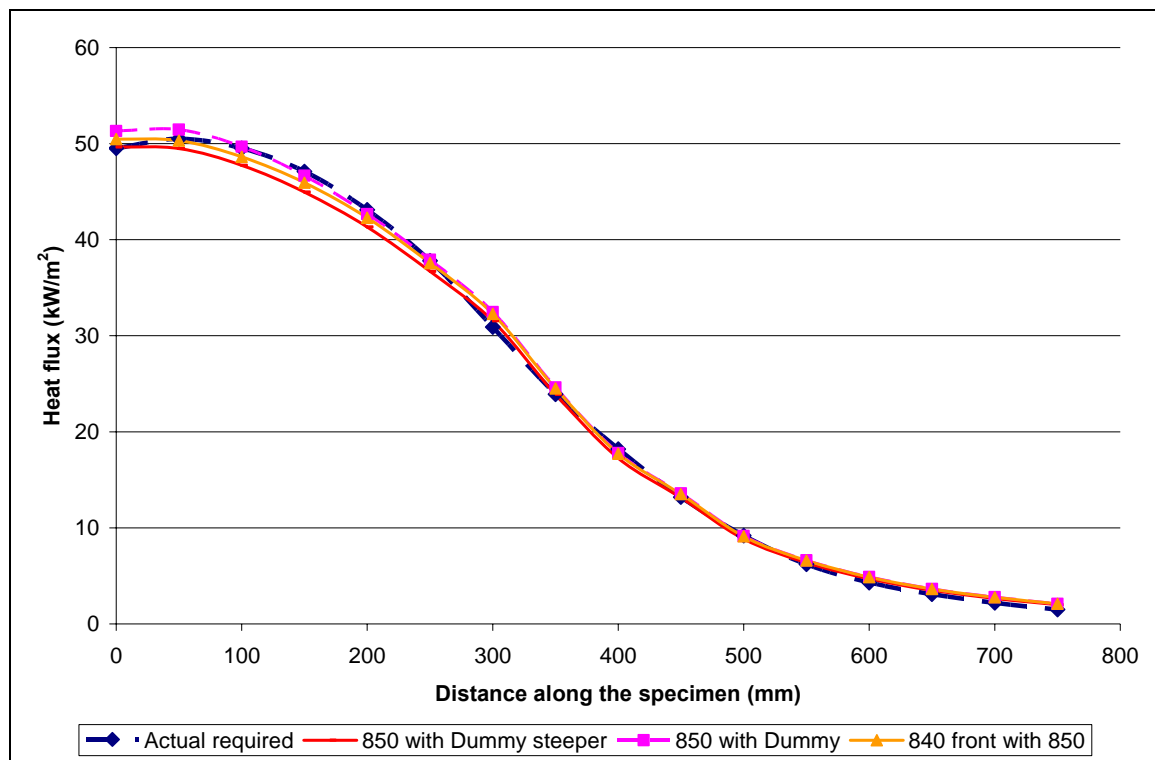


Figure 7-8: Heat flux along the dummy specimen for different scenarios

Many trial simulations were performed to find out the best scenario that matches the requirements in the standards, it is found that a temperature of 850°C on the radiant panel wall would give the best fit with the requirements. From Figure 7-8, it showed that the scenario with a steeper radiant panel is giving a lower heat flux distribution between 50 mm to 300 mm along the dummy specimen when compared to the other scenarios; therefore, this method will not be used. Additionally, the scenario with varying temperatures along the radiant panel surfaces appears to match well with the actual heat flux required, which is similar to a constant temperature. However, this will not be used as it is simpler to use a constant temperature throughout the radiant panel while getting a similar heat flux along the dummy specimen. Therefore, a temperature of 850°C is specified on the radiant panel wall to test whether the heat flux along the dummy specimen is within 10% of the standards required.

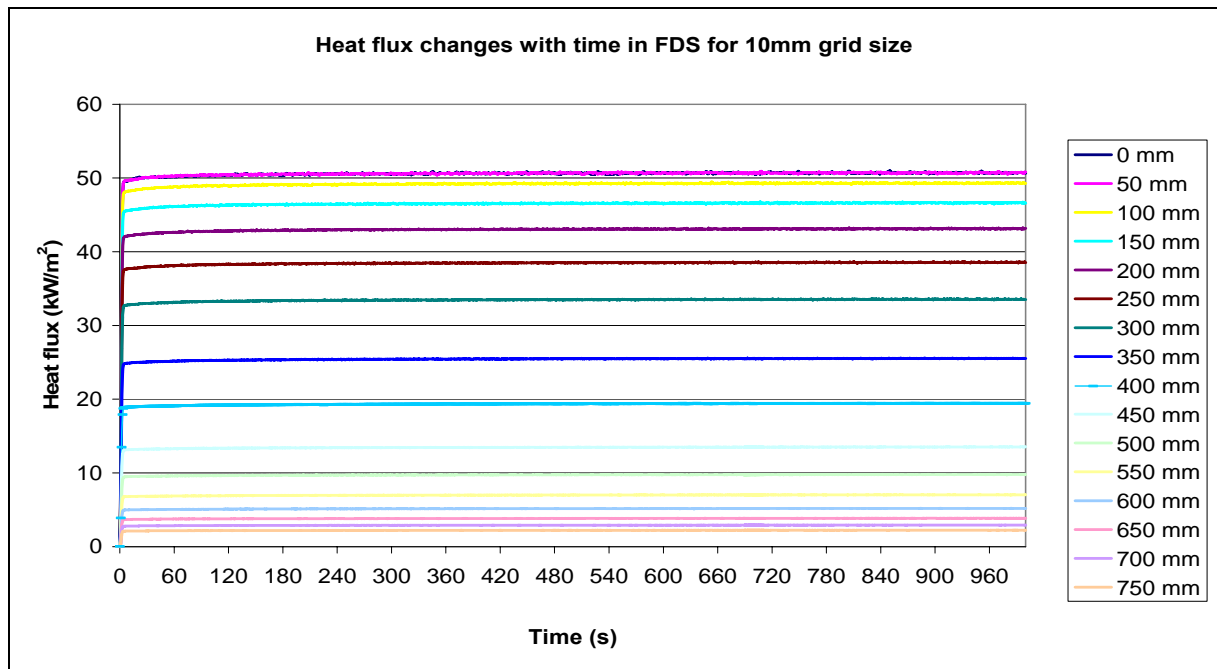


Figure 7-9: Heat flux changes with time along the specimen for 10mm grid size

Figure 7-9 is the plot of the heat flux measured against with time at different location along the dummy specimen when the constant temperature on the radiant panel is 850°C. As mentioned previously, the heat flux must be within 10% of the standards required.

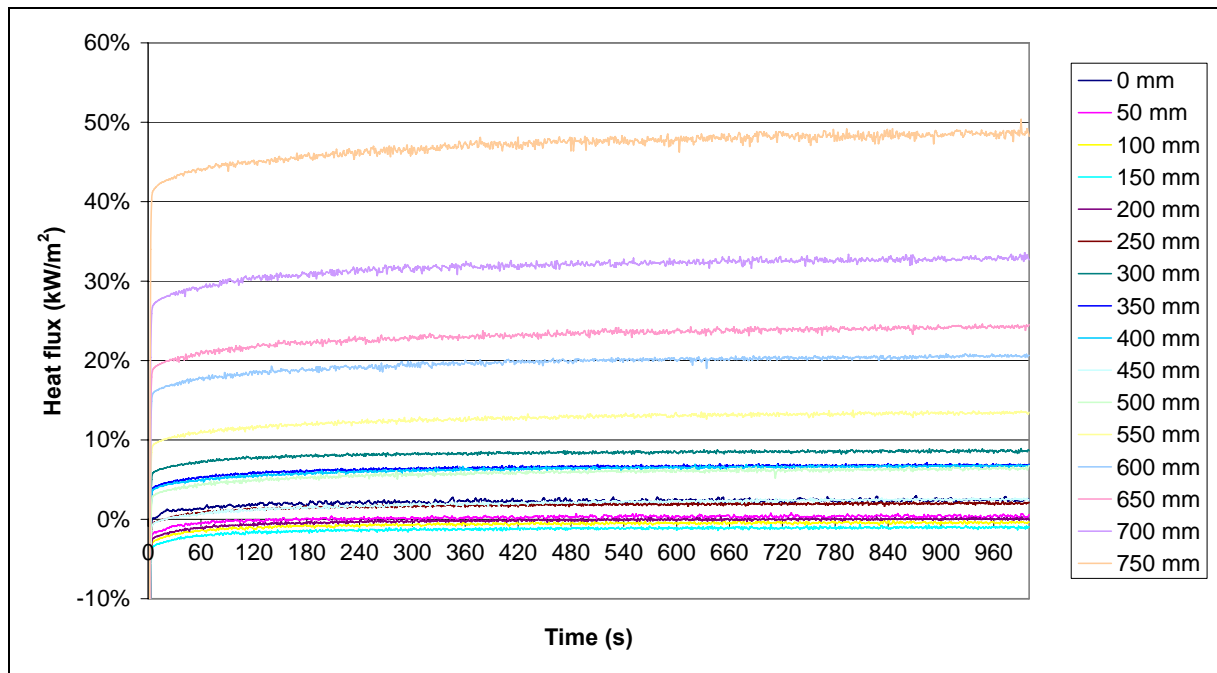


Figure 7-10: Percentage difference compared with the standards required against time for 10mm grid size

Figure 7-10 illustrates the percentage difference of the heat flux along the dummy specimen in FDS4 when compared the experimental results. It shows that the 10% margin is achieved up to 500mm along the dummy specimen. Meanwhile, for distances beyond 500 mm, the 10% error is breached and is considered to be not calibrated.

The reason for the significant increase in the percentage difference is due to the small heat flux being measured. As the LIFT test is designed so that the heat flux will decrease as the position along the specimen increases. This implies that the difference between the heat flux measured and the standards required is relatively large for lower heat fluxes and hence the position along the specimen increases.

However, it was found from the experimental results (Merryweather 2006) that the flame will not spread further than 500 mm along the specimens; therefore, using the specified geometries in the FDS4 model with a constant temperature of 850°C on the radiant panel is sufficient to perform flame spread test in FDS4.

Merryweather reported that “From 600mm onwards, the calibration results are outside the 10% limit, however this is beyond the limit of flame spread along the sample for the

materials tested, so was not considered to be important.” The plot of the calibration deviation from ASTM Fire Standard using the UC LIFT by Merryweather is reproduced as shown in Figure 7-11 below.

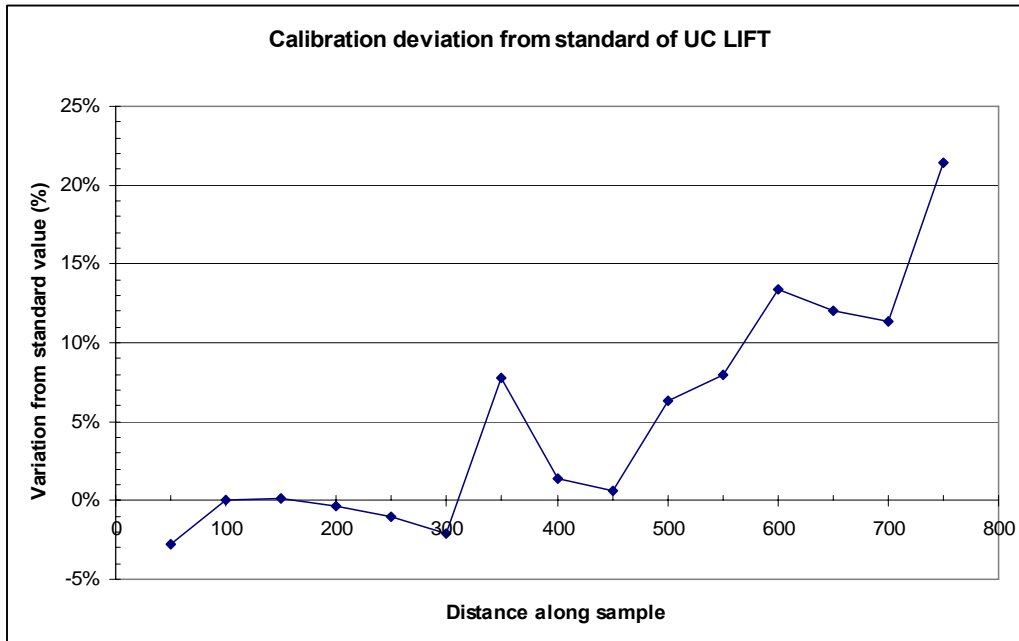


Figure 7-11: Variation from standard for LIFT calibration conducted by Merryweather (Merryweather 2006)

Additional checks are also performed at 50 mm and 350 mm along the dummy specimen as the standards require an exact match of the heat flux at both the 50 mm and 350 mm along the dummy specimen.

Figure 7-12 shows both the heat flux distribution at the 50 mm position and the percentage difference comparing to the requirements as specified in the standards. Furthermore, the heat flux attained at 50 mm is 50.0 kW/m^2 . This is considered to be an excellent match, in which it corresponds to a 0.2% error when compared to a heat flux of 50.5 kW/m^2 as required. In addition, it was found that FDS4 takes 25 simulated seconds for the heat flux to stabilise; i.e. steady state condition.

Meanwhile, Figure 7-13 is the plot for both the heat flux distribution at the 350 mm position along the dummy specimen and the percentage difference when compared to a heat flux of 23.9 kW/m^2 as required. The heat flux measured on the dummy specimen is found to be 25.0 kW/m^2 . Despite the percentage difference being found to be 7%, it is considered to be

an adequately calibrated heat flux distribution as they are relatively close to each other in terms of the degree of magnitude and is believed to have an insignificant impact on flame spread.

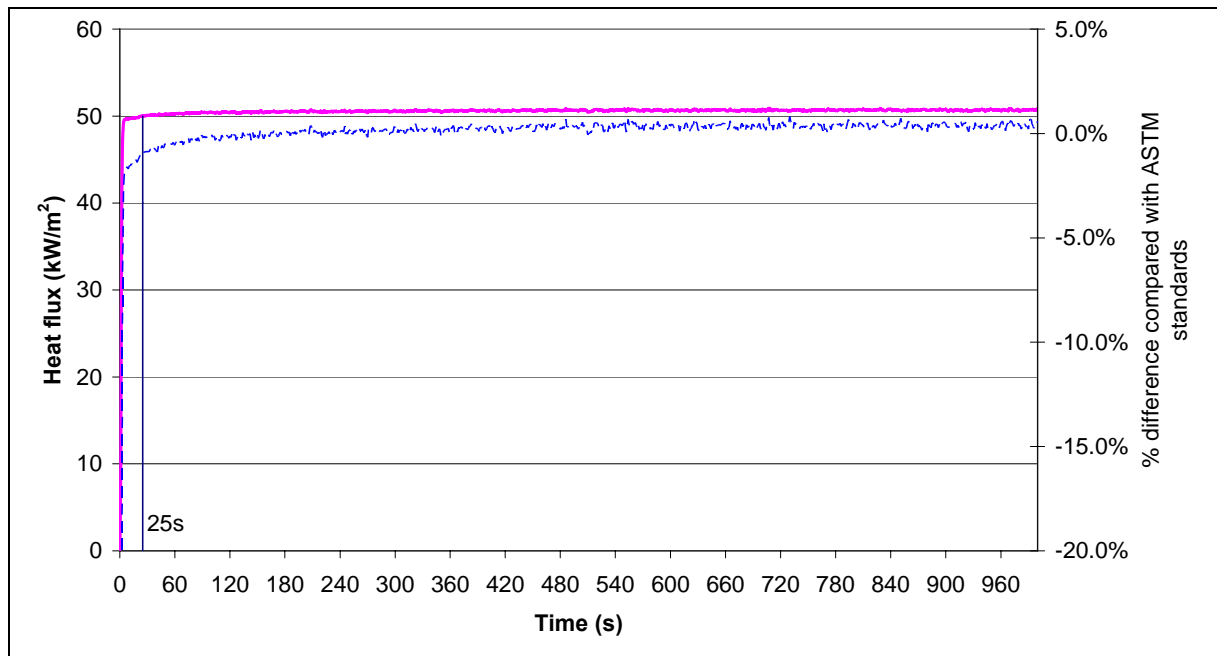


Figure 7-12: Heat flux changes with time at 50mm along the dummy specimen for 10mm grid size

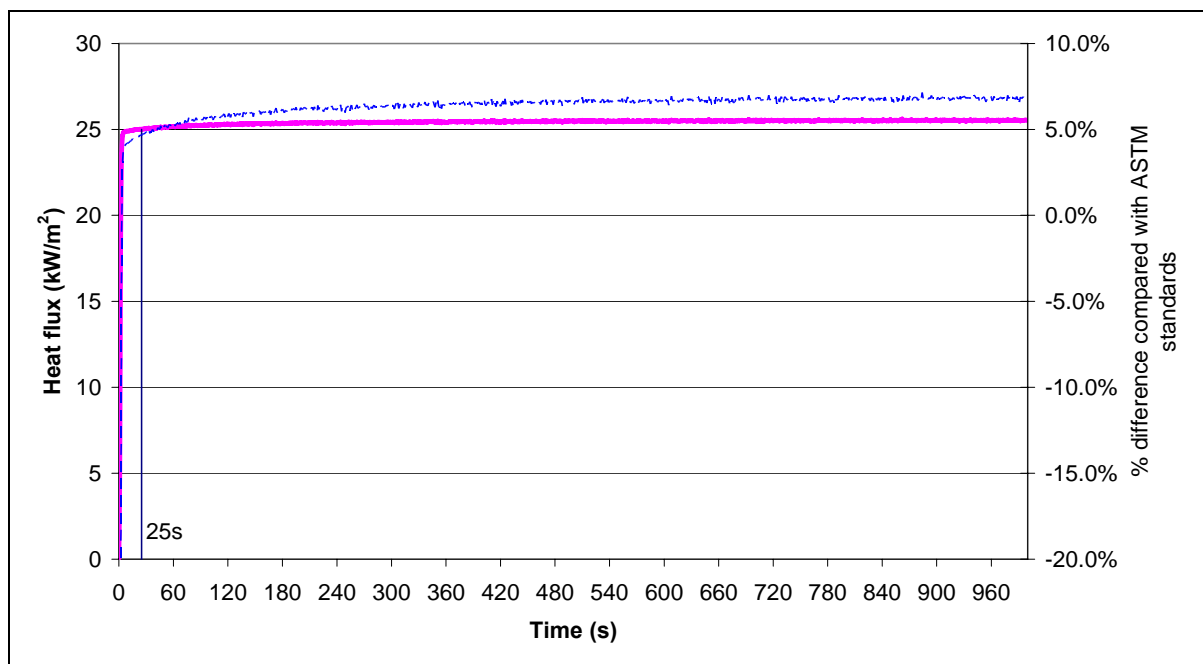


Figure 7-13: Heat flux changes with time at 350mm along the dummy specimen for 10mm grid size

Figure 7-14 compares the heat flux distribution along the dummy specimen obtained from FDS4 with the experimental results obtained by Merryweather (2006). It indicates that both heat flux profiles are similar to the required heat flux by ASTM E 1321 – 97a (2002).

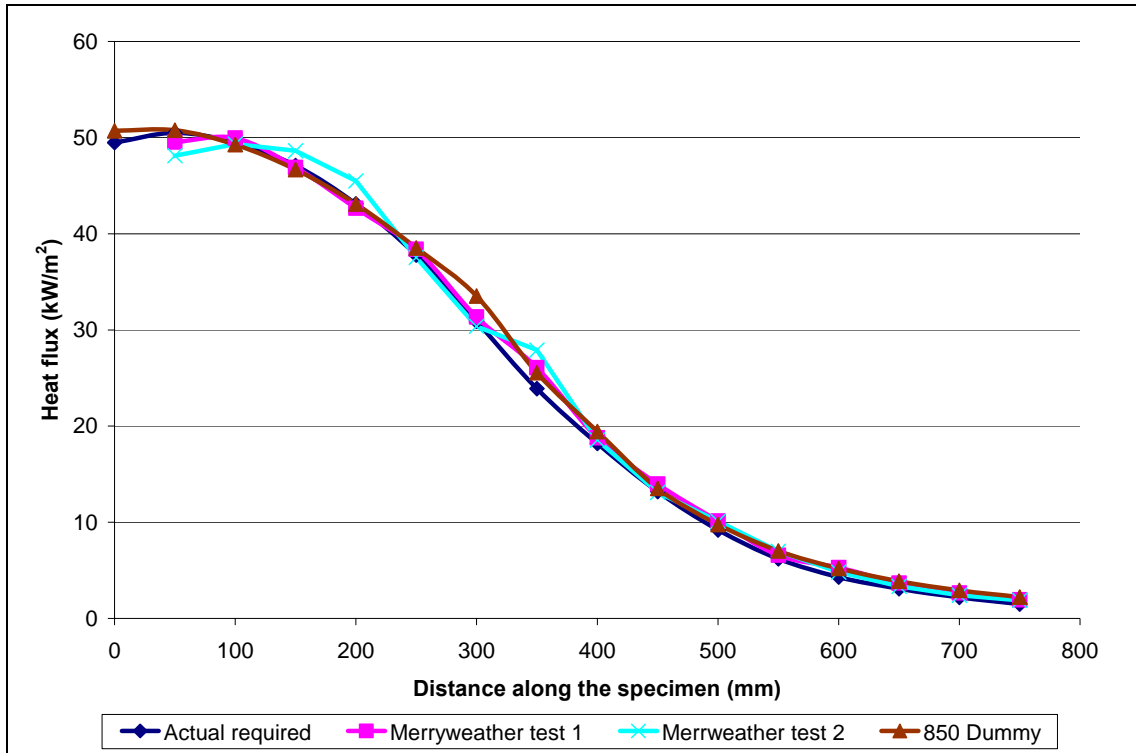


Figure 7-14: Comparison of the heat flux over the dummy specimen

7.6 Summary for the calibration of the LIFT apparatus

From the analysis above, it was demonstrated that the calibration the LIFT apparatus in FDS4 is achievable with the specified geometries (Appendix E) for the radiant panel and dummy specimen. The temperature required on the radiant panel is 850°C.

In addition, the ASTM E 1321 – 97a (2002) standards required the flame spread test of each specimen to be conducted at 5 kW/m² above its minimum heat flux for ignition. As different timber and timber based products have their own minimum heat flux for ignition, the calibration for each timber and timber based products needs to be carried out. Table 7-3 shows a summary of the temperature required on the radiant panel to meet the heat flux profile required by the ASTM standards. From the table, it demonstrated that the required temperature of the simulated radiant panel varies from 638°C to 663°C.

Table 7-3: Temperature required on the radiant panel

Type of Material	Minimum ignition flux (kW/m ²) (Merryweather 2006)	Heat flux required by the ASTM standards	Temp of the radiant panel (TMPWAL)	Corresponding heat flux after 25s (kW/m ²) at 50mm	% difference
Hardboard	17.5	22.5	650	22.6	0.4%
Medium Density Fibreboard (MDF)	16.25	21.3	638	21.5	1.2%
Melteca faced MDF	18.75	23.8	663	24.0	1.0%
Beech	18.75	23.8	663	24.0	1.0%
Macrocarpa	18.75	23.8	663	24.0	1.0%
Radiata Pine (Monterey pine)	18.75	23.8	663	24.0	1.0%
Rimu	18.5	23.5	660	23.7	1.0%
Plywood	16.3	21.3	638	21.5	0.9%
Pynefloor Particle board (chipboard)	18.75	23.8	663	24.0	1.0%

Figure 7-15 to Figure 7-17 show the comparison of the actual heat flux that is used for each timber and timber based products in FDS4 with the one obtained from the experiments. It should be noted that the heat flux profile from FDS4 is setup at 5 kW/m² above the minimum heat flux for ignition reported by Merryweather (2006).

Generally, the heat flux distribution that is determined using FDS4 matches well with the experiments. The only exception is in the case of Melteca faced MDF as indicated in Figure 7-16 (g); where it shows that the heat flux used in the experiments were much higher than the one determined from FDS4. This is because Merryweather had problem igniting the Melteca faced MDF specimen in the flame spread experiment so a higher heat flux was used for the calibration then followed by the flame spread test. Hence, the heat flux differences in the calibration of the LIFT apparatus using the FDS4 model and the experiment conducted by Merryweather 2006.

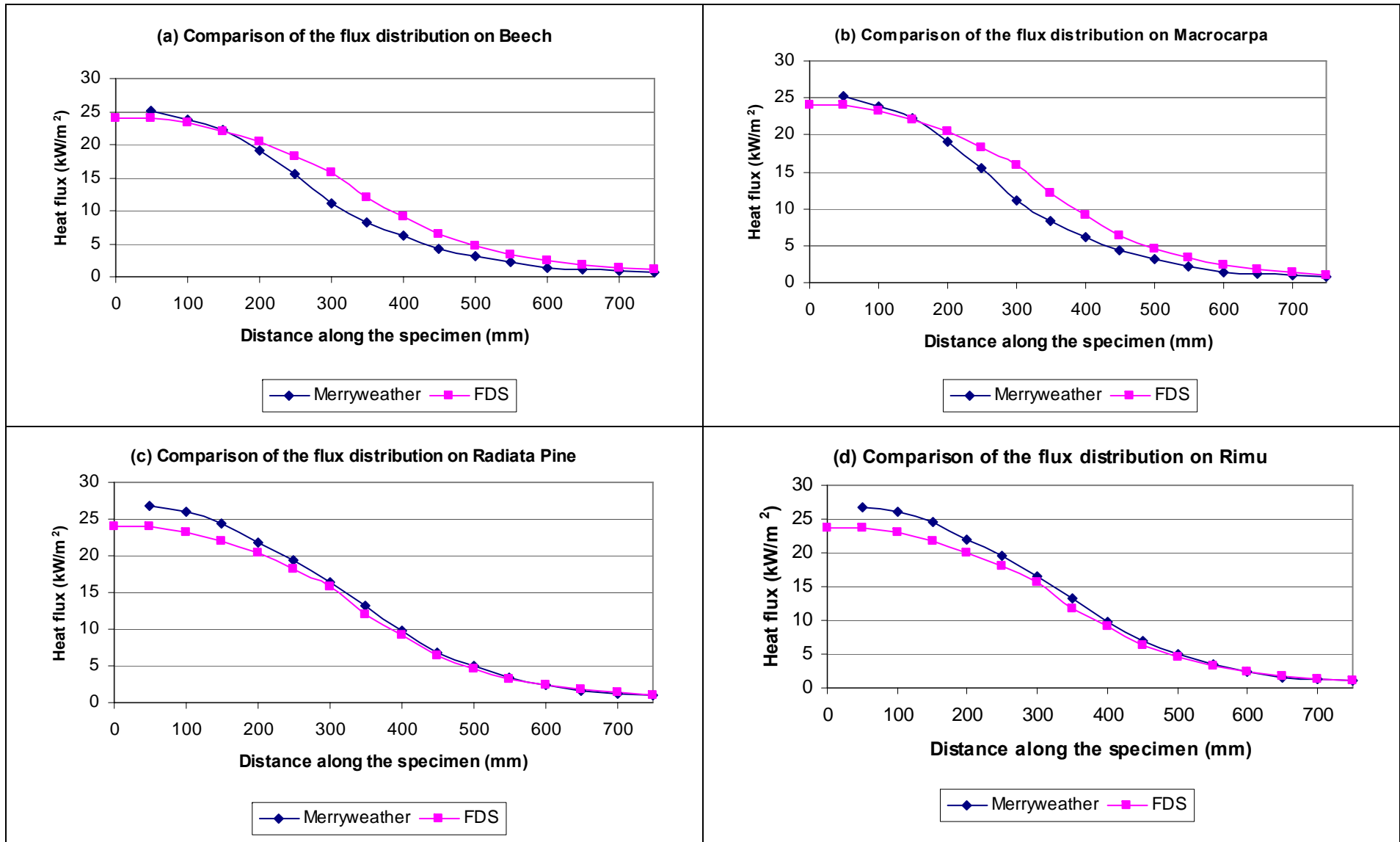


Figure 7-15: Comparison of the flux distribution on New Zealand native timber

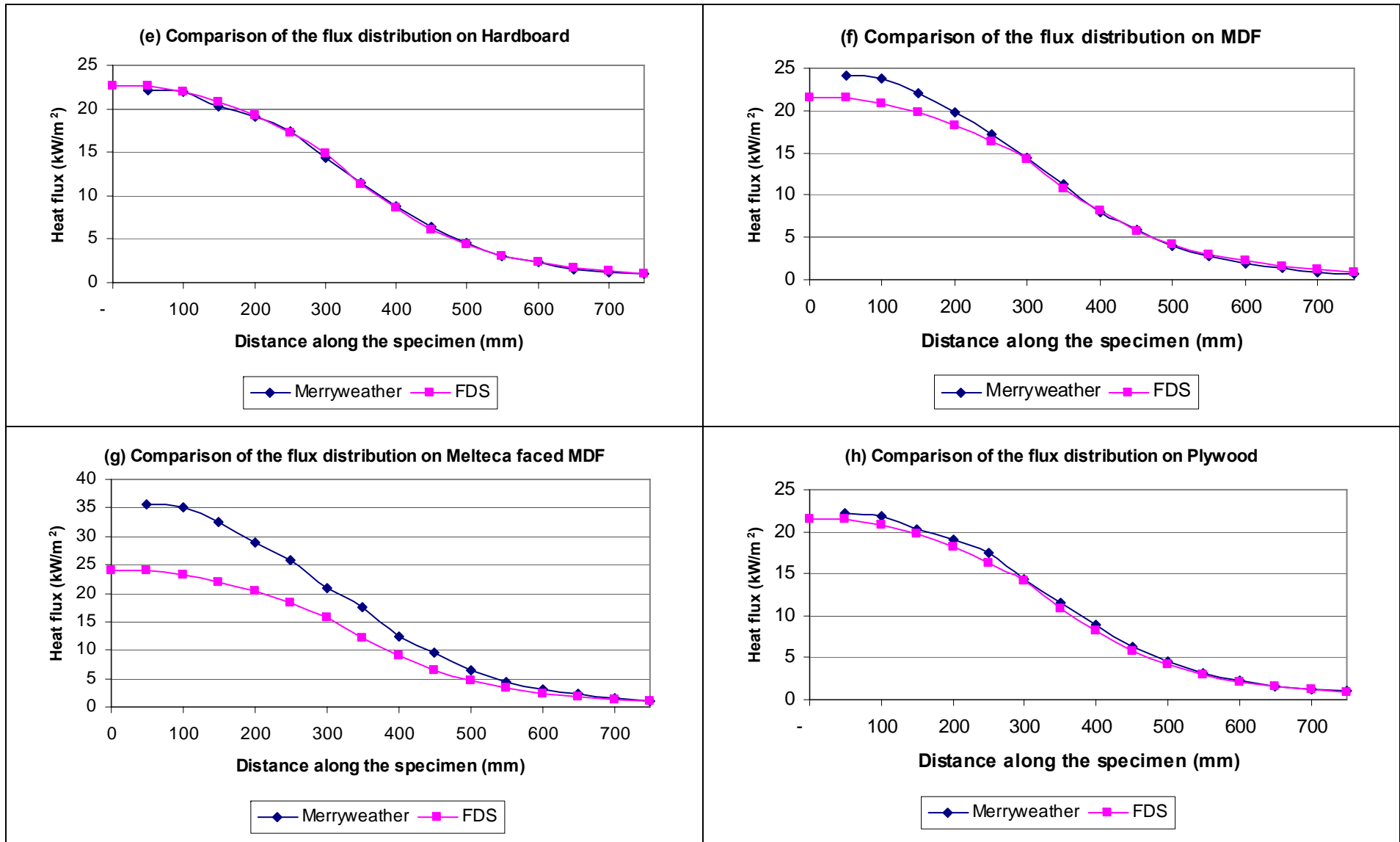


Figure 7-16: Comparison of the flux distribution on timber based products

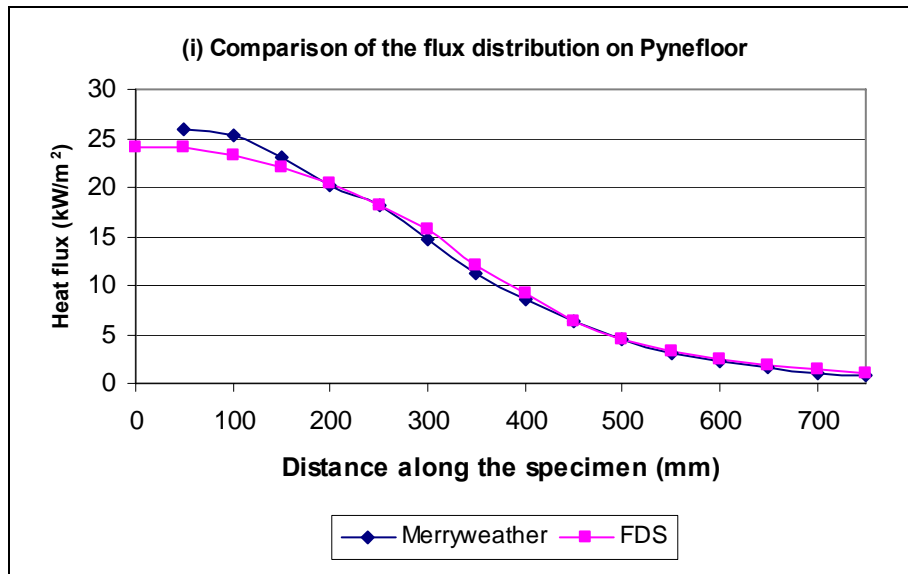


Figure 7-17: Comparison of the flux distribution on timber based product (Pynefloor)

8 Flame spread test in FDS4

This chapter describes the flame spread test procedure along with the parameters that are used in the FDS4 model. In addition, an outline of the heat transfer model used to account for the preheat time required is also described in which the surface temperature of each specimen just after the preheat time is determined.

The LIFT test consists of two procedures: First is the ignition test where ignition parameters are obtained; second is the flame spread test where flame spread parameters are obtained. As the flame spread test requires the ignition parameters, the ignition test must be carried out first before any flame spread test can be performed.

8.1 Ignition Test Procedure

The procedure and theory of the ignition test is previously described in Chapter 4 or refer to the ASTM E 1321 – 97a (2002) standards. The output of the ignition test includes parameters such as: ignition correlation parameter, preheat time, ignition temperature and minimum heat flux for ignition.

The ignition test was not simulated for the timber and timber based products as it is not within the scope of this research, but rather the ignition tests results conducted by Merryweather (2006) are used to gain consistency when comparing the results between the numerical simulation and the results from Merryweather (2006). A summary of the ignition tests results for each timber and timber based product tested by Merryweather (2006) can be found in Appendix D.

8.2 Flame Spread Test Procedure

The procedure for the flame spread test and its theory used to determine the correlations of lateral flame spread can be found in Chapter 4. From the flame spread data, the following parameters can be determined: flame heating parameter, minimum heat flux for ignition and minimum heat flux for spread. This section describes the approach that is needed to acquire a flame spread test model for the nine different timber and timber based products.

8.2.1 Calibration results from FDS4

As previously mentioned in Chapter 7, the calibration of the LIFT apparatus was performed where the radiant panel and dummy specimen is setup in FDS4. It was found that a constant temperature of 850°C is needed on the wall of the radiant panel.

Additionally, the heat flux on the specimen surface measured at 50mm from the hot end should be set at 5 kW/m² above the minimum ignition flux ($\dot{q}_{0,ig}''$). The reason for the use of a higher heat flux is for the ease in tracking the flame spread along the specimen. The heat flux profile that is applied for the timber and timber based products are shown in Figure 7-15 to Figure 7-17.

It is unnecessary to stabilise the simulated LIFT apparatus for 3 minutes as given in the ASTM standards (ASTM Committee E-5 on Fire Standards. 2004a). This is simply because the condition of the simulation in FDS4 is already considered to be steady state. However, it was found from the calibration of the LIFT apparatus that the FDS4 model needs 25 seconds to stabilise to a steady state condition as shown in Figure 7-12. Therefore, the flame spread test can only be carried out after 25 seconds from start of the simulation which leads to the use of the time remove and time create function in FDS4 i.e. at 25 seconds the dummy specimen is removed and replaced by the timber or timber based product specimen.

8.2.2 Preheat Time

A preheat time is required on the LIFT test specimen for the flame spread test as given in the ASTM E 1321 – 97a (2002) standards. This leads to an increase in the surface temperature of the specimen. In fact, the temperature profile on the test specimen will vary both along the exposed surface to the radiant panel and across the thickness of the material after a specific preheat time. Figure 8-1 shows the actual surface temperature profile after the preheat time.

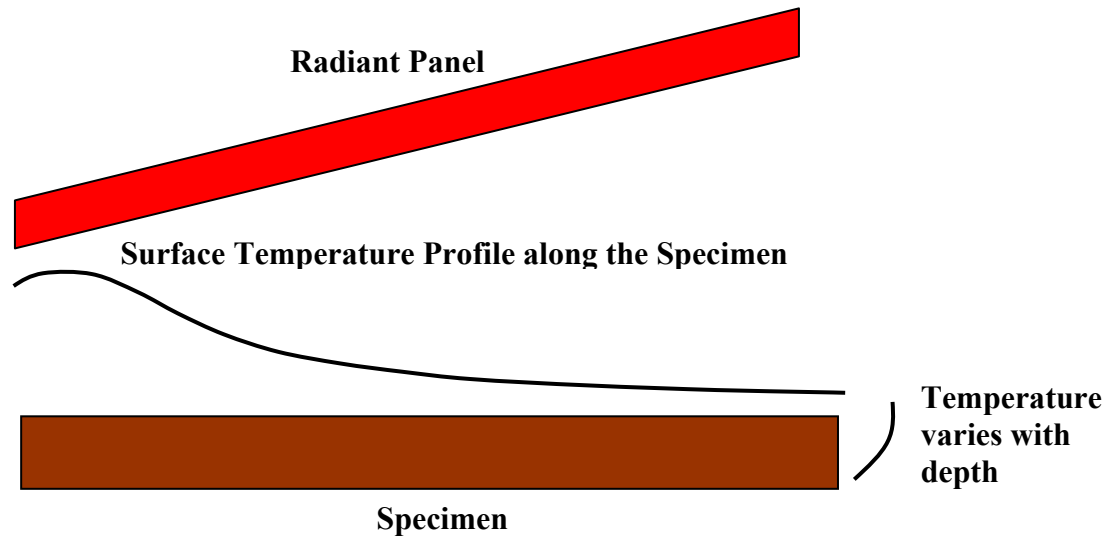


Figure 8-1: Actual surface temperature profile along the specimen and temperature varies with depth

There is no function provided in FDS4 to allow preheating of specimens because FDS4 assumes ignition to occur when the specified ignition temperature on the surface identification line is reached. This leads to the use of an initial temperature on all specimens; where the specimen is proposed to be divided into segments and applied an initial temperature to simulate the temperature just after the required preheat time.

However, Merryweather (2006) did not measured the surface temperature along the specimens after preheating the specimens; therefore it is necessary to approximate the surface temperature profile to account for the preheat time that is required by the ASTM E 1321 97a (2002) standards and applied in the FDS4 model accordingly. The approach taken to calculate the surface temperature immediately after the preheat time is to simplify the problem into a heat transfer problem; where it becomes a one dimensional heat transfer problem with the boundary condition as shown in Figure 8-2. The heat transfer problem was solved using an explicit finite difference method.

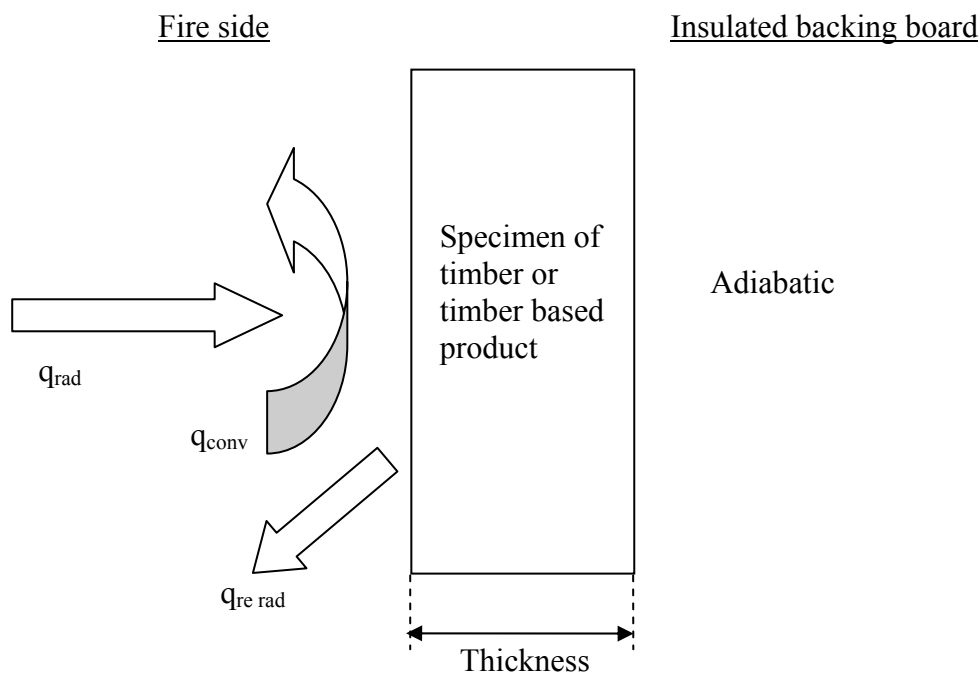


Figure 8-2: Schematic sketch of the heat transfer problem

The following sections will describe the heat transfer model that is applied to assess the surface temperature of the specimen after preheat time.

Heat Transfer Model

The heat transfer model defines the equations that are used to calculate the surface temperature of specimens. There are a total of three equations employed to determine the temperature at each node: (1) the interior node (within the specimen); (2) the other surface node (the surface of specimen adjacent to the backing board) and (3) the exposed surface node (the surface of specimen facing the radiant panel). All calculations are performed in spreadsheets with the following assumptions being made, which then allows the heat transfer problem to be solved.

Assumptions:

- 1) One dimensional heat transfer in the x direction only
- 2) The ambient temperature is $20^{\circ}C \equiv 293K$

- 3) The thermal properties of specimens are constant
- 4) No heat generation inside of specimens
- 5) Both the convective and radiation boundary condition is applied on the exposed surface node due to the heat flux from the radiant panel
- 6) Re-radiation coming off the specimen on the exposed surface node
- 7) An adiabatic boundary condition is applied on the other surface node as the specimen is adjacent to the backing board.
- 8) Radiation exchange within the specimen is ignored
- 9) A uniform grid spacing such that $\Delta x = \Delta x^+ = \Delta x^-$

Explicit Method

The explicit finite difference method is used to determine the surface temperature just after the specific preheat time; where 11 nodes in depth are assigned. The thermal transport properties of the timber and timber based products are applied in this method; which are measured from the Hot Disk test as described in Chapter 6. Meanwhile, the density of the material can be found in Appendix B.

The explicit method can only be employed in a one-dimensional heat transfer problem if the stability requirement is met; where the constraint is that the Fourier number must be less than or equal to 0.5, $Fo \leq 0.5$ (Incropera and DeWitt 2001). If this condition is not satisfied then adjustments are made until the stability requirement is met.

An example of the stability verification for Beech is shown below:

$$k = 0.1927 \frac{W}{m.K}, \rho = 1303 \frac{kg}{m^3}, c_p = 556 \frac{J}{kg.K}.$$

$$\alpha = \frac{k}{\rho c_p} = \frac{0.1927 \frac{W}{m.K}}{1303 \frac{kg}{m^3} \times 556 \frac{J}{kg.K}} = 0.000000266 \frac{m^2}{s}$$

Since 11 nodes are assigned on the timber and timber based products

$$\Delta x = \frac{\text{Thickness of the timber based product}}{\text{No. of nodes} - 1} = \frac{0.023}{11 - 1} = 0.0023, \Delta t = 1s$$

Fourier number is determined to check for stability for having 11 nodes:

$$Fo = \frac{\alpha \Delta t}{(\Delta x)^2} = \frac{0.000000266(1)}{(0.0023)^2} = 0.05031$$

As the Fourier number is less than 0.5 ($0.05 \leq 0.5$), it implies that specifying 11 nodes for this heat transfer problem is acceptable.

Moreover, the heat fluxes measured along the specimens from the LIFT experiments conducted by Merryweather (2006) were used in predicting the surface temperature along the specimen. These heat fluxes are applied as the radiation emitted from the radiant panel. However, not all of the energy is absorbed by the material; therefore an emissivity or absorption coefficient is applied to give a better representation of the actual heat flux absorbed by the specimen. From the literature by Babrauskas (2003), the emissivity for wood is found to be in the range between 0.8 and 0.9. This is similar to the other sources that are found where the typical emissivity of wood is shown in Table 8-1. It should be noted that the emissivity of a given material will vary with temperature and surface finish, and the value in the table should be used only as a guide for relative or differential temperature measurements. Therefore the exact emissivity can fluctuate depending on the types of wood species or timber based products.

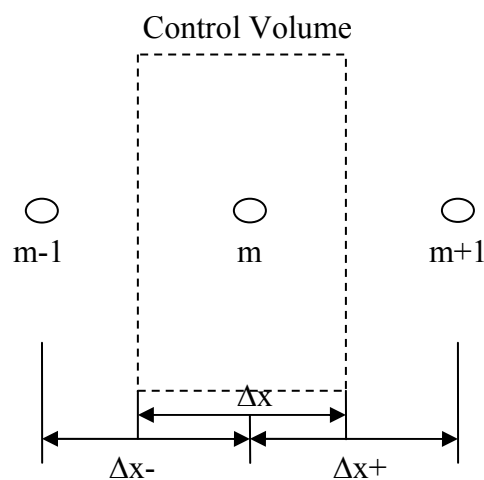
Table 8-1: Emissivity of various wood species (Anon 2006)

Material	Temp °F (°C)	Emissivity ϵ
Wood	Low	.80-.90
Beech, Planed	158 (70)	.94
Oak, Planed	100 (38)	.91
Spruce, Sanded	100 (38)	.89

The absorption coefficient is understood to be an important parameter in determining the flame spread as it will directly affect the amount of external heat flux being absorbed onto the specimen. As mentioned previously the typical absorption coefficient for wood is 0.8 – 0.9, however, an absorption coefficient of 0.9 was used during the preliminary trial flame spread test and showed the flame spread rate is overpredicted (i.e. the temperature of the specimen is set too high, which cause early ignition) therefore lower absorption coefficients were used in this research. Consequently three different absorption coefficients (0.6, 0.7 and 0.8) were examined to see the effect it has on flame spread.

- For interior nodes:

Figure 8-3 shows the heat transfer model that is applied for the interior nodes with the relevant boundary condition. In this case, there is no boundary condition as conduction is assumed to be the only means of heat transfer.

**Figure 8-3: Heat transfer model for the interior nodes**

It is assumed that there is a uniform grid spacing i.e. $\Delta x = \Delta x^+ = \Delta x^-$. The heat transfer equation that is applicable on each node is as follows:

$$q_{m+1,n}^i = k \frac{T_{m+1}^i - T_m^i}{\Delta x}, \quad q_{m-1,n}^i = k \frac{T_{m-1}^i - T_m^i}{\Delta x}, \quad q_{stored}^i = \frac{\rho c_p (T_m^{i+1} - T_m^i) \Delta x}{\Delta t}$$

An energy balance on Node m is executed as indicated below:

$$q_{stored}^i = q_{m+1,n}^i + q_{m-1,n}^i$$

$$\frac{\rho c_p (T_m^{i+1} - T_m^i) \Delta x}{\Delta t} = k \frac{T_{m+1}^i - T_m^i}{\Delta x} + k \frac{T_{m-1}^i - T_m^i}{\Delta x}$$

$$T_m^{i+1} = T_m^i + \frac{k \Delta t}{\rho c_p (\Delta x)^2} (T_{m+1}^i + T_{m-1}^i - 2T_m^i) \quad \text{Since } Fo = \frac{k \Delta t}{\rho c_p (\Delta x)^2}$$

$$T_m^{i+1} = Fo(T_{m+1}^i + T_{m-1}^i) + (1 - 2Fo)T_m^i$$

Equation 8-1

As a result, Equation 8-1 is applied in spreadsheet for calculating the change in temperature for the interior nodes.

- For other surface node:

The other surface node is the node that is adjacent to the insulated backing board. Figure 8-4 shows the heat transfer model that is applied for the other surface node with the relevant boundary condition. In this case, Node 10 is assumed to have an adiabatic boundary condition due to the insulated backing board behind the specimen.

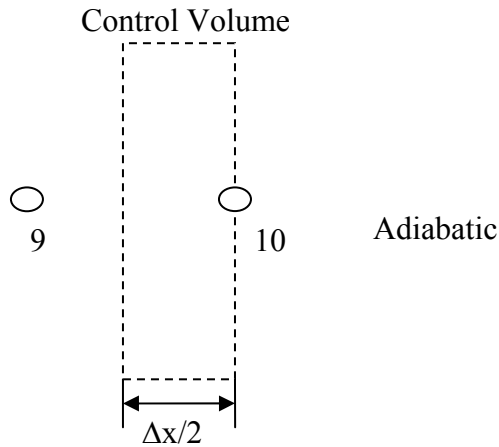


Figure 8-4: Heat transfer model for the other surface node

It is assumed that there is a uniform grid spacing i.e. $\Delta x = \Delta x^+ = \Delta x^-$. The heat transfer equation that is applicable on each node is as follows:

$$q_9^i = k \frac{T_9^i - T_{10}^i}{\Delta x}, \quad q_{stored}^i = \frac{\rho c_p \Delta x (T_{10}^{i+1} - T_{10}^i)}{2\Delta t}$$

An energy balance on Node 10 is executed as indicated below:

$$q_{stored}^i = q_9^i$$

$$\frac{\rho c_p \Delta x (T_{10}^{i+1} - T_{10}^i)}{2\Delta t} = k \frac{T_9^i - T_{10}^i}{\Delta x}$$

$$T_{10}^{i+1} - T_{10}^i = \frac{2k\Delta t}{\rho c_p \Delta x^2} (T_9^i - T_{10}^i) \quad \text{Since } Fo = \frac{k\Delta t}{\rho c_p (\Delta x)^2}$$

$$T_{10}^{i+1} = 2Fo(T_9^i - T_{10}^i) + T_{10}^i$$

$$T_{10}^{i+1} = (1 - 2Fo)T_{10}^i + 2FoT_9^i$$

Equation 8-2

As a result, Equation 8-2 is applied in the spreadsheet for calculating the change in temperature for the other surface node.

- For exposed surface (exposed to the radiant panel) node

The exposed surface node is the node that is on the surface of specimen which faces the radiant panel. Figure 8-5 shows the heat transfer model that is applied for the exposed surface node with the relevant boundary conditions. In this case, the radiation and convection for the radiant panel as well as the re-radiation coming off from the specimen.

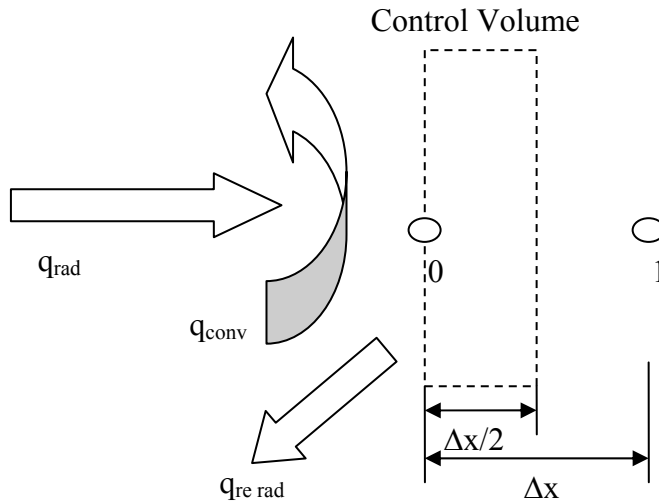


Figure 8-5: Heat transfer model for the exposed surface node

It is assumed that there is a uniform grid spacing i.e. $\Delta x = \Delta x^+ = \Delta x^-$. The heat transfer equation that is applicable on each node and the boundary condition are as follows:

$$q_{rad}^i = \text{constant}, \quad q_{conv}^i = h(T_0^i - T_\infty), \quad q_{rerad}^i = \varepsilon\sigma(T_0^{i4} - T_\infty^4),$$

$$q_1^i = k \frac{T_1^i - T_0^i}{\Delta x}, \quad q_{stored}^i = \frac{\rho c_p (T_0^{i+1} - T_0^i)}{\Delta t} \left(\frac{\Delta x}{2} \right)$$

An energy balance on Node 0 is executed as indicated below:

$$q_{stored}^i = q_1^i + q_{rad}^i - q_{conv}^i - q_{rerad}^i$$

$$\frac{\rho c_p (T_0^{i+1} - T_0^i)}{\Delta t} \left(\frac{\Delta x}{2} \right) = k \frac{T_1^i - T_0^i}{\Delta x} + q_{rad}^i - h(T_0^i - T_\infty) - \varepsilon \sigma (T_0^{i4} - T_\infty^4)$$

$$\left(\frac{\rho c_p}{\Delta t} \right) \left(\frac{\Delta x}{2} \right) (T_0^{i+1} - T_0^i) = q_{rad}^i + k \frac{T_1^i - T_0^i}{\Delta x} - h(T_0^i - T_\infty) - \varepsilon \sigma (T_0^{i4} - T_\infty^4)$$

$$T_0^{i+1} = 2Fo \left(q_{rad}^i \frac{\Delta x}{k} + T_1^i \right) + (1 - 2Fo)T_0^i - \frac{2\Delta t}{\rho c_p \Delta x} \left(h(T_0^i - T_\infty) + \varepsilon \sigma (T_0^{i4} - T_\infty^4) \right) \quad \text{Equation 8-3}$$

As a result, Equation 8-3 is applied in the spreadsheet for calculating the change in temperature for the exposed surface node. It should be noted that the term “ q_{rad}^i ” is the radiant heat flux given off from the radiant panel, which is measured at 50mm increments along the tested specimen by Merryweather (2006).

An example on the application of the explicit method in the spreadsheet can be found in Appendix F, where it shows the calculation performed to determine the surface temperature profile for Beech. The result of the analysis is plotted as shown in Figure 8-6 below.

The spreadsheets that are used for the other timber and timber based products are identical to the one shown for Beech in the example except different material properties are assigned. Nevertheless, a summary of the surface temperature profile for each timber and timber based products is plotted in Appendix F.

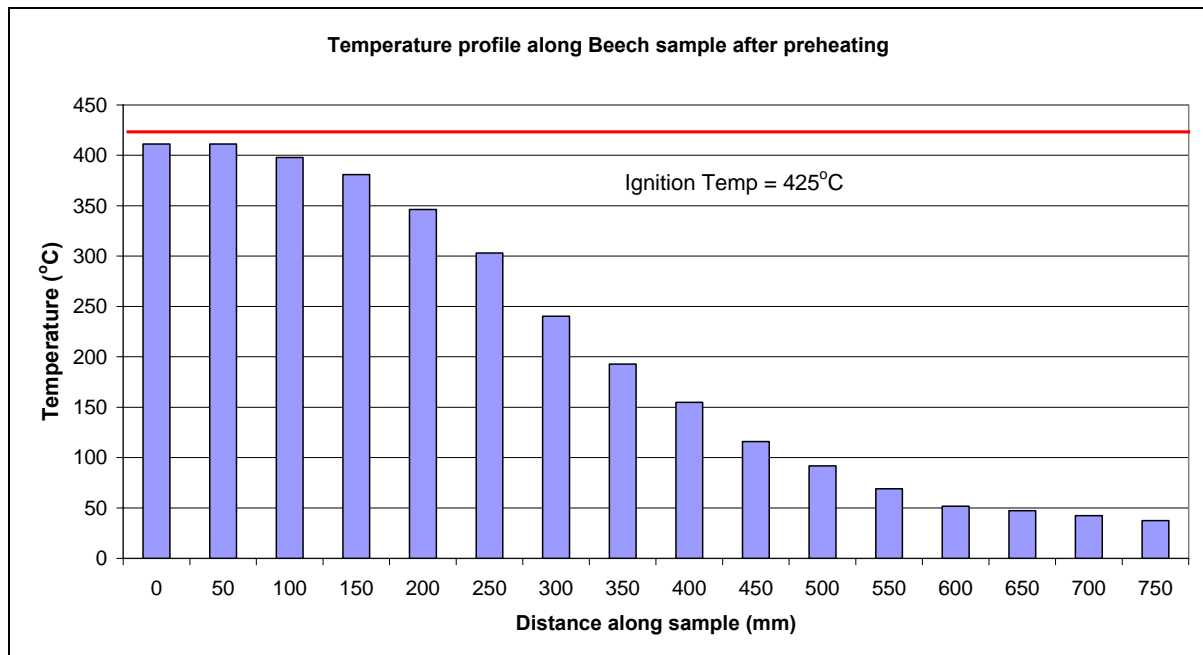


Figure 8-6: Temperature profile along Beech specimen after preheating

Despite the surface temperature profile calculated having a similar pattern as shown in Figure 8-1, the initial temperature is specified on the specimen in FDS4 as a series of segments made of 50 mm blocks. Figure 8-7 shows the preheat temperature that is applied in FDS4 on the surface of the specimen.

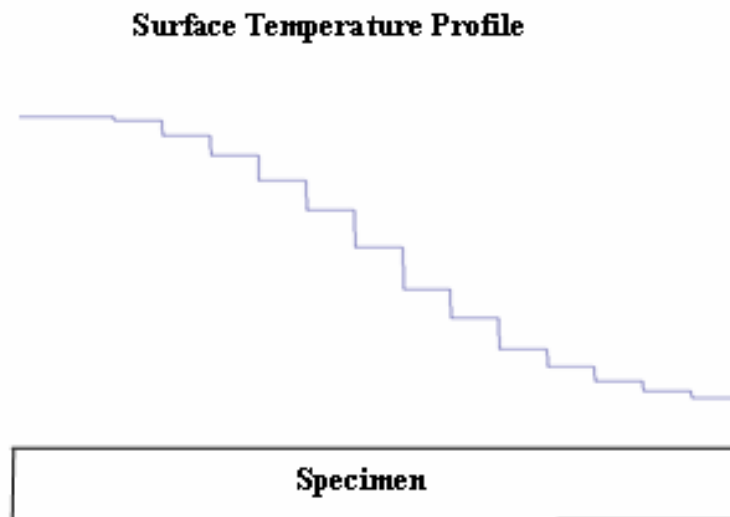


Figure 8-7: Preheat temperature modelled in FDS4

Figure 8-8 shows the setup of the flame spread test in FDS4. It demonstrates how the specimen is divided into small segment (50mm in length) as represented by different colour. These surfaces are assigned with different initial temperature to account for the effect of preheating the sample.

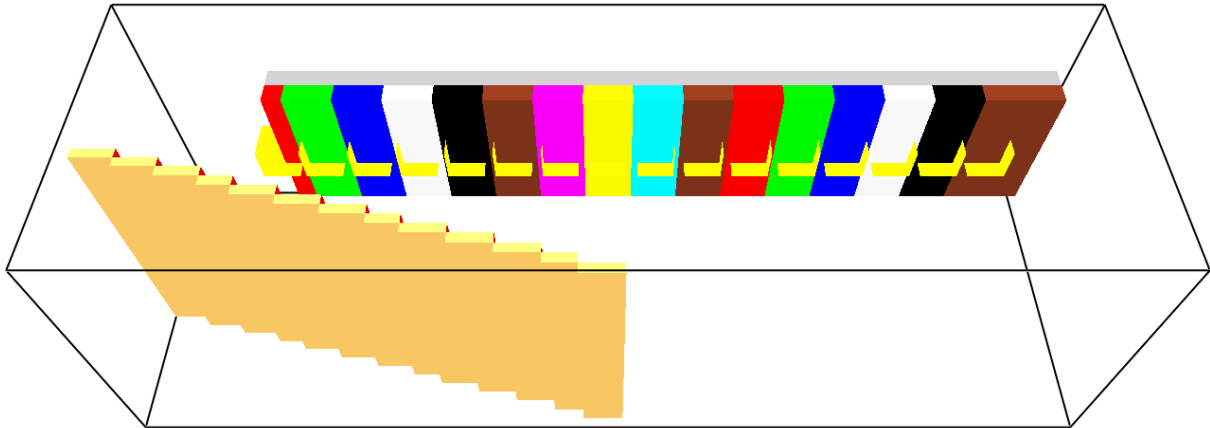


Figure 8-8: A snapshot of flame spread test setup from Smokeview

8.2.3 Other Input Variables for the flame spread test in FDS4

The basic setup of the flame spread test in FDS4 was already prepared during the calibration of the LIFT apparatus; where the size of the domain, geometries of the radiant panel and specimen inserted are used again for the flame spread test. Additionally, input variables such as the ambient temperature, grid size, open vents and length of simulation are very much identical to the calibration of the LIFT apparatus with only a few minor alternations.

Besides assigning the preheated temperature on the specimens, other parameters are also required in the FDS4 input file to accurately simulate the flame spread test in FDS4. One of these changes is the parameter for the reaction which determines the stoichiometry of the reaction. As mentioned previously, only one reaction can be specified in a FDS4 model. For flame spread test, wood is selected as the reaction as opposed to methane which is used for calibration of the LIFT apparatus. This is because the combustion material is wood.

Therefore the most representative reaction to choose for the flame spread model is wood (& REACTION='WOOD'). The reaction identification for wood is obtained from the FDS4 database and is reproduced in Figure 8-9 below:

```
&REAC ID='WOOD'
```

```

FYI='Ritchie, et al., 5th IAFSS, C_3.4 H_6.2 O_2.5'
SOOT_YIELD = 0.01
NU_O2    = 3.7
NU_CO2   = 3.4
NU_H2O   = 3.1
MW_FUEL  = 87.
EPUMO2   = 11020. /
    
```

Figure 8-9: Reaction identification for wood

The reaction fuel WOOD from the FDS4 database is taken from the paper by Ritchie et al (1997), where the material used for the experiments was Douglas Fir. Figure 8-10 shows the state relationship of mass fraction as a function of mixture fraction for wood that is applied in FDS4; where the flame is assumed to exist in the FDS4 model when the mixture fraction is 0.148.

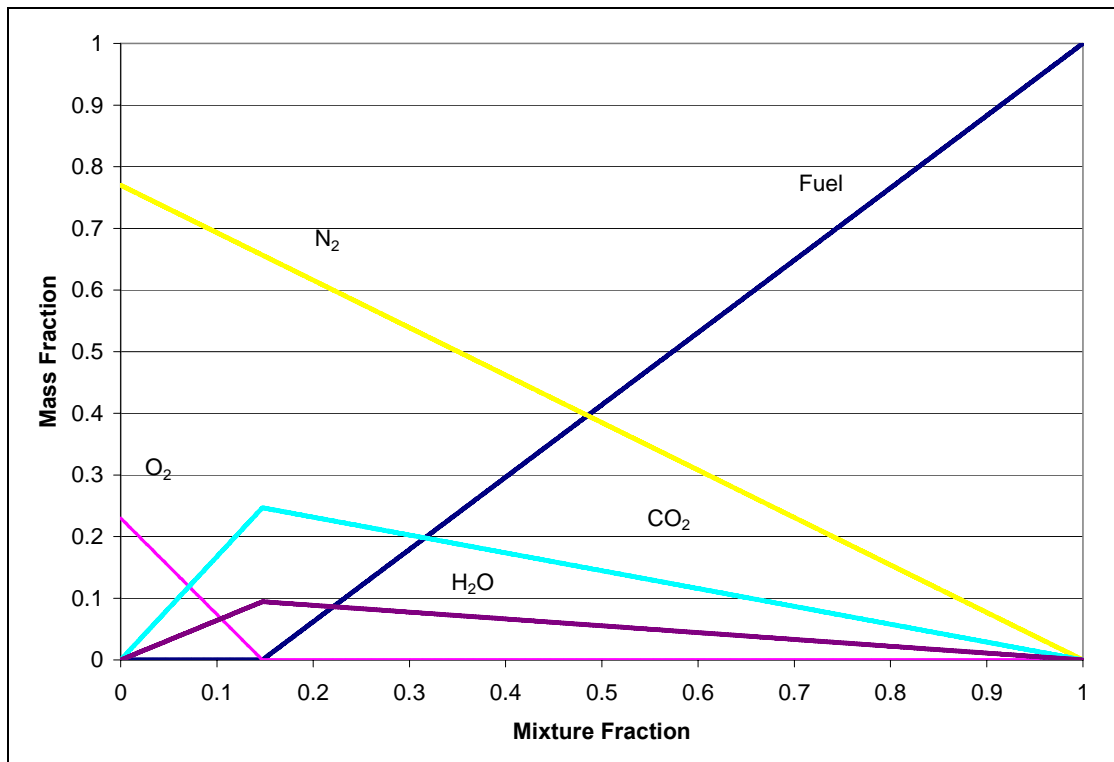


Figure 8-10: State relationship of mass fraction as a function of mixture fraction for wood

Two pyrolysis models will be used in FDS4 to simulate the pyrolysis behaviour of the materials; namely (1) Thermoplastic fuels model. This is simply a heat of vaporisation model that assumes all of the reaction occurs on the exposed surface and that no char is formed. This behaviour was chosen for its simplicity. (2) Charring fuels model. This is to investigate

whether the chosen pyrolysis model has an effect on the flame spread. An example of the FDS4 input for the thermoplastic fuels and charring fuels model is shown in Figure 8-11 and Figure 8-12 respectively.

The thermoplastic fuels model requires variables such as moisture content (MOISTURE_FRACTION), thickness of the material (DELTA), mass flux at ignition temperature (MASS_FLUX_CRITICAL), heat of vaporisation (HEAT_OF_VAPORIZATION), ignition temperature (TMPIGN), initial temperature of the material (TMPWAL0), density of the material (DENSITY), thermal conductivity (KS), specific heat capacity (C_P), internal wall points (WALL_POINTS) and back face boundary condition (BACKING). As for the charring fuels model, in addition to all of the variables listed above for the thermoplastic fuels model, thermal conductivity, specific heat capacity and density of the charred materials are also required.

```
&SURF ID      =      'Beech1'
FYI           =  'Thermoplastic material'
RGB           =  0.5,0.2,0.1
MOISTURE_FRACTION =  0.10
DELTA        =  0.023
MASS_FLUX_CRITICAL =  0.075
HEAT_OF_VAPORIZATION = 1400.
TMPIGN       =  425
TMPWAL0      =  411
DENSITY      =  556.
KS           =  0.1927
C_P         =  1.303
WALL_POINTS  =  30
BACKING      =  'INSULATED/'
```

Figure 8-11: Example of the FDS4 input for the thermoplastic fuels model

```
&SURF ID      =      'Beech1'
FYI           =  'Charring material'
RGB           =  0.5,0.2,0.1
PHASE         =  'CHAR'
MOISTURE_FRACTION =  0.10
DELTA        =  0.023
TMPIGN       =  425
HEAT_OF_VAPORIZATION = 500.
DENSITY      =  556.
```

```

TMPWAL0      = 411
RAMP_KS      = 'KS'
RAMP_C_P     = 'CPV'
RAMP_C_P_CHAR = 'CPC'
RAMP_KS_CHAR = 'KSC'
CHAR_DENSITY = 299
WALL_POINTS  = 30
BACKING      = 'INSULATED'
&RAMP ID = 'KS', T = 20., F = 0.193 /
&RAMP ID = 'KS', T = 500., F = 0.193 /
&RAMP ID = 'KSC', T = 20., F = 0.099 /
&RAMP ID = 'KSC', T = 900., F = 0.099 /
&RAMP ID = 'CPV', T = 20., F = 1.303 /
&RAMP ID = 'CPV', T = 500., F = 1.303 /
&RAMP ID = 'CPC', T = 20., F = 0.741 /
&RAMP ID = 'CPC', T = 400., F = 0.741 /
&RAMP ID = 'CPC', T = 900., F = 0.741 /

```

Figure 8-12: Example of the FDS4 input for the charring fuels model

The moisture content is required on the surface identification line for both pyrolysis models. From the Timber Design Guide (Buchanan 2002) Table 6.3, the moisture content for wood panel products are between 6 to 10% at a relative humidity of 50% and 20°C. Another coming from the research by Dietenberger (Dietenberger 2004), Redwood was tested in the LIFT test having been conditioned at 50% relative humidity. The corresponding moisture content of Redwood is 9.2%. Therefore, using a moisture content of 10% in the model is considered to be reasonable.

It should be noted that the moisture content of the tested specimen was not measured by Merryweather. However, it was stated in the Merryweather report that “For the allowable range given in the ASTM LIFT standard, then the moisture content of the samples would be between 8.5% and 9.9% MC.”

The burning behaviour of a fuel is governed by its heat of vaporisation as for wood, its typical heat of vaporisation is found to be 0.95 – 1.82 kJ/g (Icove and DeHaan 2004). Initial trial models were simulated and it showed that an average value would predict a better flame spread than using an upper or lower bound value. Therefore, the heat of vaporisation is entered as 1400 kJ/kg for the thermoplastic fuels model. However, the heat of vaporisation in the charring fuels model actually refers to the gasification of the virgin material at the pyrolysis front and is not an “effective” value that is often used to model the effect of the

char shielding the virgin material from the heat flux at the surface (McGrattan (editor) July 2004). A heat of vaporisation of 500 kJ/kg is selected for the charring fuels model based on the fact that char materials are very similar for different type of wood species as char is composed primarily of carbon; this value comes from the FDS4 database for 'Spruce'. The typical heats of mass burning rates for wood is found to have a mass flux of 70 - 80 g/m²s (Icove and DeHaan 2004); which is equivalent to 0.07 – 0.08 kg/m²s. Therefore, the mass flux at ignition temperature is entered as 0.075 kg/m²/s. These values are taken as a base case for the FDS4 model and sensitivity of these values were later investigated in Chapter 9.

The ignition temperature (TMPIGN) of the specimen extracted from the experiment performed by Merryweather (2006), which are reproduced in Appendix D. While the initial temperature of the material (TMPWAL0) is specified to account for the preheat time. The method of calculating the temperature just after the preheat time is described in Chapter 8.2.2 and the results for all materials used in this research can be found in Appendix F.

The thermal transport properties of each specimen are determined using the Hot Disk test. The results showing the thermal conductivity, specific heat capacity and density of the material and the method details can be found in Chapter 6. These properties are entered appropriately into both the thermoplastic fuels and charring fuels model.

In FDS4, the prescription of the thermal conductivity directs the code to perform a one-dimensional heat transfer calculation across the thickness of the material; where the default number of nodes used in the one-dimensional heat conduction calculation into a thermally-thick solid is 20. On the other hand, the number of nodes can be specified manually by adding the parameter WALL POINTS to the SURF line. In this research, 30 nodes are assigned to accurately account for the heat conduction during flame spread.

By default, the FDS4 model assumed that the wall liner backs up to an air gap. However, in the flame spread test as specified in the ASTM E 1321-97a (2002) standards, the wall liner is assumed to be backed up against a fiber insulating board with a sheet of aluminium foil separating the two materials to prevent any heat loss from the back side of the material.

Therefore the back face boundary condition is specified as insulated; where the expression `BACKING='INSULATED'` is entered on the on the SURF line.

Finally as discussed in Chapter 7, no restart function should be assigned into the model as restarting ultimately affects the heat flux distribution along the specimen and the resulting rate of flame spread. The overall FDS4 input files for the flame spread test by adapting the LIFT apparatus can be found in Appendix G; which shows both the thermoplastic and charring fuels model for Beech. FDS4 input files for other timber and timber based products are not provided in this research as it is very similar to the one shown in Appendix G with some changes in the initial temperature and thermal properties of the material. The thermal properties for each species of wood are also given in Appendix G in FDS4 format.

8.3 Analysis method of flame spread

There are a total of 54 scenarios simulated in FDS4 which represent the nine different timber and timber based products. Two different scenarios are investigated to see the effect of the selected pyrolysis model has on modelling flame spread. The two pyrolysis models tested are (1) thermoplastic fuels and (2) charring fuels model. As well as different types of model, three different absorption coefficients (0.6, 0.7 and 0.8) for each specimen are also examined; this parameter contributed significantly to the rate of flame spread as it determines the amount of heat flux being absorbed by the specimen during the time of preheating.

A fire is basically modelled as the ejection of pyrolysed fuel from a solid surface or vent that burns when mixed with oxygen (McGrattan (editor) July 2004), which is the default mixture fraction model of combustion. Another method that can be applied to model flame in FDS4 is known as Heat Release Rate per Unit Volume (HRRPUV).

As the flame structure in Smokeview can be visualised in different ways, the flame spread extent simulated by FDS4 may also differ depending on the technique used. Consequently, the flame spread test for the selected timber and timber based products was analysed using both the Mixture Fraction (0.6, 0.7 and 0.8) and HRRPUV model resulting in a total of 108 different flame spread rates.

The flame spread data is obtained by visually tracking the flame front progress along the longitudinal centreline of the specimen in FDS4; where the arrival time of the flame front at 25 mm increments is recorded. Figure 8-13 and Figure 8-14 show perspective views of the flame spread test that is carried out in FDS4; all flame spread measurements are taken by zooming into the specimens in Smokeview.

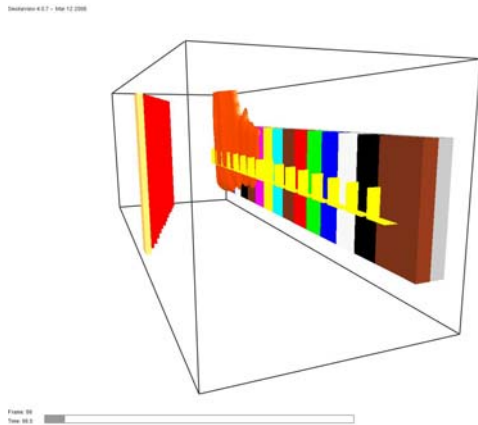


Figure 8-13: A perspective view of the flame spread test in Smokeview

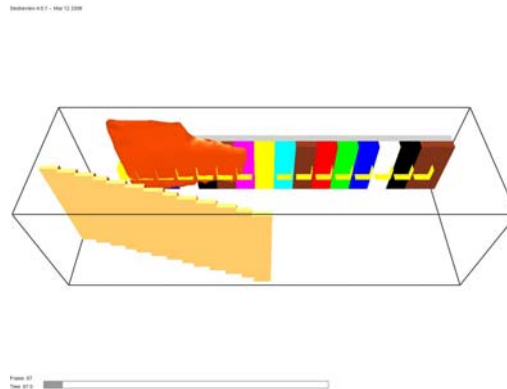


Figure 8-14: Front view of the flame spread test in Smokeview

8.4 Flame spread results from FDS4

All nine different timber and timber based specimens are analysed. However, only the results using the Mixture Fraction to model flame spread are shown in this section as this was the base case approach to measuring the flame spread and the HRRPUV method was investigated later as a comparison; where the plots of the flame spread using HRRPUV to model can be found in Appendix I. It should be noted that using the Mixture Fraction model give a slightly better flame spread results when compared to the HRRPUV model.

The arrival time against the flame front position using Mixture Fraction model is plotted for all timber and timber based products as shown below in Figure 8-15 to Figure 8-23. It shows both the thermoplastic and charring fuels model as well as for the effect of flame spread by changing the absorption coefficient.

8.4.1 Flame spread for Beech

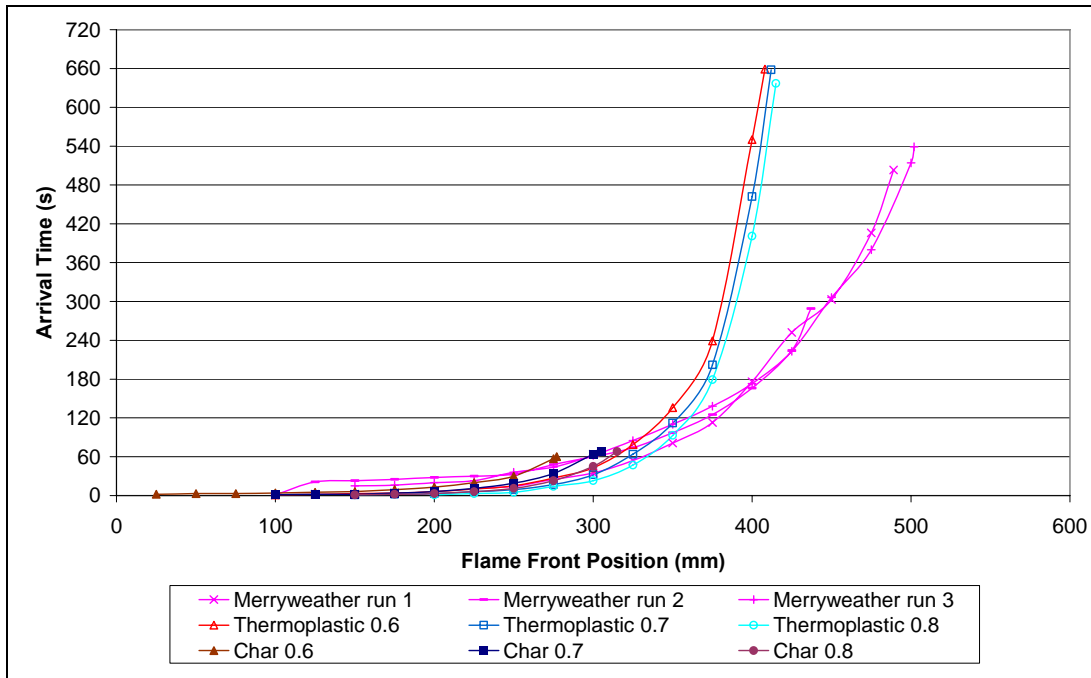


Figure 8-15: Arrival time versus flame front position for Beech (using Mixture Fraction)

8.4.2 Flame spread for Hardboard

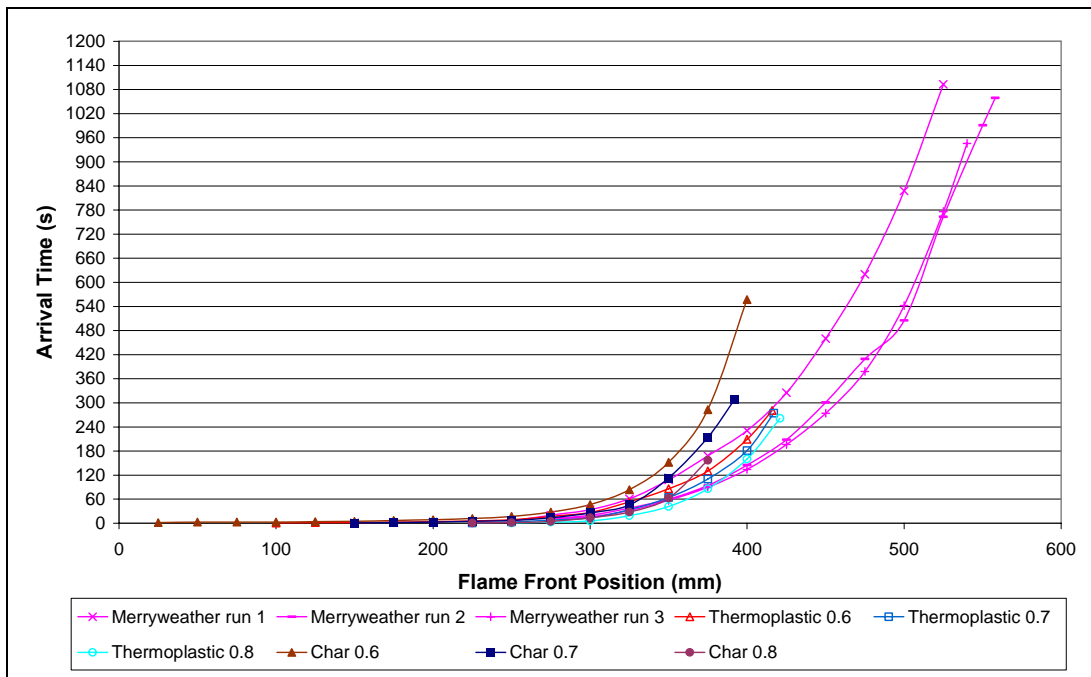


Figure 8-16: Arrival time versus flame front position for Hardboard (using Mixture Fraction)

8.4.3 Flame spread for Macrocarpa

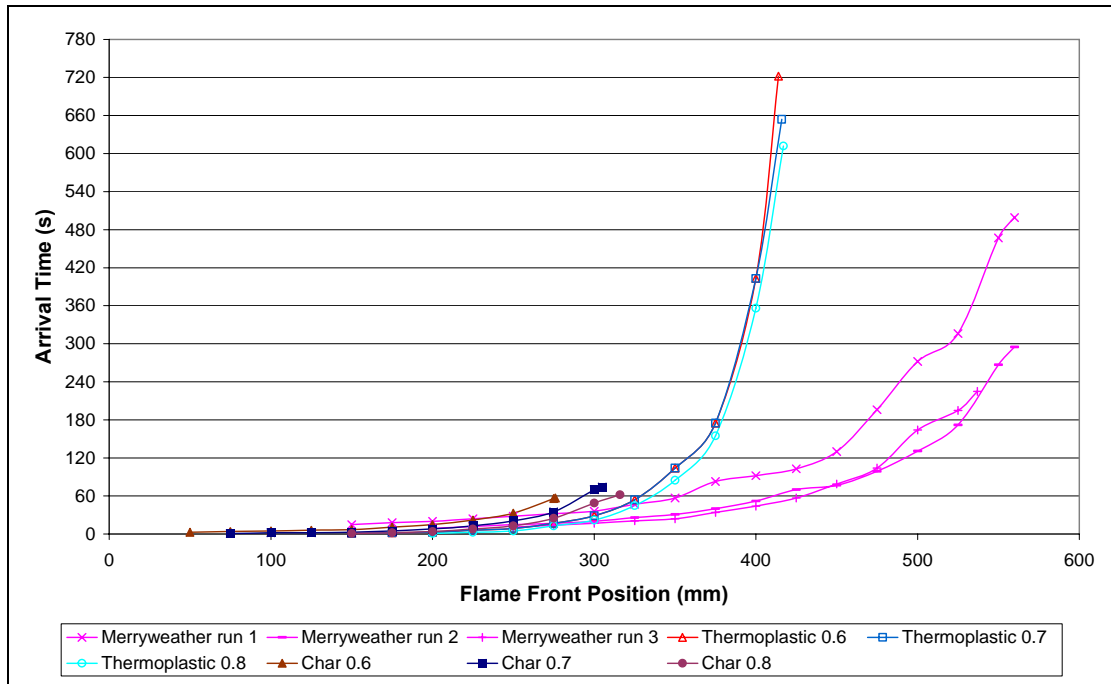


Figure 8-17: Arrival time versus flame front position for Macrocarpa (using Mixture Fraction)

8.4.4 Flame spread for MDF

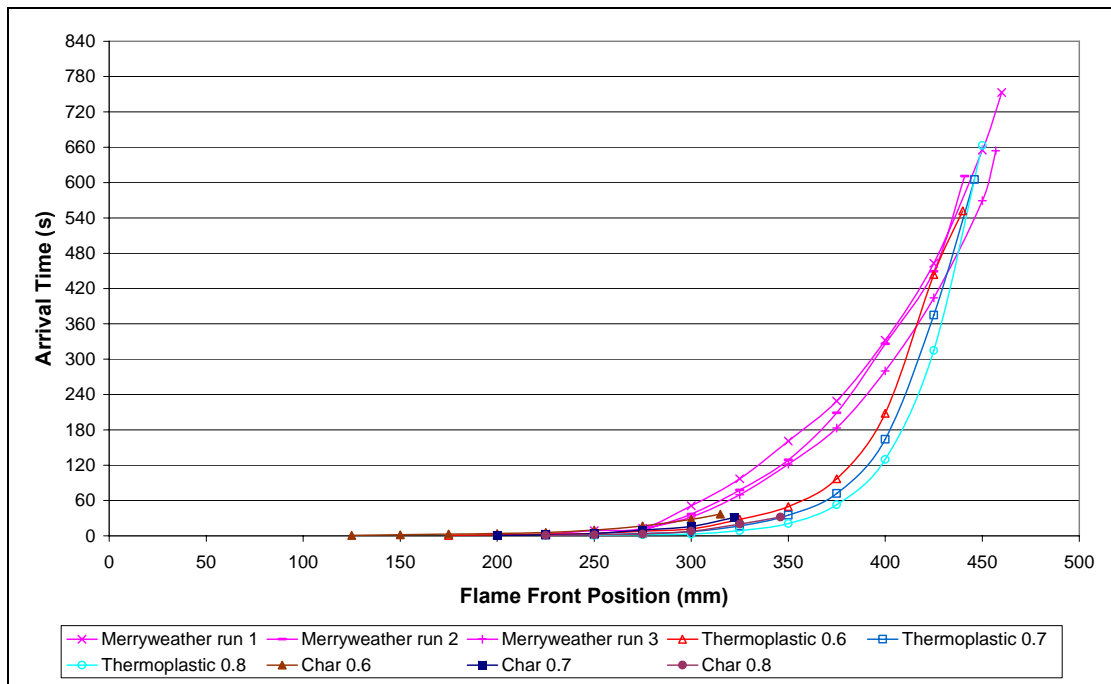


Figure 8-18: Arrival time versus flame front position for MDF (using Mixture Fraction)

8.4.5 Flame spread for Melteca faced MDF

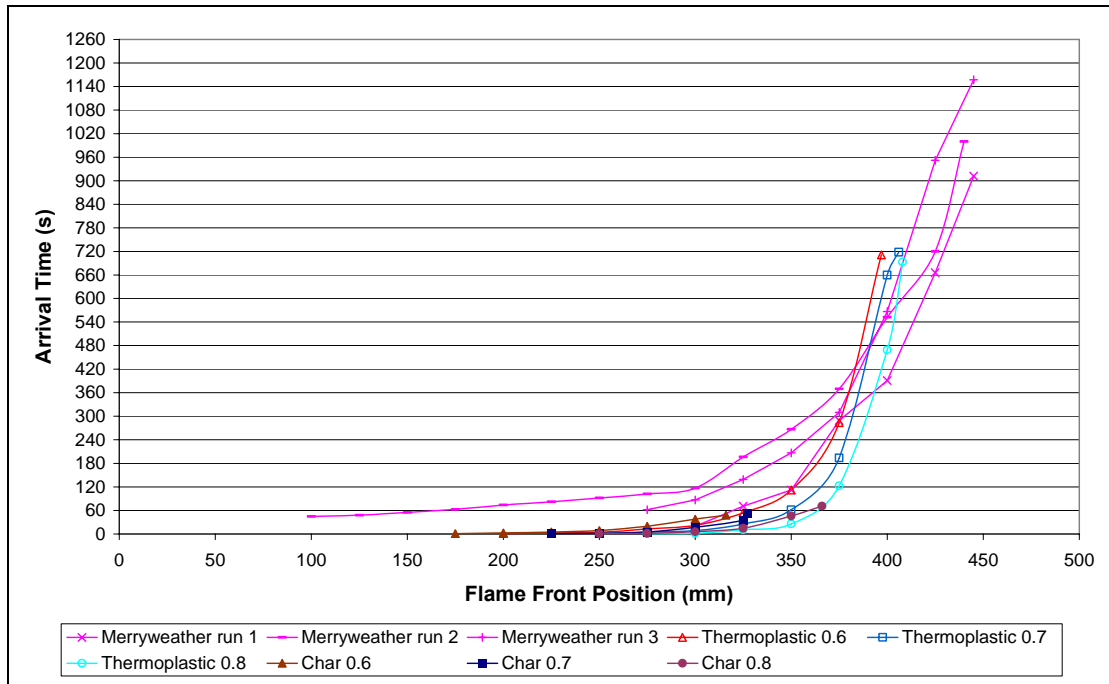


Figure 8-19: Arrival time versus flame front position for Melteca faced MDF (using Mixture Fraction)

8.4.6 Flame spread for Radiata Pine

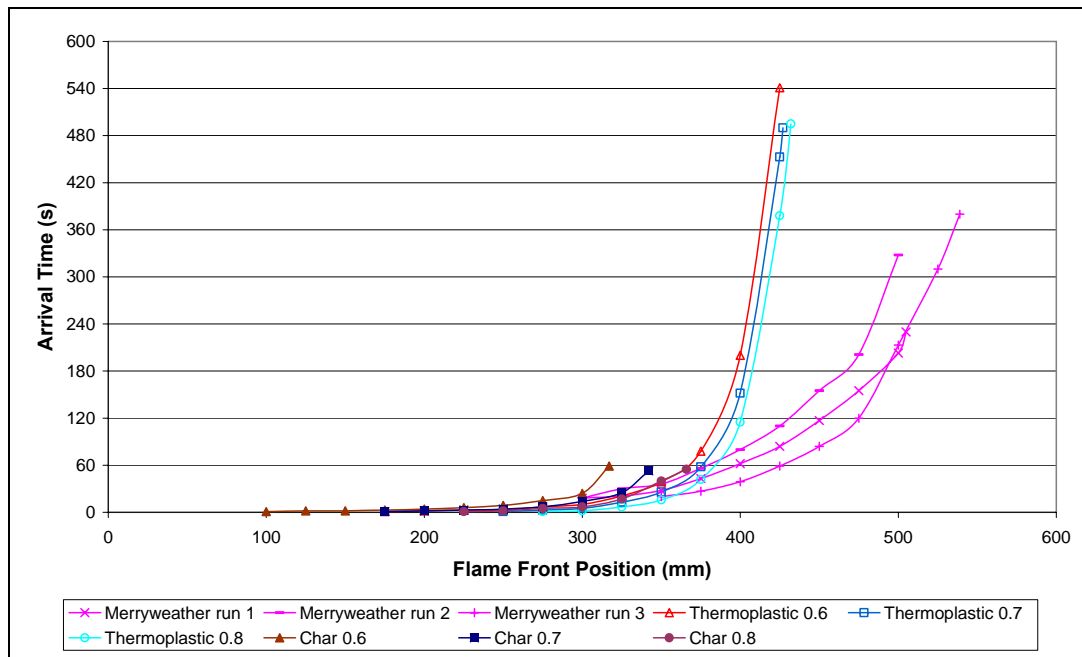


Figure 8-20: Arrival time versus flame front position for Radiata Pine (using Mixture Fraction)

8.4.7 Flame spread for Plywood

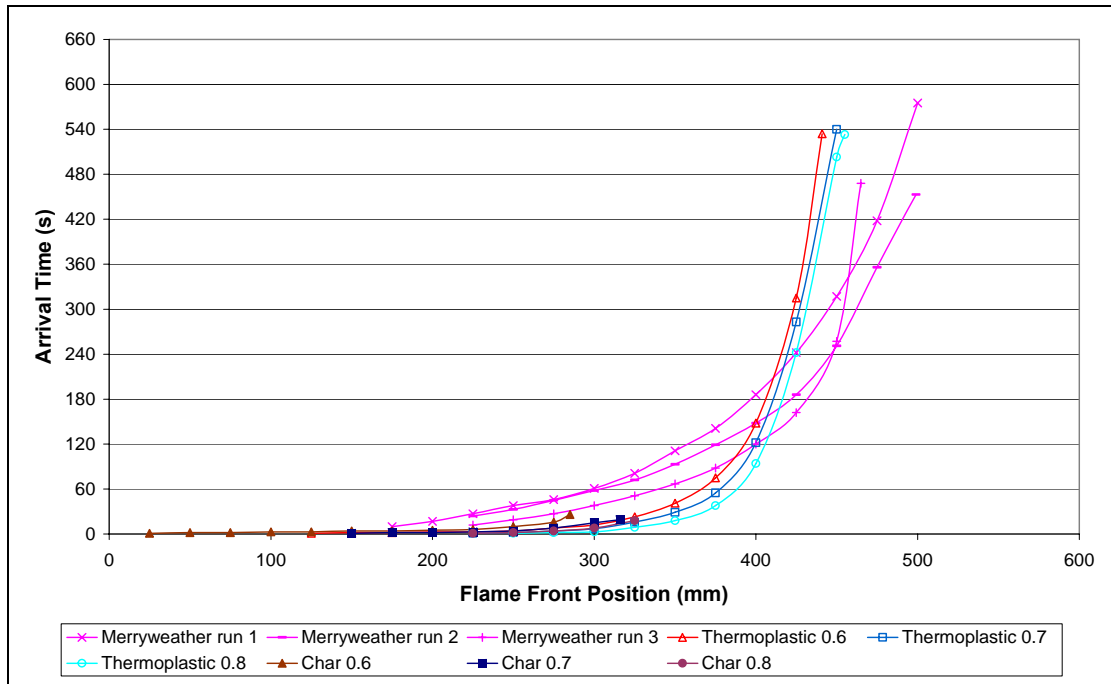


Figure 8-21: Arrival time versus flame front position for Plywood (using Mixture Fraction)

8.4.8 Flame spread for Pynefloor

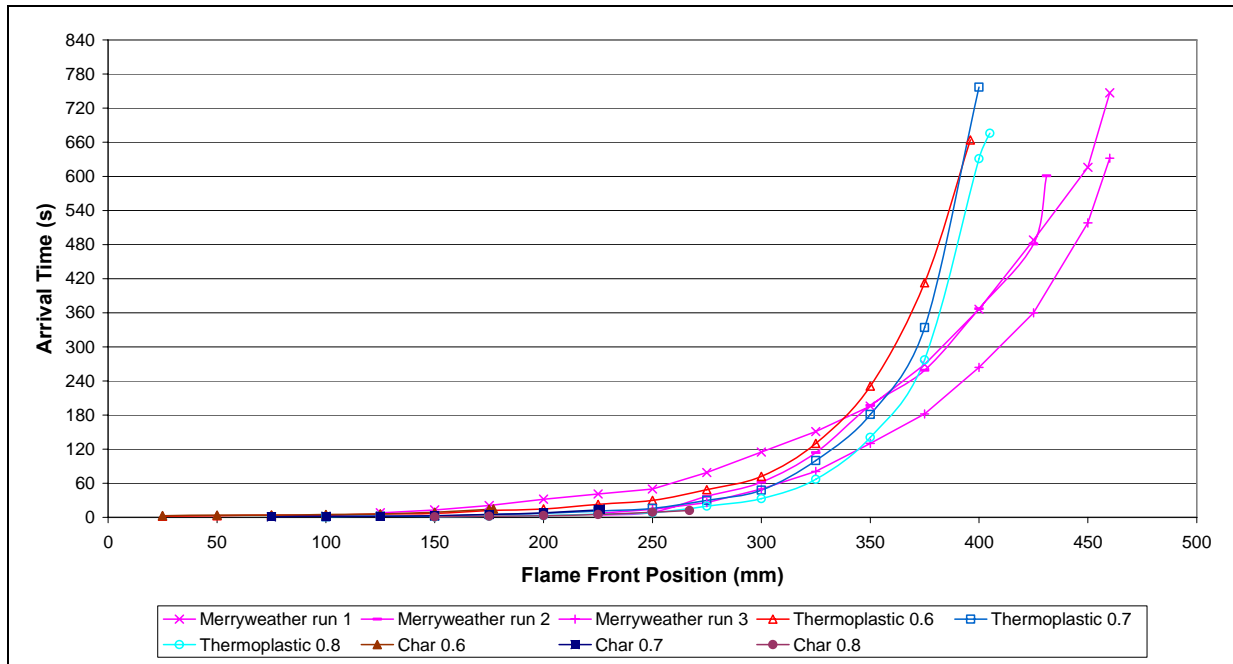


Figure 8-22: Arrival time versus flame front position for Pynefloor (using Mixture Fraction)

8.4.9 Flame spread for Rimu

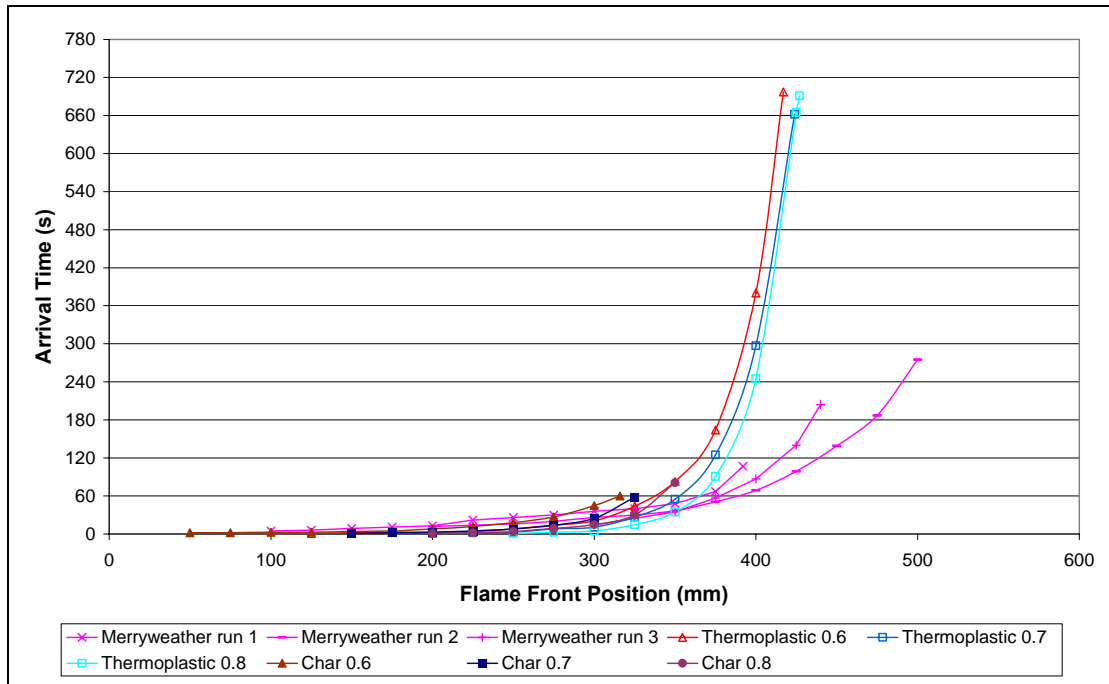


Figure 8-23: Arrival time versus flame front position for Rimu (using Mixture Fraction)

8.5 Flame spread correlations parameters

The correlations of lateral flame spread for different timber and timber based products, using Mixture Fraction as the basis of analysis, are shown in Figure 8-24 to Figure 8-32 below. These are calculated using the flame spread test calculations and are tabulated in Appendix H and its theory can be found in Chapter 4.

The flame spread correlations are determined for both the thermoplastic and charring fuels model. The legend on the left and right hand side represent the correlations for the thermoplastic and charring fuels model respectively from an absorption coefficient of 0.6 to 0.8.

8.5.1 Flame heating correlations for Beech

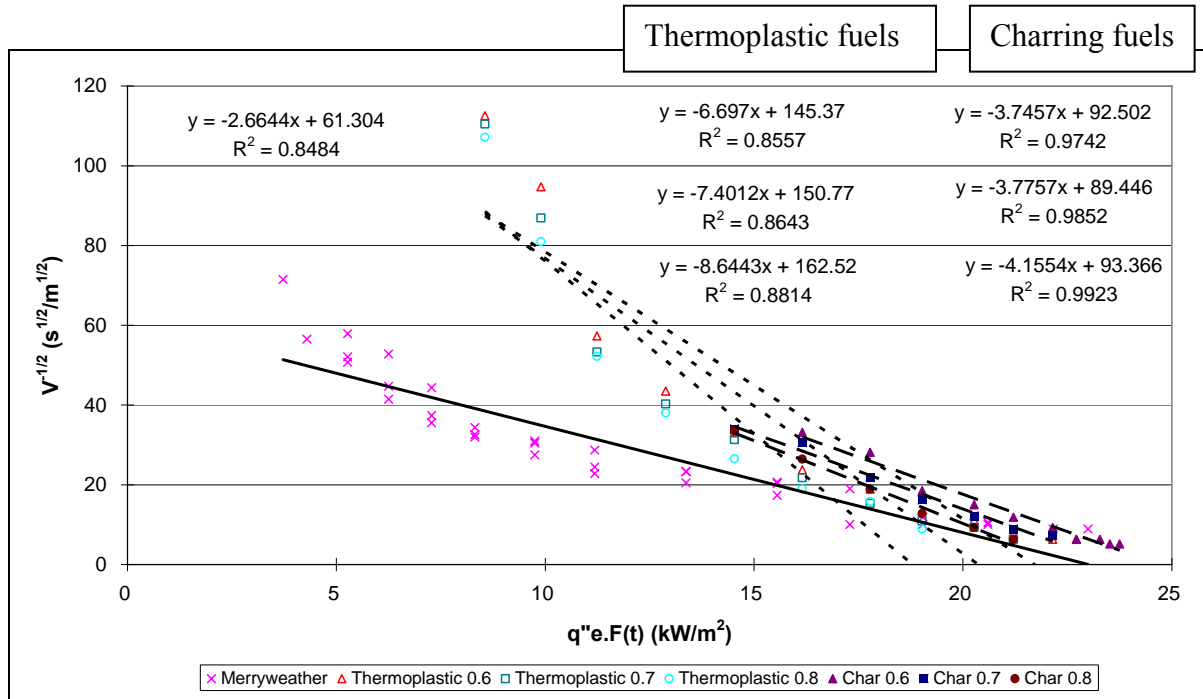


Figure 8-24: Correlations of lateral flame spread for Beech (using Mixture Fraction)

8.5.2 Flame heating correlations for Hardboard

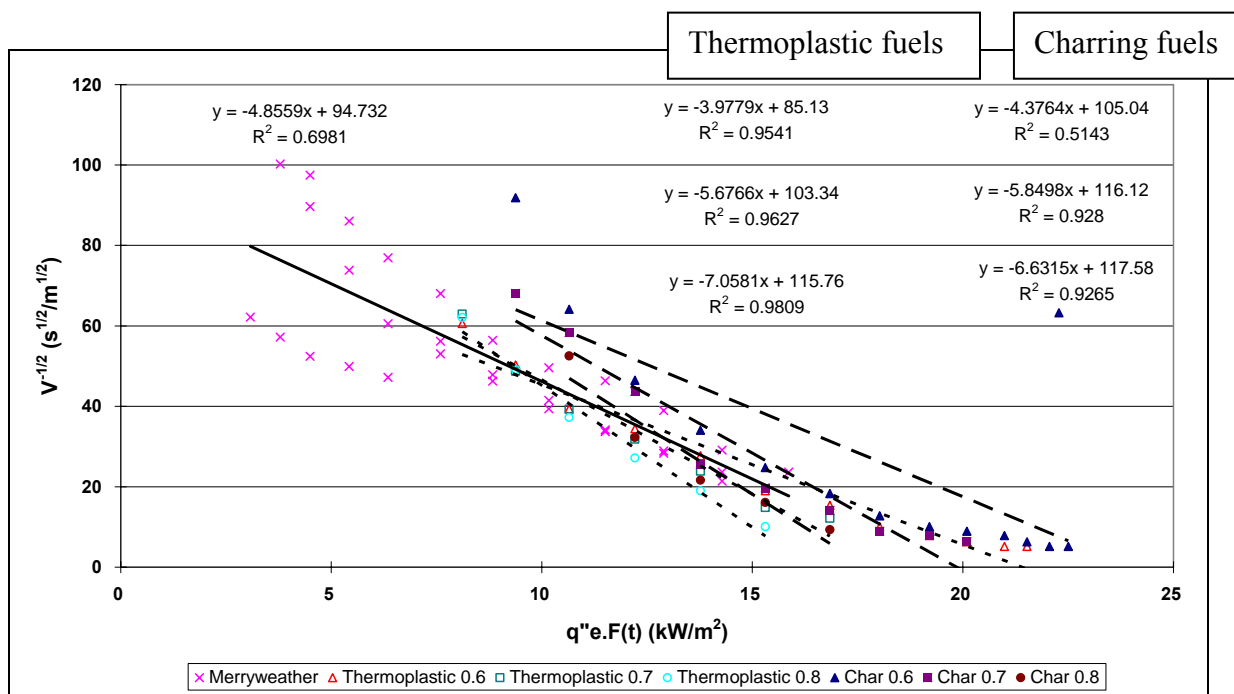


Figure 8-25: Correlations of lateral flame spread for Hardboard (using Mixture Fraction)

8.5.3 Flame heating correlations for Macrocarpa

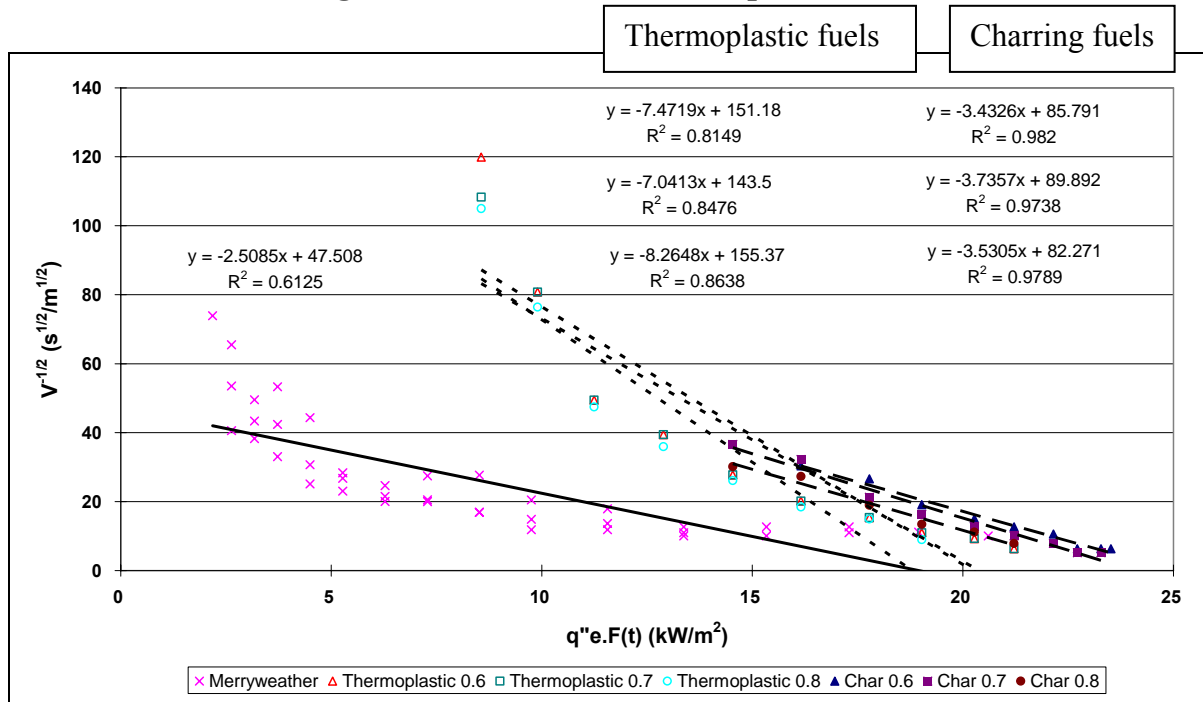


Figure 8-26: Correlations of lateral flame spread for Macrocarpa (using Mixture Fraction)

8.5.4 Flame heating correlations for MDF

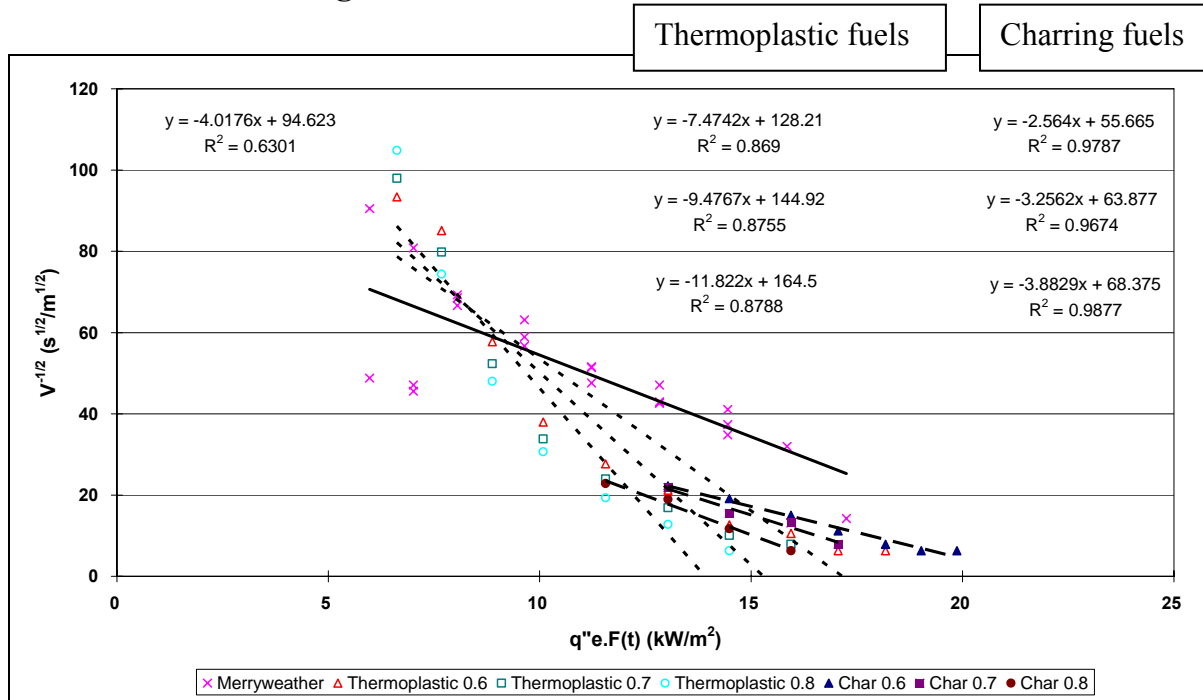


Figure 8-27: Correlations of lateral flame spread for MDF (using Mixture Fraction)

8.5.5 Flame heating correlations for Melteca faced MDF

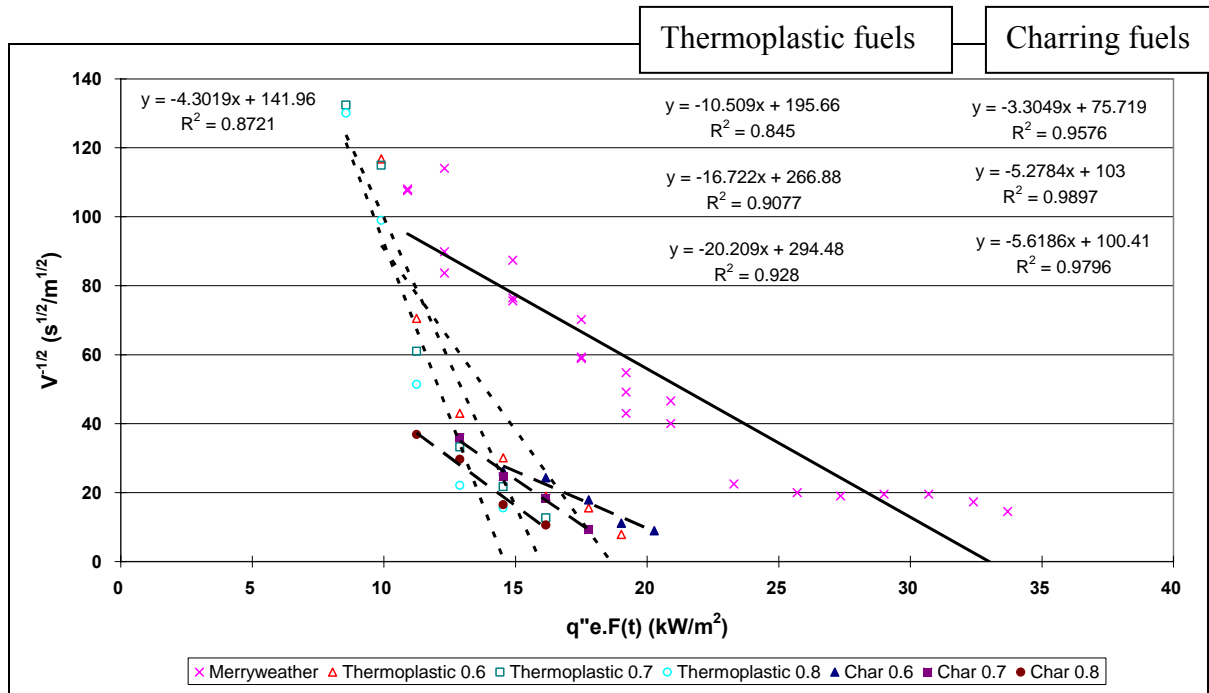


Figure 8-28: Correlations of lateral flame spread for Melteca faced MDF (using Mixture Fraction)

8.5.6 Flame heating correlations for Radiata Pine

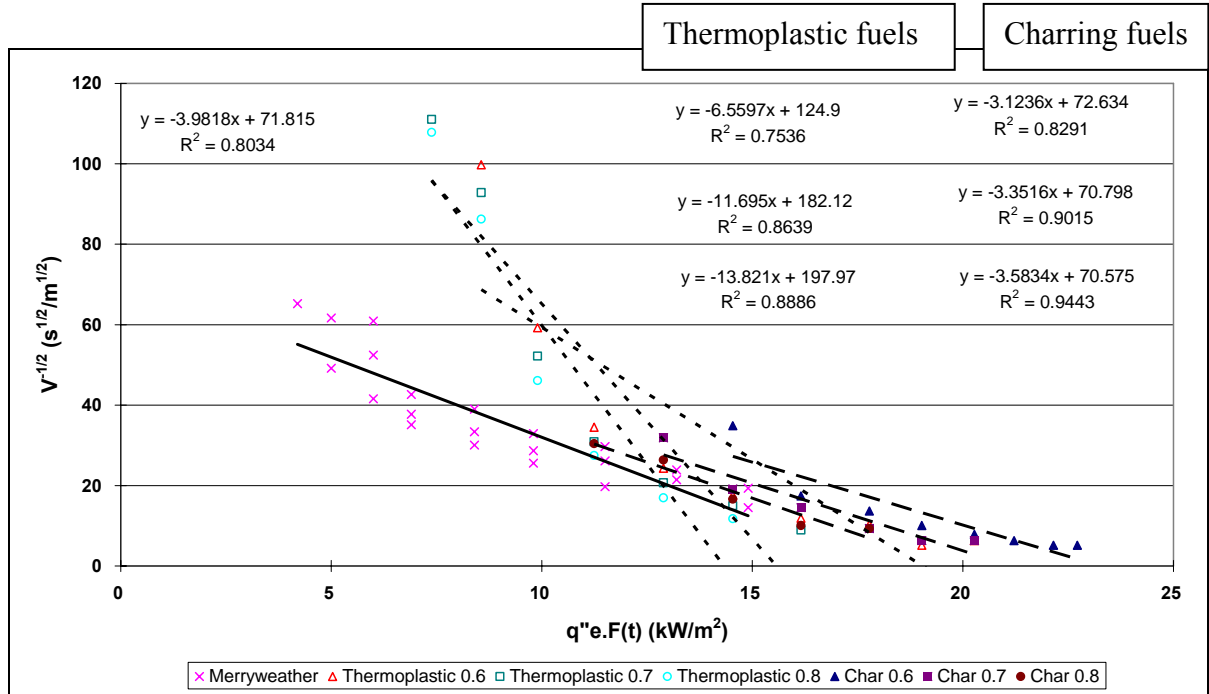


Figure 8-29: Correlations of lateral flame spread for Radiata Pine (using Mixture Fraction)

8.5.7 Flame heating correlations for Plywood

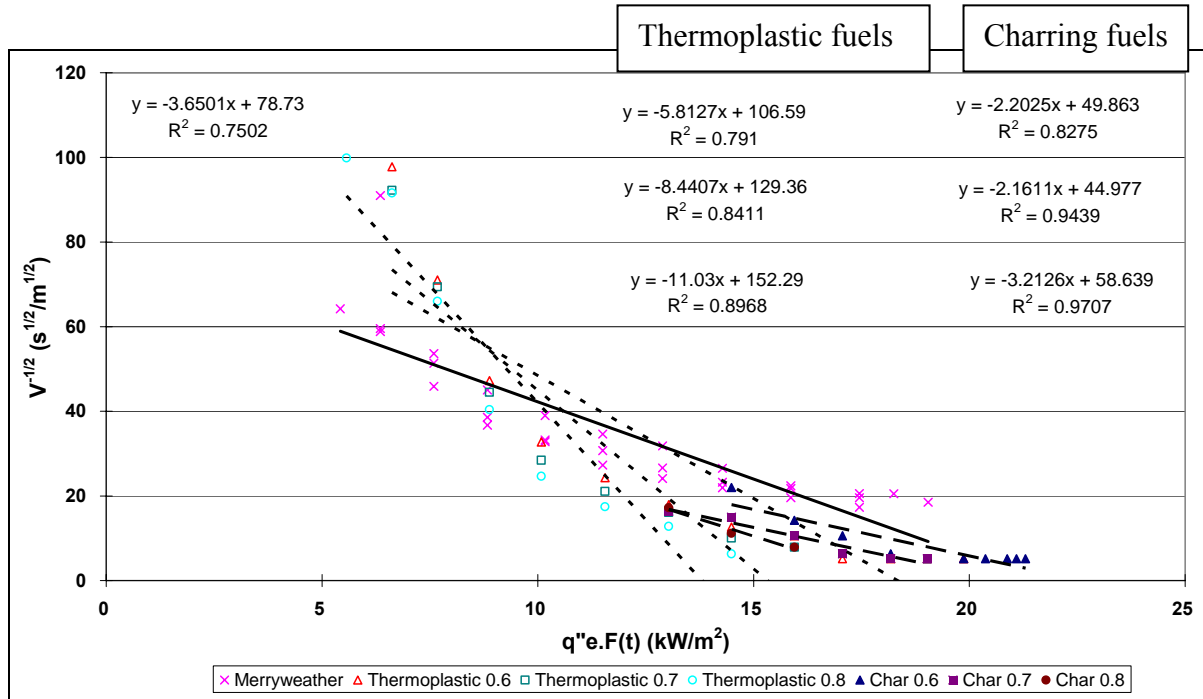


Figure 8-30: Correlations of lateral flame spread for Plywood (using Mixture Fraction)

8.5.8 Flame heating correlations for Pynefloor

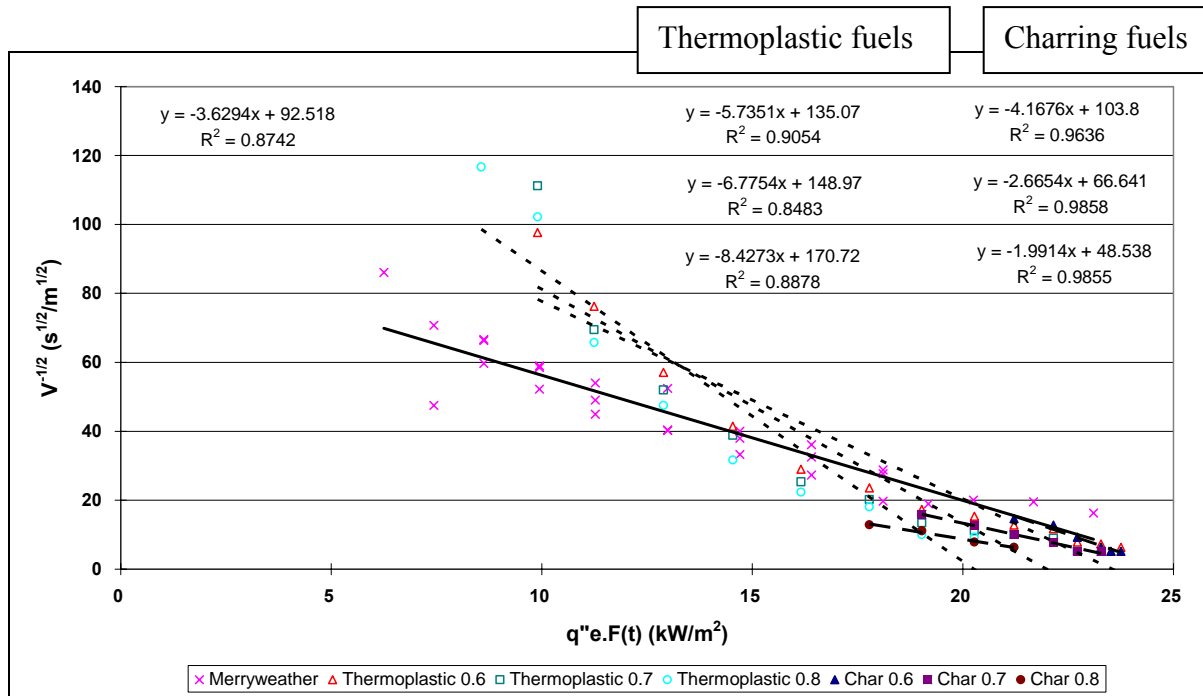


Figure 8-31: Correlations of lateral flame spread for Pynefloor (using Mixture Fraction)

8.5.9 Flame heating correlations for Rimu

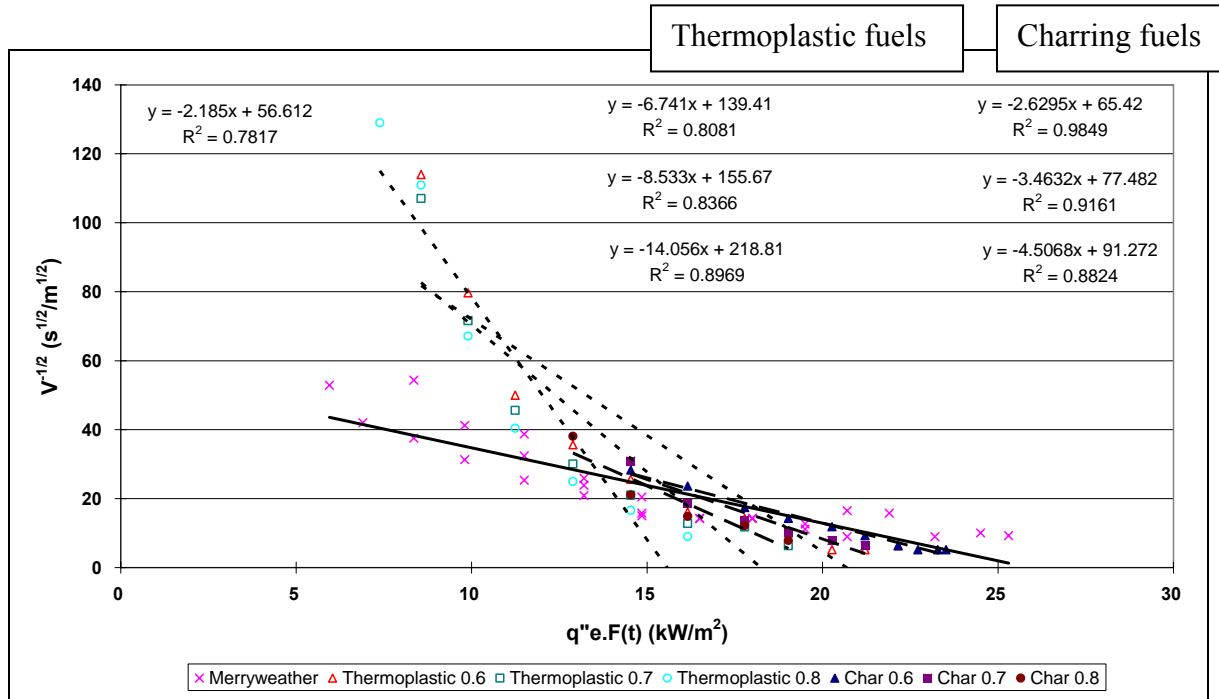


Figure 8-32: Correlations of lateral flame spread for Rimu (using Mixture Fraction)

8.5.10 Summary of the flame spread parameters

Summary of the flame spread parameters such as flame heating parameters, minimum heat flux required for ignition and minimum heat flux required for spread is tabulated in Table 8-2 to Table 8-4 respectively. These tables shows the correlated values obtained from FDS4 using different absorption coefficient in conjunction with the experimental data obtained from Merryweather 2006.

Table 8-2: Flame heating parameters for the selected timber and timber based products

Type of wood panels	Flame Heating Parameter, Φ (using an absorption coefficient of 0.6)	Flame Heating Parameter, Φ (using an absorption coefficient of 0.7)	Flame Heating Parameter, Φ (using an absorption coefficient of 0.8)	Flame Heating Parameter, Φ (from Merryweather 2006)
Macrocarpa	31.2	26.3	29.5	58.3
Plywood	77.0	80.0	36.2	28.0
Beech	35.9	35.3	29.1	54.7
Radiata pine (Monterey pine)	44.5	38.7	33.8	27.4
Medium Density Fibreboard (MDF)	88.4	54.8	38.5	23.4
Pynefloor Particle board (chipboard)	28.3	69.1	123.8	37.3
Melteca faced MDF	65.3	25.6	22.6	38.5
Hardboard	24.9	14.0	10.9	20.3
Rimu	72.8	42.0	24.8	106.6

Table 8-3: Minimum heat flux for ignition for the selected timber and timber based products

Type of wood panels	$q''_{o,ig}$ (Correlation) (using an absorption coefficient of 0.6)	$q''_{o,ig}$ (Correlation) (using an absorption coefficient of 0.7)	$q''_{o,ig}$ (Correlation) (using an absorption coefficient of 0.8)	$q''_{o,ig}$ (Correlation) (from Merryweather 2006)
Macrocarpa	25.0	24.1	23.3	18.9
Plywood	22.6	20.8	18.3	21.6
Beech	24.7	23.7	23.7	21.3
Radiata pine (Monterey pine)	23.3	21.1	19.7	18.0
Medium Density Fibreboard (MDF)	21.7	19.6	17.6	14.9
Pynefloor Particle board (chipboard)	24.9	25.0	24.4	25.5
Melteca faced MDF	22.9	19.5	17.9	33.0
Hardboard	24.0	19.9	17.7	19.5
Rimu	24.9	22.4	20.3	26.0

Table 8-4: Critical heat flux for spread for the selected timber and timber based products

Type of wood panels	Critical flux for spread, $q''_{o,s}$ (From Graph) (using an absorption coefficient of 0.6)	Critical flux for spread, $q''_{o,s}$ (From Graph) (using an absorption coefficient of 0.7)	Critical flux for spread, $q''_{o,s}$ (From Graph) (using an absorption coefficient of 0.8)	Critical flux for spread, $q''_{o,s}$ (from Merryweather 2006)
Macrocarpa	14.5	12.9	12.9	2.2
Plywood	14.5	11.6	11.6	5.4
Beech	14.5	12.9	12.9	3.7
Radiata pine (Monterey pine)	12.9	11.2	9.9	4.2
Medium Density Fibreboard (MDF)	11.6	11.6	10.1	8.7
Pynefloor Particle board (chipboard)	20.3	17.8	16.2	6.2
Melteca faced MDF	12.9	11.2	9.9	10.9
Hardboard	8.1	8.1	9.4	3.1
Rimu	12.9	12.9	11.2	6.0

9 Sensitivity Analysis

This chapter presents the sensitivity analysis performed for the flame spread test FDS4 model; which includes the grid size of the FDS4 setup, the type of pyrolysis model and FDS4 input variables (both the heat of vaporisation and moisture content of the specimen), this enables the effect that each parameter has on the flame spread to be compared.

9.1 Grid Sizing

The grid resolution that was used for the flame spread test model was 10 mm. However, the processing of the model is considered to be time-consuming due to the fine grids i.e. the computation time for this is 72 hours using a Pentium 4 3.2 GHz with 1 gigabyte of RAM. The aim of this section is to determine an appropriate grid size that represents the flame spread test and minimises the computational time while maintaining accuracy of the results. This analysis comprises of coarser grid sizes (15 mm, 20 mm and 25 mm). Despite different grid sizes being used in the flame spread test model, calibration of the LIFT apparatus is also required as stated in the ASTM E 1321 97a (2002) standards. This is to ensure the heat flux exposed on the specimens is identical for every specimen.

9.1.1 Calibration of the LIFT apparatus for different grid sizes

As mentioned earlier, the chosen grid size for analysis is 15, 20 and 25 mm. In principle all other inputs in the FDS4 input files are identical with the exception of the temperature on the radiant panel and the settings of the grid size in the model. The FDS4 input for the selected grid size is shown in Figure 9-1, Figure 9-2 and Figure 9-3 respectively for 15, 20 and 25 mm.

```
&HEAD CHID='Lift 15mm calibration 860',TITLE='Lift 15mm calibration 860' /
&GRID IBAR=63.33,JBAR=20,KBAR=20 / Specify number of grid cells in the x, y, and z
directions, respectively
&PDIM XBAR=0.95,YBAR=0.3,ZBAR=0.3 /
&TIME TWFIN=1000. / Time when finished (length of simulation)
```

Figure 9-1: FDS4 input for a grid size of 15mm

```
&HEAD CHID='Lift 20mm calibration 853',TITLE='Lift 20mm calibration 853' /
&GRID IBAR=47.5,JBAR=15,KBAR=15 / Specify number of grid cells in the x, y, and z
directions, respectively
&PDIM XBAR=0.95,YBAR=0.3,ZBAR=0.3 /
&TIME TWFIN=1000. / Time when finished (length of simulation)
```

Figure 9-2: FDS4 input for a grid size of 20mm

```
&HEAD CHID='Lift 25mm calibration 843',TITLE='Lift 25mm calibration 843' /
&GRID IBAR=38,JBAR=12,KBAR=12 / Specify number of grid cells in the x, y, and z
directions, respectively
&PDIM XBAR=0.95,YBAR=0.3,ZBAR=0.3 /
&TIME TWFIN=1000. / Time when finished (length of simulation)
```

Figure 9-3: FDS4 input for a grid size of 25mm

Calibration for each grid size is carried out individually to determine the required temperature on the radiant panel walls. As increasing the grid size in the domain also affects the heat flux exposed on the specimen; where the geometry of the radiant panel is distorted when compared to a 10mm grid size as indicated in Figure 9-4 to Figure 9-6. Results for the calibration of the LIFT apparatus in FDS4 are summarised in **Table 9-1**, which includes the temperature required on the radiant panel for the selected grid size.

Finally, these temperatures are implemented appropriately on the walls of radiant panel with the addition of coarser grid sizes into the flame spread test model in order to carry out the FDS4 simulation.

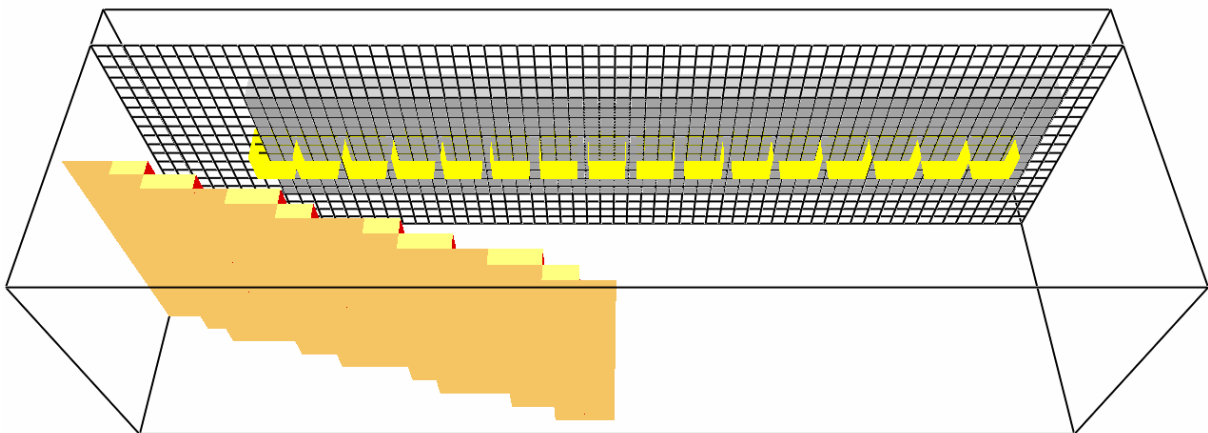


Figure 9-4: LIFT test setup in FDS4 using a grid size of 15mm (a view from Smokeview)

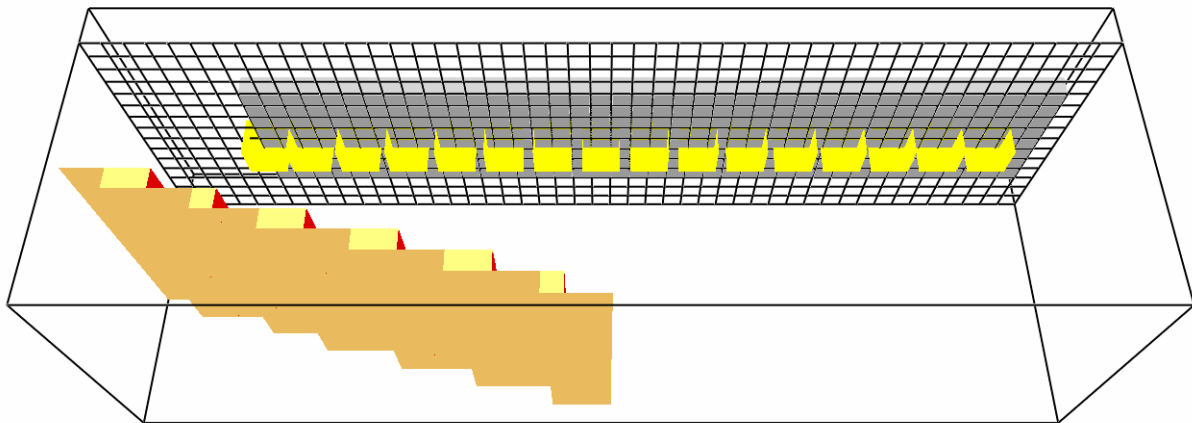


Figure 9-5: LIFT test setup in FDS4 using a grid size of 20mm (a view from Smokeview)

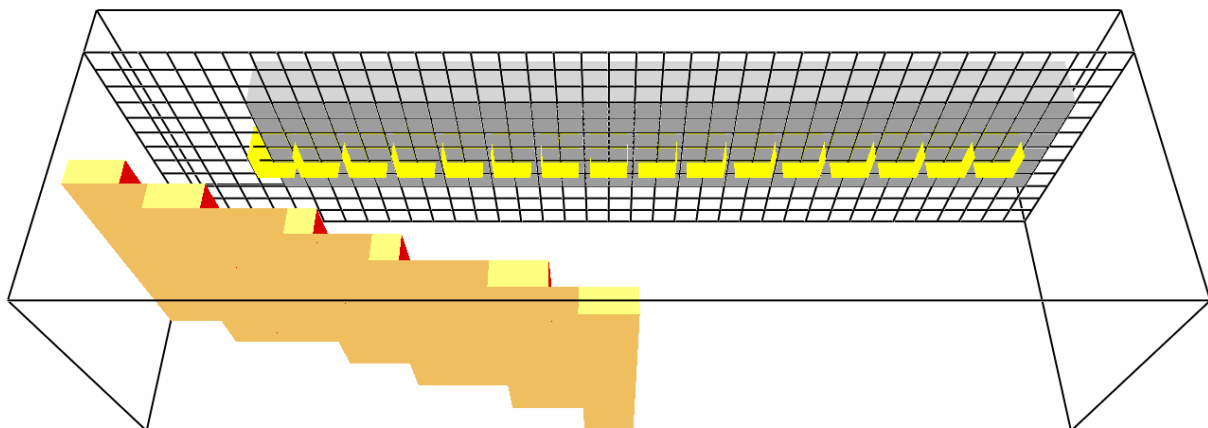


Figure 9-6: LIFT test setup in FDS4 using a grid size of 25mm (a view from Smokeview)

Table 9-1: Summary for the calibration of the LIFT apparatus in FDS4

For 15mm

Type of Material	Minimum Ignition Flux (kW/m ²) (Merryweather 2006)	Heat Flux required by ASTM standards	Temp of the radiant panel (TMPWAL, K)	Corresponding heat flux after 25s (kW/m ²)	% difference
Hardboard	17.5	22.5	654	22.5	0.0%
Medium Density Fibreboard (MDF)	16.25	21.3	641	21.2	-0.2%
Melteca faced MDF	18.75	23.8	665	23.6	-0.6%
Beech	18.75	23.8	665	23.6	-0.6%
Macrocarpa	18.75	23.8	665	23.6	-0.6%
Radiata Pine (Monterey pine)	18.75	23.8	665	23.6	-0.6%
Rimu	18.5	23.5	663	23.4	-0.4%
Plywood	16.3	21.3	641	21.2	-0.5%
Pynefloor Particle board (chipboard)	18.75	23.8	665	23.6	-0.6%

For 20mm

Type of Material	Minimum Ignition Flux (kW/m ²) (Merryweather 2006)	Heat Flux required by ASTM standards	Temp of the radiant panel (TMPWAL, K)	Corresponding heat flux after 25s (kW/m ²)	% difference
Hardboard	17.5	22.5	656	22.5	0.0%
Medium Density Fibreboard (MDF)	16.25	21.3	644	21.3	0.2%
Melteca faced MDF	18.75	23.8	669	23.7	-0.2%
Beech	18.75	23.8	669	23.7	-0.2%
Macrocarpa	18.75	23.8	669	23.7	-0.2%
Radiata Pine (Monterey pine)	18.75	23.8	669	23.7	-0.2%
Rimu	18.5	23.5	666	23.4	-0.4%
Plywood	16.3	21.3	644	21.3	0.0%
Pynefloor Particle board (chipboard)	18.75	23.8	669	23.7	-0.2%

For 25mm

Type of Material	Minimum Ignition Flux (kW/m ²) (Merryweather 2006)	Heat Flux required by ASTM standards	Temp of the radiant panel (TMPWAL)	Corresponding heat flux after 25s (kW/m ²)	% difference
Hardboard	17.5	22.5	646	22.4	-0.4%
Medium Density Fibreboard (MDF)	16.25	21.3	634	21.3	0.2%
Melteca faced MDF	18.75	23.8	659	23.7	-0.2%
Beech	18.75	23.8	659	23.7	-0.2%
Macrocarpa	18.75	23.8	659	23.7	-0.2%
Radiata Pine (Monterey pine)	18.75	23.8	659	23.7	-0.2%
Rimu	18.5	23.5	656	23.4	-0.4%
Plywood	16.3	21.3	634	21.3	0.0%
Pynefloor Particle board (chipboard)	18.75	23.8	659	23.7	-0.2%

9.1.2 Flame spread results for different grid sizes

Flame spread results are obtained for different grid sizes using thermoplastic fuels model in conjunction with Mixture Fraction for analysis. This is to see how FDS4 predicts flame spread when a coarser grid size is selected. Figure 9-7 shows the arrival time against the flame front position for the Beech specimen using different grid sizes (ranging from 10mm to 25mm) and compared with the experimental results obtained by Merryweather (2006). From this figure, it indicated that the prediction of flame spread using a fine grid size (i.e. 10 mm) is better than a coarse grid size as more details are capture by the finer grid cells; hence flame can travel further along the specimen. Furthermore, the extent of flame spread occurs much earlier than expected for coarser grid size due to the details of the reaction is not being captured in FDS4.

It should be noted that other specimens behave very similar in terms of the spread of flame when compared to Beech and for this reason it is not shown in this section.

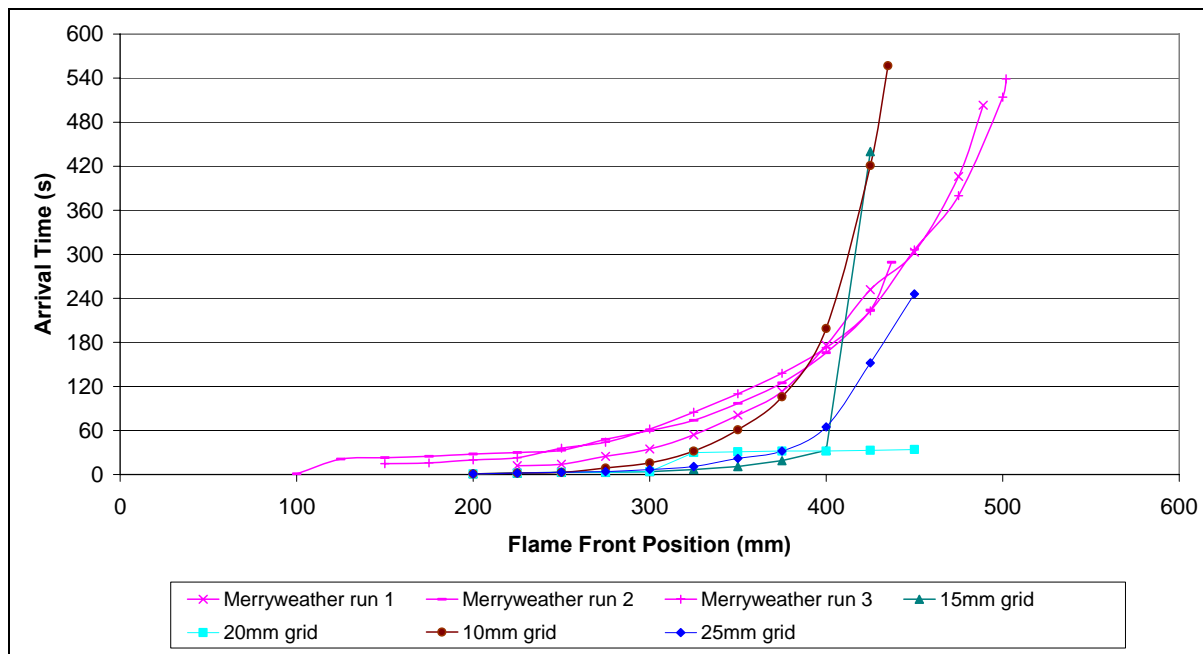


Figure 9-7: Arrival Time versus Flame Front Position for Beech with different grid sizes (using Mixture Fraction)

Figure 9-8 shows the correlations of lateral flame spread for Beech using FDS4 and comparing it with the experimental results. Again the correlation equations for each grid size

are presented on the right hand side of the figure; where the grid size increases from top to bottom (i.e. 10 mm to 25 mm) as indicated.

Interestingly, a grid size of 15 mm and 25 mm correlates better than the finer grid sizes. Overall, it indicates the lack of consistency in using FDS4 to correlate flame spread parameters. This is due to the extent of flame spread being simulated too early (i.e. the flame spreads faster in FDS) when compared to the experimental results, the extent of flame spread does not spread as far as the experimental results and the fact that the flame heating parameter is very sensitive to the slope of the correlation.

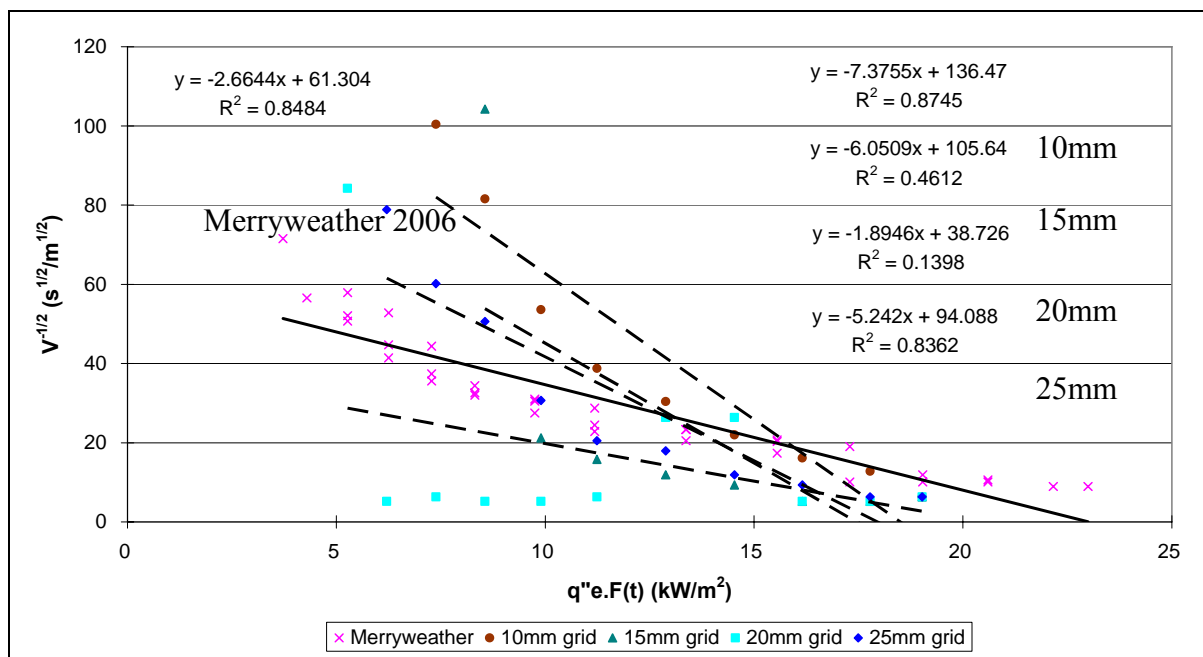


Figure 9-8: Correlations of Lateral Flame Spread for Beech with different grid sizes (using Mixture Fraction)

9.1.3 Discussion on the effect of the grid size on flame spread

Calibration results from Section 9.1.1 already indicated that the radiant panel in the FDS4 model can accurately simulate the required heat flux to perform a flame spread test despite grid size is changed. Similarly, flame spread data are collected for all nine timber and timber based products using Smokeview. In order to understand the effect of grid size has on modelling flame spread in FDS4, the results from the correlations are directly compared with

the experimental data; where percentage difference is used as a parameter for comparing the prediction of flame spread using different grid sizes in the FDS4 model.

Table 9-2 shows the percentage difference of the flame heating parameter between the experimental results and the FDS4 results. It demonstrates that the flame heating parameter predicted using a grid size of 25 mm is the best overall; where it is within 75% error. The reason of a 10mm grid size not giving the best prediction of the flame heating parameter is due to the calculation of the flame heating parameter strongly depends on the slope of the correlation, i.e. extent of flame spread that is simulated in FDS4 will affect the flame heating parameter, despite that fact that it can simulated the best flame front arrival time.

On the other hand, the percentage difference of the critical flux required for ignition between the experimental results and the FDS4 results indicates that as the grid size increases, the percentage difference for the critical heat flux required for ignition increases. In particular, this parameter is poorly correlated than all other parameters as the percentage error is over 100% for both grid size of 20mm and 25mm. This is due to the early ignition of the specimen where the temperature along the specimen is simulated insufficiently i.e. the reaction along the specimen is not correctly modelled.

Finally, the percentage difference of the critical flux required for spread between the experimental results and the FDS4 results also suggested that the prediction of the critical flux required for flame spread contains the largest error. The reason for coarser grid cells to have a longer flame extent is that an average temperature is taken over a larger grid cells.

Table 9-2: Summary of the flame spread parameters from Merryweather (2006) and FDS4 using different grid sizes

Source	Flame Heating Parameter, Φ	% difference	$q''_{o,ig}$ (Correlation)	% difference	Critical flux for spread, $q''_{o,s}$ (From Graph)	% difference
Merryweather	70.9	0.0%	23.0	0.0%	3.7	0.0%
10mm	9.2	-87.0%	18.5	-19.6%	6.2	66.8%
15mm	13.7	-80.6%	17.5	-24.1%	7.4	98.3%
20mm	140.1	97.8%	-1.9	-108.1%	5.3	41.5%
25mm	18.3	-74.2%	493.2	2043.5%	5.3	41.5%

Based on the analysis of grid size presented above, there seems to be a minor difference in the correlation of flame spread when a coarser grid size (i.e. larger than 10 mm) is used. However, it is noticed that the extinction of the flame occurs much earlier than expected when the selected grid size increases.

Despite of all this, the arrival time versus the flame front position indicates that the prediction of the flame spread using FDS4 is plausible in the early stages of flame spread; where a grid size of up to 25mm can be use for the prediction flame spread up to 230 mm along the specimen (also the point where extent of flame spread occurs). Nevertheless, a grid size of 10 mm is chosen for the flame spread test model so that finer reaction details are captured.

9.2 Sensitivity on the pyrolysis model

Two pyrolysis models are examined to see the effect it has on the flame spread. The selected models include thermoplastic fuels and charring fuels, as the timber and timber based products are assumed to pyrolyse and ignite. These models are based on a one dimensional heat transfer model as mentioned in Chapter 4. Besides this, two different flame visualisation in Smokeview is used to simulate the flame spread namely Mixture Fraction and HRRPUV; this option is selected in the Smokeview window.

9.2.1 FDS4 input for the pyrolysis models

As mentioned in the previous chapter (Chapter 8), the FDS4 input required for the two models are similar. However, the charring fuels model consists of more variables relating to the properties of char. This is to account for the insulation provided by the charred materials.

In general, the thermoplastic fuels model requires variables such as moisture content, thickness of the material, mass flux at ignition temperature, heat of vaporisation, ignition temperature, initial temperature of the material, density of the material, thermal conductivity, specific heat capacity, internal wall points and back face boundary condition. While, the charring fuels model requires the additional variables such as the thermal conductivity, specific heat capacity and density of the charred materials.

Additionally, the charring fuels model used in this research have constant char properties employed, i.e. char properties are constant at different temperature. This is due to the equipment available where the thermal transport properties can only be measured at room temperature (21°C) using the Hot Disk test.

9.2.2 Flame spread results for the pyrolysis models

Figure 9-9 is a plot of the percentage difference when comparing the flame heating parameter between the results obtained from FDS4 and Merryweather (2006). From this graph, the flame heating parameters obtained using the charring fuels model shows a significant variation when compared to the thermoplastic model. It is also noticeable that both the thermoplastic fuels model and HRRPUV used to simulate flame always underestimates the flame heating parameters with the exception of one case for Radiata Pine having an absorption coefficient of 0.6. In general, it is still considered to underestimate the flame heating parameter.

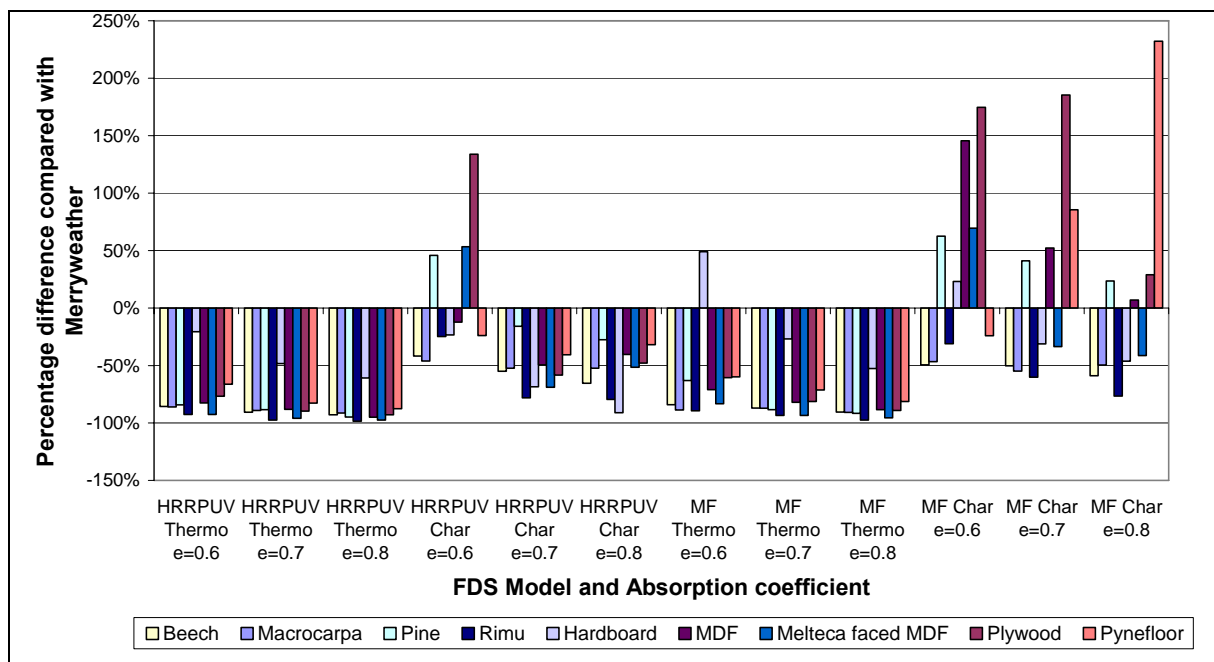


Figure 9-9: Comparison of flame heating parameter between the results from Merryweather (2006) and FDS4 using different FDS4 model and absorption coefficient

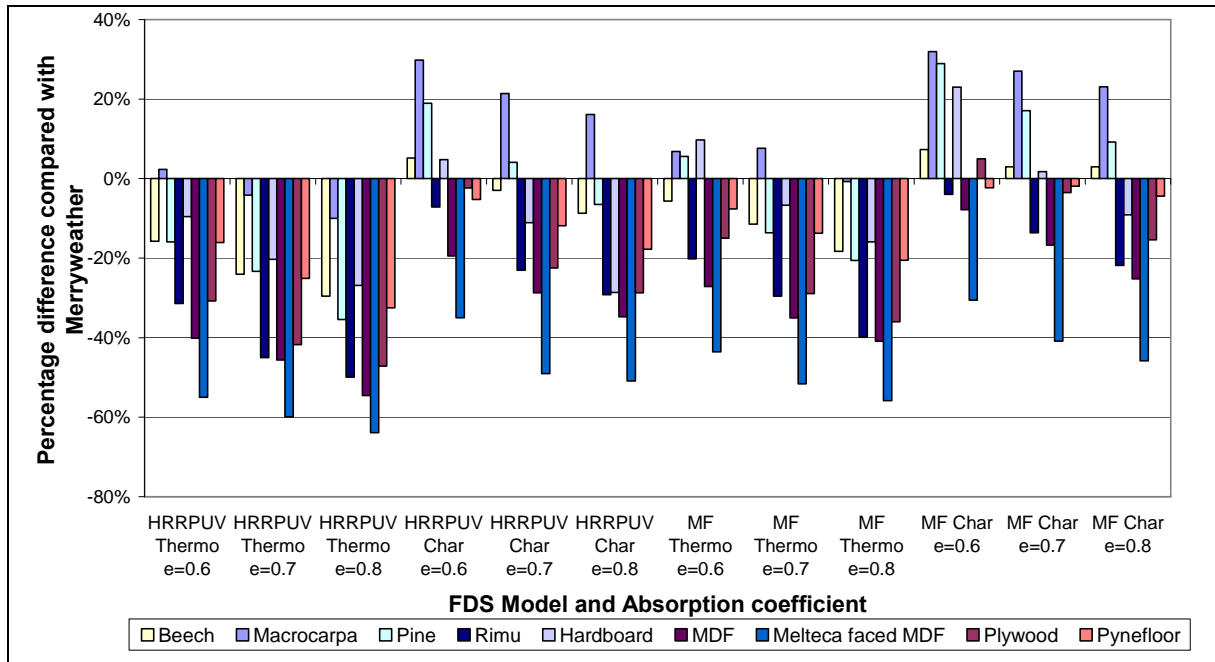


Figure 9-10: Comparison of critical flux for ignition between the results from Merryweather (2006) and FDS4 using different FDS4 model and absorption coefficient

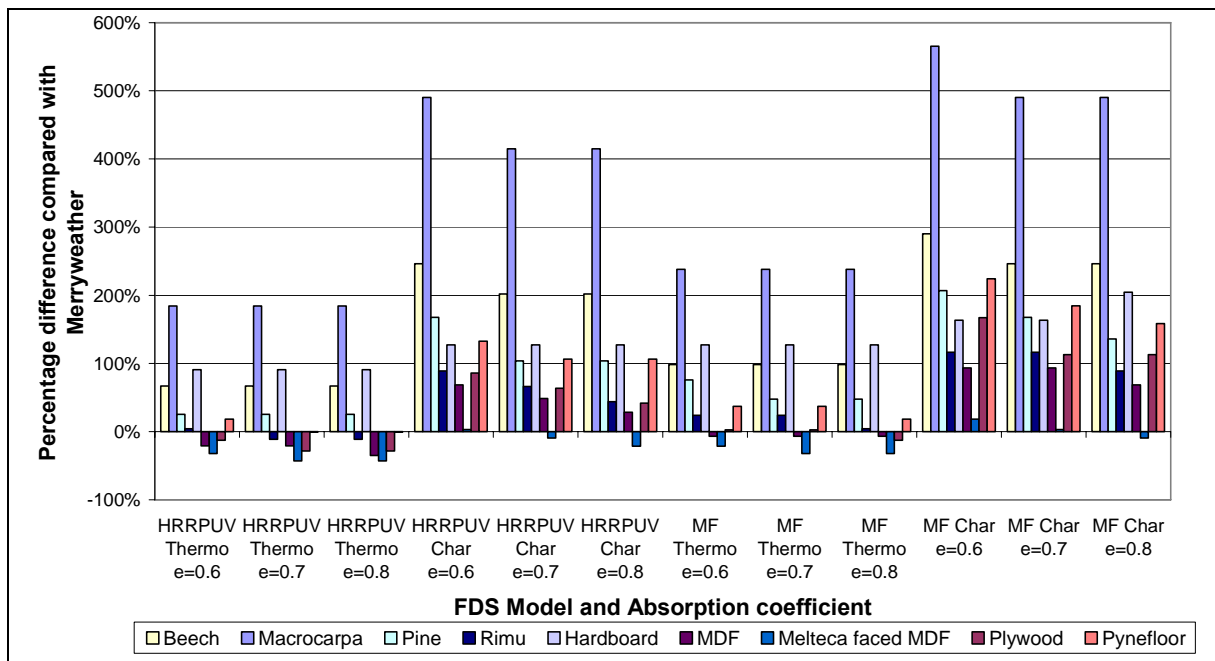


Figure 9-11: Comparison of critical flux for spread between the results from Merryweather (2006) and FDS4 using different FDS4 model and absorption coefficient

Meanwhile, Figure 9-10 and Figure 9-11 is a plot of the percentage difference comparing the critical heat flux required for ignition and spread respectively between the results obtained from FDS4 and Merryweather (2006). For the critical flux required for ignition, the thermoplastic fuels model displays a similar trend as in the flame heating parameter where it underestimates the critical flux for ignition. Again, as for the charring fuels model, this parameter fluctuates between specimens but it is within 40% of accuracy when compared to the experimental results.

Conversely from Figure 9-11, the thermoplastic fuels model correlates a better match in the critical heat flux for flame spread when compared to the charring fuels model. This is because the extent of flame spread using the thermoplastic fuels model is closer to the experimental results as shown by the arrival time against flame front position in Appendix I. In addition, this figure indicates that the correlation of critical flux for flame spread from the charring fuels model is very poor where the percentage difference is 200% on average.

9.2.3 Discussion on the technique of analysing the flame spread

From the sensitivity analysis on the technique of simulating flame spread, it is indicated that using the mixture fraction to model the flame is more appropriate than using HRRPUV. This is because using HRRPUV tends to underestimate the flame heating parameters.

In addition, it is determined that the most appropriate pyrolysis model to be used in predicting the flame spread would be the thermoplastic fuels model. The reason is due to the extent of flame spread is modelled better in the thermoplastic fuels model than the charring fuels model. Despite, the thermoplastic fuels predicting the extent of the flame spread to occur later when compared to the experimental results. By using this scenario as the basis, the plot of the arrival time against the distance along the specimen exhibits a similar trend of flame spread with the experimental results initially, but later on, the extent of flame spread gradually slows down and stops at a similar location along the specimen as the experimental results indicated.

In this research, a thermoplastic fuels model is chosen to simulate the pyrolysis process while the flame spread data is analysed using mixture fraction. Overall, the correlated critical heat

flux for ignition appears to be by far the best correlations from the flame spread data where the results are within 50% of accuracy.

9.3 Sensitivity on the FDS4 inputs

A number of parameters have been assumed and applied in the flame spread test model; these variables include heat of vaporisation and moisture content. This section tries to determine the effect these variables has on flame spread. In this case, only the Beech specimen is selected to carry out this process; while the charring fuels model is used as the pyrolysis model and mixture fraction is implemented to simulate the flame spread in Smokeview as discussed in the previous section.

9.3.1 Heat of vaporisation

As mentioned in the previous chapter, the heat of vaporisation for the charring fuels model refers to the gasification of the virgin material at the pyrolysis front. And it is not an “effective” value that is often used to model the effect of the char shielding the virgin material from the heat flux at the surface (McGrattan (editor) July 2004). As it is reasonable to assume that the char materials are similar regardless of the type of wood species, the selected heat of vaporisation for the charring fuels model is 500 kJ/kg which comes from the FDS4 database for ‘Spruce’.

Nevertheless, this variable is still considered to be uncertain. Therefore, an investigation is carried out to examine the effect the heat of vaporisation has on flame spread. Different heat of vaporisation value was selected to see the impact it has on flame spread; these values were 500kJ/kg, 1000 kJ/kg, 1500 kJ/kg and 2000 kJ/kg.

Again the Beech specimen is selected as the benchmark model for testing. Figure 9-12 is a plot for the arrival time versus the flame front position for Beech compared with the experimental results. It indicates that as the heat of vaporisation increases, the spread of flame decreases. This seems reasonable as higher heat of vaporisation implies the material needs more energy to vaporise and turn into fuel gases. Therefore, it requires additional time for flame to spread along specimen.

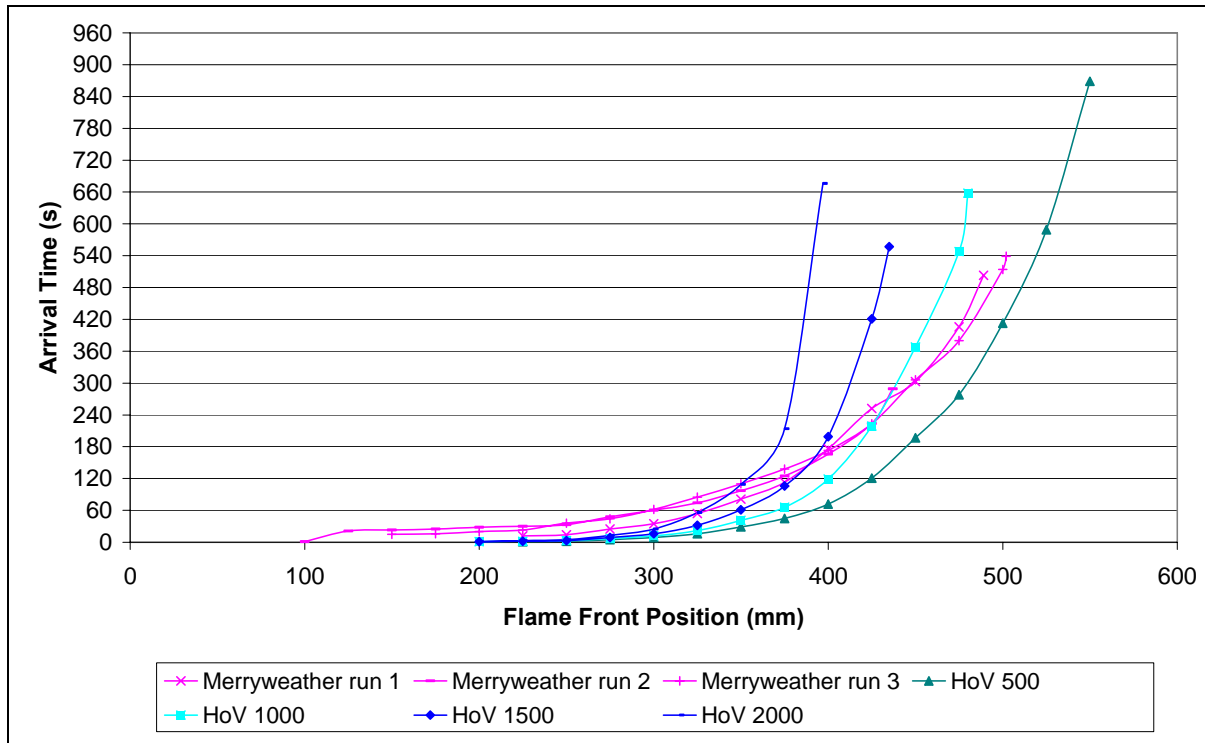


Figure 9-12: Arrival Time versus Flame Front Position for Beech with different heat of vaporisation (using Mixture Fraction)

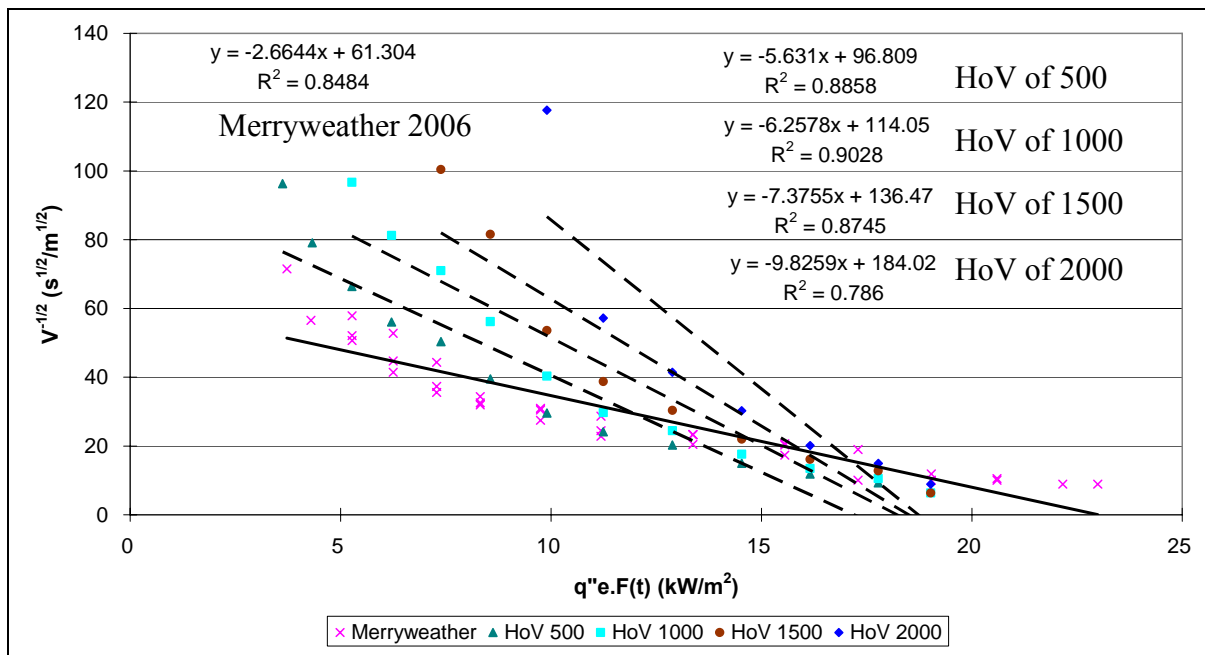


Figure 9-13: Correlations of Lateral Flame Spread for Beech with different heat of vaporisations (using Mixture Fraction)

Figure 9-13 shows the correlations of lateral flame spread for Beech with the experimental results for comparison. As can be seen in the figure, only two data points are available in the

flame spread correlations when the heat of vaporisation is 2000 kJ/kg. In addition, it demonstrates that similar flame heating parameters can be obtained even though the arrival time versus flame front position is different compared to the experimental results. Due to the fact that the extent of the flame spread occurs further along the specimen, the selected 500 kJ/kg (from FDS4 database) as the heat of vaporisation in the charring fuels model is considered to be reasonable.

It should be noted that the heat of vaporisation for charred materials is generally not measured in experiments. Hence no published data can be found to compare with the heat of vaporisation that was used in the charring fuels model.

Table 9-3: Summary of the flame spread parameters using different heat of vaporisation

Source	Flame Heating Parameter, Φ	Percentage difference	$q''_{o,ig}$ (Correlation)	Percentage difference	Critical flux for spread, $q''_{o,s}$ (From Graph)	Percentage difference
Merryweather	70.9	0.0%	23.0	0.0%	3.7	0.0%
HoV 500	15.9	-77.6%	17.2	-25.3%	2.9	-21.7%
HoV 1000	12.8	-81.9%	18.2	-20.8%	4.3	16.2%
HoV 1500	9.2	-87.0%	18.5	-19.6%	6.2	66.8%
HoV 2000	5.2	-92.6%	18.7	-18.6%	8.6	129.9%

From the flame spread data, it is found that as the heat of vaporisation increases, the spread of flame decreases which is expected as higher heat of vaporisation meaning the material needs more energy to vaporise and turn into fuel gases. Additionally the prediction of flame front position using FDS4 compared better with the experimental data when a lower heat of vaporisation is selected (i.e. using 500 kJ/kg instead of 1400kJ/kg).

9.3.2 Moisture Content

The moisture content is the second variable that is studied to determine the effect it has on flame spread as this term is also unknown variable; as Merryweather (2006) did not measure it. Previously, a moisture content of 10% is employed in the FDS4 model. This is because the moisture content for wood panel products are between 6 to 10% at a relative humidity of

50% and 20°C (Buchanan 2002). Once more, the Beech specimen is selected as the benchmark model for the analysis.

Figure 9-14 shows the comparison of the arrival time versus the flame front position for the results obtained from FDS4 and experiments. It indicated that as the moisture content decreases, the rate of flame spread increases. This is because lower moisture content implies that the material contains less moisture in the material and therefore, it needs less energy for flame to spread and easier to ignite.

Figure 9-15 is a plot of the correlations of lateral flame spread for Beech. It indicated that the flame spread parameters obtained using different moisture content does not vary significantly. It is also illustrated in Table 9-4; where the flame spread parameters and its percentage difference are compared with the experimental results.

Therefore, a moisture content of 10% seems reasonable to be employed in the FDS4 model.

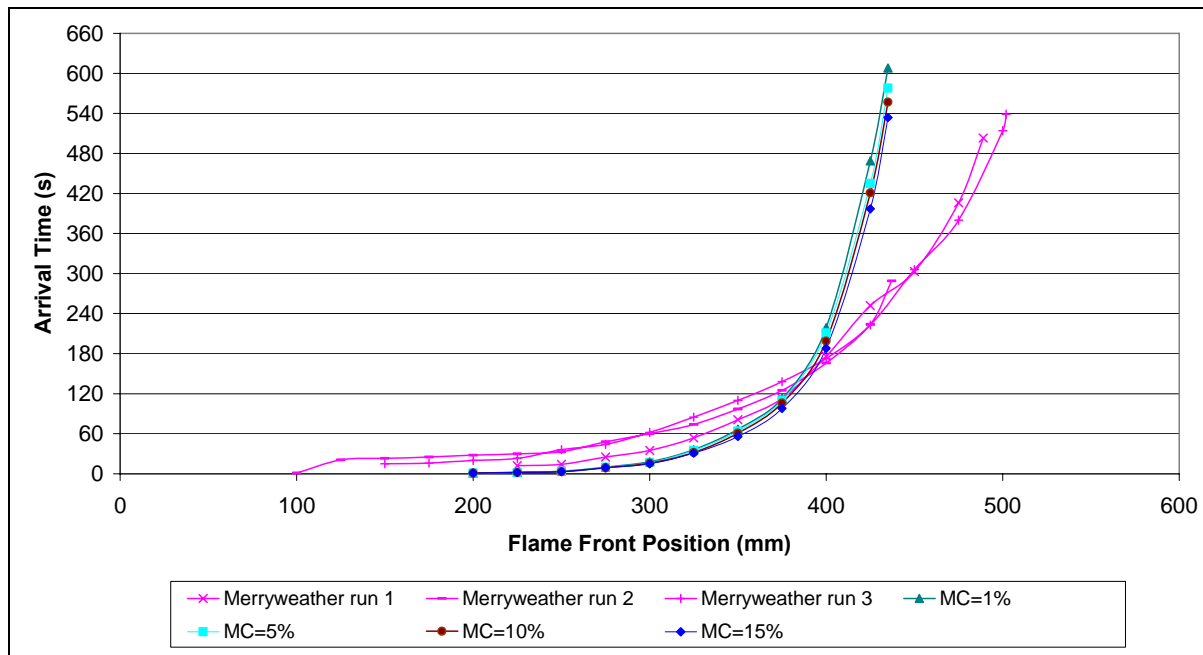


Figure 9-14: Arrival Time versus Flame Front Position for Beech with different moisture contents (using Mixture Fraction)

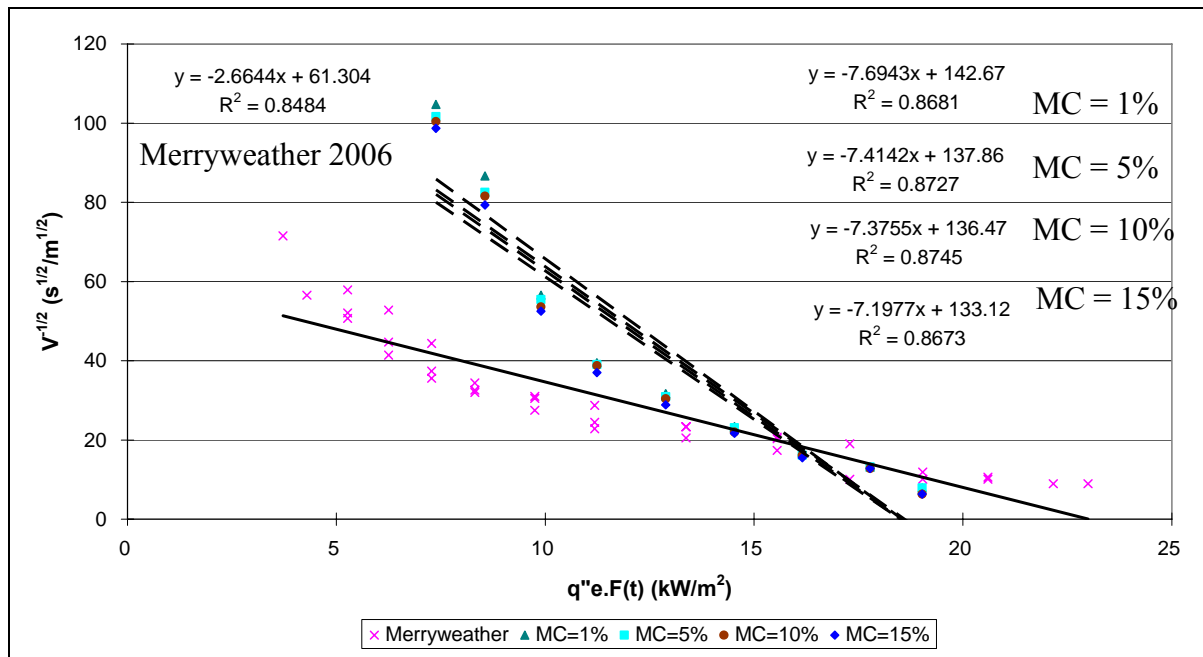


Figure 9-15: Correlations of Lateral Flame Spread for Beech with different moisture contents (using Mixture Fraction)

Table 9-4: Summary of the flame spread parameters using different moisture content

Source	Flame Heating Parameter, Φ	Percentage difference	$q''o,ig$ (Correlation)	Percentage difference	Critical flux for spread, $q''o,s$ (From Graph)	Percentage difference
Merryweather	70.9	0.0%	23.0	0.0%	3.7	0.0%
MC=1%	8.5	-88.0%	18.5	-19.4%	6.2	66.8%
MC=5%	9.2	-87.1%	18.6	-19.2%	6.2	66.8%
MC=10%	9.2	-87.0%	18.5	-19.6%	6.2	66.8%
MC=15%	9.7	-86.3%	18.5	-19.6%	6.2	66.8%

In summary, it is found that as the moisture content decreases, the rate of flame spread decreases. Again it is what is likely to be, as low moisture content implies that the material contains less moisture in the material and therefore, it is easier to ignite and needing less energy for flame to spread. This is indicated by the arrival time versus flame front position in Figure 9-14. Nevertheless, moisture content does not to have a significant role in flame spread modelling using FDS4 (in terms of correlating the flame spread parameters). This is shown by the output of the flame spread parameters as tabulated in Table 9-4.

10 Discussion

This chapter discusses the prediction of flame spread in FDS4 by directly comparing with the experimental results obtained by Merryweather (2006). Both the arrival time against the flame front position and the correlated flame spread parameters are plotted to determine the predictions of opposed-flow flame spread in FDS4; where flame spread data obtained using Smokeview were employed. The flame spread parameters includes flame heating parameter, minimum flux for ignition and spread. Beside the flame spread properties, variables such as thermal transport properties (thermal conductivity and specific heat capacity), density and ignition temperature are also being compared. The aim of this section is to give an overview of the accuracy in using FDS4 for modelling flame spread.

10.1 Comparison of thermal properties

10.1.1 Thermal conductivity and specific heat capacity

Charred material should have a lower thermal conductivity than virgin material due to an insulated layer provided by the charred material. This insulated layer actually minimises the heat transfer across the material and consequently giving a lower thermal conductivity. A plot of the thermal conductivity and specific heat capacity between the charred and virgin materials is shown in Figure 10-1 and Figure 10-2 respectively.

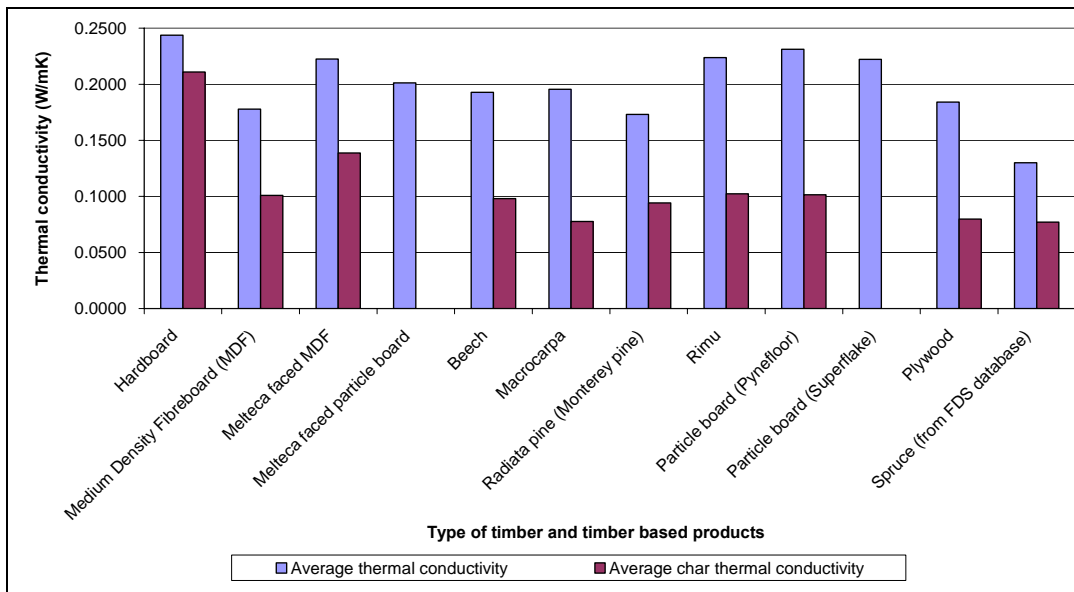


Figure 10-1: Comparison between the thermal conductivity for charred and virgin wood

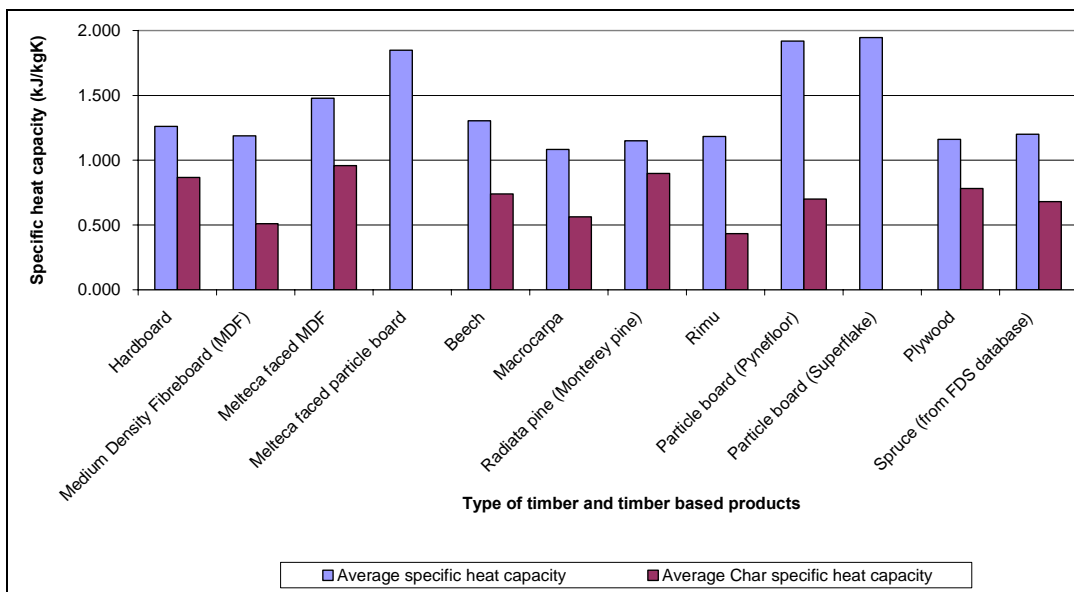


Figure 10-2: Comparison between the specific heat capacity for charred and virgin wood

From these figures, it indicated that the thermal conductivities measured are consistent for all timber and timber based products and compared well with ‘Spruce’ in the FDS4 database; where the ratio of the virgin and charred material was used as the benchmark. However, the thermal conductivity obtained for charred hardboard seems to be higher than expected. This is probably due to the thermal bowing of the specimen which leads to the difficulties in carrying out the Hot Disk test to obtain the thermal transport properties. This is particularly a

problem to hardboard as the thickness of hardboard is very thin (i.e. 5mm) compared to other specimens which have a thickness from 15mm to 24mm. Hence, it was difficult to conduct the Hot Disk test using the charred hardboard specimen. Nevertheless, it is still reasonable to assume that the thermal transport properties obtained from the Hot Disk test represents the selected material; hence applied in the FDS4 model.

It should also be noted that the thermal properties for other charred materials (such as Superflake particle board and Melteca faced particle board) are not in the graphs. This is because these thermal properties are expected to be very similar to those of Pynefloor particle board and Melteca faced MDF respectively and hence the reason that is not used by Merryweather (2006) in the LIFT test.

10.2 Comparison of ignition temperature

Ignition temperature for each timber and timber based products were measured when undertaking the charring experiments based on the cone calorimeter setup as described in Chapter 5. The ignition temperature obtained is compared directly with the experimental results as illustrated in Figure 10-3. From this figure, it indicated that the measured ignition temperature corresponds to those found by Merryweather (2006). This further suggests that the ignition temperature applied in the FDS4 model is reasonable.

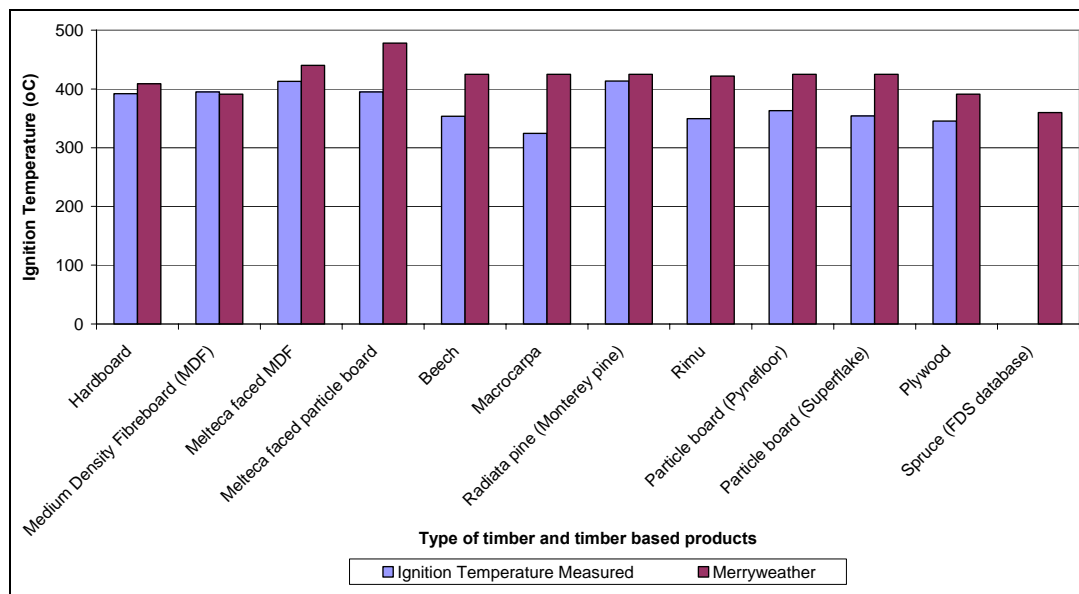


Figure 10-3: Comparison of ignition temperature

10.3 Comparison of density of virgin wood and char material

As mentioned previously in Section 6.4, the mass and volume approach was adopted when measuring the density of all timber and timber based products. A plot between the calculated densities with the experimental results by Merryweather (2006) is shown in Figure 10-4 below; where the former one is implemented in the FDS4 model. From this figure, it indicated that the measured density of each material is very similar to those published by Merryweather (2006); hence the percentage difference between the two densities is within +/- 15%.

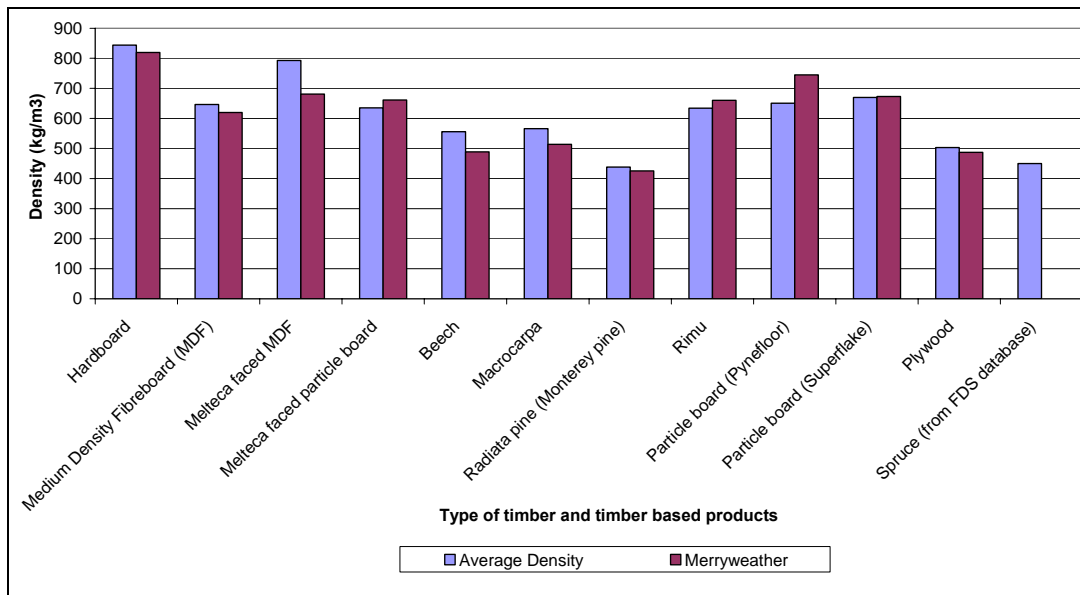


Figure 10-4: Comparison of wood density between measured and Merryweather (2006)

Additionally, the density for both virgin wood and charred materials is plotted in Figure 10-5 for comparison. The char density for various wood species ranges from 156 to 360 kg/m³ according to Tran and White (1992) and that table is reproduced as shown in Table 10-1 below. However, the results of the experiments showed that the char density of the timber and timber based products ranges from 250 to 580 kg/m³. It should be noted that the manufactured boards generally gave a higher wood and char densities.

Despite the higher upper range compared to the one suggested by Tran and White (1992), the measured char density was applied for the charring fuels model in FDS4. This is because the change in char density does not have a major impact on the rate of flame spread.

As mentioned earlier in the section, the methodology in determining char density is only a crude approximation. Nevertheless, by making use of the ratio between the virgin and charred material’s density for ‘Spruce’ that is found in the FDS4 database, it demonstrated that the calculated ratio compares well with ‘Spruce’. Therefore, it illustrates that the char density measured is reasonable and applicable in the charring fuels model.

Table 10-1: Char properties for various wood species (Tran and White 1992)

Species	Flux (kW m ⁻²)	f_c	Char yield γ_c	Apparent ρ_c (kg m ⁻³)
Redwood	17.8	0.523	0.27	181
	17.7	0.512	0.27	174
	25.8	0.563	0.26	168
	26.2	—	—	—
	38.5	0.613	0.27	183
	38.7	0.634	0.28	180
	53.6	0.835	0.32	156
	56.3	0.747	0.31	191
Southern pine	17.4	0.475	0.20	272
	17.4	0.456	0.24	287
	25.2	0.530	0.30	287
	26.9	0.469	0.20	294
	38.5	0.479	0.25	358
	38.6	0.444	0.23	355
	55.5	0.616	0.25	256
	56.0	0.583	0.26	312
Red oak	17.8	0.547	0.25	327
	18.7	0.567	0.26	328
	25.0	0.559	0.24	317
	25.8	0.564	0.25	333
	37.8	0.625	0.25	360
	38.4	0.606	0.25	345
	53.1	0.753	0.27	256
	53.6	0.705	0.31	312
Basswood	17.6	0.428	0.24	264
	17.8	0.408	0.22	251
	27.7	0.421	0.23	288
	25.5	0.430	0.22	260
	38.1	0.450	0.23	255
	38.7	0.409	0.20	227
	51.6	0.519	—	—
	53.4	0.523	0.23	239

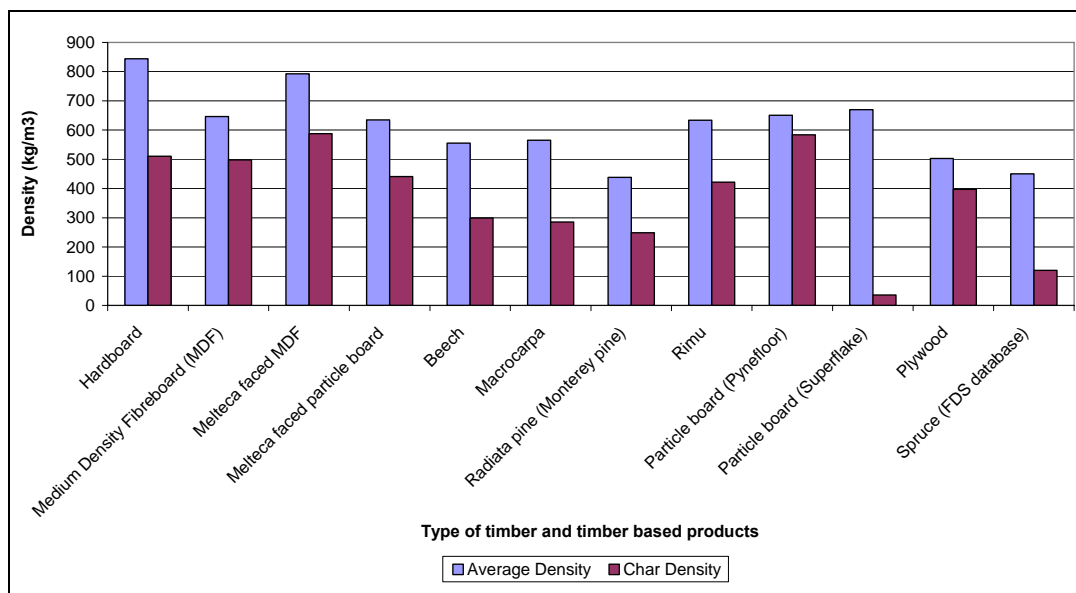


Figure 10-5: Comparison between the wood and char density

10.4 Flame Spread data

10.4.1 Arrival time versus distance along specimen

Smokeview was used to obtain the simulated flame spread data from FDS4 where the arrival time and its corresponding distance along specimen were recorded. Figure 10-6 shows the comparison of the arrival time against the flame front along Beech specimen between the prediction from FDS4 and the data obtained by Merryweather (2006); where the graph includes both the thermoplastic fuels and charring fuels model as well as the selected absorption coefficient (0.6, 0.7 and 0.8).

This graph is only used to demonstrate the typical prediction of the flame front position simulated by FDS4. For all other timber and timber based products, the comparison of the arrival time against the flame front position between FDS4 and the experimental results are shown in Section 8.4. It is also noted that similar flame spread pattern was observed for all other timber and timber based products.

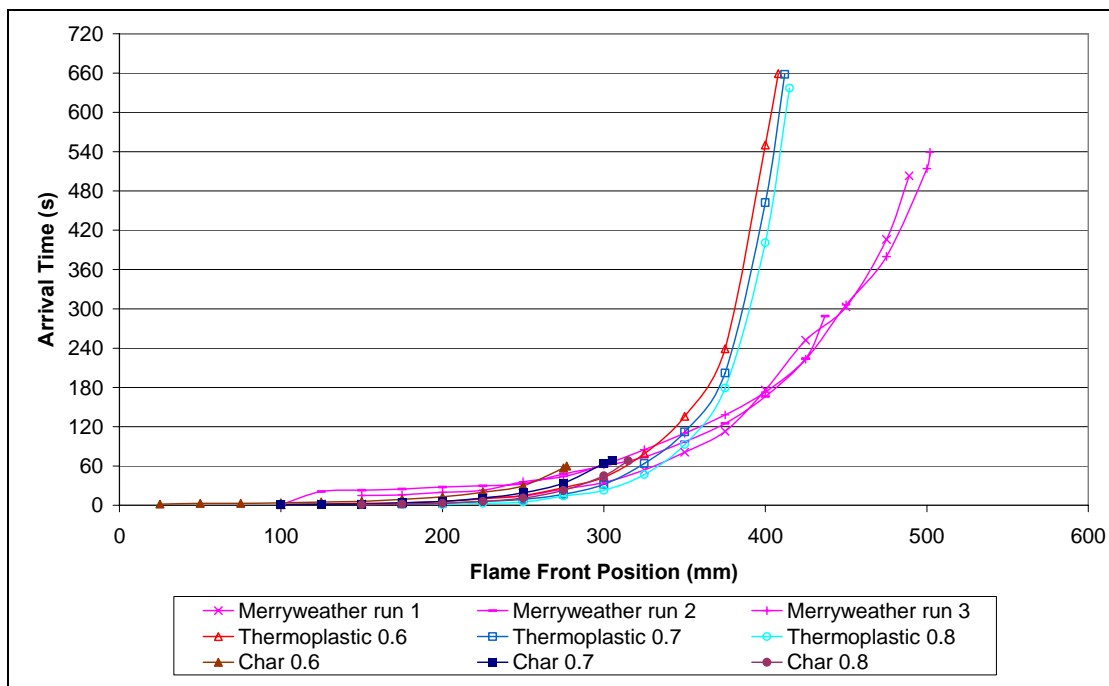


Figure 10-6: Comparison between the prediction of flame front’s arrival time for Beech in FDS4 and the results from Merryweather (2006) using Mixture Fraction

From Figure 10-6, it indicates that the plot of the arrival time against the flame front position shifts to the left as the absorption coefficient decreases. This is because the absorption coefficient influences the amount of heat flux absorbed by the specimen. In another word, it has an effect on how fast the flame front travels. Therefore, decreasing the absorption coefficient is effectively reducing the heat flux that is absorbed at the surface of the specimen and increases the time it takes for the specimen to ignite.

The thermoplastic fuels model predicting similar flame front arrival trends when compared to the data from Merryweather (2006). However, the arrival time is generally slower than the experimental results. This is because the specimen is not being heated as quick when compared to the data from the experiment by Merryweather (2006). Additionally the sensitivity analysis section indicated that by selecting a lower heat of vaporisation value, the prediction of flame front position using FDS4 compares better with the data from the experiments (i.e. using 500 kJ/kg instead of 1400kJ/kg).

Meanwhile, the charring fuels model does not simulate the flame spread as indicated by the early flame extinction; where the extent of flame spread actually stops much earlier when compared to both the thermoplastic fuels model and the experimental results. This is likely due to the char layer on the surface of the specimen acting as an insulation layer.

Overall, the flame spread rate is greatly affected by the selection of the pyrolysis model in simulating the LIFT test and the prediction of the arrival time of the flame front is considered to be reasonable only when thermoplastic fuels model is used.

10.5 Flame spread correlations parameters

The flame spread correlations are determined for both the thermoplastic and charring fuels model. The correlated parameters include flame heating parameter, critical heat flux for ignition and critical heat flux for flame spread. These correlations using the results from the FDS4 models were compared with those from the experiments by Merryweather (2006).

Figure 10-7 shows the comparison of the lateral flame spread correlations between FDS4 and experimental results for Beech specimen. Again, this graph is only intended to demonstrate the typical lateral flame spread correlations between FDS4 and the data from Merryweather

(2006). The correlations of lateral flame spread for all other selected specimens are shown in Section 8.5. The equation located on the left hand corner indicates the correlations obtained by Merryweather (2006), while the equations located at the centre and the right hand corner indicate the correlations predicted by using the thermoplastic fuels and charring fuels model respectively.

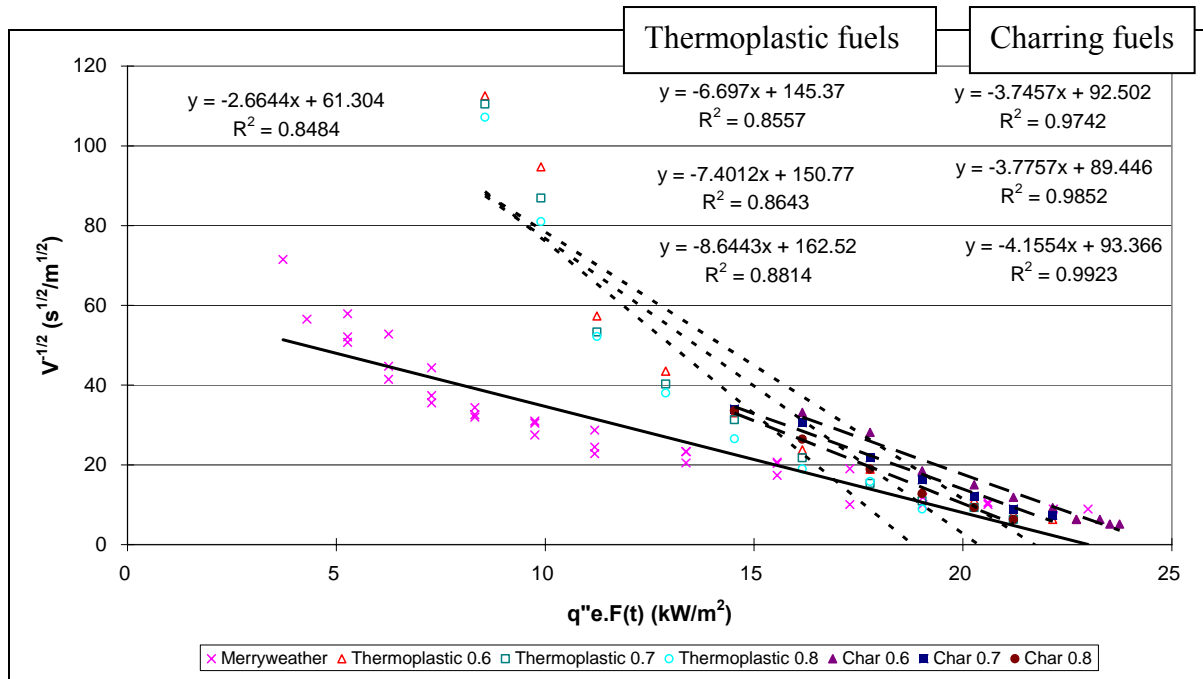


Figure 10-7: Comparison of the correlations of lateral flame spread for Beech specimen

The flame spread correlation parameter is calculated using Equation 4-16 as described in Section 4.3.1. For convenience, this equation is reproduced below; where the flame heat transfer factor (C) is the slope of the graph and b is the ignition correlation parameter.

$$\phi = \frac{4}{(Cb)^2}$$

The flame heat transfer factor (C) will strongly influence the outcome of the flame heating parameter as indicated in the equation above, i.e. C is inversely square proportional to Φ . If the ignition correlation parameter b is constant due to the identical specimen, then the Φ is dependent on the C factor.

In general, the charring fuels model gives a shorter trend line in the correlations plot compared to the thermoplastic fuels model as shown in Figure 10-7 above. The reason is due to the early flame front extinction simulated by the charring fuels model, i.e. flame does not spread when the heat flux exposed on the specimen surface is low; hence less data points are available to correlate. Therefore, only the correlations from the thermoplastic fuels model will be used for discussion.

10.5.1 Flame heating parameter, Φ

The term flame heating parameter is an indicator of how a material is susceptible to opposed flow flame spread. If a material is ignited and flame spread rapidly then the flame heating parameter for the material is large. On the contrary, if flame spread slowly across the material then the flame heating parameter is small.

Direct comparison between the correlations of flame spread parameter that is determined from FDS4 results and the experimental results are plotted for all timber and timber based products; where the thermoplastic fuels model and mixture fraction were used as the technique to visualise flame in Smokeview. This is illustrated in Figure 10-8 to Figure 10-10 for an absorption coefficient of 0.6 to 0.8 respectively. Note that the New Zealand native timber is indicated by the solid symbol while the manufacturer timber based product has a hollow symbol.

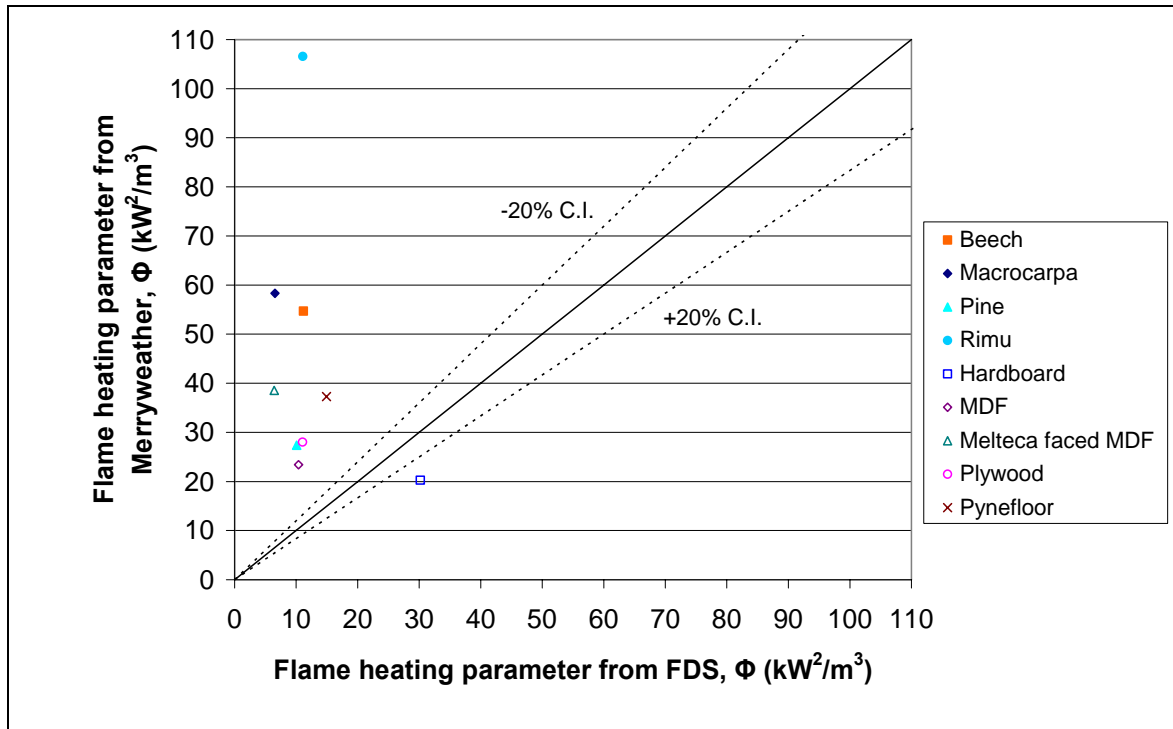


Figure 10-8: Comparison of flame heating parameter between the results from Merryweather (2006) and FDS4 (Thermoplastic fuels $\epsilon=0.6$ Mixture Fraction)

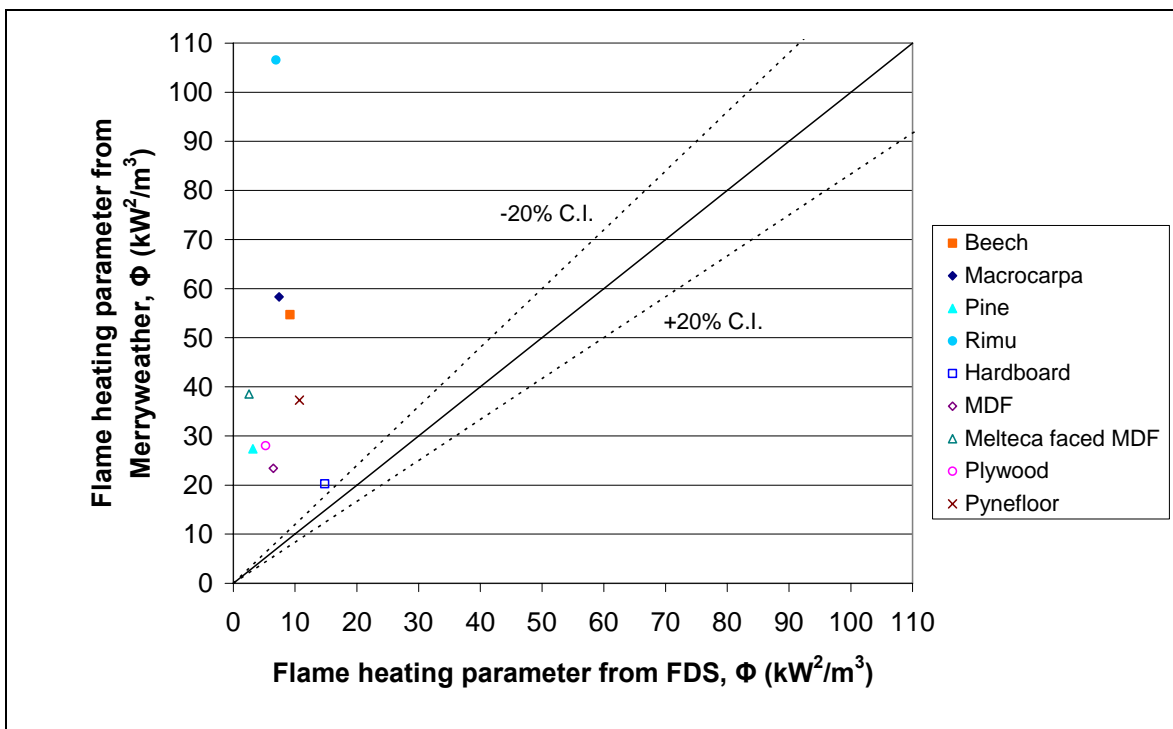


Figure 10-9: Comparison of flame heating parameter between the results from Merryweather (2006) and FDS4 (Thermoplastic fuels $\epsilon=0.7$ Mixture Fraction)

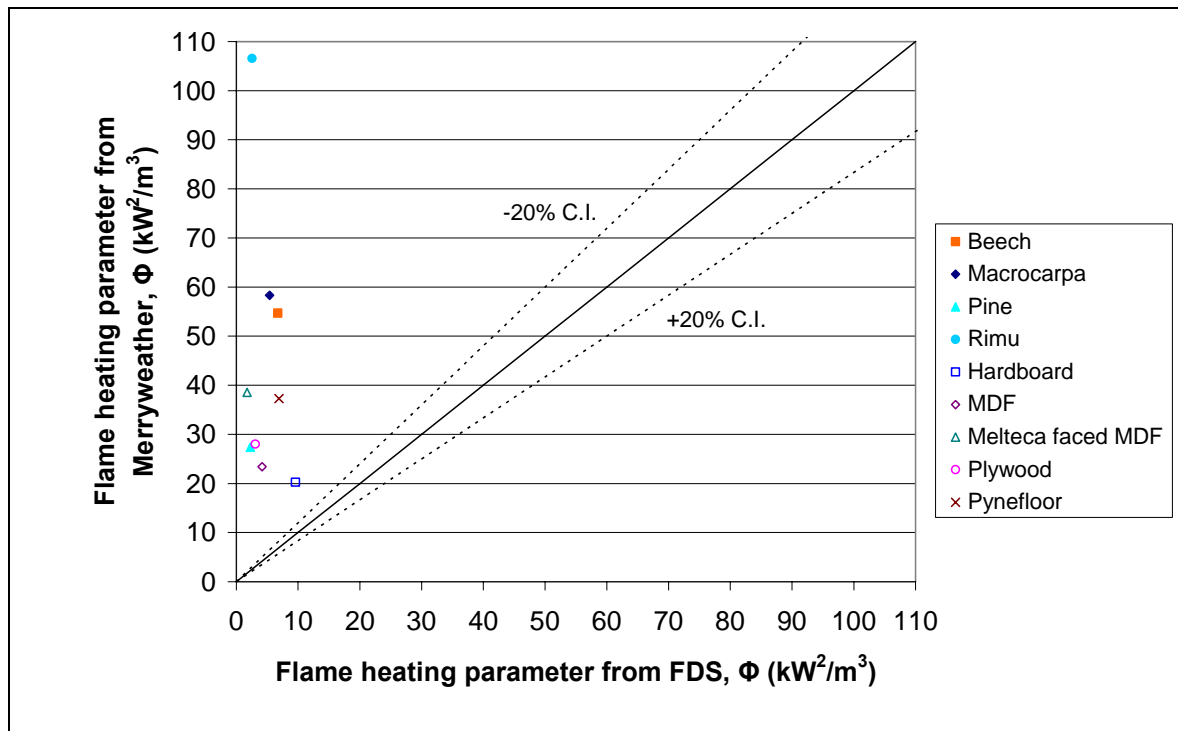


Figure 10-10: Comparison of flame heating parameter between the results from Merryweather (2006) and FDS4 (Thermoplastic fuels $\epsilon=0.8$ Mixture Fraction)

If the data points on the direct comparison graphs are positioned in the upper region then it implies that FDS4 model underestimated the Φ . And vice versa if the data points are located in the lower region of the graph then it implies that FDS4 model overestimated the Φ value. And lastly, if the data points lie on the diagonal line in the figure then it means the prediction from the FDS4 model is identical to the experimental results.

Since the data points in the direct comparison figures for the flame heating parameters lie mostly in the upper portion of the graph, it implies that the Φ value determined from the FDS4 model is larger than the one found from the experiments, i.e. overestimate the Φ value, which means that actual flame spread will be quicker than the prediction by the FDS4 model.

The reason why the thermoplastic fuels model cannot predict the flame heating parameter well is due to the spread of flame simulated happens much slower than it was found in the experiments. This also reduces the flame heat transfer factor (C) as the velocity is inversely squared proportional to the exposed heat flux, i.e. $1/\sqrt{V^2}$ vs. q'' .

The term C is the slope of the graph for the correlation of flame spread parameters. If C is large or the slope is steep, it means that there is not much change in flame spread (flame spread of the material is limited) and hence a small Φ . However, if C is small or the slope is flat, it means that the material is very susceptible to flame spread and it spreads rapidly; hence a large Φ .

From Table 10-2, it indicated that the all C values predicted using FDS4 models tend to be larger than the experimental results as a result of the delayed arrival time of flame front when compared to the experimental results (the slower flame spread rate). Again, this leads to the difference between the predicted Φ and the experimental Φ values.

Table 10-2: Comparison of the flame spread parameter using thermoplastic fuels model $\varepsilon=0.7$

Type of wood panels	Ignition Correlation Parameter, b	Flame Spread Parameter, C (Found from the slope of the lateral flame spread graph)	Flame Spread Parameter (FDS), C (Found from the slope of the lateral flame spread graph)	Flame Heating Parameter, Φ	Flame Heating Parameter (FDS), Φ
Macrocarpa	0.0589	2.5	7.0	58.3	7.4
Plywood	0.0584	3.7	8.4	28.0	5.2
Beech	0.0503	3.0	7.4	54.7	9.2
Radiata pine (Monterey pine)	0.0541	4.0	11.7	27.4	3.2
Medium Density Fibreboard (MDF)	0.0468	5.0	9.5	23.4	6.5
Pynefloor Particle board (chipboard)	0.0509	3.6	6.8	37.3	10.7
Melteca faced MDF	0.0423	4.3	16.7	38.5	2.6
Hardboard	0.0516	4.9	5.7	20.3	14.8
Rimu	0.0503	2.2	8.5	106.6	6.9

Additionally, NZ native timbers trend to lie in the upper most region that is above timber based products which implies the prediction of these timbers are worst than the one for timber based products.

The correlations of the flame spread parameters actually differ between the FDS4 results and the one derived from the experiments; where the flame heating parameters were overestimated by the FDS4 models. This implies that the FDS4 models underestimate the flame spread rate as it is observed from the arrival time versus the flame front position. For

example: the results from Merryweather (2006) showed that the flame front takes 50 seconds (after the required preheat time) to spread to 350mm along the Beech specimen; while the prediction from the FDS4 model indicated that the time for the flame to spread to the same location is 120 seconds.

Nevertheless, the rate of flame spread can increase in the FDS4 model if the heat of vaporisation parameter is reduced i.e. from 1400 kJ/kg to 500 kJ/kg. The actual heat of vaporisation of the specimen was not used, as the actual heat of vaporisation was not measured; where it can be obtained from a cone calorimeter test. This was not conducted due to the lack of material available and time constraint. As a result, an average value of 1400 kJ/kg that is used where the typical heat of vaporisation for wood is found to be 0.95 – 1.82 kJ/g (Icove and DeHaan 2004). As the heat of vaporisation implies the amount of energy needed to vaporise a fuel. Therefore, lowering the heat of vaporisation value implies the flame will travel faster.

Due to the slower flame spread rate that is simulated in the FDS4 models, the prediction of the flame heating parameters is underestimated. Overall, it can be concluded that the correlations of the flame spread parameters from the FDS4 results are not within the desired accuracy to be used as the result from the flame spread test.

10.5.2 Critical heat flux for ignition, $\dot{q}_{o,ig}''$

The term critical heat flux for ignition means that the minimum heat flux required before the specimen ignites. Figure 10-11 to Figure 10-13 show the direct comparison between the correlations of critical flux for ignition that is determined from FDS4 results and the experimental results for all timber and timber based products; where the thermoplastic fuels model and mixture fraction were used as the technique to visualise flame in Smokeview. Again, the three figures represent the comparison when using different absorption coefficient (0.6 to 0.8).

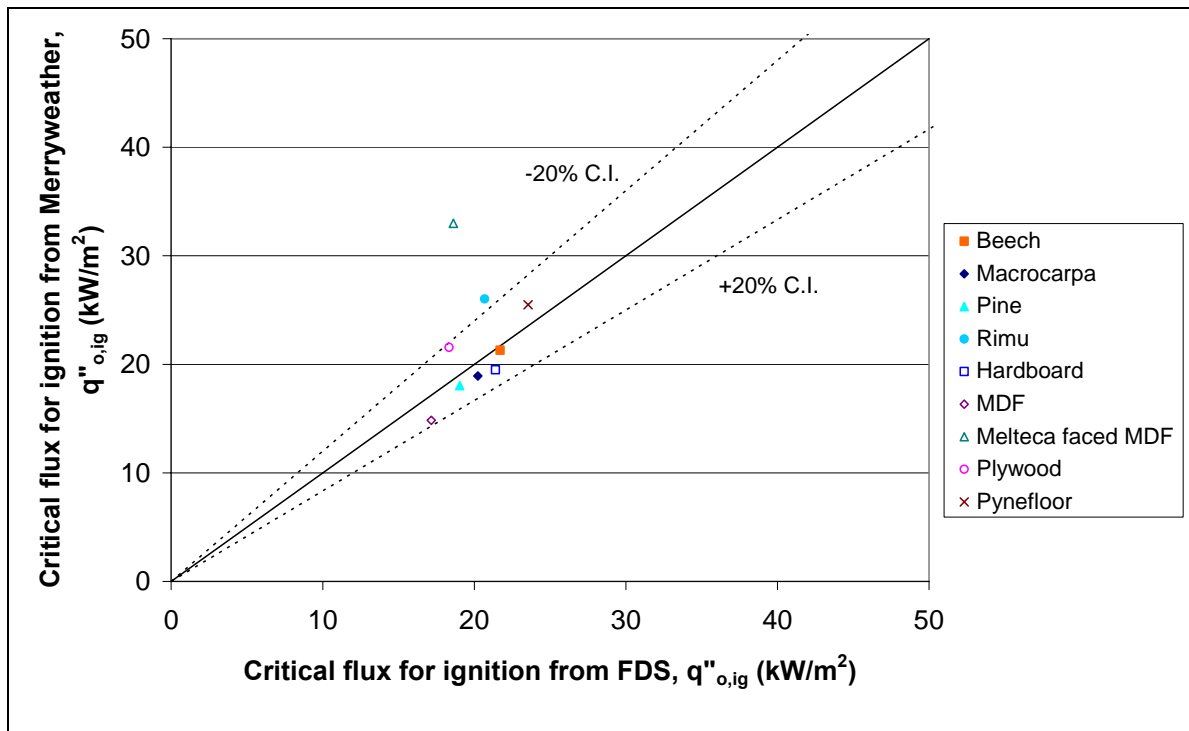


Figure 10-11: Comparison of critical flux for ignition between the results from Merryweather (2006) and FDS4 (Thermoplastic fuels $\epsilon=0.6$ Mixture Fraction)

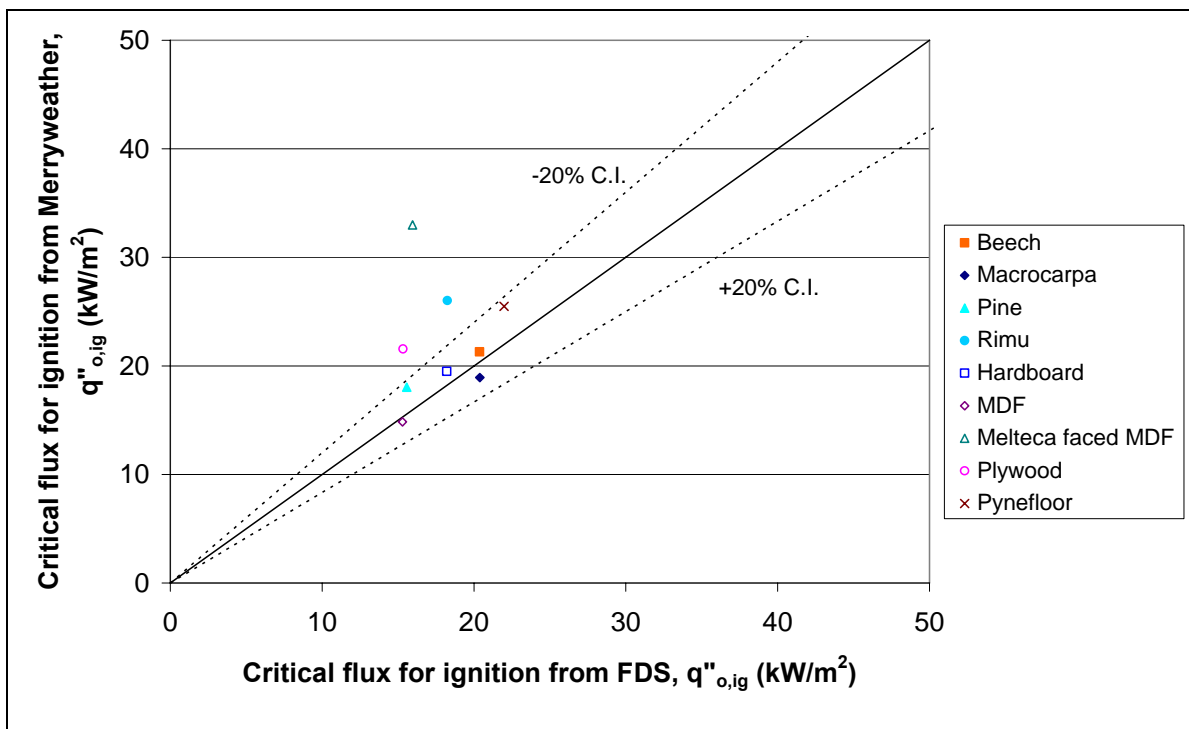


Figure 10-12: Comparison of critical flux for ignition between the results from Merryweather (2006) and FDS4 (Thermoplastic fuels $\epsilon=0.7$ Mixture Fraction)

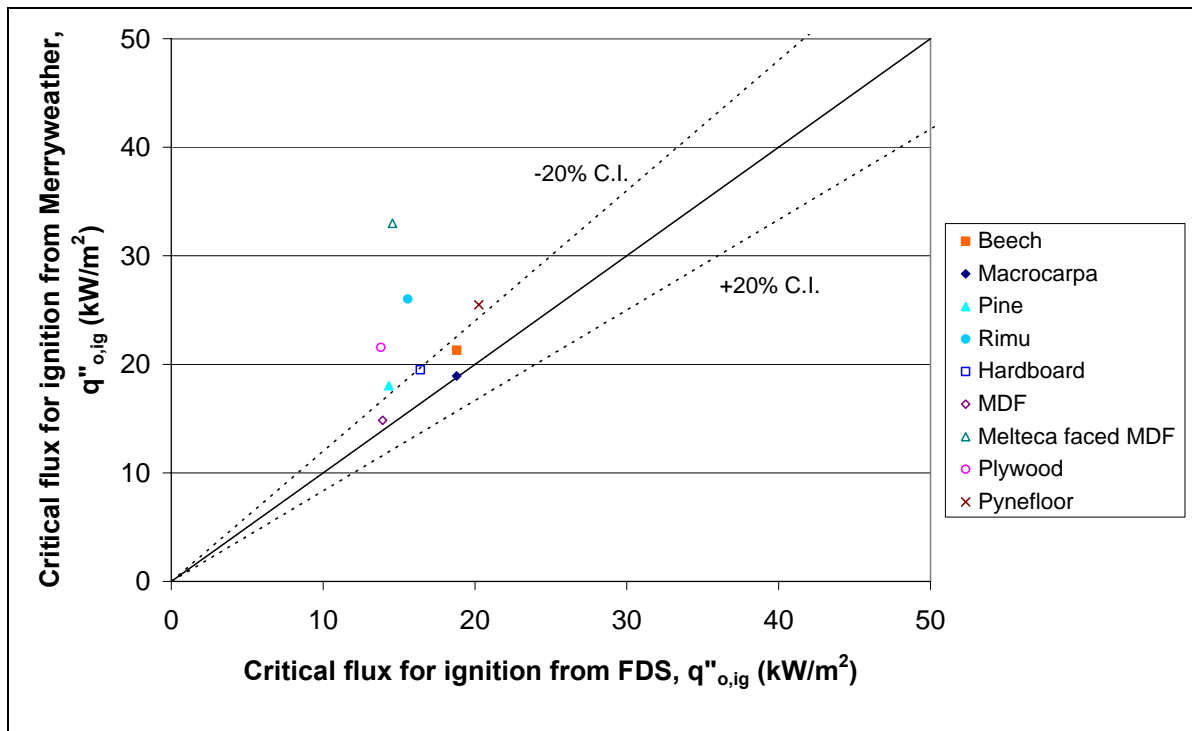


Figure 10-13: Comparison of critical flux for ignition between the results from Merryweather (2006) and FDS4 (Thermoplastic fuels $\epsilon=0.8$ Mixture Fraction)

In general, the prediction of the minimum heat flux for ignition $\dot{q}_{o,ig}''$ compares well with the experimental results as indicated by the data points being relatively close to the line i.e. within 20%. Consequently, it implies the initial ignition of the specimen simulated in the FDS4 model agreed with the results from the experiments. This also means that the initial temperature implemented in the FDS4 model in which it simulates the preheating of the specimen was reasonable.

It should be noted that the Melteca faced MDF specimen is an outlier where the minimum heat flux for ignition was overestimated having a percentage difference of 33%. This implies that the time it takes for initial ignition of the specimen is longer in the FDS4 model than the experiments. One reason would be the measurement of the thermal transport properties was not measured correctly i.e. incorrect use of the Hot Disk test apparatus. The likely reason is that the Melteca facing affects the radiant heat flux being exposed to the particleboard behind the facing. Hence a higher radiant heat flux was used by Merryweather (2006).

Studies by Ngu (Ngu 2001) found that the minimum heat flux, \dot{q}_{\min}'' from the ISO Ignitability Test for each type of timber, in the order of highest to the lowest are: Macrocarpa, Beech, Medium Density Fibreboard (MDF), Radiata Pine, Rimu and Plywood. The simulated results agreed well with the experimental data. However, the correlated minimum heat flux for ignition from the FDS4 model does not show this trend, where in the order of highest to the lowest are: Rimu, Plywood, Beech, Radiata Pine, Macrocarpa and Medium Density Fibreboard (MDF).

Preheat temperature is a major factor that influences the minimum heat flux for ignition. This is because the ignition of the specimen in the FDS4 model is controlled by the specified ignition temperature. This allows the ignition of the specimen and hence flame spread to be measured.

Overall, the FDS4 model does give a reasonable correlation of the minimum heat flux for ignition but this is all because the ignition temperature of the specimen was specified.

10.5.3 Critical heat flux for flame spread, $\dot{q}_{o,s}''$

The term critical heat flux for flame spread simply means that the minimum heat flux required before the flame extinct. Direct comparison between the correlations of critical heat flux for flame spread that is determined from FDS4 results and the experimental results are plotted for all timber and timber based products; where the thermoplastic fuels model and mixture fraction were used as the technique to visualise flame in Smokeview. This is illustrated in Figure 10-14 to Figure 10-16 for an absorption coefficient of 0.6 to 0.8 respectively.

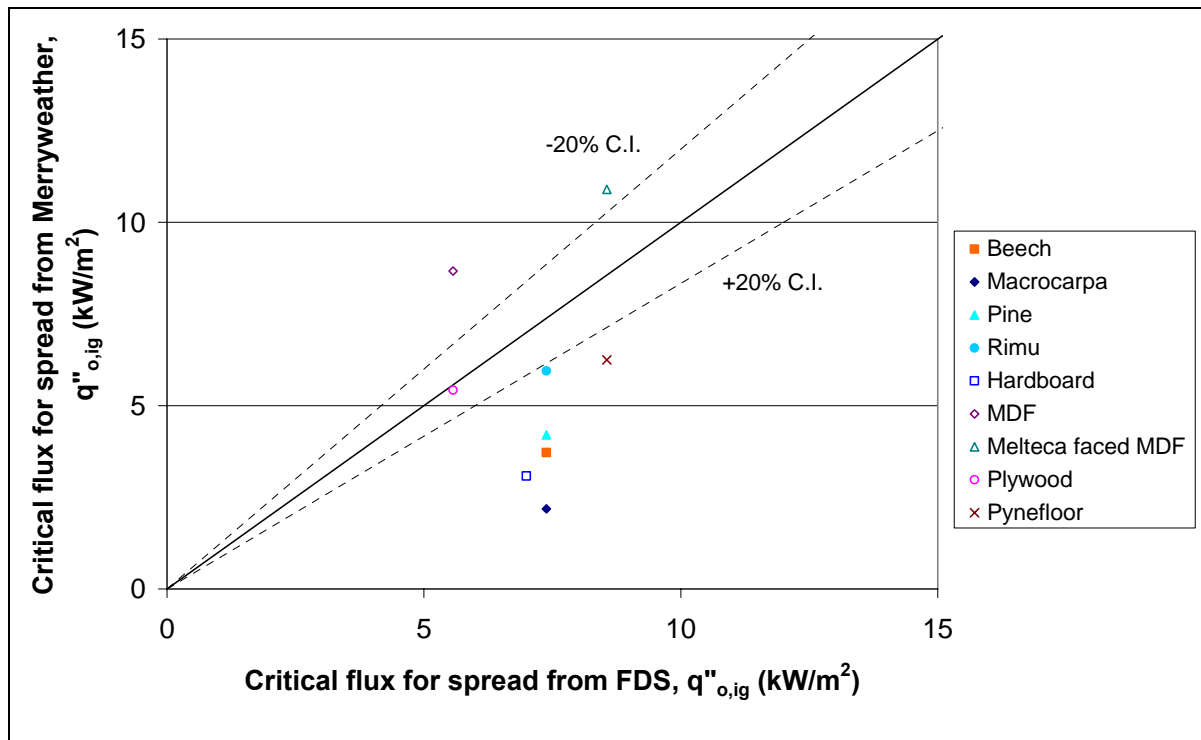


Figure 10-14: Comparison of critical flux for spread between the results from Merryweather (2006) and FDS4 (Thermoplastic fuels $\epsilon=0.6$ Mixture Fraction)

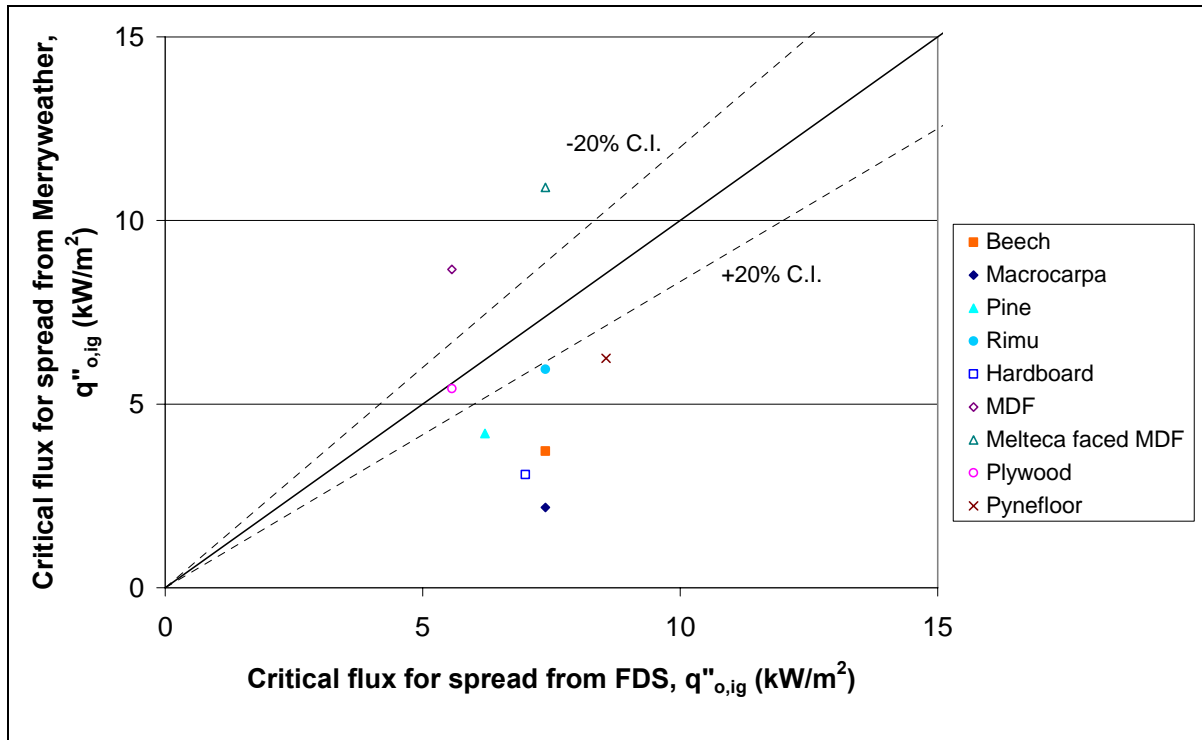


Figure 10-15: Comparison of critical flux for spread between the results from Merryweather (2006) and FDS4 (Thermoplastic fuels $\epsilon=0.7$ Mixture Fraction)

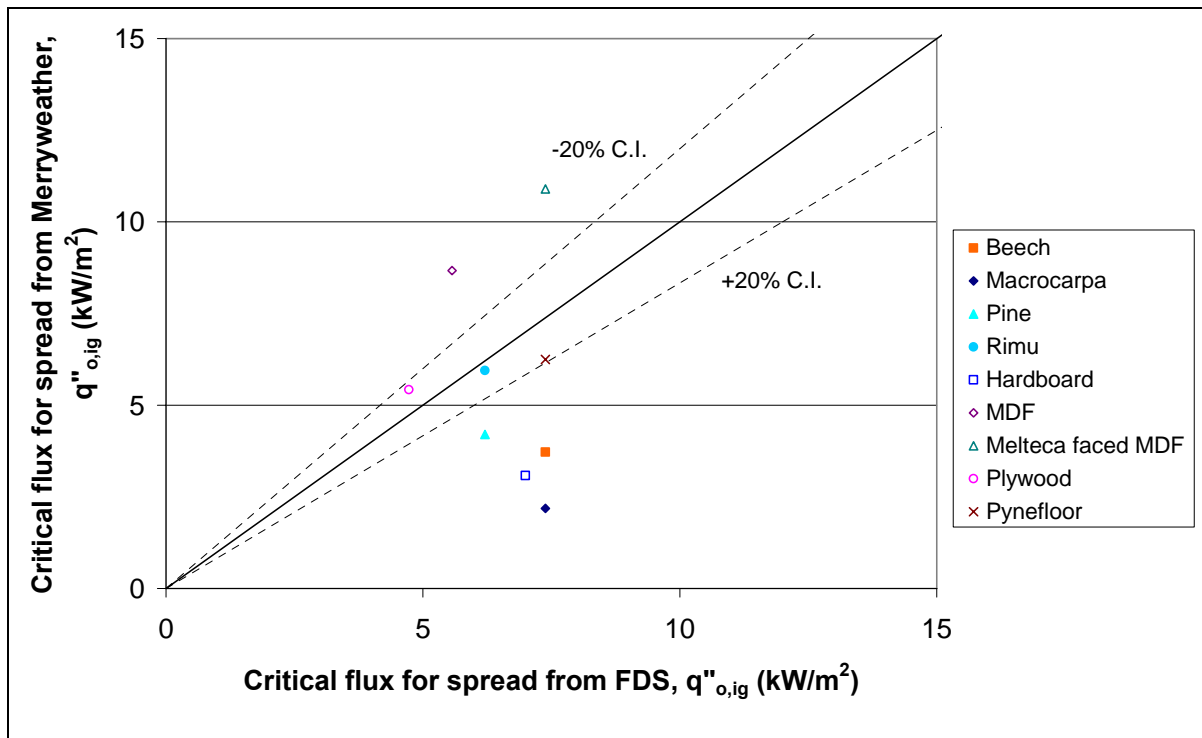


Figure 10-16: Comparison of critical flux for spread between the results from Merryweather (2006) and FDS4 (Thermoplastic fuels $\epsilon=0.8$ Mixture Fraction)

These figures indicate that the FDS4 model generally overestimates the critical flux for spread. This is also indicated in the plot of the arrival time versus the flame front position along the specimen (Figure 10-6) where flame front actually stopped much earlier than the experimental results. This relationship can again be seen in the correlations of lateral flame spread graph as illustrated in Figure 10-7.

In general, the correlated minimum heat flux for flame spread is much higher than the experimental results. This means that the flame does not spread further than the actual experiments. Additionally, this also leads to the inaccurate prediction of the flame heating parameter for all specimens as discussed in Section 10.5.1. Therefore, it showed that the FDS4 model cannot accurately predicts when flame spread will stop.

11 Conclusions

The FDS4 CFD model was used to simulate the LIFT test to predict the opposed flow flame spread for timber and timber based products. The conclusions and findings from each aspect of this research are described below:

- Ignition temperature, density, heat capacity and thermal conductivity (in virgin and charred state) of the timber and timber based products were determined experimentally and compare well with the values found in literature.
- FDS4 cannot model an object that is preheated but this is overcome by implementing an initial temperature on the object.
- FDS4 model was setup to simulate the LIFT test based on the standard geometries.
- Calibration of the LIFT apparatus was successfully performed in which demonstrated that it is achievable in FDS4.
- The flame spread rate is greatly affected by the selection of the pyrolysis model in simulating the LIFT test.
- The prediction of the arrival time of the flame front is considered to be reasonable only when thermoplastic fuels model is used.
- The charring fuels model gives a shorter trend line in the correlations plot compared to the thermoplastic fuels model due to the early extinction of the flame front.
- The prediction of the flame heating parameters is underestimated due to the slower flame spread rate that is simulated in the FDS4 models.
- The prediction of the minimum heat flux for ignition is compared well but this is all because the ignition temperature of the specimen was specified.
- The prediction of the minimum heat flux for spread is generally overestimated by FDS4.

- Due to the slower flame spread rate in the thermoplastic fuels model, the correlations of the flame spread parameters differ from the results derived from the actual experiment.
- Only minor difference in the correlation of flame spread when a coarser grid size is used i.e. the extinction of the flame spread occurs earlier when the grid size increases. However, finer grid size was chosen so that finer flame details are captured.
- The prediction of flame front position using FDS4 compared better with the experimental data when a lower heat of vaporisation is selected (i.e. using 500 kJ/kg instead of 1400kJ/kg).
- Preheat temperature is a major factor that influences the minimum heat flux for ignition.
- Absorption coefficient has an effect on the flame spread rate as it determines the amount of heat flux that is exposed on the surface of the specimen.
- The variable “moisture content” does not have a significant role in flame spread modelling using FDS4.
- Based on the LIFT apparatus setup in FDS4, both thermoplastic fuels and charring fuels model cannot perform the flame spread test. However the modelling of the arrival time of the flame front is considered to be reasonable.

12 Further work and Recommendations

As this research work has been limited in scope and duration, future work should consider the following:

- To recalculate the char density of the timber and timber based products using a more accurate technique.
- To measure the surface temperature of each specimen after the calculated preheat time during the LIFT test.
- To work out the heat of vaporisation of the material using the cone calorimeter tests.
- To perform more flame spread tests on a wider range of materials.
- To use FDS5 new solid phase models.

For further flame spread tests, it is recommended to conduct more flame spread test on a wider range of materials that have been tested previously using the LIFT, such as gypsum board, polyurethane foam and polymethymethacrylate (PMMA). Comparison between different materials other than timber products will provide a further validation on the prediction of opposed flow flame spread in FDS4.

Additionally, if this research was to start over from the beginning, more LIFT experiments should be performed without preheat time (only preheating the sample to an ambient temperature). This enable a direct comparison with the FDS4 prediction of opposed flow flame spread. As a result, the implication of preheating the specimen can be neglected. Hence a more accurate comparison due to fewer assumptions is being made in the FDS4 model. It should be noted that this method will not be considered to be a LIFT test as the sample is not preheated.

13 References

- Anis-ur-Rehman, M., and Maqsood, A. (2003). "Measurement of Thermal Transport Properties with an Improved Transient Plane Source Technique." *International journal of thermophysics*, Vol 24(3), 867-883.
- Anon. (1986). "ISO 5657, Method of measuring the ignitability of products subjected to thermal irradiance." International Organisation of Standards, Geneva, Switzerland.
- Anon. (2004). "E471-96(2002) Standard Test Method for Obtaining Char Density Profile of Ablative Materials by Machining and Weighing." ASTM fire standards, ASTM International, West Conchohocken, PA.
- Anon. (2006). "Emissivity of common materials: Emissivity of wood." Omega Engineering inc., One Omega Drive, Stamford, Connecticut.
- ASTM Committee E-5 on Fire Standards. (2004a). ASTM fire standards, ASTM International, West Conchohocken, PA.
- ASTM Committee E-5 on Fire Standards. (2004b). "Standard Test Method for Determining Material Ignition and Flame Spread Properties E1321-97a (2002)." ASTM fire standards, ASTM International, West Conchohocken, PA.
- Atreya, A., Capentier, C., and Harkleroad, M. (1985). "Effect of Sample Orientation on Piloted Ignition and Flame Spread." *Fire Safety Science : Proceedings of The First International Symposium*, C. E. Grant and P. J. Pagni, eds., Hemisphere Publishing Corporation, NIST, USA, pp 97-109.
- Azhakesan, M. A., Shields, T. J., and Silcock, G. W. H. (1998). "Ignition and opposed flow flame spread using a reduced scale attachment to the cone calorimeter." *Fire Technology*, Vol 34(2), pp. 99-116.
- Azhakesan, M. A., Shields, T. J., and Silcock, G. W. H. (2000). "On the nature, influence and magnitudes of flame heat transfer during surface flame spread." *Fire Safety Journal*, 35(3), 189-222.

References

- Babrauskas, V. (1995). "Flame fluxes in opposed-flow flame spread : a review of the literature." 9178485347, Swedish National Testing and Research Institute Fire Technology, Borås, Sweden.
- Babrauskas, V. (2002). "The Cone Calorimeter." SFPE handbook of fire protection engineering, P. J. DiNenno, ed., National Fire Protection Association, Society of Fire Protection Engineers, Quincy, Mass, pp 3-63 to 3-81.
- Babrauskas, V., and Wetterlund, I. (1999). "Comparative Data from LIFT and Cone Calorimeter Tests on 6 Products, Including Flame Flux Measurements." SP Swedish National Testing and Research Institute, Borås, Sweden.
- Blass, H. J. (1995). "Timber engineering - Structural Timber Education Programme." Centrum Hout, Almere, Netherlands.
- Buchanan, A. H. (2002). "Timber design guide." New Zealand Timber Industry Federation, Wellington, New Zealand, 259.
- Chao, Y. H., and Fernandez-Pello, A. C. (1996). "Concurrent Horizontal Flame Spread: The Combined Effect of Flow Velocity, Turbulence and Oxygen Concentration." Combustion science and technology, V 110 to 111 (19), pp.1-6.
- Cholin, J. M. (2003). "Wood and Wood-Based Products." Fire protection handbook, A. E. Cote, ed., National Fire Protection Association, Quincy, Mass., pp. 8-29 to 8-45.
- Cox, G. (1995a). "Combustion fundamentals of fire: Chapter 1 - Basic considerations." G. Cox, ed., Academic Press, London, 476.
- Cox, G. (1995b). "Combustion fundamentals of fire: Chapter 2 - The Solid Phase." Combustion fundamentals of fire, Academic Press, London, 476.
- deRis, J. N. (1968). "The spread of a diffusion flame over a combustible surface," PhD. Thesis, Harvard University.
- Dietenberger, M. A. (1996a). "Ignitability Analysis of Siding Materials Using Modified Protocol for Lift Apparatus." Fire and materials, Vol 20, pp. 115-121.

References

Dietenberger, M. A. (1996b). "Ignitability Analysis using the Cone Calorimeter and LIFT Apparatus." Proceedings of the International Conference on Fire Safety, July 22-26, 1996, Columbus, OH, pp. 189-197.

Dietenberger, M. A. (2004). "Ignitability of Materials in Transitional Heating Regimes." 5th International Scientific Conference, Wood and Fire Safety, April 18-22, 2004, The Patria Hotel, Slovak Republic, pp. 31-41.

Drysdale, D. (1999). "An Introduction to Fire Dynamics." Wiley, Chichester ; New York.

Fernandez-Pello, A. C., Ray, S. R., and Glassman, I. (1981). "18th Symposium (International) on Combustion." Pittsburgh, PA.

Fernandez-Pello, A. C., and Williams, F. A. (1977). "A Theory of Laminar Flame Spread Over Flat Surfaces of Solid Combustibles." Combustion and flame, Vol. 28, pp. 251-277.

Forney, G. P., and McGrattan, K. B. (2004). "User's Guide for Smokeview Version 4." NIST Special Publication 1017, National Institute of Standards and Technology, Gaithersburg, Maryland.

Frey, A. E., and T'ien, J. S. (1979). "A theory of flame spread over a solid fuel including finite-rate chemical kinetics." Combustion and flame, Vol 36, pp. 263-268.

Gustafsson, S. E. (1998). "Instruction Manual for Hot Disk Thermal Constants Analyser." American Institute of Physics, pp. 1-44.

Heskestad, G. (2002). "Fire Plumes, Flame Height, and Air Entrainment." SFPE handbook of fire protection engineering, P. J. DiNenno, ed., National Fire Protection Association ; Society of Fire Protection Engineers, Quincy, Mass. Bethesda, MD.

Icove, D. J., and DeHaan, J. D. (2004). "Forensic fire scene reconstruction." Brady fire, Pearson/Prentice Hall, Upper Saddle River, N.J.

Incropera, F. P., and DeWitt, D. P. (2001). "Fundamentals of heat and mass transfer." Wiley, New York.

References

Janssens, M. (2002). "Calorimetry." SFPE handbook of fire protection engineering, P. J. DiNenno, ed., National Fire Protection Association ; Society of Fire Protection Engineers, Quincy, Mass. Bethesda, MD., pp 3-38 to 3-62.

Kollmann, F. F. P., and Cote, W. A. (1968). "Principles of wood science and technology." Solid Wood, Vol 1, pp 592.

McAlevy, R. F., and Magee, R. S. (1969). "The mechanisms of flame spreading over the surface of igniting condensed-phase materials." Twelfth Symposium (International) on Combustion, pp. 215-227.

McGrattan (editor), K. B. (2004). "Fire Dynamics Simulator (Version 4) Technical Reference Guide." NIST Special Publication 1018, National Institute of Standards and Technology, Gaithersburg, Maryland.

McGrattan, K. B., and Forney, G. P. (2004). "Fire Dynamics Simulator (Version 4) User's Guide." NIST Special Publication 1019, National Institute of Standards and Technology, Gaithersburg, Maryland.

McGrattan, K. B. e. (2004). "Fire Dynamics Simulator (Version 4) Technical Reference Guide." NIST Special Publication 1018, National Institute of Standards and Technology, Gaithersburg, Maryland.

Merryweather, G. (2006). "Comparison of Flame Spread Measurements Using the ASTM E 1321 LIFT and a Reduced Scale Adaptation of the Cone Calorimeter Apparatus," University of Canterbury, Christchurch.

Ngu, C. K. (2001). "Ignition properties of New Zealand timber," University of Canterbury, Christchurch.

Nisted, T. (1991). "Flame spread experiments in bench scale : project 5 of the EUREFIC fire research programme." Dantest, Fire Technology (Dansk institut for prøvning og justering), København.

Olson, S. L., Ferkul, P. V., and Tien, J. S. (1988). "22nd Symposium (International) on Combustion." Pittsburgh, PA, pp. 1213.

References

Quintiere, J. G. (1981). "A Simplified Theory for Generalizing Results from a Radiant Panel Rate of Flame Spread Apparatus." *Fire and materials*, Vol. 2(2), pp. 52-60.

Quintiere, J. G. (1998). "Principles of fire behavior." Delmar Publishers, Albany, N.Y.

Quintiere, J. G. (2002). "Surface Flame Spread." *SFPE handbook of fire protection engineering*, P. J. DiNenno, ed., National Fire Protection Association ; Society of Fire Protection Engineers, Quincy, Mass. Bethesda, MD.

Quintiere, J. G., and Harkleroad, M. (1984). "New Concepts for Measuring Flame Spread Properties, NBSIR 84-2943." National Bureau of Standards, Gaithersburg, MD.

Saito, K., Quintiere, J. G., and Williams, F. A. (1985). *Fire Safety Science : Proceedings of The First International Symposium*, C. E. Grant and P. J. Pagni, eds., Hemisphere Publishing Corporation, NIST, USA, pp 75.

Spearpoint, M. J. (1999). "Predicting the ignition and burning rate of wood in the cone calorimeter using an integral model." Building and Fire Research Laboratory (U.S.), Gaithersburg, MD.

Tannehill, J. C., Anderson, D. A., and Pletcher, R. H. (1997). "Computational fluid mechanics and heat transfer." *Series in computational and physical processes in mechanics and thermal sciences*, Taylor & Francis, Washington, DC.

Tran, H. C., and White, R. H. (1992). "Burning Rate of Solid Wood Measured in a Heat Release Rate Calorimeter." *Fire and Materials*, 16(1), 197-206.

White, R. H. (2002). "Analytical Methods for Determining Fire Resistance of Timber Members." *SFPE handbook of fire protection engineering*, P. J. DiNenno, ed., National Fire Protection Association ; Society of Fire Protection Engineers, Quincy, Mass. Bethesda, MD.

Wichman, I. S. (1992). "Theory of opposed-flow flame spread." *Progress in Energy and Combustion Science*, Vol 18(6), pp 553-593.

Williams, F. A. (1976). "Sixteenth Symposium (International) on Combustion." The Combustion Institute, pp. 1281-1294.

References

Zhou, L., Cheng, R., and Fernandez-Pello, A. C. (1990). "Flame spread in an opposed turbulent flow." *Combustion and flame*, 81(1), pp 40 to 49.

Appendix A – LIFT calibration data

Appendix A 1: Flux distribution values required in the ASTM E 1321 -97a (2002) standards

Distance From Exposed End of the Specimen (mm)	Typical Flux Levels at the Specimen (kW/m ²)	Flux distribution F(x)
0	49.5	0.980
50	50.5	1.000
100	49.5	0.980
150	47.1	0.933
200	43.1	0.853
250	37.8	0.749
300	30.9	0.612
350	23.9	0.473
400	18.2	0.360
450	13.2	0.261
500	9.2	0.182
550	6.2	0.123
600	4.3	0.085
650	3.1	0.061
700	2.2	0.044
750	1.5	0.030

Distance in 25mm increment (mm)	Flux distribution F(x)
0	0.980
25	0.990
50	1.000
75	0.990
100	0.980
125	0.956
150	0.933
175	0.893
200	0.853
225	0.801
250	0.749
275	0.680
300	0.612
325	0.543
350	0.473
375	0.417
400	0.360
425	0.311
450	0.261
475	0.222
500	0.182
525	0.152
550	0.123
575	0.104
600	0.085

625	0.073
650	0.061
675	0.052
700	0.044
725	0.037
750	0.030

Appendix B – Calculation for density

Appendix B 1: Dimension of specimens and its density for virgin materials

Material	Mass (g)	Mass (kg)	Breath (mm)	Length (mm)	Thickness (mm)	Volume (mm ³)	Volume (m ³)	Density (kg/m ³)	Average Density	Density of tested samples kg/m ³ (Merryweather (2006))	Percentage difference in Density
Hardboard	42.21	0.04221	100	100	5	50000	0.00005	844	844	819.5	-3.0%
	42.20	0.0422	100	100	5	50000	0.00005	844			
Medium Density Fibreboard (MDF)	111.88	0.11188	96	100	18	172800	0.0001728	647	647	620	-4.3%
	111.57	0.11157	96	100	18	172800	0.0001728	646			
Melteca faced MDF	140.94	0.14094	97	100	18	174600	0.0001746	807	793	681	-16.4%
	134.55	0.13455	96	100	18	172800	0.0001728	779			
Melteca faced particle board	96.58	0.09658	95	94	17	151810	0.00015181	636	635	661	3.9%
	97.24	0.09724	95	95	17	153425	0.000153425	634			
Beech	115.50	0.1155	94	97	23	209714	0.000209714	551	556	489	-13.6%
	121.19	0.12119	94	100	23	216200	0.0002162	561			
Macrocarpa	129.68	0.12968	96	100	24	230400	0.0002304	563	566	514	-10.0%

Appendix B

Calculation for density

	130.91	0.13091	96	100	24	230400	0.0002304	568			
Radiata Pine (Monterey pine)	91.48	0.09148	96	100	22	211200	0.0002112	433	438	425	-3.1%
	93.65	0.09365	96	100	22	211200	0.0002112	443			
Rimu	128.03	0.12803	96	100	21	201600	0.0002016	635	634	660	3.9%
	127.64	0.12764	96	100	21	201600	0.0002016	633			
Particle board (chipboard)	126.54	0.12654	97	100	20	194000	0.000194	652	650	745	12.7%
	125.85	0.12585	97	100	20	194000	0.000194	649			
	128.69	0.12869	96	100	20	192000	0.000192	670	670	673	0.5%
	127.07	0.12707	95	100	20	190000	0.00019	669			
Plywood	104.72	0.10472	100	100	21	210000	0.00021	499	503	487	-3.3%
	106.52	0.10652	100	100	21	210000	0.00021	507			
Calcium Silicate	168.55	0.16855	93	115	15	160425	0.000160425	1051	1055	-	-
	170.06	0.17006	93	115	15	160425	0.000160425	1060			

Appendix B 2: Measured ignition temperature and calculation of the char density

Beech	Specimen 1	Specimen 2
Ignition Temperature (°C)	360	347
Ignition Time (s)	47	46
Non char depth (mm)	11	10
x (mm)	97	101
y (mm)	91	87
Volume of the virgin material (mm ³)	97097	87870
Average Density (kg/m ³)	556	
Mass of the virgin material (g)	53.95	48.82
Total Mass (g)	65.34	64.04
Char mass (g)	11.39	15.22
Char depth (mm)	5.0	6.0
x (mm)	96	98
y (mm)	84	82
Char volume (mm ³)	40320	48216
Char density (kg/m ³)	282	316

Macrocarpa	Specimen 1	Specimen 2
Ignition Temperature (°C)	329	320
Ignition Time (s)	39	39
Non char depth (mm)	13.0	14
x (mm)	95	96
y (mm)	100	100

Melteca faced MDF	Specimen 1	Specimen 2
Ignition Temperature (°C)	406	420
Ignition Time (s)	93	81
Non char depth (mm)	5.0	5
x (mm)	97	97
y (mm)	100	100
Volume of the virgin material (mm ³)	48500	48500
Average Density (kg/m ³)	793	
Mass of the virgin material (g)	38.46	38.46
Total Mass (g)	78.64	83.58
Char mass (g)	40.18	45.12
Char depth (mm)	8	8
x (mm)	94	93
y (mm)	97	97
Char volume (mm ³)	72944	72168
Char density (kg/m ³)	551	625

Melteca faced particle board	Specimen 1	Specimen 2
Ignition Temperature (°C)	385	405
Ignition Time (s)	92	85
Non char depth (mm)	5	5
x (mm)	95	95
y (mm)	95	95

Appendix B

Calculation for density

Volume of the virgin material (mm ³)	123500	134400
Average Density (kg/m ³)	566	
Mass of the virgin material (g)	69.84	76.01
Total Mass (g)	90.22	90.36
Char mass (g)	20.38	14.35
Char depth (mm)	7.0	6.0
x (mm)	92	94
y (mm)	100	100
Char volume (mm ³)	64400	56400
Char density (kg/m ³)	316	255

Volume of the virgin material (mm ³)	45125	45125
Average Density (kg/m ³)	635	
Mass of the virgin material (g)	28.65	28.65
Total Mass (g)	60.67	57.35
Char mass (g)	32.02	28.70
Char depth (mm)	8.0	8.0
x (mm)	93	92
y (mm)	93	93
Char volume (mm ³)	69192	68448
Char density (kg/m ³)	463	419

Radiata Pine (Monterey pine)	Specimen 1	Specimen 2
Ignition Temperature (°C)	431	396
Ignition Time (s)	51	46
Non char depth (mm)	8.0	8
x (mm)	94	95
y (mm)	100	100
Volume of the virgin material (mm ³)	75200	76000
Average Density (kg/m ³)	438	
Mass of the virgin material (g)	32.96	33.31
Total Mass (g)	50.95	48.74
Char mass (g)	17.99	15.43
Char depth (mm)	8.0	8.0

Pynefloor Particle board (chipboard)	Specimen 1	Specimen 2
Ignition Temperature (°C)	356	335
Ignition Time (s)	60	58
Non char depth (mm)	4	5
x (mm)	96	96
y (mm)	100	100
Volume of the virgin material (mm ³)	38400	48000
Average Density (kg/m ³)	670	
Mass of the virgin material (g)	25.71	32.14
Total Mass (g)	62.88	68.13
Char mass (g)	37.17	35.99
Char depth (mm)	10	10

Appendix B

Calculation for density

x (mm)	99	96
y (mm)	86	86
Char volume (mm ³)	68112	66048
Char density (kg/m ³)	264	234

x (mm)	94	94
y (mm)	98	98
Char volume (mm ³)	92120	92120
Char density (kg/m ³)	403	391

Rimu	Specimen 1	Specimen 2
Ignition Temperature (°C)	338	361
Ignition Time (s)	54	54
Non char depth (mm)	9.0	9
x (mm)	95	94
y (mm)	100	100
Volume of the virgin material (mm ³)	85500	84600
Average Density (kg/m ³)	634	
Mass of the virgin material (g)	54.22	53.65
Total Mass (g)	76.60	78.21
Char mass (g)	22.38	24.56
Char depth (mm)	7.0	7.0
x (mm)	77	82
y (mm)	100	100
Char volume (mm ³)	53900	57400
Char density (kg/m ³)	415	428

Superflake Particle board (chipboard)	Specimen 1	Specimen 2
Ignition Temperature (°C)	358	368
Ignition Time (s)	55	63
Non char depth (mm)	4.0	4
x (mm)	94	95
y (mm)	100	100
Volume of the virgin material (mm ³)	37600	38000
Average Density (kg/m ³)	503	
Mass of the virgin material (g)	18.91	19.11
Total Mass (g)	70.83	71.93
Char mass (g)	51.92	52.82
Char depth (mm)	10.0	10.0
x (mm)	91	92
y (mm)	98	98
Char volume (mm ³)	89180	90160
Char density (kg/m ³)	582	586

Appendix B**Calculation for density**

Plywood	Specimen 1	Specimen 2
Ignition Temperature (°C)	343	365
Ignition Time (s)	43	39
Non char depth (mm)	9.0	8
x (mm)	101	101
y (mm)	100	101
Volume of the virgin material (mm ³)	90900	81608
Average Density (kg/m ³)	650	
Mass of the virgin material (g)	59.13	53.09
Total Mass (g)	61.45	56.47
Char mass (g)	2.32	3.38
Char depth (mm)	8.0	9.0
x (mm)	97	98
y (mm)	98	96
Char volume (mm ³)	76048	84672
Char density (kg/m ³)	31	40

Hardboard	Specimen 1	Specimen 2
Ignition Temperature (°C)	398	386
Ignition Time (s)	66	58
Non char depth (mm)	0.5	0.5
x (mm)	90	91
y (mm)	85	91
Volume of the virgin material (mm ³)	3825	4141
Average Density (kg/m ³)	844	
Mass of the virgin material (g)	3.23	3.49
Total Mass (g)	20.25	23.10
Char mass (g)	17.02	19.61
Char depth (mm)	4.5	4.5
x (mm)	90	91
y (mm)	85	91
Char volume (mm ³)	34425	37265
Char density (kg/m ³)	494	526

Medium Density Fibreboard (MDF)	Specimen 1	Specimen 2
Ignition Temperature (°C)	390	400
Ignition Time (s)	75	80
Non char depth (mm)	5	3
x (mm)	95	95
y (mm)	100	100
Volume of the virgin material (mm ³)	47500	28500
Average Density (kg/m ³)	647	
Mass of the virgin material (g)	30.71	18.43
Total Mass (g)	63.29	58.01
Char mass (g)	32.58	39.58
Char depth (mm)	8	9
x (mm)	92	90
y (mm)	94	93
Char volume (mm ³)	69184	75330
Char density (kg/m ³)	471	525

Appendix C – Hot Disk test results

Beech					
Test	k (W/m.K)	α (mm²/s)	c (MJ/m³.K)	Temp Increase (K)	Total to Characteristic Time
1	0.1908	0.2569	0.7425	3.11	0.412
2	0.1983	0.2699	0.7347	3.00	0.433
3	0.1906	0.2636	0.7233	3.11	0.423
4	0.1928	0.2668	0.7226	3.09	0.428
5	0.1909	0.274	0.6968	3.12	0.440
Average	0.1927	0.2662	0.7240		
Std dev	0.0033	0.0065	0.0173		

Charred Beech					
Test	k (W/m.K)	α (mm²/s)	c (MJ/m³.K)	Temp Increase (K)	Total to Characteristic Time
1	0.1050	0.3939	0.2667	2.76	0.632
2	0.1046	0.3345	0.3126	3.70	0.537
3	0.1002	0.3981	0.2516	3.03	0.639
4	0.0955	0.6460	0.1478	2.81	0.674
5	0.0848	0.6637	0.1278	2.49	0.799
Average	0.0980	0.4872	0.2213		
Std dev	0.0083	0.1552	0.0798		

Radiata Pine					
Test	k (W/m.K)	α (mm ² /s)	c (MJ/m ³ .K)	Temp Increase (K)	Total to Characteristic Time
1	0.1721	0.2897	0.5939	3.48	0.465
2	0.1771	0.3669	0.4826	3.43	0.589
3	0.1702	0.3529	0.4822	3.55	0.567
4	0.1733	0.3621	0.4786	3.48	0.581
5	0.1726	0.3597	0.4799	3.50	0.577
Average	0.1731	0.3463	0.5034		
Std dev	0.0025	0.0320	0.0506		

Charred Radiata Pine					
Test	k (W/m.K)	α (mm ² /s)	c (MJ/m ³ .K)	Temp Increase (K)	Total to Characteristic Time
1	0.08160	0.3907	0.2088	3.42	0.470
2	0.08547	0.619	0.1381	3.13	0.745
3	0.09713	0.4623	0.2101	2.89	0.557
4	0.09786	0.3304	0.2962	2.78	0.398
5	0.10920	0.4138	0.2638	3.27	0.565
Average	0.09425	0.4432	0.2234		
Std dev	0.01098	0.1091	0.0604		

Rimu					
Test	k (W/m.K)	α (mm ² /s)	c (MJ/m ³ .K)	Temp Increase (K)	Total to Characteristic Time
1	0.2288	0.3287	0.6963	2.63	0.528
2	0.2296	0.3277	0.7008	2.63	0.526
3	0.2165	0.2964	0.7306	2.78	0.476
4	0.2204	0.2834	0.7775	2.71	0.455
5	0.2231	0.2638	0.8457	2.66	0.424
Average	0.2237	0.3000	0.7502		
Std dev	0.0056	0.0282	0.0624		

Charred Rimu					
Test	k (W/m.K)	α (mm ² /s)	c (MJ/m ³ .K)	Temp Increase (K)	Total to Characteristic Time
1	0.1047	0.5071	0.2065	2.59	0.611
2	0.1004	0.5513	0.1821	2.70	0.664
3	0.1008	0.5681	0.1775	2.67	0.684
4	0.1048	0.6704	0.1563	2.51	0.807
5	0.1009	0.7344	0.1373	2.56	0.884
Average	0.1023	0.6063	0.1719		
Std dev	0.0022	0.0933	0.0263		

Macrocarpa					
Test	k (W/m.K)	α (mm²/s)	c (MJ/m³.K)	Temp Increase (K)	Total to Characteristic Time
1	0.2015	0.2966	0.6794	2.98	0.476
2	0.1895	0.3003	0.6309	3.17	0.482
3	0.1941	0.337	0.5759	3.11	0.541
4	0.2042	0.3673	0.5561	2.97	0.590
5	0.1881	0.3045	0.6176	3.19	0.489
Average	0.1955	0.3211	0.6120		
Std dev	0.0071	0.0304	0.0484		

Charred Macrocarpa					
Test	k (W/m.K)	α (mm²/s)	c (MJ/m³.K)	Temp Increase (K)	Total to Characteristic Time
1	0.08119	0.35	0.2320	3.19	0.506
2	0.07188	0.6505	0.1105	3.68	0.783
3	0.08133	0.3948	0.2212	3.28	0.539
4	0.08033	0.7085	0.1134	2.57	0.739
5	0.07348	0.5752	0.1277	2.79	0.923
Average	0.07764	0.5358	0.1610		
Std dev	0.00458	0.1573	0.0604		

MDF					
Test	k (W/m.K)	α (mm ² /s)	c (MJ/m ³ .K)	Temp Increase (K)	Total to Characteristic Time
1	0.1766	0.1949	0.9058	3.41	0.626
2	0.1749	0.2461	0.7109	3.41	0.790
3	0.1775	0.2422	0.7328	3.36	0.778
4	0.1783	0.2260	0.7888	3.36	0.726
5	0.1820	0.2596	0.7009	3.28	0.834
Average	0.1779	0.2338	0.7678		
Std dev	0.0026	0.0248	0.0843		

Charred MDF					
Test	k (W/m.K)	α (mm ² /s)	c (MJ/m ³ .K)	Temp Increase (K)	Total to Characteristic Time
1	0.1058	0.3676	0.2878	2.87	0.590
2	0.0976	0.3879	0.2517	3.09	0.623
3	0.0942	0.4774	0.1972	3.12	0.766
4	0.1018	0.3979	0.2560	2.94	0.639
5	0.1048	0.3788	0.2767	2.87	0.608
Average	0.1008	0.4019	0.2539		
Std dev	0.0049	0.0437	0.0350		

Melteca faced MDF					
Test	k (W/m.K)	α (mm²/s)	c (MJ/m³.K)	Temp Increase (K)	Total to Characteristic Time
1	0.2174	0.1772	1.227	2.77	0.569
2	0.2188	0.1864	1.174	2.75	0.599
3	0.2224	0.1947	1.142	2.71	0.625
4	0.2225	0.1876	1.186	2.70	0.602
5	0.2311	0.2037	1.134	2.60	0.654
Average	0.2224	0.1899	1.173		
Std dev	0.0053	0.0099	0.037		

Charred Melteca faced MDF					
Test	k (W/m.K)	α (mm²/s)	c (MJ/m³.K)	Temp Increase (K)	Total to Characteristic Time
1	0.1397	0.2385	0.5857	2.13	0.766
2	0.1427	0.2431	0.5871	2.05	0.780
3	0.1336	0.2586	0.5167	2.06	0.623
4	-	-	-	-	-
5	-	-	-	-	-
Average	0.1387	0.2467	0.5632		
Std dev	0.0046	0.0105	0.0402		

Plywood					
Test	k (W/m.K)	α (mm ² /s)	c (MJ/m ³ .K)	Temp Increase (K)	Total to Characteristic Time
1	0.1794	0.3063	0.5857	3.35	0.492
2	0.1784	0.2912	0.6126	3.34	0.467
3	0.1774	0.2745	0.6463	3.35	0.441
4	0.1933	0.3593	0.5378	3.12	0.577
5	0.1919	0.3567	0.5379	3.15	0.573
Average	0.1841	0.3176	0.5841		
Std dev	0.0078	0.0386	0.0473		

Charred Plywood					
Test	k (W/m.K)	α (mm ² /s)	c (MJ/m ³ .K)	Temp Increase (K)	Total to Characteristic Time
1	0.07997	0.5396	0.1482	3.56	0.866
2	0.08175	0.5116	0.1598	2.57	0.821
3	0.07646	0.7251	0.1054	3.38	0.873
4	0.08443	0.6314	0.1337	3.14	0.760
5	0.07616	0.6271	0.1215	3.47	0.755
Average	0.07975	0.6070	0.1337		
Std dev	0.00352	0.0845	0.0215		

Pynefloor					
Test	k (W/m.K)	α (mm ² /s)	c (MJ/m ³ .K)	Temp Increase (K)	Total to Characteristic Time
1	0.2016	0.1488	1.355	2.97	0.478
2	0.2377	0.1932	1.231	2.54	0.620
3	0.2394	0.2089	1.146	2.52	0.671
4	0.2286	0.1746	1.309	2.66	0.561
5	0.2490	0.2077	1.199	2.42	0.667
Average	0.2313	0.1866	1.248		
Std dev	0.0181	0.0253	0.084		

Charred Pynefloor					
Test	k (W/m.K)	α (mm ² /s)	c (MJ/m ³ .K)	Temp Increase (K)	Total to Characteristic Time
1	0.0943	0.2780	0.3391	3.24	0.446
2	0.1040	0.3952	0.2632	2.92	0.634
3	0.1017	0.2767	0.3677	2.98	0.444
4	0.1033	0.5162	0.2000	2.87	0.829
5	0.1044	0.4177	0.2498	2.85	0.671
Average	0.1015	0.3768	0.2840		
Std dev	0.0042	0.1015	0.0684		

Hardboard					
Test	k (W/m.K)	α (mm ² /s)	c (MJ/m ³ .K)	Temp Increase (K)	Total to Characteristic Time
1	0.2538	0.2734	0.928	2.37	0.439
2	0.2518	0.2326	1.082	2.32	0.373
3	0.2412	0.2267	1.064	2.42	0.364
4	0.2339	0.2120	1.103	3.74	0.340
5	0.2380	0.2084	1.142	2.42	0.335
Average	0.2437	0.2306	1.064		
Std dev	0.0087	0.0259	0.081		

Charred Hardboard					
Test	k (W/m.K)	α (mm ² /s)	c (MJ/m ³ .K)	Temp Increase (K)	Total to Characteristic Time
1	0.2278	0.6284	0.3625	1.22	0.757
2	0.2068	0.5104	0.4051	2.00	0.819
3	0.2000	0.3329	0.6008	2.86	0.534
4	0.2118	0.4885	0.4335	3.25	0.784
5	0.2079	0.5061	0.4108	2.64	0.731
Average	0.2109	0.4933	0.4425		
Std dev	0.0104	0.1054	0.0921		

Melteca faced Particle board					
Test	k (W/m.K)	α (mm²/s)	c (MJ/m³.K)	Temp Increase (K)	Total to Characteristic Time
1	0.1995	0.1680	1.188	3.02	0.539
2	0.2098	0.1805	1.163	2.87	0.579
3	0.1980	0.1621	1.222	3.03	0.520
4	0.2000	0.1694	1.180	3.01	0.544
5	0.1991	0.1783	1.116	3.02	0.573
Average	0.2013	0.1717	1.174		
Std dev	0.0048	0.0076	0.039		

Charred Melteca faced Particle board					
Test	k (W/m.K)	α (mm²/s)	c (MJ/m³.K)	Temp Increase (K)	Total to Characteristic Time
1	N/A	N/A	N/A	N/A	N/A
2	N/A	N/A	N/A	N/A	N/A
3	N/A	N/A	N/A	N/A	N/A
4	N/A	N/A	N/A	N/A	N/A
5	N/A	N/A	N/A	N/A	N/A
Average	N/A	N/A	N/A		
Std dev	N/A	N/A	N/A		

Superflake					
Test	k (W/m.K)	α (mm ² /s)	c (MJ/m ³ .K)	Temp Increase (K)	Total to Characteristic Time
1	0.2157	0.1711	1.261	2.79	0.549
2	0.2497	0.2083	1.199	2.41	0.669
3	0.2217	0.1622	1.367	2.71	0.521
4	0.2154	0.1539	1.400	2.79	0.494
5	0.2089	0.1621	1.288	2.88	0.521
Average	0.2223	0.1715	1.303		
Std dev	0.0160	0.0214	0.081		

Charred Superflake					
Test	k (W/m.K)	α (mm ² /s)	c (MJ/m ³ .K)	Temp Increase (K)	Total to Characteristic Time
1	N/A	N/A	N/A	N/A	N/A
2	N/A	N/A	N/A	N/A	N/A
3	N/A	N/A	N/A	N/A	N/A
4	N/A	N/A	N/A	N/A	N/A
5	N/A	N/A	N/A	N/A	N/A
Average	N/A	N/A	N/A		
Std dev	N/A	N/A	N/A		

Calcium Silicate					
Test	k (W/m.K)	α (mm ² /s)	c (MJ/m ³ .K)	Temp Increase (K)	Total to Characteristic Time
1	0.3045	0.3930	0.7747	1.98	0.631
2	0.3292	0.4757	0.6921	1.81	0.764
3	0.3127	0.3973	0.7870	1.92	0.638
4	0.3119	0.3804	0.8198	1.93	0.611
5	0.3103	0.3909	0.7940	1.94	0.627
Average	0.3137	0.4075	0.7735		
Std dev	0.0092	0.0387	0.0484		

Appendix D – Ignition test results from Merryweather (2006)

MDF	LIFT	ISO5657-1986	Ngu (ISO5657)	Ignition in RIFT	
Ignition parameter "b"	0.047	0.053	0.043	0.053	s ^{0.5}
t* intercept of ignition parameter graph	21	19	23	19	s ^{0.5}
Preheat time t*	456	355	544	357	sec
Critical ignition flux q"crit	3.4	3.7	4.7	-0.3	kW/m ²
Thermal inertia kpc	1.10	0.86	1.04	0.86	(kW/m ² K) ²
Minimum ignition flux q"ig,min	16.25	16.25	13.5	16.25	kW/m ²
Heat transfer coefficient at ignition h	0.044	0.044	0.039	0.043	kW/m ² K
Ignition temperature T _{ig}	391	391	348	391	°C
Plywood - 17mm	LIFT	ISO5657-1986	Ngu (ISO5657)	Ignition in RIFT	
Ignition parameter "b"	0.058	0.048	0.034	0.061	s ^{0.5}
t* intercept of ignition parameter graph	17	21	29	17	s ^{0.5}
Preheat time t*	293	432	870	273	sec
Critical ignition flux q"crit	7.2	4.6	7.2	9.9	kW/m ²
Thermal inertia kpc	0.71	0.93	1.76	0.66	(kW/m ² K) ²
Minimum ignition flux q"ig,min	16.3	13.8	12.0	16.3	kW/m ²
Heat transfer coefficient at ignition h	0.044	0.041	0.040	0.043	kW/m ² K
Ignition temperature T _{ig}	391	352	321	391	°C

Melteca faced MDF	LIFT	ISO5657-1986	Ignition in RIFT	
Ignition parameter "b"	0.0423	0.0429	0.051	s ^{0.5}
t* intercept of ignition parameter graph	24	23	19.5	s ^{0.5}
Preheat time t*	560	542	382	sec
Critical ignition flux q"crit	-6.44	2.58	- 1.06	kW/m ²
Thermal inertia kpc	1.475	1.474	1.07	(kW/m ² K) ²
Minimum ignition flux q"ig,min	18.75	20	21.25	kW/m ²
Heat transfer coefficient at ignition h	0.045	0.046	0.047	kW/m ² K
Ignition temperature T _{ig}	440	425	454	°C
Melteca/ Particle board	LIFT	ISO5657-1986	Ignition in RIFT	
Ignition parameter "b"	Not tested	0.044	0.057	s ^{0.5}
t* intercept of ignition parameter graph	-	22.6	17.5	s ^{0.5}
Preheat time t*	-	512	308	sec
Critical ignition flux q"crit	-	2.00	10.1	kW/m ²
Thermal inertia kpc	-	1.27	0.97	(kW/m ² K) ²
Minimum ignition flux q"ig,min	-	18.75	23.75	kW/m ²
Heat transfer coefficient at ignition h	-	0.044	0.050	kW/m ² K
Ignition temperature T _{ig}	-	425	478	°C

Pynefloor particle Board	LIFT	ISO5657-1986	Ignition in RIFT	
Ignition parameter "b"	0.0509	0.0364	0.063	s ^{0.5}
t* intercept of ignition parameter graph	19.6	27.5	16	s ^{0.5}
Preheat time t*	385.6	754.6	250	sec
Critical ignition flux q"crit	1.7	3.5	4.3	kW/m ²
Thermal inertia kpc	0.96	1.64	0.70	(kW/m ² K) ²
Minimum ignition flux q"ig,min	18.75	13.75	21.25	kW/m ²
Heat transfer coefficient at ignition h	0.044	0.041	0.047	kW/m ² K
Ignition temperature T _{ig}	425	352	454	°C
Superflake particle board	LIFT	ISO5657-1986	Ignition in RIFT	
Ignition parameter "b"	Not tested	0.0327	0.05	s ^{0.5}
t* intercept of ignition parameter graph	Not tested	30.6	19.72	s ^{0.5}
Preheat time t*	Not tested	935	389	sec
Critical ignition flux q"crit	Not tested	3.44	5.24	kW/m ²
Thermal inertia kpc	Not tested	2.11	1.05	(kW/m ² K) ²
Minimum ignition flux q"ig,min	Not tested	13.75	18.75	kW/m ²
Heat transfer coefficient at ignition h	Not tested	0.042	0.05	kW/m ² K
Ignition temperature T _{ig}	Not tested	352	424.87	°C

Hardboard	LIFT	ISO5657-1986	Ignition in RIFT		
Ignition parameter "b"	0.052	0.033	0.032		s ^{0.5}
t* intercept of ignition parameter graph	19	31	31.3		s ^{0.5}
Preheat time t*	375	944	977		sec
Critical ignition flux q"crit	2.172	- 0.588	2.6		kW/m ²
Thermal inertia kpc	0.88	1.83	1.67		(kW/m ² K) ²
Minimum ignition flux q"ig,min	17.5	11.25	11.25		kW/m ²
Heat transfer coefficient at ignition h	0.043	0.039	0.037		kW/m ² K
Ignition temperature T _{ig}	409	307	307		°C
Beech	LIFT	ISO5657-1986	Ngu (ISO5657)	Ignition in RIFT	
Ignition parameter "b"	0.050	0.053	0.025	0.034	s ^{0.5}
t* intercept of ignition parameter graph	20	19	40	29.1	s ^{0.5}
Preheat time t*	395	355	1,618	844	sec
Critical ignition flux q"crit	9.24	11.83	11.14	12.8	kW/m ²
Thermal inertia kpc	0.98	0.85	3.27	2.30	(kW/m ² K) ²
Minimum ignition flux q"ig,min	18.75	18	12	18.75	kW/m ²
Heat transfer coefficient at ignition h	0.044	0.043	0.040	0.046	kW/m ² K
Ignition temperature T _{ig}	425	415	321	425	°C

Radiata Pine	LIFT	ISO5657-1986	Ngu (ISO5657)	Ignition in RIFT	
Ignition parameter "b"	0.054	0.039	0.047	0.043	s ^{0.5}
t* intercept of ignition parameter graph	18	25	21	23	s ^{0.5}
Preheat time t*	341	643	460	531	sec
Critical ignition flux q ["] _{crit}	9.7	12.0	7.8	10.9	kW/m ²
Thermal inertia kpc	0.92	1.54	1.08	1.45	(kW/m ² K) ²
Minimum ignition flux q ["] _{ig,min}	18.75	16.25	15.5	18.75	kW/m ²
Heat transfer coefficient at ignition h	0.046	0.043	0.043	0.046	kW/m ² K
Ignition temperature T _{ig}	425	391	380	425	°C
Rimu	LIFT	ISO5657-1986	Ngu (ISO5657)	Ignition in RIFT	
Ignition parameter "b"	0.050	0.050	0.033	0.047	s ^{0.5}
t* intercept of ignition parameter graph	20	20	30	21.5	s ^{0.5}
Preheat time t*	395	397	893	462	sec
Critical ignition flux q ["] _{crit}	9.62	12.75	7.52	13.9	kW/m ²
Thermal inertia kpc	1.06	1.03	1.93	1.41	(kW/m ² K) ²
Minimum ignition flux q ["] _{ig,min}	18.5	18	13.5	21.25	kW/m ²
Heat transfer coefficient at ignition h	0.046	0.045	0.041	0.049	kW/m ² K
Ignition temperature T _{ig}	422	415	348	454	°C

Macrocarpa	LIFT	ISO5657-1986	Ngu (ISO5657)	Ignition in RIFT	
Ignition parameter "b"	0.059	0.048	0.055	0.056	s ^{0.5}
t* intercept of ignition parameter graph	17	21	18	18.0	s ^{0.5}
Preheat time t*	288	436	337	325	sec
Critical ignition flux q ["] _{crit}	14.7	15.2	12.9	15.6	kW/m ²
Thermal inertia kpc	0.78	1.13	0.79	0.89	(kW/m ² K) ²
Minimum ignition flux q ["] _{ig,min}	18.75	18	15.5	18.75	kW/m ²
Heat transfer coefficient at ignition h	0.046	0.045	0.043	0.046	kW/m ² K
Ignition temperature T _{ig}	425	415	380	425	°C

Appendix E – Calibration FDS4 input files

```
&HEAD CHID='Lift calibration 638',TITLE='Lift calibration 638' /
&GRID IBAR=95,JBAR=30,KBAR=30 / Specify number of grid cells in the x, y, and z
directions, respectively
&PDIM XBAR=0.95,YBAR=0.3,ZBAR=0.3 /
&TIME TWFIN=1000. / Time when finished (length of simulation)
```

```
&SURF ID = 'PANEL',TMPWAL=638,RGB = 1.0,0.0,0.0 /
```

```
&MISC SURF_DEFAULT='SPRUCE', REACTION='METHANE', NFRAMES=1000,
TMPA=25, TMPO=25, DTCORE=30./, RESTART=.TRUE./
```

```
*****
```

Properties

```
*****
```

```
&REAC ID='METHANE'
  FYI='Methane, C H_4'
  MW_FUEL=16
  NU_O2=2.
  NU_CO2=1.
  NU_H2O=2.
  RADIATIVE_FRACTION=0.15
  SOOT_YIELD=0.01 /
```

```
*****
```

```
&SURF ID      = 'DUMMY'
  FYI  = 'Calcium Silicate'
  RGB  = 0.66,0.66,0.66
  C_P  =0.6697
  DENSITY=1080.
  KS   = 0.3442
  DELTA = 0.19/
```

```
*****
```

```
*****
```

BACKING BOARD (Calcium Silicate)

```
*****
```

```
&OBST XB = 0.125,0.925,0.27,0.285,0.0625,0.2175 , SURF_ID='DUMMY' /
```

Special calibration board

&OBST XB = 0.125,0.925,0.25,0.27,0.0625,0.2175 , SURF_ID='DUMMY',/ 20mm thick,
750kg/m3

Radiant Panel

&OBST

XB=0,0.04,0.13,0.14,0,0.28,SURF_ID6='INERT','PANEL','INERT','PANEL','INERT','INERT',BNDF_BLOCK =FALSE /

&OBST

XB=0.04,0.08,0.12,0.13,0,0.28,SURF_ID6='INERT','PANEL','INERT','PANEL','INERT','INERT',BNDF_BLOCK =FALSE /

&OBST

XB=0.08,0.12,0.11,0.12,0,0.28,SURF_ID6='INERT','PANEL','INERT','PANEL','INERT','INERT',BNDF_BLOCK =FALSE /

&OBST

XB=0.12,0.15,0.1,0.11,0,0.28,SURF_ID6='INERT','PANEL','INERT','PANEL','INERT','INERT',BNDF_BLOCK =FALSE /

&OBST

XB=0.15,0.19,0.09,0.1,0,0.28,SURF_ID6='INERT','PANEL','INERT','PANEL','INERT','INERT',BNDF_BLOCK =FALSE /

&OBST

XB=0.19,0.23,0.08,0.09,0,0.28,SURF_ID6='INERT','PANEL','INERT','PANEL','INERT','INERT',BNDF_BLOCK =FALSE /

&OBST

XB=0.23,0.27,0.07,0.08,0,0.28,SURF_ID6='INERT','PANEL','INERT','PANEL','INERT','INERT',BNDF_BLOCK =FALSE /

&OBST

XB=0.27,0.3,0.06,0.07,0,0.28,SURF_ID6='INERT','PANEL','INERT','PANEL','INERT','INERT',BNDF_BLOCK =FALSE /

&OBST

XB=0.3,0.34,0.05,0.06,0,0.28,SURF_ID6='INERT','PANEL','INERT','PANEL','INERT','INERT',BNDF_BLOCK =FALSE /

&OBST

XB=0.34,0.38,0.04,0.05,0,0.28,SURF_ID6='INERT','PANEL','INERT','PANEL','INERT','INERT',BNDF_BLOCK =FALSE /

&OBST

XB=0.38,0.42,0.03,0.04,0,0.28,SURF_ID6='INERT','PANEL','INERT','PANEL','INERT','INERT',BNDF_BLOCK =FALSE /

&OBST

XB=0.42,0.45,0.02,0.03,0,0.28,SURF_ID6='INERT','PANEL','INERT','PANEL','INERT','INERT',BNDF_BLOCK =FALSE /

&OBST

XB=0.45,0.49,0.01,0.02,0,0.28,SURF_ID6='INERT','INERT','INERT','PANEL','INERT','INERT',BNDF_BLOCK =FALSE /

Vents

&VENT CB='XBAR0',SURF_ID='OPEN' /

&VENT CB='XBAR' ,SURF_ID='OPEN' /

&VENT CB='YBAR0',SURF_ID='OPEN' /

&VENT CB='YBAR' ,SURF_ID='OPEN' /

&VENT CB='ZBAR0' ,SURF_ID='OPEN' /

&VENT CB='ZBAR' ,SURF_ID='OPEN' /

Position of the gauge heat fluxmeters along the specimen

&THCP XYZ=0.13,0.25,0.14,QUANTITY='GAUGE_HEAT_FLUX', IOR=-2, LABEL='0mm away'/

&THCP XYZ=0.175,0.25,0.14,QUANTITY='GAUGE_HEAT_FLUX', IOR=-2, LABEL='50mm away'/

&THCP XYZ=0.225,0.25,0.14,QUANTITY='GAUGE_HEAT_FLUX', IOR=-2, LABEL='100mm away'/

&THCP XYZ=0.275,0.25,0.14,QUANTITY='GAUGE_HEAT_FLUX', IOR=-2, LABEL='150mm away'/

&THCP XYZ=0.325,0.25,0.14,QUANTITY='GAUGE_HEAT_FLUX', IOR=-2, LABEL='200mm away'/

&THCP XYZ=0.375,0.25,0.14,QUANTITY='GAUGE_HEAT_FLUX', IOR=-2, LABEL='250mm away'/

&THCP XYZ=0.425,0.25,0.14,QUANTITY='GAUGE_HEAT_FLUX', IOR=-2, LABEL='300mm away'/

&THCP XYZ=0.475,0.25,0.14,QUANTITY='GAUGE_HEAT_FLUX', IOR=-2, LABEL='350mm away'/

&THCP XYZ=0.525,0.25,0.14,QUANTITY='GAUGE_HEAT_FLUX', IOR=-2, LABEL='400mm away'/

&THCP XYZ=0.575,0.25,0.14,QUANTITY='GAUGE_HEAT_FLUX', IOR=-2, LABEL='450mm away'/

&THCP XYZ=0.625,0.25,0.14,QUANTITY='GAUGE_HEAT_FLUX', IOR=-2, LABEL='500mm away'/

&THCP XYZ=0.675,0.25,0.14,QUANTITY='GAUGE_HEAT_FLUX', IOR=-2, LABEL='550mm away'/

&THCP XYZ=0.725,0.25,0.14,QUANTITY='GAUGE_HEAT_FLUX', IOR=-2, LABEL='600mm away'/

&THCP XYZ=0.775,0.25,0.14,QUANTITY='GAUGE_HEAT_FLUX', IOR=-2, LABEL='650mm away'/

```
&THCP XYZ=0.825,0.25,0.14,QUANTITY='GAUGE_HEAT_FLUX', IOR=-2, LABEL=  
'700mm away'/  
&THCP XYZ=0.875,0.25,0.14,QUANTITY='GAUGE_HEAT_FLUX', IOR=-2, LABEL=  
'750mm away'/
```

&BNDF QUANTITY='GAUGE_HEAT_FLUX' / Tells FDS4 to record the Gauge heat flux of all solid surfaces.

Appendix F – Preheat Temperature Profiles

Appendix F 1: An example of the implicit method applied in spreadsheet

Solve this as a transient problem with the following boundary conditions:

Condition $q''(\text{Fire})$
 1 = 25.2 kW/m²
 Ignition temp = 425

Emissivity off the specimen (absorbed by the specimen) 0.8

Temperature at the surface = 411.2 C
 No ignition cell
 Preheat time = 395 C: 414

Assume convection boundary on the other side and the initial temperature is 293 K.
 The ignition temperature is 391 degree C
 Therefore 391+273 = 639 K

$$\alpha = \frac{k}{\rho c}$$

$$Fo = \frac{\alpha \Delta t}{\Delta x^2}$$

$$Bi = \frac{h\Delta x}{k}$$

Known properties:

$$q_{conv}'' = h(T_s - T_\infty)$$

$$q_{rad}'' = \epsilon\sigma(T_s^4 - T_\infty^4)$$

$$q_{net}'' = q_{Fire}'' - q_{conv}'' - q_{rad}''$$

k = 0.1927 W/m.K	x = 0.023 m	Δt = 1 s	ε = 0.8
c = 1303 J/kg.K	Δx = 0.0023 m	Fo = 0.05031	h = 15 W/m ²
ρ = 556 kg/m ³	α = 2.66E-07 m ² /s	σ = 5.7E-08 W/m ² K ⁴	Bi = 0.1791

$$T_0^{i+1} = 2Fo \left(\frac{q_0'' \Delta x}{k} + T_1^i \right) + (1 - 2Fo)T_0^i + h(T_0^i - T_\infty) - \epsilon\sigma(T_0^i - T_\infty^4)$$

$$T_m^{i+1} = Fo(T_{m+1}^i + T_{m-1}^i) + (1 - 2Fo)T_m^i$$

$$T_{10}^{i+1} = (1 - 2Fo)T_9^i + 2FoT_9^i$$

Condition 1

q''(rad heat flux)	Time (s)	Node 0	Node 1	Node 2	Node 3	Node 4	Node 5	Node 6	Node 7	Node 8	Node 9	Node 10	Time (s)
20156	0	293.0	293.0	293.0	293.0	293.0	293.0	293.0	293.0	293.0	293.0	293.0	0
20156	1	317.2	293.0	293.0	293.0	293.0	293.0	293.0	293.0	293.0	293.0	293.0	1
20156	2	338.4	294.2	293.0	293.0	293.0	293.0	293.0	293.0	293.0	293.0	293.0	2
20156	3	357.0	296.4	293.1	293.0	293.0	293.0	293.0	293.0	293.0	293.0	293.0	3
20156	4	373.5	299.3	293.2	293.0	293.0	293.0	293.0	293.0	293.0	293.0	293.0	4
20156	5	388.1	302.7	293.5	293.0	293.0	293.0	293.0	293.0	293.0	293.0	293.0	5
20156	6	401.2	306.5	294.0	293.0	293.0	293.0	293.0	293.0	293.0	293.0	293.0	6
20156	7	412.9	310.7	294.5	293.1	293.0	293.0	293.0	293.0	293.0	293.0	293.0	7

Appendix F

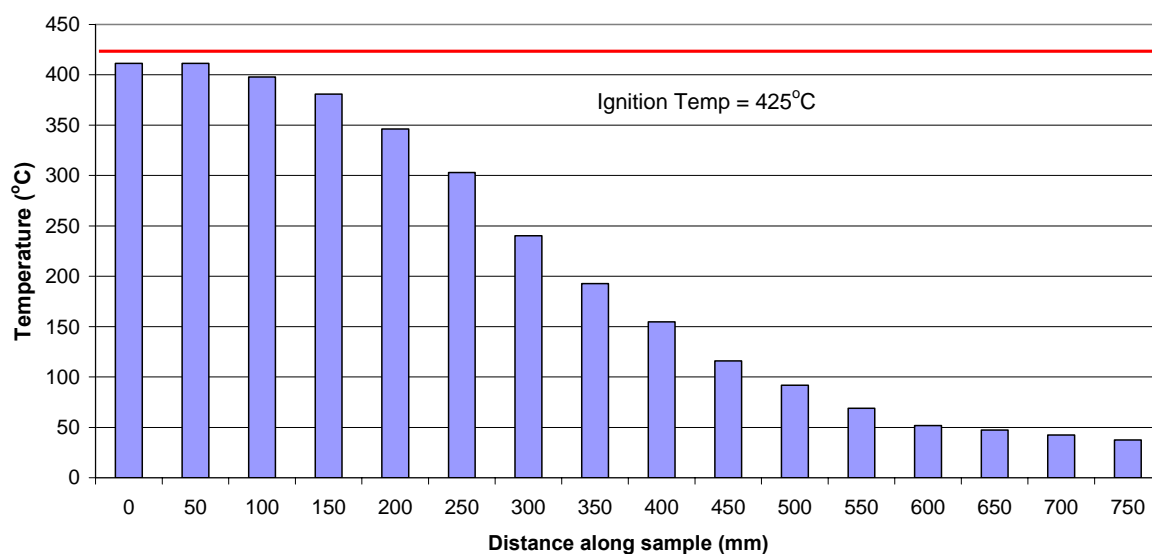
Preheat Temperature Profiles

20156	8	423.5	315.0	295.3	293.2	293.0	293.0	293.0	293.0	293.0	293.0	293.0	293.0	8
20156	9	433.1	319.5	296.2	293.3	293.0	293.0	293.0	293.0	293.0	293.0	293.0	293.0	9
20156	10	441.8	324.0	297.2	293.4	293.0	293.0	293.0	293.0	293.0	293.0	293.0	293.0	10
20156	11	449.8	328.6	298.3	293.6	293.0	293.0	293.0	293.0	293.0	293.0	293.0	293.0	11
20156	12	457.2	333.2	299.6	293.8	293.1	293.0	293.0	293.0	293.0	293.0	293.0	293.0	12
20156	13	464.0	337.7	301.0	294.0	293.1	293.0	293.0	293.0	293.0	293.0	293.0	293.0	13
20156	14	470.3	342.2	302.5	294.3	293.1	293.0	293.0	293.0	293.0	293.0	293.0	293.0	14
20156	15	476.1	346.7	304.1	294.7	293.2	293.0	293.0	293.0	293.0	293.0	293.0	293.0	15
20156	16	481.6	351.0	305.8	295.1	293.3	293.0	293.0	293.0	293.0	293.0	293.0	293.0	16
20156	17	486.8	355.3	307.5	295.5	293.3	293.0	293.0	293.0	293.0	293.0	293.0	293.0	17
20156	18	491.6	359.5	309.3	296.0	293.4	293.0	293.0	293.0	293.0	293.0	293.0	293.0	18
20156	19	496.2	363.7	311.2	296.6	293.5	293.1	293.0	293.0	293.0	293.0	293.0	293.0	19
20156	20	500.5	367.7	313.1	297.1	293.7	293.1	293.0	293.0	293.0	293.0	293.0	293.0	20
20156	21	504.6	371.6	315.0	297.8	293.8	293.1	293.0	293.0	293.0	293.0	293.0	293.0	21
20156	22	508.5	375.5	317.0	298.4	294.0	293.1	293.0	293.0	293.0	293.0	293.0	293.0	22
20156	23	512.2	379.2	319.0	299.2	294.2	293.2	293.0	293.0	293.0	293.0	293.0	293.0	23
20156	24	515.7	382.9	321.0	299.9	294.4	293.2	293.0	293.0	293.0	293.0	293.0	293.0	24
20156	25	519.1	386.4	323.1	300.7	294.6	293.3	293.0	293.0	293.0	293.0	293.0	293.0	25
20156	26	522.3	389.9	325.1	301.5	294.8	293.3	293.0	293.0	293.0	293.0	293.0	293.0	26
20156	27	525.4	393.3	327.2	302.4	295.1	293.4	293.1	293.0	293.0	293.0	293.0	293.0	27
20156	28	528.4	396.6	329.3	303.2	295.4	293.5	293.1	293.0	293.0	293.0	293.0	293.0	28
20156	29	531.3	399.9	331.4	304.2	295.7	293.5	293.1	293.0	293.0	293.0	293.0	293.0	29
20156	30	534.0	403.0	333.4	305.1	296.0	293.6	293.1	293.0	293.0	293.0	293.0	293.0	30
20156	31	536.7	406.1	335.5	306.1	296.3	293.7	293.1	293.0	293.0	293.0	293.0	293.0	31
20156	32	539.2	409.2	337.6	307.1	296.7	293.8	293.2	293.0	293.0	293.0	293.0	293.0	32
20156	33	541.7	412.1	339.7	308.1	297.1	293.9	293.2	293.0	293.0	293.0	293.0	293.0	33
20156	34	544.1	415.0	341.7	309.1	297.5	294.0	293.2	293.0	293.0	293.0	293.0	293.0	34
20156	35	546.4	417.8	343.8	310.2	297.9	294.2	293.2	293.0	293.0	293.0	293.0	293.0	35
20156	36	548.7	420.5	345.8	311.2	298.3	294.3	293.3	293.1	293.0	293.0	293.0	293.0	36
20156	37	550.9	423.2	347.8	312.3	298.8	294.5	293.3	293.1	293.0	293.0	293.0	293.0	37

For Beech

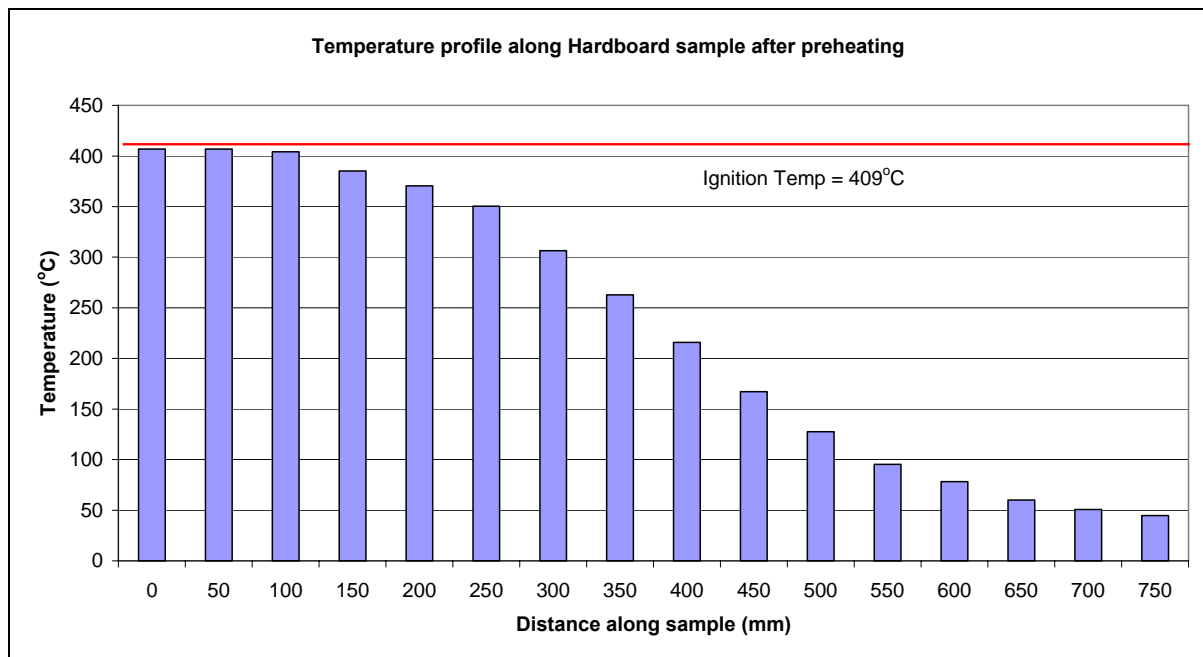
Distance along sample (mm)	Heat flux (kW/m ²)	Temperature (°C)
0	-	411
50	24.2	411
100	23.7	398
150	22.0	381
200	19.8	346
250	17.3	303
300	14.4	240
350	11.2	193
400	8.1	155
450	6.0	116
500	3.9	92
550	2.8	69
600	1.9	52
650	1.3	47
700	0.9	42
750	0.7	37

Temperature profile along Beech sample after preheating



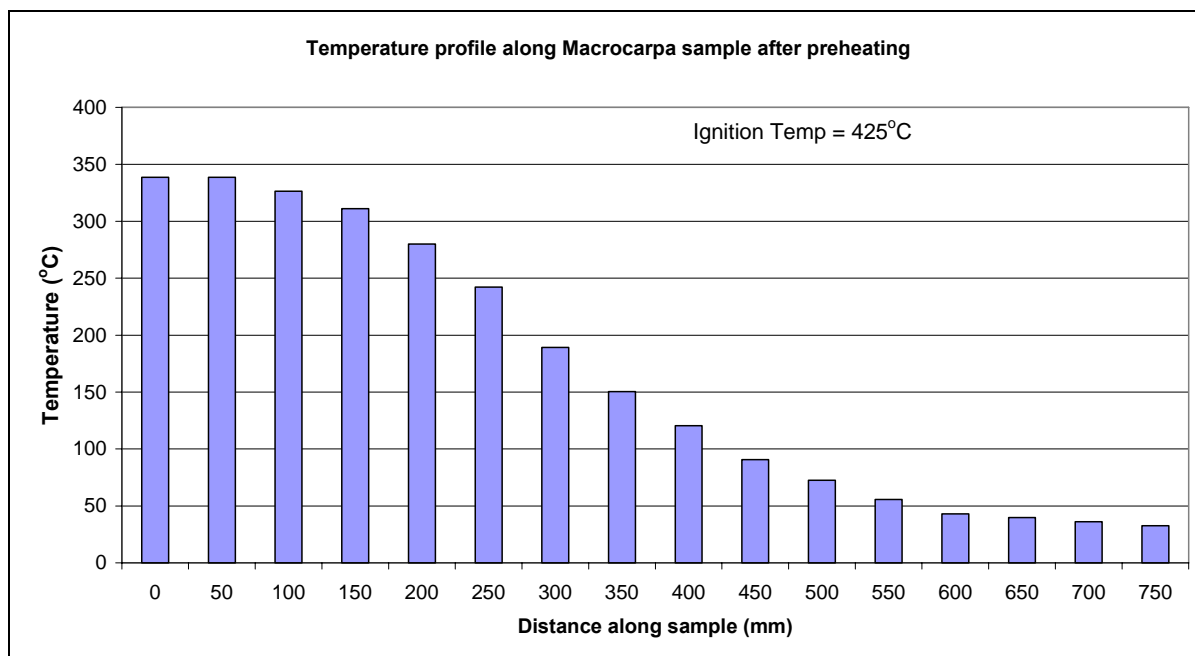
For Hardboard

Distance along sample (mm)	Heat flux (kW/m ²)	Temperature (°C)
0	-	407
50	24.2	407
100	23.7	404
150	22.0	385
200	19.8	371
250	17.3	350
300	14.4	306
350	11.2	263
400	8.1	216
450	6.0	167
500	3.9	128
550	2.8	95
600	1.9	78
650	1.3	60
700	0.9	51
750	0.7	45



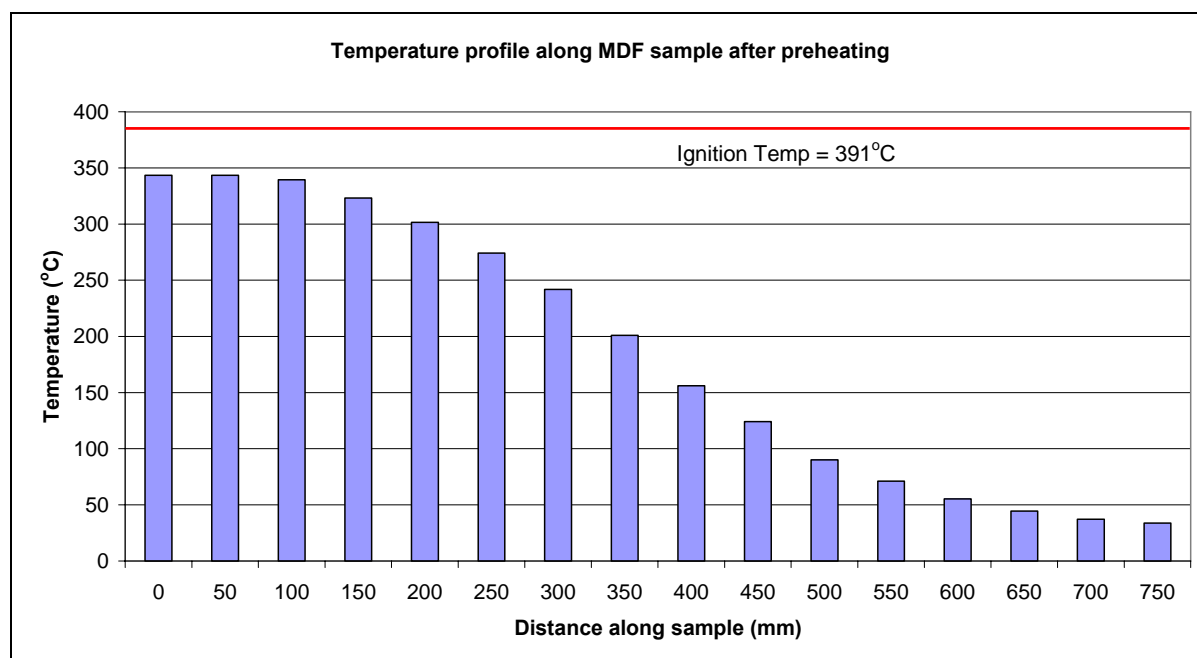
For Macrocarpa

Distance along sample (mm)	Heat flux (kW/m ²)	Temperature (°C)
0	-	339
50	24.2	339
100	23.7	326
150	22.0	311
200	19.8	280
250	17.3	242
300	14.4	189
350	11.2	150
400	8.1	121
450	6.0	91
500	3.9	73
550	2.8	56
600	1.9	43
650	1.3	40
700	0.9	36
750	0.7	33



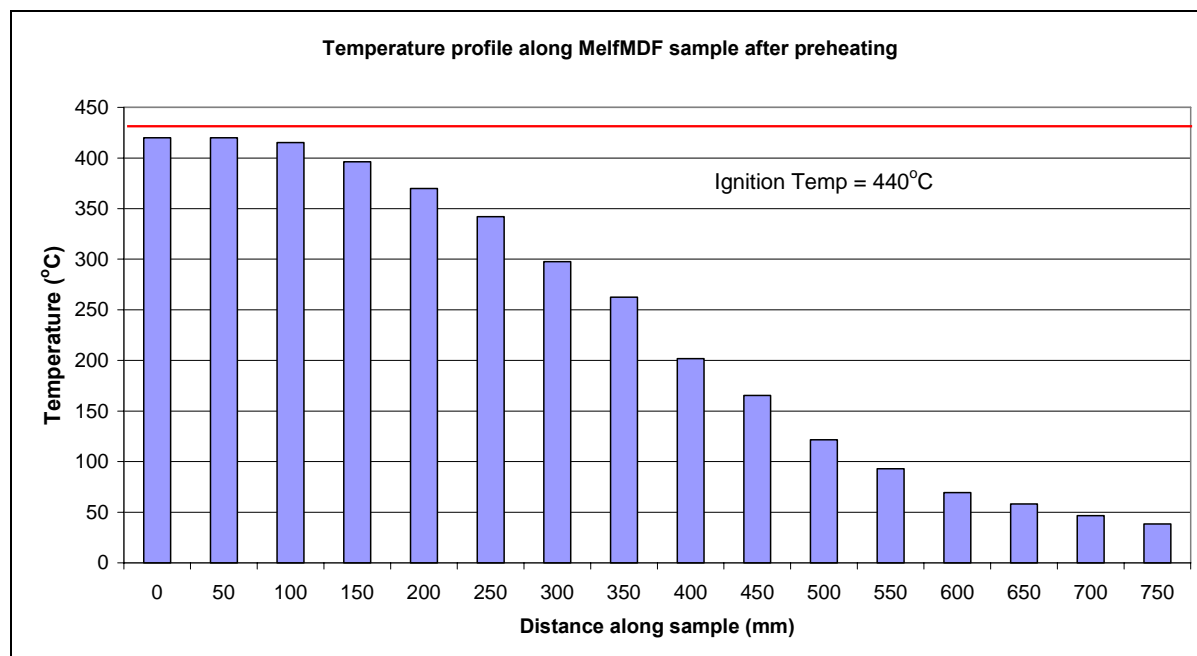
For MDF

Distance along sample (mm)	Heat flux (kW/m ²)	Temperature (°C)
0	-	344
50	24.2	344
100	23.7	339
150	22.0	323
200	19.8	302
250	17.3	274
300	14.4	242
350	11.2	201
400	8.1	156
450	6.0	124
500	3.9	90
550	2.8	71
600	1.9	55
650	1.3	45
700	0.9	37
750	0.7	34



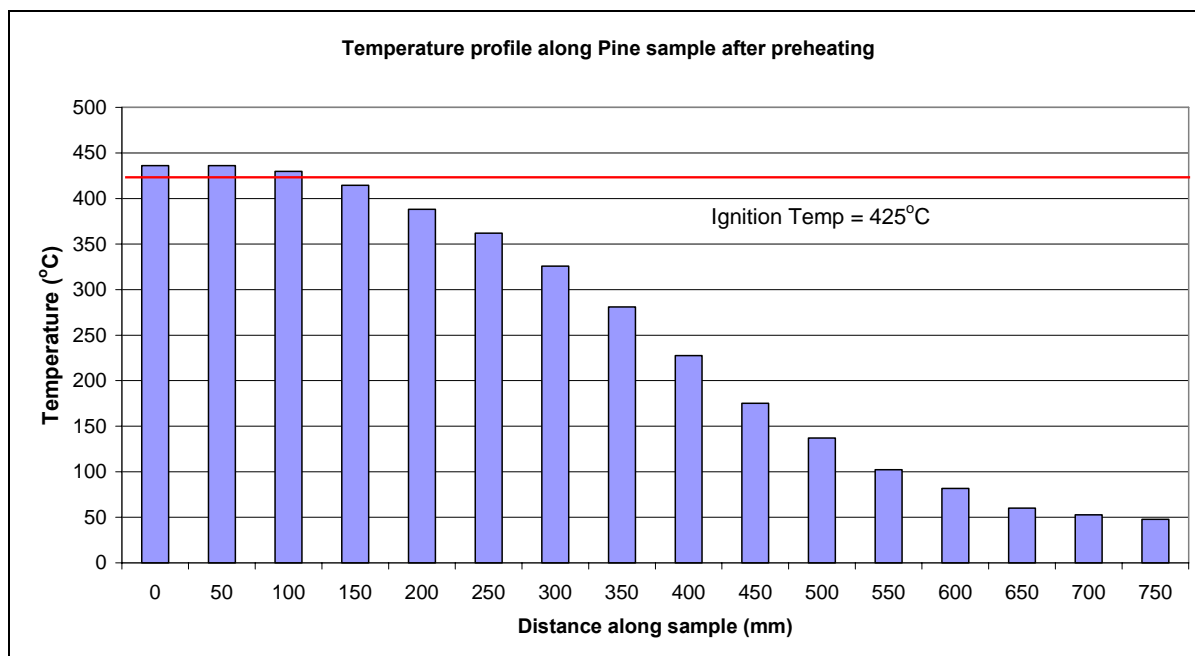
For MelfMDF

Distance along sample (mm)	Heat flux (kW/m ²)	Temperature (°C)
0	-	420
50	24.2	420
100	23.7	415
150	22.0	396
200	19.8	370
250	17.3	342
300	14.4	298
350	11.2	262
400	8.1	202
450	6.0	165
500	3.9	122
550	2.8	93
600	1.9	69
650	1.3	58
700	0.9	47
750	0.7	38



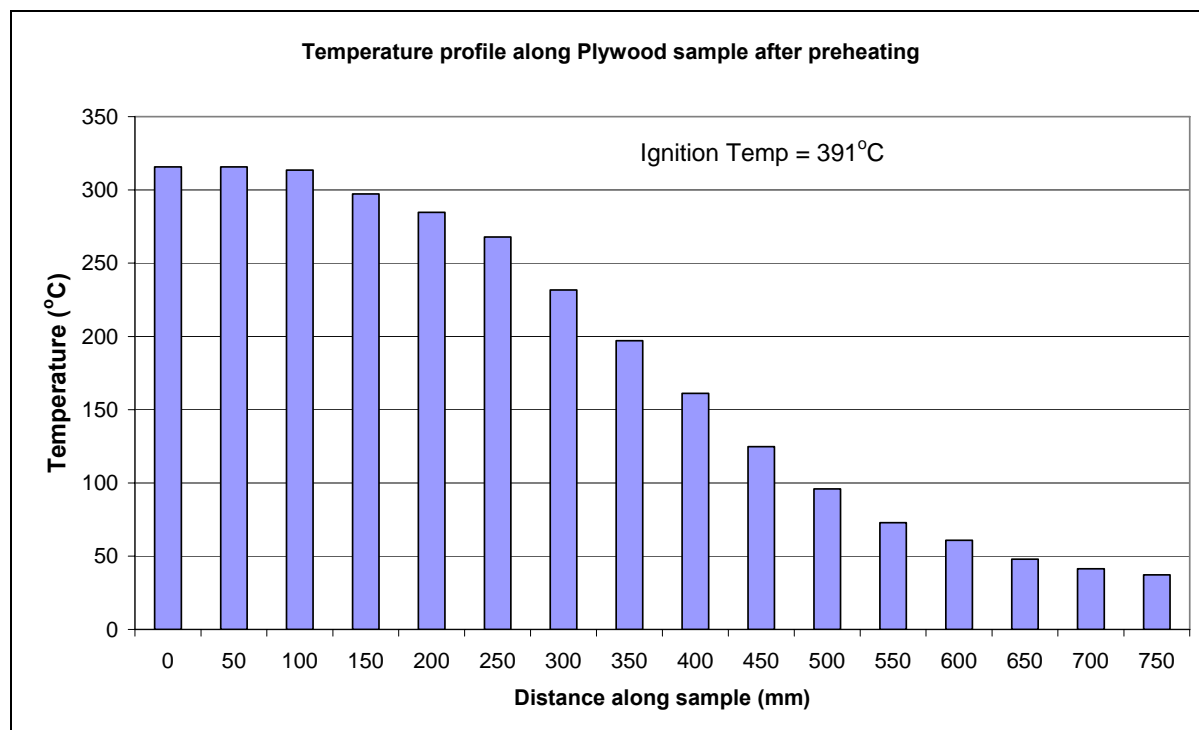
For Pine

Distance along sample (mm)	Heat flux (kW/m ²)	Temperature (°C)
0	-	436
50	24.2	436
100	23.7	430
150	22.0	414
200	19.8	388
250	17.3	362
300	14.4	326
350	11.2	281
400	8.1	228
450	6.0	175
500	3.9	137
550	2.8	102
600	1.9	82
650	1.3	60
700	0.9	53
750	0.7	48



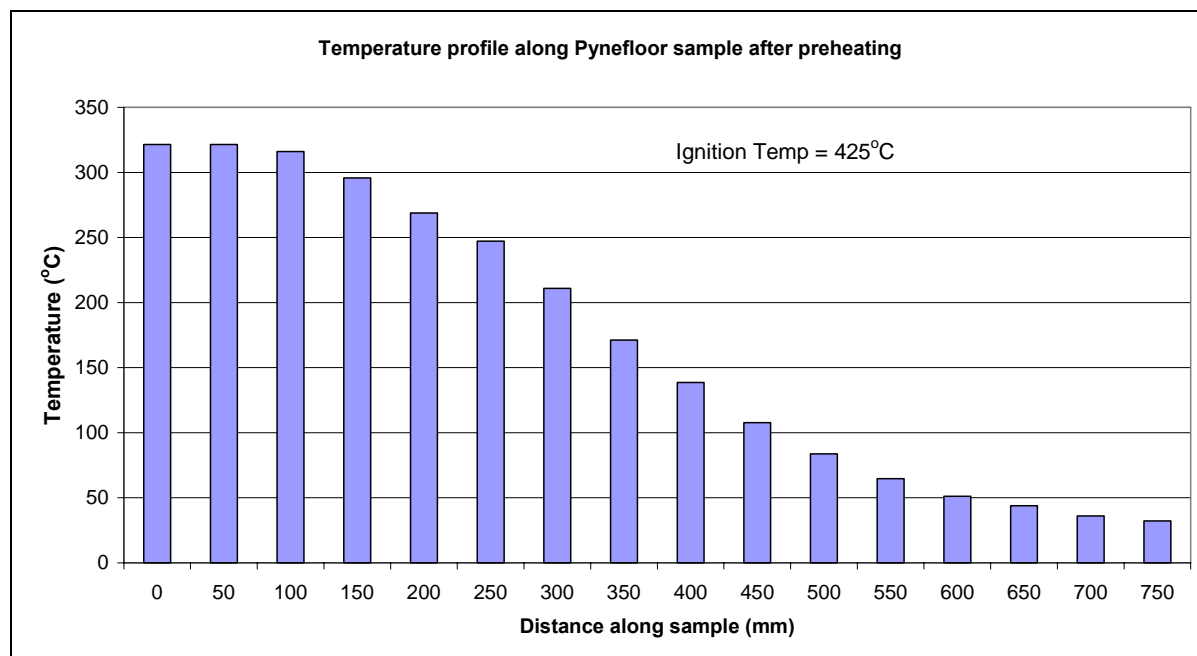
For Plywood

Distance along sample (mm)	Heat flux (kW/m ²)	Temperature (°C)
0	-	316
50	24.2	316
100	23.7	314
150	22.0	297
200	19.8	285
250	17.3	268
300	14.4	232
350	11.2	197
400	8.1	161
450	6.0	125
500	3.9	96
550	2.8	73
600	1.9	61
650	1.3	48
700	0.9	41
750	0.7	37



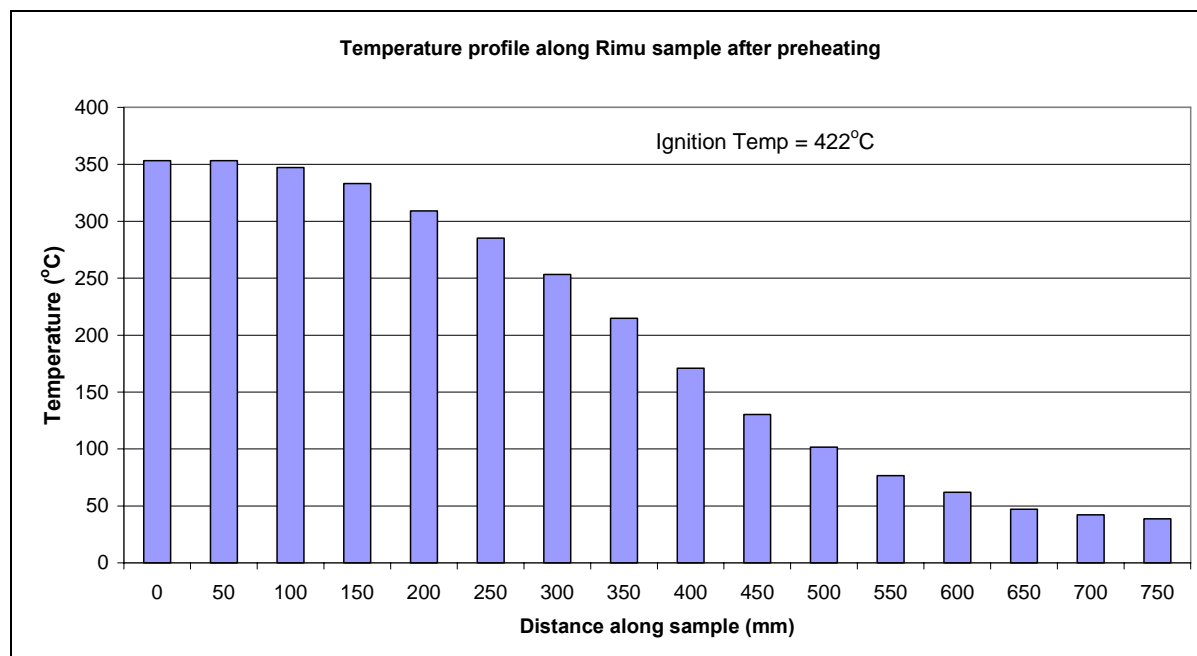
For Pynefloor

Distance along sample (mm)	Heat flux (kW/m ²)	Temperature (°C)
0	-	321
50	24.2	321
100	23.7	316
150	22.0	296
200	19.8	269
250	17.3	247
300	14.4	211
350	11.2	171
400	8.1	139
450	6.0	108
500	3.9	84
550	2.8	65
600	1.9	51
650	1.3	44
700	0.9	36
750	0.7	32



For Rimu

Distance along sample (mm)	Heat flux (kW/m ²)	Temperature (°C)
0	-	353
50	24.2	353
100	23.7	347
150	22.0	333
200	19.8	309
250	17.3	285
300	14.4	253
350	11.2	215
400	8.1	171
450	6.0	130
500	3.9	102
550	2.8	77
600	1.9	62
650	1.3	47
700	0.9	42
750	0.7	39



Appendix G – Flame spread test FDS4 input files

Thermoplastic Fuels Model for Beech with an absorption coefficient of 0.8

```
&HEAD CHID='Beech e0.8',TITLE='Beech e0.8' /
&GRID IBAR=95,JBAR=30,KBAR=30 / Specify number of grid cells in the x, y, and z
directions, respectively
&PDIM XBAR=0.95,YBAR=0.3,ZBAR=0.3 /
&TIME TWFIN=1000. / Time when finished (length of simulation)
```

```
&SURF ID = 'PANEL',TMPWAL=660,RGB = 1.0,0.0,0.0 /
```

```
&MISC SURF_DEFAULT='SPRUCE', REACTION='WOOD', NFRAMES=1000,
TMPA=25, TMPO=25, DTCORE=30./, RESTART=.TRUE./
```

```
*****
```

Properties

```
*****
```

```
&REAC ID='WOOD'
  FYI='Ritchie, et al., 5th IAFSS, C_3.4 H_6.2 O_2.5'
  SOOT_YIELD = 0.01
  NU_O2      = 3.7
  NU_CO2     = 3.4
  NU_H2O     = 3.1
  MW_FUEL    = 87.
  EPUMO2     = 11020. /
```

```
*****
```

```
&SURF ID          = 'SPRUCE'
  FYI              = 'Thermoplastic material'
  RGB              = 0.5,0.2,0.1
  PHASE            = 'CHAR'
  MOISTURE_FRACTION = 0.10
  DELTA            = 0.028
  TMPIGN           = 360.0
  HEAT_OF_VAPORIZATION = 500.
  DENSITY          = 450.
  RAMP_KS          = 'KS'
  RAMP_C_P         = 'CPV'
  RAMP_C_P_CHAR    = 'CPC'
  RAMP_KS_CHAR     = 'KSC'
  CHAR_DENSITY     = 120.
  WALL_POINTS      = 30
  BACKING          = 'EXPOSED' /
```

```

&RAMP ID = 'KS', T = 20., F = 0.13 /
&RAMP ID = 'KS', T = 500., F = 0.29 /
&RAMP ID = 'KSC', T = 20., F = 0.077 /
&RAMP ID = 'KSC', T = 900., F = 0.16 /
&RAMP ID = 'CPV', T = 20., F = 1.2 /
&RAMP ID = 'CPV', T = 500., F = 3.0 /
&RAMP ID = 'CPC', T = 20., F = 0.68 /
&RAMP ID = 'CPC', T = 400., F = 1.5 /
&RAMP ID = 'CPC', T = 900., F = 1.8 /

```

```
*****
```

```

&SURF ID      =      'Beech1'
  FYI         = 'Thermoplastic material'
  RGB         = 0.5,0.2,0.1
  MOISTURE_FRACTION = 0.10
  DELTA       = 0.023
  MASS_FLUX_CRITICAL = 0.075
  HEAT_OF_VAPORIZATION = 1400.
  TMPIGN      = 425
  TMPWAL0     = 411
  DENSITY     = 556.
  KS = 0.1927
  C_P = 1.303
  WALL_POINTS = 30
  BACKING     = 'INSULATED/'

```

```
*****
```

```

&SURF ID      =      'Beech2'
  FYI         = 'Thermoplastic material'
  RGB         = 0.5,0.2,0.1
  MOISTURE_FRACTION = 0.10
  DELTA       = 0.023
  MASS_FLUX_CRITICAL = 0.075
  HEAT_OF_VAPORIZATION = 1400.
  TMPIGN      = 425
  TMPWAL0     = 411
  DENSITY     = 556.
  KS = 0.1927
  C_P = 1.303
  WALL_POINTS = 30
  BACKING     = 'INSULATED/'

```

```
*****
```

```

&SURF ID      =      'Beech3'
  FYI         = 'Thermoplastic material'
  RGB         = 0.5,0.2,0.1
  MOISTURE_FRACTION = 0.10

```

```

DELTA          =      0.023
MASS_FLUX_CRITICAL =    0.075
HEAT_OF_VAPORIZATION = 1400.
TMPIGN        =      425
TMPWAL0       =      398
DENSITY       =      556.
KS            =    0.1927
C_P          =    1.303
WALL_POINTS   =      30
BACKING       =    'INSULATED'/
*****
&SURF ID      =          'Beech4'
FYI          = 'Thermoplastic material'
RGB          = 0.5,0.2,0.1
MOISTURE_FRACTION = 0.10
DELTA        =      0.023
MASS_FLUX_CRITICAL =    0.075
HEAT_OF_VAPORIZATION = 1400.
TMPIGN        =      425
TMPWAL0       =      381
DENSITY       =      556.
KS            =    0.1927
C_P          =    1.303
WALL_POINTS   =      30
BACKING       =    'INSULATED'/
*****
&SURF ID      =          'Beech5'
FYI          = 'Thermoplastic material'
RGB          = 0.5,0.2,0.1
MOISTURE_FRACTION = 0.10
DELTA        =      0.023
MASS_FLUX_CRITICAL =    0.075
HEAT_OF_VAPORIZATION = 1400.
TMPIGN        =      425
TMPWAL0       =      346
DENSITY       =      556.
KS            =    0.1927
C_P          =    1.303
WALL_POINTS   =      30
BACKING       =    'INSULATED'/
*****
&SURF ID      =          'Beech6'
FYI          = 'Thermoplastic material'
RGB          = 0.5,0.2,0.1
MOISTURE_FRACTION = 0.10
DELTA        =      0.023
MASS_FLUX_CRITICAL =    0.075
HEAT_OF_VAPORIZATION = 1400.

```

```

TMPIGN      = 425
TMPWAL0    = 303
DENSITY     = 556.
KS = 0.1927
C_P = 1.303
WALL_POINTS = 30
BACKING     = 'INSULATED'/
*****
&SURF ID    = 'Beech7'
FYI        = 'Thermoplastic material'
RGB        = 0.5,0.2,0.1
MOISTURE_FRACTION = 0.10
DELTA      = 0.023
MASS_FLUX_CRITICAL = 0.075
HEAT_OF_VAPORIZATION = 1400.
TMPIGN     = 425
TMPWAL0    = 240
DENSITY    = 556.
KS = 0.1927
C_P = 1.303
WALL_POINTS = 30
BACKING    = 'INSULATED'/
*****
&SURF ID    = 'Beech8'
FYI        = 'Thermoplastic material'
RGB        = 0.5,0.2,0.1
MOISTURE_FRACTION = 0.10
DELTA      = 0.023
MASS_FLUX_CRITICAL = 0.075
HEAT_OF_VAPORIZATION = 1400.
TMPIGN     = 425
TMPWAL0    = 193
DENSITY    = 556.
KS = 0.1927
C_P = 1.303
WALL_POINTS = 30
BACKING    = 'INSULATED'/
*****
&SURF ID    = 'Beech9'
FYI        = 'Thermoplastic material'
RGB        = 0.5,0.2,0.1
MOISTURE_FRACTION = 0.10
DELTA      = 0.023
MASS_FLUX_CRITICAL = 0.075
HEAT_OF_VAPORIZATION = 1400.
TMPIGN     = 425
TMPWAL0    = 155
DENSITY    = 556.

```

```

KS = 0.1927
C_P = 1.303
WALL_POINTS = 30
BACKING = 'INSULATED'/
*****
&SURF ID = 'Beech10'
FYI = 'Thermoplastic material'
RGB = 0.5,0.2,0.1
MOISTURE_FRACTION = 0.10
DELTA = 0.023
MASS_FLUX_CRITICAL = 0.075
HEAT_OF_VAPORIZATION = 1400.
TMPIGN = 425
TMPWAL0 = 116
DENSITY = 556.
KS = 0.1927
C_P = 1.303
WALL_POINTS = 30
BACKING = 'INSULATED'/
*****
&SURF ID = 'Beech11'
FYI = 'Thermoplastic material'
RGB = 0.5,0.2,0.1
MOISTURE_FRACTION = 0.10
DELTA = 0.023
MASS_FLUX_CRITICAL = 0.075
HEAT_OF_VAPORIZATION = 1400.
TMPIGN = 425
TMPWAL0 = 92
DENSITY = 556.
KS = 0.1927
C_P = 1.303
WALL_POINTS = 30
BACKING = 'INSULATED'/
*****
&SURF ID = 'Beech12'
FYI = 'Thermoplastic material'
RGB = 0.5,0.2,0.1
MOISTURE_FRACTION = 0.10
DELTA = 0.023
MASS_FLUX_CRITICAL = 0.075
HEAT_OF_VAPORIZATION = 1400.
TMPIGN = 425
TMPWAL0 = 69
DENSITY = 556.
KS = 0.1927
C_P = 1.303
WALL_POINTS = 30

```

```
BACKING      = 'INSULATED'/
*****
&SURF ID     = 'Beech13'
FYI          = 'Thermoplastic material'
RGB          = 0.5,0.2,0.1
MOISTURE_FRACTION = 0.10
DELTA        = 0.023
MASS_FLUX_CRITICAL = 0.075
HEAT_OF_VAPORIZATION = 1400.
TMPIGN       = 425
TMPWAL0      = 52
DENSITY      = 556.
KS           = 0.1927
C_P          = 1.303
WALL_POINTS  = 30
BACKING      = 'INSULATED'/
*****
&SURF ID     = 'Beech14'
FYI          = 'Thermoplastic material'
RGB          = 0.5,0.2,0.1
MOISTURE_FRACTION = 0.10
DELTA        = 0.023
MASS_FLUX_CRITICAL = 0.075
HEAT_OF_VAPORIZATION = 1400.
TMPIGN       = 425
TMPWAL0      = 47
DENSITY      = 556.
KS           = 0.1927
C_P          = 1.303
WALL_POINTS  = 30
BACKING      = 'INSULATED'/
*****
&SURF ID     = 'Beech15'
FYI          = 'Thermoplastic material'
RGB          = 0.5,0.2,0.1
MOISTURE_FRACTION = 0.10
DELTA        = 0.023
MASS_FLUX_CRITICAL = 0.075
HEAT_OF_VAPORIZATION = 1400.
TMPIGN       = 425
TMPWAL0      = 42
DENSITY      = 556.
KS           = 0.1927
C_P          = 1.303
WALL_POINTS  = 30
BACKING      = 'INSULATED'/
*****
&SURF ID     = 'Beech16'
```

```

FYI          = 'Thermoplastic material'
RGB          = 0.5,0.2,0.1
MOISTURE_FRACTION = 0.10
DELTA       = 0.023
MASS_FLUX_CRITICAL = 0.075
HEAT_OF_VAPORIZATION = 1400.
TMPIGN      = 425
TMPWAL0     = 37
DENSITY     = 556.
KS          = 0.1927
C_P        = 1.303
WALL_POINTS = 30
BACKING     = 'INSULATED'/
*****
&SURF ID    = 'DUMMY'
FYI        = 'Calcium Silicate'
RGB        = 0.66,0.66,0.66
C_P        = 0.7329
DENSITY    = 1055.
KS         = 0.3137
DELTA     = 0.15/
*****
*****
*****
*****
BACKING BOARD (Calcium Silicate)
*****

&OBST XB = 0.125,0.925,0.27,0.29,0.0625,0.2175 , SURF_ID='DUMMY' /

*****
Special calibration board
*****

&OBST XB = 0.125,0.925,0.25,0.27,0.0625,0.2175 , SURF_ID='DUMMY',
T_REMOVE=25./

*****
Beech specimen
*****
&OBST XB=0.125,0.15,0.25,0.27,0.0625,0.2175, SURF_ID='Beech1', T_CREATE=25.,
COLOR='RED' /
&OBST XB=0.15,0.2,0.25,0.27,0.0625,0.2175, SURF_ID='Beech2', T_CREATE=25.,
COLOR='GREEN' /

```

```

&OBST XB=0.2,0.25,0.25,0.27,0.0625,0.2175, SURF_ID='Beech3', T_CREATE=25.,
COLOR='BLUE' /
&OBST XB=0.25,0.3,0.25,0.27,0.0625,0.2175, SURF_ID='Beech4', T_CREATE=25.,
COLOR='WHITE' /
&OBST XB=0.3,0.35,0.25,0.27,0.0625,0.2175, SURF_ID='Beech5', T_CREATE=25.,
COLOR='BLACK' /
&OBST XB=0.35,0.4,0.25,0.27,0.0625,0.2175, SURF_ID='Beech6', T_CREATE=25.,
COLOR='GRAY' /
&OBST XB=0.4,0.45,0.25,0.27,0.0625,0.2175, SURF_ID='Beech7', T_CREATE=25.,
COLOR='MAGENTA' /
&OBST XB=0.45,0.5,0.25,0.27,0.0625,0.2175, SURF_ID='Beech8', T_CREATE=25.,
COLOR='YELLOW' /
&OBST XB=0.5,0.55,0.25,0.27,0.0625,0.2175, SURF_ID='Beech9', T_CREATE=25.,
COLOR='CYAN' /
&OBST XB=0.55,0.6,0.25,0.27,0.0625,0.2175, SURF_ID='Beech10', T_CREATE=25.,
COLOR='TAN' /
&OBST XB=0.6,0.65,0.25,0.27,0.0625,0.2175, SURF_ID='Beech11', T_CREATE=25.,
COLOR='RED' /
&OBST XB=0.65,0.7,0.25,0.27,0.0625,0.2175, SURF_ID='Beech12', T_CREATE=25.,
COLOR='GREEN' /
&OBST XB=0.7,0.75,0.25,0.27,0.0625,0.2175, SURF_ID='Beech13', T_CREATE=25.,
COLOR='BLUE' /
&OBST XB=0.75,0.8,0.25,0.27,0.0625,0.2175, SURF_ID='Beech14', T_CREATE=25.,
COLOR='WHITE' /
&OBST XB=0.8,0.85,0.25,0.27,0.0625,0.2175, SURF_ID='Beech15', T_CREATE=25.,
COLOR='BLACK' /
&OBST XB=0.85,0.925,0.25,0.27,0.0625,0.2175, SURF_ID='Beech16', T_CREATE=25.,
COLOR='GRAY' /

```

```
*****
```

```
Radiant Panel
```

```
*****
```

```
&OBST
```

```
XB=0,0.04,0.13,0.14,0,0.28,SURF_ID6='INERT','PANEL','INERT','PANEL','INERT','INERT',BNDF_BLOCK =FALSE /
```

```
&OBST
```

```
XB=0.04,0.08,0.12,0.13,0,0.28,SURF_ID6='INERT','PANEL','INERT','PANEL','INERT','INERT',BNDF_BLOCK =FALSE /
```

```
&OBST
```

```
XB=0.08,0.12,0.11,0.12,0,0.28,SURF_ID6='INERT','PANEL','INERT','PANEL','INERT','INERT',BNDF_BLOCK =FALSE /
```

```
&OBST
```

```
XB=0.12,0.15,0.1,0.11,0,0.28,SURF_ID6='INERT','PANEL','INERT','PANEL','INERT','INERT',BNDF_BLOCK =FALSE /
```

```
&OBST
```

```
XB=0.15,0.19,0.09,0.1,0,0.28,SURF_ID6='INERT','PANEL','INERT','PANEL','INERT','INERT',BNDF_BLOCK =FALSE /
```

```

&OBST
XB=0.19,0.23,0.08,0.09,0,0.28,SURF_ID6='INERT','PANEL','INERT','PANEL','INERT','IN
ERT',BNDF_BLOCK =FALSE /
&OBST
XB=0.23,0.27,0.07,0.08,0,0.28,SURF_ID6='INERT','PANEL','INERT','PANEL','INERT','IN
ERT',BNDF_BLOCK =FALSE /
&OBST
XB=0.27,0.3,0.06,0.07,0,0.28,SURF_ID6='INERT','PANEL','INERT','PANEL','INERT','IN
ERT',BNDF_BLOCK =FALSE /
&OBST
XB=0.3,0.34,0.05,0.06,0,0.28,SURF_ID6='INERT','PANEL','INERT','PANEL','INERT','IN
ERT',BNDF_BLOCK =FALSE /
&OBST
XB=0.34,0.38,0.04,0.05,0,0.28,SURF_ID6='INERT','PANEL','INERT','PANEL','INERT','IN
ERT',BNDF_BLOCK =FALSE /
&OBST
XB=0.38,0.42,0.03,0.04,0,0.28,SURF_ID6='INERT','PANEL','INERT','PANEL','INERT','IN
ERT',BNDF_BLOCK =FALSE /
&OBST
XB=0.42,0.45,0.02,0.03,0,0.28,SURF_ID6='INERT','PANEL','INERT','PANEL','INERT','IN
ERT',BNDF_BLOCK =FALSE /
&OBST
XB=0.45,0.49,0.01,0.02,0,0.28,SURF_ID6='INERT','INERT','INERT','PANEL','INERT','IN
ERT',BNDF_BLOCK =FALSE /

```

```

*****
*****

```

```

*****

```

Vents

```

*****

```

```

&VENT CB='XBAR0',SURF_ID='OPEN' /
&VENT CB='XBAR' ,SURF_ID='OPEN' /
&VENT CB='YBAR0',SURF_ID='OPEN' /
&VENT CB='YBAR' ,SURF_ID='OPEN' /
&VENT CB='ZBAR0' ,SURF_ID='OPEN' /
&VENT CB='ZBAR' ,SURF_ID='OPEN' /

```

```

*****
*****

```

Output files

```

*****
*****

```

```

&THCP XYZ=0.13,0.25,0.14,QUANTITY='GAUGE_HEAT_FLUX', IOR=-2, LABEL=
'0mm away'/

```

```
&THCP XYZ=0.175,0.25,0.14,QUANTITY='GAUGE_HEAT_FLUX', IOR=-2, LABEL='50mm away'/
&THCP XYZ=0.225,0.25,0.14,QUANTITY='GAUGE_HEAT_FLUX', IOR=-2, LABEL='100mm away'/
&THCP XYZ=0.275,0.25,0.14,QUANTITY='GAUGE_HEAT_FLUX', IOR=-2, LABEL='150mm away'/
&THCP XYZ=0.325,0.25,0.14,QUANTITY='GAUGE_HEAT_FLUX', IOR=-2, LABEL='200mm away'/
&THCP XYZ=0.375,0.25,0.14,QUANTITY='GAUGE_HEAT_FLUX', IOR=-2, LABEL='250mm away'/
&THCP XYZ=0.425,0.25,0.14,QUANTITY='GAUGE_HEAT_FLUX', IOR=-2, LABEL='300mm away'/
&THCP XYZ=0.475,0.25,0.14,QUANTITY='GAUGE_HEAT_FLUX', IOR=-2, LABEL='350mm away'/
&THCP XYZ=0.525,0.25,0.14,QUANTITY='GAUGE_HEAT_FLUX', IOR=-2, LABEL='400mm away'/
&THCP XYZ=0.575,0.25,0.14,QUANTITY='GAUGE_HEAT_FLUX', IOR=-2, LABEL='450mm away'/
&THCP XYZ=0.625,0.25,0.14,QUANTITY='GAUGE_HEAT_FLUX', IOR=-2, LABEL='500mm away'/
&THCP XYZ=0.675,0.25,0.14,QUANTITY='GAUGE_HEAT_FLUX', IOR=-2, LABEL='550mm away'/
&THCP XYZ=0.725,0.25,0.14,QUANTITY='GAUGE_HEAT_FLUX', IOR=-2, LABEL='600mm away'/
&THCP XYZ=0.775,0.25,0.14,QUANTITY='GAUGE_HEAT_FLUX', IOR=-2, LABEL='650mm away'/
&THCP XYZ=0.825,0.25,0.14,QUANTITY='GAUGE_HEAT_FLUX', IOR=-2, LABEL='700mm away'/
&THCP XYZ=0.875,0.25,0.14,QUANTITY='GAUGE_HEAT_FLUX', IOR=-2, LABEL='750mm away'/
```

```
&ISOF QUANTITY = 'MIXTURE_FRACTION', VALUE(1)=0.148/
&PL3D DTSAM=10000000./ Do not produce any Plot3D files
```

Charring Fuels Model for Beech with a absorption coefficient of 0.8

```
&HEAD CHID='Char beech delay e0.8',TITLE='Char beech delay e0.8' /
&GRID IBAR=95,JBAR=30,KBAR=30 / Specify number of grid cells in the x, y, and z
directions, respectively
&PDIM XBAR=0.95,YBAR=0.3,ZBAR=0.3 /
&TIME TWFIN=1000. / Time when finished (length of simulation)

&SURF ID = 'PANEL',TMPWAL=660,RGB = 1.0,0.0,0.0 /

&MISC SURF_DEFAULT='SPRUCE', REACTION='WOOD', NFRAMES=1000,
TMPA=25,TMPO=25,DTCORE=30./, RESTART=.TRUE./
```

```
*****
```

Properties

```
*****
```

```
&REAC ID='WOOD'
  FYI='Ritchie, et al., 5th IAFSS, C_3.4 H_6.2 O_2.5'
  SOOT_YIELD = 0.01
  NU_O2      = 3.7
  NU_CO2     = 3.4
  NU_H2O     = 3.1
  MW_FUEL    = 87.
  EPUMO2     = 11020. /
```

```
*****
```

```
&SURF ID          = 'SPRUCE'
  FYI              = 'Charring material'
  RGB              = 0.5,0.2,0.1
  PHASE            = 'CHAR'
  MOISTURE_FRACTION = 0.10
  DELTA            = 0.028
  TMPIGN           = 360.0
  HEAT_OF_VAPORIZATION = 500.
  DENSITY          = 450.
  RAMP_KS          = 'KS'
  RAMP_C_P         = 'CPV'
  RAMP_C_P_CHAR    = 'CPC'
  RAMP_KS_CHAR     = 'KSC'
  CHAR_DENSITY     = 120.
  WALL_POINTS      = 30
  BACKING          = 'EXPOSED' /
&RAMP ID = 'KS', T = 20., F = 0.13 /
&RAMP ID = 'KS', T = 500., F = 0.29 /
&RAMP ID = 'KSC', T = 20., F = 0.077 /
&RAMP ID = 'KSC', T = 900., F = 0.16 /
```

```
&RAMP ID = 'CPV', T = 20., F = 1.2 /
&RAMP ID = 'CPV', T = 500., F = 3.0 /
&RAMP ID = 'CPC', T = 20., F = 0.68 /
&RAMP ID = 'CPC', T = 400., F = 1.5 /
&RAMP ID = 'CPC', T = 900., F = 1.8 /
```

```
*****
```

```
&SURF ID          =          'Beech1'
  FYI              =  'Charring material'
  RGB              =  0.5,0.2,0.1
  PHASE            =  'CHAR'
  MOISTURE_FRACTION =  0.10
  DELTA            =  0.023
  TMPIGN           =  425
  HEAT_OF_VAPORIZATION = 500.
  DENSITY          =  556.
  TMPWAL0         =  411
  RAMP_KS          =  'KS'
  RAMP_C_P         =  'CPV'
  RAMP_C_P_CHAR    =  'CPC'
  RAMP_KS_CHAR     =  'KSC'
  CHAR_DENSITY     = 299
  WALL_POINTS      =  30
  BACKING          =  'INSULATED'/
&RAMP ID = 'KS', T = 20., F = 0.193 /
&RAMP ID = 'KS', T = 500., F = 0.193 /
&RAMP ID = 'KSC', T = 20., F = 0.099 /
&RAMP ID = 'KSC', T = 900., F = 0.099 /
&RAMP ID = 'CPV', T = 20., F = 1.303 /
&RAMP ID = 'CPV', T = 500., F = 1.303 /
&RAMP ID = 'CPC', T = 20., F = 0.741 /
&RAMP ID = 'CPC', T = 400., F = 0.741 /
&RAMP ID = 'CPC', T = 900., F = 0.741 /
```

```
*****
```

```
&SURF ID          =          'Beech2'
  FYI              =  'Charring material'
  RGB              =  0.5,0.2,0.1
  PHASE            =  'CHAR'
  MOISTURE_FRACTION =  0.10
  DELTA            =  0.023
  TMPIGN           =  425
  HEAT_OF_VAPORIZATION = 500.
  DENSITY          =  556.
  TMPWAL0         =  411
  RAMP_KS          =  'KS'
  RAMP_C_P         =  'CPV'
  RAMP_C_P_CHAR    =  'CPC'
```

```

RAMP_KS_CHAR      = 'KSC'
CHAR_DENSITY      = 299
WALL_POINTS       = 30
BACKING           = 'INSULATED'/
&RAMP ID = 'KS', T = 20., F = 0.193 /
&RAMP ID = 'KS', T = 500., F = 0.193 /
&RAMP ID = 'KSC', T = 20., F = 0.099 /
&RAMP ID = 'KSC', T = 900., F = 0.099 /
&RAMP ID = 'CPV', T = 20., F = 1.303 /
&RAMP ID = 'CPV', T = 500., F = 1.303 /
&RAMP ID = 'CPC', T = 20., F = 0.741 /
&RAMP ID = 'CPC', T = 400., F = 0.741 /
&RAMP ID = 'CPC', T = 900., F = 0.741 /
*****
&SURF ID          =          'Beech3'
FYI               = 'Charring material'
RGB               = 0.5,0.2,0.1
PHASE             = 'CHAR'
MOISTURE_FRACTION = 0.10
DELTA             = 0.023
TMPIGN           = 425
HEAT_OF_VAPORIZATION = 500.
DENSITY          = 556.
TMPWAL0         = 398
RAMP_KS          = 'KS'
RAMP_C_P         = 'CPV'
RAMP_C_P_CHAR    = 'CPC'
RAMP_KS_CHAR     = 'KSC'
CHAR_DENSITY     = 299
WALL_POINTS      = 30
BACKING          = 'INSULATED'/
&RAMP ID = 'KS', T = 20., F = 0.193 /
&RAMP ID = 'KS', T = 500., F = 0.193 /
&RAMP ID = 'KSC', T = 20., F = 0.099 /
&RAMP ID = 'KSC', T = 900., F = 0.099 /
&RAMP ID = 'CPV', T = 20., F = 1.303 /
&RAMP ID = 'CPV', T = 500., F = 1.303 /
&RAMP ID = 'CPC', T = 20., F = 0.741 /
&RAMP ID = 'CPC', T = 400., F = 0.741 /
&RAMP ID = 'CPC', T = 900., F = 0.741 /
*****
&SURF ID          =          'Beech4'
FYI               = 'Charring material'
RGB               = 0.5,0.2,0.1
PHASE             = 'CHAR'
MOISTURE_FRACTION = 0.10
DELTA             = 0.023
TMPIGN           = 425

```

```

HEAT_OF_VAPORIZATION = 500.
DENSITY      = 556.
TMPWAL0     = 381
RAMP_KS      = 'KS'
RAMP_C_P     = 'CPV'
RAMP_C_P_CHAR = 'CPC'
RAMP_KS_CHAR = 'KSC'
CHAR_DENSITY = 299
WALL_POINTS  = 30
BACKING      = 'INSULATED'/
&RAMP ID = 'KS', T = 20., F = 0.193 /
&RAMP ID = 'KS', T = 500., F = 0.193 /
&RAMP ID = 'KSC', T = 20., F = 0.099 /
&RAMP ID = 'KSC', T = 900., F = 0.099 /
&RAMP ID = 'CPV', T = 20., F = 1.303 /
&RAMP ID = 'CPV', T = 500., F = 1.303 /
&RAMP ID = 'CPC', T = 20., F = 0.741 /
&RAMP ID = 'CPC', T = 400., F = 0.741 /
&RAMP ID = 'CPC', T = 900., F = 0.741 /
*****
&SURF ID      = 'Beech5'
FYI           = 'Charring material'
RGB           = 0.5,0.2,0.1
PHASE        = 'CHAR'
MOISTURE_FRACTION = 0.10
DELTA        = 0.023
TMPIGN       = 425
HEAT_OF_VAPORIZATION = 500.
DENSITY      = 556.
TMPWAL0     = 346
RAMP_KS      = 'KS'
RAMP_C_P     = 'CPV'
RAMP_C_P_CHAR = 'CPC'
RAMP_KS_CHAR = 'KSC'
CHAR_DENSITY = 299
WALL_POINTS  = 30
BACKING      = 'INSULATED'/
&RAMP ID = 'KS', T = 20., F = 0.193 /
&RAMP ID = 'KS', T = 500., F = 0.193 /
&RAMP ID = 'KSC', T = 20., F = 0.099 /
&RAMP ID = 'KSC', T = 900., F = 0.099 /
&RAMP ID = 'CPV', T = 20., F = 1.303 /
&RAMP ID = 'CPV', T = 500., F = 1.303 /
&RAMP ID = 'CPC', T = 20., F = 0.741 /
&RAMP ID = 'CPC', T = 400., F = 0.741 /
&RAMP ID = 'CPC', T = 900., F = 0.741 /
*****
&SURF ID      = 'Beech6'

```

```

FYI          = 'Charring material'
RGB          = 0.5,0.2,0.1
PHASE       = 'CHAR'
MOISTURE_FRACTION = 0.10
DELTA       = 0.023
TMPIGN      = 425
HEAT_OF_VAPORIZATION = 500.
DENSITY     = 556.
TMPWAL0    = 303
RAMP_KS     = 'KS'
RAMP_C_P    = 'CPV'
RAMP_C_P_CHAR = 'CPC'
RAMP_KS_CHAR = 'KSC'
CHAR_DENSITY = 299
WALL_POINTS = 30
BACKING     = 'INSULATED'/
&RAMP ID = 'KS', T = 20., F = 0.193 /
&RAMP ID = 'KS', T = 500., F = 0.193 /
&RAMP ID = 'KSC', T = 20., F = 0.099 /
&RAMP ID = 'KSC', T = 900., F = 0.099 /
&RAMP ID = 'CPV', T = 20., F = 1.303 /
&RAMP ID = 'CPV', T = 500., F = 1.303 /
&RAMP ID = 'CPC', T = 20., F = 0.741 /
&RAMP ID = 'CPC', T = 400., F = 0.741 /
&RAMP ID = 'CPC', T = 900., F = 0.741 /
*****
&SURF ID    = 'Beech7'
FYI         = 'Charring material'
RGB         = 0.5,0.2,0.1
PHASE      = 'CHAR'
MOISTURE_FRACTION = 0.10
DELTA      = 0.023
TMPIGN     = 425
HEAT_OF_VAPORIZATION = 500.
DENSITY    = 556.
TMPWAL0   = 240
RAMP_KS    = 'KS'
RAMP_C_P   = 'CPV'
RAMP_C_P_CHAR = 'CPC'
RAMP_KS_CHAR = 'KSC'
CHAR_DENSITY = 299
WALL_POINTS = 30
BACKING    = 'INSULATED'/
&RAMP ID = 'KS', T = 20., F = 0.193 /
&RAMP ID = 'KS', T = 500., F = 0.193 /
&RAMP ID = 'KSC', T = 20., F = 0.099 /
&RAMP ID = 'KSC', T = 900., F = 0.099 /
&RAMP ID = 'CPV', T = 20., F = 1.303 /

```

```

&RAMP ID = 'CPV', T = 500., F = 1.303 /
&RAMP ID = 'CPC', T = 20., F = 0.741 /
&RAMP ID = 'CPC', T = 400., F = 0.741 /
&RAMP ID = 'CPC', T = 900., F = 0.741 /
*****
&SURF ID          =          'Beech8'
  FYI              =  'Charring material'
  RGB              =  0.5,0.2,0.1
  PHASE            =  'CHAR'
  MOISTURE_FRACTION =  0.10
  DELTA            =  0.023
  TMPIGN           =  425
  HEAT_OF_VAPORIZATION = 500.
  DENSITY          =  556.
  TMPWAL0         =  193
  RAMP_KS          =  'KS'
  RAMP_C_P         =  'CPV'
  RAMP_C_P_CHAR    =  'CPC'
  RAMP_KS_CHAR     =  'KSC'
  CHAR_DENSITY     =  299
  WALL_POINTS      =  30
  BACKING          =  'INSULATED'
&RAMP ID = 'KS', T = 20., F = 0.193 /
&RAMP ID = 'KS', T = 500., F = 0.193 /
&RAMP ID = 'KSC', T = 20., F = 0.099 /
&RAMP ID = 'KSC', T = 900., F = 0.099 /
&RAMP ID = 'CPV', T = 20., F = 1.303 /
&RAMP ID = 'CPV', T = 500., F = 1.303 /
&RAMP ID = 'CPC', T = 20., F = 0.741 /
&RAMP ID = 'CPC', T = 400., F = 0.741 /
&RAMP ID = 'CPC', T = 900., F = 0.741 /
*****
&SURF ID          =          'Beech9'
  FYI              =  'Charring material'
  RGB              =  0.5,0.2,0.1
  PHASE            =  'CHAR'
  MOISTURE_FRACTION =  0.10
  DELTA            =  0.023
  TMPIGN           =  425
  HEAT_OF_VAPORIZATION = 500.
  DENSITY          =  556.
  TMPWAL0         =  155
  RAMP_KS          =  'KS'
  RAMP_C_P         =  'CPV'
  RAMP_C_P_CHAR    =  'CPC'
  RAMP_KS_CHAR     =  'KSC'
  CHAR_DENSITY     =  299
  WALL_POINTS      =  30

```

```

BACKING          = 'INSULATED'/
&RAMP ID = 'KS', T = 20., F = 0.193 /
&RAMP ID = 'KS', T = 500., F = 0.193 /
&RAMP ID = 'KSC', T = 20., F = 0.099 /
&RAMP ID = 'KSC', T = 900., F = 0.099 /
&RAMP ID = 'CPV', T = 20., F = 1.303 /
&RAMP ID = 'CPV', T = 500., F = 1.303 /
&RAMP ID = 'CPC', T = 20., F = 0.741 /
&RAMP ID = 'CPC', T = 400., F = 0.741 /
&RAMP ID = 'CPC', T = 900., F = 0.741 /
*****
&SURF ID        = 'Beech10'
FYI             = 'Charring material'
RGB             = 0.5,0.2,0.1
PHASE          = 'CHAR'
MOISTURE_FRACTION = 0.10
DELTA          = 0.023
TMPIGN        = 425
HEAT_OF_VAPORIZATION = 500.
DENSITY       = 556.
TMPWAL0      = 116
RAMP_KS      = 'KS'
RAMP_C_P     = 'CPV'
RAMP_C_P_CHAR = 'CPC'
RAMP_KS_CHAR = 'KSC'
CHAR_DENSITY = 299
WALL_POINTS  = 30
BACKING      = 'INSULATED'/
&RAMP ID = 'KS', T = 20., F = 0.193 /
&RAMP ID = 'KS', T = 500., F = 0.193 /
&RAMP ID = 'KSC', T = 20., F = 0.099 /
&RAMP ID = 'KSC', T = 900., F = 0.099 /
&RAMP ID = 'CPV', T = 20., F = 1.303 /
&RAMP ID = 'CPV', T = 500., F = 1.303 /
&RAMP ID = 'CPC', T = 20., F = 0.741 /
&RAMP ID = 'CPC', T = 400., F = 0.741 /
&RAMP ID = 'CPC', T = 900., F = 0.741 /
*****
&SURF ID        = 'Beech11'
FYI             = 'Charring material'
RGB             = 0.5,0.2,0.1
PHASE          = 'CHAR'
MOISTURE_FRACTION = 0.10
DELTA          = 0.023
TMPIGN        = 425
HEAT_OF_VAPORIZATION = 500.
DENSITY       = 556.
TMPWAL0      = 92

```

```

RAMP_KS      = 'KS'
RAMP_C_P     = 'CPV'
RAMP_C_P_CHAR = 'CPC'
RAMP_KS_CHAR = 'KSC'
CHAR_DENSITY = 299
WALL_POINTS  = 30
BACKING      = 'INSULATED'/
&RAMP ID = 'KS', T = 20., F = 0.193 /
&RAMP ID = 'KS', T = 500., F = 0.193 /
&RAMP ID = 'KSC', T = 20., F = 0.099 /
&RAMP ID = 'KSC', T = 900., F = 0.099 /
&RAMP ID = 'CPV', T = 20., F = 1.303 /
&RAMP ID = 'CPV', T = 500., F = 1.303 /
&RAMP ID = 'CPC', T = 20., F = 0.741 /
&RAMP ID = 'CPC', T = 400., F = 0.741 /
&RAMP ID = 'CPC', T = 900., F = 0.741 /
*****
&SURF ID      = 'Beech12'
FYI           = 'Charring material'
RGB           = 0.5,0.2,0.1
PHASE         = 'CHAR'
MOISTURE_FRACTION = 0.10
DELTA         = 0.023
TMPIGN        = 425
HEAT_OF_VAPORIZATION = 500.
DENSITY       = 556.
TMPWAL0       = 69
RAMP_KS       = 'KS'
RAMP_C_P      = 'CPV'
RAMP_C_P_CHAR = 'CPC'
RAMP_KS_CHAR  = 'KSC'
CHAR_DENSITY  = 299
WALL_POINTS   = 30
BACKING       = 'INSULATED'/
&RAMP ID = 'KS', T = 20., F = 0.193 /
&RAMP ID = 'KS', T = 500., F = 0.193 /
&RAMP ID = 'KSC', T = 20., F = 0.099 /
&RAMP ID = 'KSC', T = 900., F = 0.099 /
&RAMP ID = 'CPV', T = 20., F = 1.303 /
&RAMP ID = 'CPV', T = 500., F = 1.303 /
&RAMP ID = 'CPC', T = 20., F = 0.741 /
&RAMP ID = 'CPC', T = 400., F = 0.741 /
&RAMP ID = 'CPC', T = 900., F = 0.741 /
*****
&SURF ID      = 'Beech13'
FYI           = 'Charring material'
RGB           = 0.5,0.2,0.1
PHASE         = 'CHAR'

```

```

MOISTURE_FRACTION = 0.10
DELTA = 0.023
TMPIGN = 425
HEAT_OF_VAPORIZATION = 500.
DENSITY = 556.
TMPWAL0 = 52
RAMP_KS = 'KS'
RAMP_C_P = 'CPV'
RAMP_C_P_CHAR = 'CPC'
RAMP_KS_CHAR = 'KSC'
CHAR_DENSITY = 299
WALL_POINTS = 30
BACKING = 'INSULATED'/
&RAMP ID = 'KS', T = 20., F = 0.193 /
&RAMP ID = 'KS', T = 500., F = 0.193 /
&RAMP ID = 'KSC', T = 20., F = 0.099 /
&RAMP ID = 'KSC', T = 900., F = 0.099 /
&RAMP ID = 'CPV', T = 20., F = 1.303 /
&RAMP ID = 'CPV', T = 500., F = 1.303 /
&RAMP ID = 'CPC', T = 20., F = 0.741 /
&RAMP ID = 'CPC', T = 400., F = 0.741 /
&RAMP ID = 'CPC', T = 900., F = 0.741 /
*****
&SURF ID = 'Beech14'
FYI = 'Charring material'
RGB = 0.5,0.2,0.1
PHASE = 'CHAR'
MOISTURE_FRACTION = 0.10
DELTA = 0.023
TMPIGN = 425
HEAT_OF_VAPORIZATION = 500.
DENSITY = 556.
TMPWAL0 = 47
RAMP_KS = 'KS'
RAMP_C_P = 'CPV'
RAMP_C_P_CHAR = 'CPC'
RAMP_KS_CHAR = 'KSC'
CHAR_DENSITY = 299
WALL_POINTS = 30
BACKING = 'INSULATED'/
&RAMP ID = 'KS', T = 20., F = 0.193 /
&RAMP ID = 'KS', T = 500., F = 0.193 /
&RAMP ID = 'KSC', T = 20., F = 0.099 /
&RAMP ID = 'KSC', T = 900., F = 0.099 /
&RAMP ID = 'CPV', T = 20., F = 1.303 /
&RAMP ID = 'CPV', T = 500., F = 1.303 /
&RAMP ID = 'CPC', T = 20., F = 0.741 /
&RAMP ID = 'CPC', T = 400., F = 0.741 /

```

```

&RAMP ID = 'CPC', T = 900., F = 0.741 /
*****
&SURF ID          =          'Beech15'
  FYI              =  'Charring material'
  RGB              =  0.5,0.2,0.1
  PHASE            =  'CHAR'
  MOISTURE_FRACTION =  0.10
  DELTA            =  0.023
  TMPIGN           =  425
  HEAT_OF_VAPORIZATION = 500.
  DENSITY          =  556.
  TMPWAL0         =  42
  RAMP_KS          =  'KS'
  RAMP_C_P        =  'CPV'
  RAMP_C_P_CHAR   =  'CPC'
  RAMP_KS_CHAR    =  'KSC'
  CHAR_DENSITY    =  299
  WALL_POINTS     =  30
  BACKING         =  'INSULATED'
&RAMP ID = 'KS', T = 20., F = 0.193 /
&RAMP ID = 'KS', T = 500., F = 0.193 /
&RAMP ID = 'KSC', T = 20., F = 0.099 /
&RAMP ID = 'KSC', T = 900., F = 0.099 /
&RAMP ID = 'CPV', T = 20., F = 1.303 /
&RAMP ID = 'CPV', T = 500., F = 1.303 /
&RAMP ID = 'CPC', T = 20., F = 0.741 /
&RAMP ID = 'CPC', T = 400., F = 0.741 /
&RAMP ID = 'CPC', T = 900., F = 0.741 /
*****
&SURF ID          =          'Beech16'
  FYI              =  'Charring material'
  RGB              =  0.5,0.2,0.1
  PHASE            =  'CHAR'
  MOISTURE_FRACTION =  0.10
  DELTA            =  0.023
  TMPIGN           =  425
  HEAT_OF_VAPORIZATION = 500.
  DENSITY          =  556.
  TMPWAL0         =  37
  RAMP_KS          =  'KS'
  RAMP_C_P        =  'CPV'
  RAMP_C_P_CHAR   =  'CPC'
  RAMP_KS_CHAR    =  'KSC'
  CHAR_DENSITY    =  299
  WALL_POINTS     =  30
  BACKING         =  'INSULATED'
&RAMP ID = 'KS', T = 20., F = 0.193 /
&RAMP ID = 'KS', T = 500., F = 0.193 /

```

```
&RAMP ID = 'KSC', T = 20., F = 0.099 /
&RAMP ID = 'KSC', T = 900., F = 0.099 /
&RAMP ID = 'CPV', T = 20., F = 1.303 /
&RAMP ID = 'CPV', T = 500., F = 1.303 /
&RAMP ID = 'CPC', T = 20., F = 0.741 /
&RAMP ID = 'CPC', T = 400., F = 0.741 /
&RAMP ID = 'CPC', T = 900., F = 0.741 /
*****
&SURF ID      = 'DUMMY'
  FYI  = 'Calcium Silicate'
  RGB  = 0.66,0.66,0.66
  C_P  = 0.7329
  DENSITY=1055.
  KS   = 0.3137
  DELTA = 0.15/
*****

*****
*****

*****
BACKING BOARD (Calcium Silicate)
*****

&OBST XB = 0.125,0.925,0.27,0.29,0.0625,0.2175 , SURF_ID='DUMMY' /

*****
Special calibration board
*****

&OBST XB = 0.125,0.925,0.25,0.27,0.0625,0.2175 , SURF_ID='DUMMY',
T_REMOVE=25./

*****
Beech specimen
*****
&OBST XB=0.125,0.15,0.25,0.27,0.0625,0.2175, SURF_ID='Beech1', T_CREATE=25.,
COLOR='RED' /
&OBST XB=0.15,0.2,0.25,0.27,0.0625,0.2175, SURF_ID='Beech2', T_CREATE=25.,
COLOR='GREEN' /
&OBST XB=0.2,0.25,0.25,0.27,0.0625,0.2175, SURF_ID='Beech3', T_CREATE=25.,
COLOR='BLUE' /
&OBST XB=0.25,0.3,0.25,0.27,0.0625,0.2175, SURF_ID='Beech4', T_CREATE=25.,
COLOR='WHITE' /
&OBST XB=0.3,0.35,0.25,0.27,0.0625,0.2175, SURF_ID='Beech5', T_CREATE=25.,
COLOR='BLACK' /
```

```

&OBST XB=0.35,0.4,0.25,0.27,0.0625,0.2175, SURF_ID='Beech6', T_CREATE=25.,
COLOR='GRAY' /
&OBST XB=0.4,0.45,0.25,0.27,0.0625,0.2175, SURF_ID='Beech7', T_CREATE=25.,
COLOR='MAGENTA' /
&OBST XB=0.45,0.5,0.25,0.27,0.0625,0.2175, SURF_ID='Beech8', T_CREATE=25.,
COLOR='YELLOW' /
&OBST XB=0.5,0.55,0.25,0.27,0.0625,0.2175, SURF_ID='Beech9', T_CREATE=25.,
COLOR='CYAN' /
&OBST XB=0.55,0.6,0.25,0.27,0.0625,0.2175, SURF_ID='Beech10', T_CREATE=25.,
COLOR='TAN' /
&OBST XB=0.6,0.65,0.25,0.27,0.0625,0.2175, SURF_ID='Beech11', T_CREATE=25.,
COLOR='RED' /
&OBST XB=0.65,0.7,0.25,0.27,0.0625,0.2175, SURF_ID='Beech12', T_CREATE=25.,
COLOR='GREEN' /
&OBST XB=0.7,0.75,0.25,0.27,0.0625,0.2175, SURF_ID='Beech13', T_CREATE=25.,
COLOR='BLUE' /
&OBST XB=0.75,0.8,0.25,0.27,0.0625,0.2175, SURF_ID='Beech14', T_CREATE=25.,
COLOR='WHITE' /
&OBST XB=0.8,0.85,0.25,0.27,0.0625,0.2175, SURF_ID='Beech15', T_CREATE=25.,
COLOR='BLACK' /
&OBST XB=0.85,0.925,0.25,0.27,0.0625,0.2175, SURF_ID='Beech16', T_CREATE=25.,
COLOR='GRAY' /

```

```
*****
```

```
Radiant Panel
```

```
*****
```

```

&OBST
XB=0,0.04,0.13,0.14,0,0.28,SURF_ID6='INERT','PANEL','INERT','PANEL','INERT','INER
T',BNDF_BLOCK =FALSE /
&OBST
XB=0.04,0.08,0.12,0.13,0,0.28,SURF_ID6='INERT','PANEL','INERT','PANEL','INERT','IN
ERT',BNDF_BLOCK =FALSE /
&OBST
XB=0.08,0.12,0.11,0.12,0,0.28,SURF_ID6='INERT','PANEL','INERT','PANEL','INERT','IN
ERT',BNDF_BLOCK =FALSE /
&OBST
XB=0.12,0.15,0.1,0.11,0,0.28,SURF_ID6='INERT','PANEL','INERT','PANEL','INERT','IN
ERT',BNDF_BLOCK =FALSE /
&OBST
XB=0.15,0.19,0.09,0.1,0,0.28,SURF_ID6='INERT','PANEL','INERT','PANEL','INERT','IN
ERT',BNDF_BLOCK =FALSE /
&OBST
XB=0.19,0.23,0.08,0.09,0,0.28,SURF_ID6='INERT','PANEL','INERT','PANEL','INERT','IN
ERT',BNDF_BLOCK =FALSE /
&OBST
XB=0.23,0.27,0.07,0.08,0,0.28,SURF_ID6='INERT','PANEL','INERT','PANEL','INERT','IN
ERT',BNDF_BLOCK =FALSE /

```

```

&OBST
XB=0.27,0.3,0.06,0.07,0,0.28,SURF_ID6='INERT','PANEL','INERT','PANEL','INERT','IN
ERT',BNDF_BLOCK =FALSE /
&OBST
XB=0.3,0.34,0.05,0.06,0,0.28,SURF_ID6='INERT','PANEL','INERT','PANEL','INERT','IN
ERT',BNDF_BLOCK =FALSE /
&OBST
XB=0.34,0.38,0.04,0.05,0,0.28,SURF_ID6='INERT','PANEL','INERT','PANEL','INERT','IN
ERT',BNDF_BLOCK =FALSE /
&OBST
XB=0.38,0.42,0.03,0.04,0,0.28,SURF_ID6='INERT','PANEL','INERT','PANEL','INERT','IN
ERT',BNDF_BLOCK =FALSE /
&OBST
XB=0.42,0.45,0.02,0.03,0,0.28,SURF_ID6='INERT','PANEL','INERT','PANEL','INERT','IN
ERT',BNDF_BLOCK =FALSE /
&OBST
XB=0.45,0.49,0.01,0.02,0,0.28,SURF_ID6='INERT','INERT','INERT','PANEL','INERT','IN
ERT',BNDF_BLOCK =FALSE /

```

```

*****
*****

```

```

*****

```

Vents

```

*****

```

```

&VENT CB='XBAR0',SURF_ID='OPEN' /
&VENT CB='XBAR' ,SURF_ID='OPEN' /
&VENT CB='YBAR0',SURF_ID='OPEN' /
&VENT CB='YBAR' ,SURF_ID='OPEN' /
&VENT CB='ZBAR0' ,SURF_ID='OPEN' /
&VENT CB='ZBAR' ,SURF_ID='OPEN' /

```

```

*****
*****

```

Output files

```

*****
*****

```

```

&THCP XYZ=0.13,0.25,0.14,QUANTITY='GAUGE_HEAT_FLUX', IOR=-2, LABEL=
'0mm away'/
&THCP XYZ=0.175,0.25,0.14,QUANTITY='GAUGE_HEAT_FLUX', IOR=-2, LABEL=
'50mm away'/
&THCP XYZ=0.225,0.25,0.14,QUANTITY='GAUGE_HEAT_FLUX', IOR=-2, LABEL=
'100mm away'/
&THCP XYZ=0.275,0.25,0.14,QUANTITY='GAUGE_HEAT_FLUX', IOR=-2, LABEL=
'150mm away'/

```

&THCP XYZ=0.325,0.25,0.14,QUANTITY='GAUGE_HEAT_FLUX', IOR=-2, LABEL='200mm away'/
&THCP XYZ=0.375,0.25,0.14,QUANTITY='GAUGE_HEAT_FLUX', IOR=-2, LABEL='250mm away'/
&THCP XYZ=0.425,0.25,0.14,QUANTITY='GAUGE_HEAT_FLUX', IOR=-2, LABEL='300mm away'/
&THCP XYZ=0.475,0.25,0.14,QUANTITY='GAUGE_HEAT_FLUX', IOR=-2, LABEL='350mm away'/
&THCP XYZ=0.525,0.25,0.14,QUANTITY='GAUGE_HEAT_FLUX', IOR=-2, LABEL='400mm away'/
&THCP XYZ=0.575,0.25,0.14,QUANTITY='GAUGE_HEAT_FLUX', IOR=-2, LABEL='450mm away'/
&THCP XYZ=0.625,0.25,0.14,QUANTITY='GAUGE_HEAT_FLUX', IOR=-2, LABEL='500mm away'/
&THCP XYZ=0.675,0.25,0.14,QUANTITY='GAUGE_HEAT_FLUX', IOR=-2, LABEL='550mm away'/
&THCP XYZ=0.725,0.25,0.14,QUANTITY='GAUGE_HEAT_FLUX', IOR=-2, LABEL='600mm away'/
&THCP XYZ=0.775,0.25,0.14,QUANTITY='GAUGE_HEAT_FLUX', IOR=-2, LABEL='650mm away'/
&THCP XYZ=0.825,0.25,0.14,QUANTITY='GAUGE_HEAT_FLUX', IOR=-2, LABEL='700mm away'/
&THCP XYZ=0.875,0.25,0.14,QUANTITY='GAUGE_HEAT_FLUX', IOR=-2, LABEL='750mm away'/

&ISOF QUANTITY = 'MIXTURE_FRACTION', VALUE(1)=0.148/
&PL3D DTSAM=1000000./ Do not produce any Plot3D files

Material properties for each species of wood**Beech**

```

&SURF ID          =          'Beech1'
  FYI              =  'Thermoplastic material'
  RGB              =  0.5,0.2,0.1
  MOISTURE_FRACTION =  0.10
  DELTA            =  0.023
  MASS_FLUX_CRITICAL =  0.075
  HEAT_OF_VAPORIZATION = 1400.
  TMPIGN          =  425
  TMPWAL0        =  345
  DENSITY         =  556.
  KS              =  0.1927
  C_P             =  1.303
  WALL_POINTS     =  30
  BACKING         =  'INSULATED/'

```

Char Beech

```

&SURF ID          =          'Beech1'
  FYI              =  'Charring material'
  RGB              =  0.5,0.2,0.1
  PHASE            =  'CHAR'
  MOISTURE_FRACTION =  0.10
  DELTA            =  0.023
  TMPIGN          =  425
  HEAT_OF_VAPORIZATION = 500.
  DENSITY         =  556.
  TMPWAL0        =  345
  RAMP_KS         =  'KS'
  RAMP_C_P        =  'CPV'
  RAMP_C_P_CHAR   =  'CPC'
  RAMP_KS_CHAR    =  'KSC'
  CHAR_DENSITY    =  299
  WALL_POINTS     =  30
  BACKING         =  'INSULATED/'

```

```

&RAMP ID = 'KS', T = 20., F = 0.193 /
&RAMP ID = 'KS', T = 500., F = 0.193 /
&RAMP ID = 'KSC', T = 20., F = 0.099 /
&RAMP ID = 'KSC', T = 900., F = 0.099 /
&RAMP ID = 'CPV', T = 20., F = 1.303 /
&RAMP ID = 'CPV', T = 500., F = 1.303 /
&RAMP ID = 'CPC', T = 20., F = 0.741 /
&RAMP ID = 'CPC', T = 400., F = 0.741 /
&RAMP ID = 'CPC', T = 900., F = 0.741 /

```

Hardboard

```

&SURF ID          =          'Hardboard1'
  FYI              =  'Thermoplastic material'
  RGB              =  0.5,0.2,0.1
  MOISTURE_FRACTION =  0.10
  DELTA            =  0.005
  MASS_FLUX_CRITICAL =  0.075
  HEAT_OF_VAPORIZATION = 1400.
  TMPIGN           =  409
  TMPWAL0          =  339
  DENSITY          =  845.
  KS               =  0.2437
  C_P              =  1.260
  WALL_POINTS      =  30
  BACKING          =  'INSULATED/'

```

Char Hardboard

```

&SURF ID          =          'Hardboard1'
  FYI              =  'Charring material'
  RGB              =  0.5,0.2,0.1
  PHASE            =  'CHAR'
  MOISTURE_FRACTION =  0.10
  DELTA            =  0.005
  TMPIGN           =  409
  HEAT_OF_VAPORIZATION = 500.
  DENSITY          =  845.
  TMPWAL0          =  339
  RAMP_KS          =  'KS'
  RAMP_C_P         =  'CPV'
  RAMP_C_P_CHAR    =  'CPC'
  RAMP_KS_CHAR     =  'KSC'
  CHAR_DENSITY     =  510
  WALL_POINTS      =  30
  BACKING          =  'INSULATED/'
&RAMP ID = 'KS', T = 20., F = 0.244 /
&RAMP ID = 'KS', T = 500., F = 0.244 /
&RAMP ID = 'KSC', T = 20., F = 0.211 /
&RAMP ID = 'KSC', T = 900., F = 0.211 /
&RAMP ID = 'CPV', T = 20., F = 1.261 /
&RAMP ID = 'CPV', T = 500., F = 1.261 /
&RAMP ID = 'CPC', T = 20., F = 0.868 /
&RAMP ID = 'CPC', T = 400., F = 0.868 /
&RAMP ID = 'CPC', T = 900., F = 0.868 /

```

Macrocarpa

```

&SURF ID      =      'Macrocarpa1'
  FYI         =  'Thermoplastic material'
  RGB         =  0.5,0.2,0.1
  MOISTURE_FRACTION =  0.10
  DELTA       =  0.024
  MASS_FLUX_CRITICAL =  0.075
  HEAT_OF_VAPORIZATION = 1400.
  TMPIGN      =  425
  TMPWAL0     =  339
  DENSITY     =  566.
  KS          =  0.1955
  C_P        =  1.082
  WALL_POINTS =  30
  BACKING    =  'INSULATED/'

```

Char Macrocarpa

```

&SURF ID      =      'Macrocarpa1'
  FYI         =  'Charring material'
  RGB         =  0.5,0.2,0.1
  PHASE       =  'CHAR'
  MOISTURE_FRACTION =  0.10
  DELTA       =  0.024
  TMPIGN      =  425
  HEAT_OF_VAPORIZATION = 500.
  DENSITY     =  566.
  TMPWAL0     =  339
  RAMP_KS     =  'KS'
  RAMP_C_P    =  'CPV'
  RAMP_C_P_CHAR =  'CPC'
  RAMP_KS_CHAR =  'KSC'
  CHAR_DENSITY = 285
  WALL_POINTS =  30
  BACKING    =  'INSULATED/'
&RAMP ID = 'KS', T = 20., F = 0.196 /
&RAMP ID = 'KS', T = 500., F = 0.196 /
&RAMP ID = 'KSC', T = 20., F = 0.078 /
&RAMP ID = 'KSC', T = 900., F = 0.078 /
&RAMP ID = 'CPV', T = 20., F = 1.083 /
&RAMP ID = 'CPV', T = 500., F = 1.083 /
&RAMP ID = 'CPC', T = 20., F = 0.564 /
&RAMP ID = 'CPC', T = 400., F = 0.564 /
&RAMP ID = 'CPC', T = 900., F = 0.564 /

```

MDF

```

&SURF ID      =      'MDF1'
  FYI          =  'Thermoplastic material'
  RGB          =  0.5,0.2,0.1
  MOISTURE_FRACTION =  0.10
  DELTA        =  0.018
  MASS_FLUX_CRITICAL =  0.075
  HEAT_OF_VAPORIZATION = 1400.
  TMPIGN       =  391
  TMPWAL0      =  344
  DENSITY       =  647.
  KS           =  0.1779
  C_P          =  1.188
  WALL_POINTS   =  30
  BACKING       =  'INSULATED/'

```

Char MDF

```

&SURF ID      =      'MDF1'
  FYI          =  'Charring material'
  RGB          =  0.5,0.2,0.1
  PHASE        =  'CHAR'
  MOISTURE_FRACTION =  0.10
  DELTA        =  0.018
  TMPIGN       =  391
  HEAT_OF_VAPORIZATION = 500.
  DENSITY       =  647.
  TMPWAL0      =  344
  RAMP_KS      =  'KS'
  RAMP_C_P     =  'CPV'
  RAMP_C_P_CHAR =  'CPC'
  RAMP_KS_CHAR =  'KSC'
  CHAR_DENSITY =  498
  WALL_POINTS   =  30
  BACKING       =  'INSULATED/'
&RAMP ID = 'KS', T = 20., F = 0.178 /
&RAMP ID = 'KS', T = 500., F = 0.178 /
&RAMP ID = 'KSC', T = 20., F = 0.101 /
&RAMP ID = 'KSC', T = 900., F = 0.101 /
&RAMP ID = 'CPV', T = 20., F = 1.188 /
&RAMP ID = 'CPV', T = 500., F = 1.188 /
&RAMP ID = 'CPC', T = 20., F = 0.51 /
&RAMP ID = 'CPC', T = 400., F = 0.51 /
&RAMP ID = 'CPC', T = 900., F = 0.51 /

```

Melteca faced MDF

```

&SURF ID      =      'Melfmdf1'
  FYI          =  'Thermoplastic material'
  RGB          =  0.5,0.2,0.1
  MOISTURE_FRACTION =  0.10
  DELTA        =  0.018
  MASS_FLUX_CRITICAL =  0.075
  HEAT_OF_VAPORIZATION = 1400.
  TMPIGN       =  440
  TMPWAL0      =  420
  DENSITY      =  793.
  KS           =  0.2224
  C_P          =  1.479
  WALL_POINTS  =  30
  BACKING      =  'INSULATED/'

```

Char Melteca faced MDF

```

&SURF ID      =      'Melfmdf1'
  FYI          =  'Charring material'
  RGB          =  0.5,0.2,0.1
  PHASE        =  'CHAR'
  MOISTURE_FRACTION =  0.10
  DELTA        =  0.018
  TMPIGN       =  440
  HEAT_OF_VAPORIZATION = 500.
  DENSITY      =  793.
  TMPWAL0      =  420
  RAMP_KS      =  'KS'
  RAMP_C_P     =  'CPV'
  RAMP_C_P_CHAR =  'CPC'
  RAMP_KS_CHAR =  'KSC'
  CHAR_DENSITY =  588
  WALL_POINTS  =  30
  BACKING      =  'INSULATED/'
&RAMP ID = 'KS', T = 20., F = 0.223 /
&RAMP ID = 'KS', T = 500., F = 0.223 /
&RAMP ID = 'KSC', T = 20., F = 0.139 /
&RAMP ID = 'KSC', T = 900., F = 0.139 /
&RAMP ID = 'CPV', T = 20., F = 1.479 /
&RAMP ID = 'CPV', T = 500., F = 1.479 /
&RAMP ID = 'CPC', T = 20., F = 0.958 /
&RAMP ID = 'CPC', T = 400., F = 0.958 /
&RAMP ID = 'CPC', T = 900., F = 0.958 /

```

Radiata Pine

```

&SURF ID      =      'Pine1'
  FYI          =  'Thermoplastic material'
  RGB          =  0.5,0.2,0.1
  MOISTURE_FRACTION =  0.10
  DELTA        =  0.022
  MASS_FLUX_CRITICAL =  0.075
  HEAT_OF_VAPORIZATION = 1400.
  TMPIGN       =  425
  TMPWAL0      =  369
  DENSITY      =  439.
  KS           =  0.1731
  C_P          =  1.149
  WALL_POINTS  =  30
  BACKING      =  'INSULATED/'

```

Char Radiata Pine

```

&SURF ID      =      'Pine1'
  FYI          =  'Charring material'
  RGB          =  0.5,0.2,0.1
  PHASE        =  'CHAR'
  MOISTURE_FRACTION =  0.10
  DELTA        =  0.022
  TMPIGN       =  425
  HEAT_OF_VAPORIZATION = 500.
  DENSITY      =  439.
  TMPWAL0      =  369
  RAMP_KS      =  'KS'
  RAMP_C_P     =  'CPV'
  RAMP_C_P_CHAR =  'CPC'
  RAMP_KS_CHAR =  'KSC'
  CHAR_DENSITY =  249
  WALL_POINTS  =  30
  BACKING      =  'INSULATED/'
&RAMP ID = 'KS', T = 20., F = 0.174 /
&RAMP ID = 'KS', T = 500., F = 0.174 /
&RAMP ID = 'KSC', T = 20., F = 0.095 /
&RAMP ID = 'KSC', T = 900., F = 0.095 /
&RAMP ID = 'CPV', T = 20., F = 1.149 /
&RAMP ID = 'CPV', T = 500., F = 1.149 /
&RAMP ID = 'CPC', T = 20., F = 0.898 /
&RAMP ID = 'CPC', T = 400., F = 0.898 /
&RAMP ID = 'CPC', T = 900., F = 0.898 /

```

Plywood

```

&SURF ID      =      'Plywood1'
  FYI          =  'Thermoplastic material'
  RGB          =  0.5,0.2,0.1
  MOISTURE_FRACTION =  0.10
  DELTA        =  0.021
  MASS_FLUX_CRITICAL =  0.075
  HEAT_OF_VAPORIZATION = 1400.
  TMPIGN       =  391
  TMPWAL0     =  316
  DENSITY      =  503.
  KS           =  0.1841
  C_P          =  1.161
  WALL_POINTS  =  30
  BACKING      =  'INSULATED/'

```

Char Plywood

```

&SURF ID      =      'Plywood1'
  FYI          =  'Charring material'
  RGB          =  0.5,0.2,0.1
  PHASE        =  'CHAR'
  MOISTURE_FRACTION =  0.10
  DELTA        =  0.021
  TMPIGN       =  391
  HEAT_OF_VAPORIZATION = 500.
  DENSITY      =  503.
  TMPWAL0     =  316
  RAMP_KS      =  'KS'
  RAMP_C_P     =  'CPV'
  RAMP_C_P_CHAR =  'CPC'
  RAMP_KS_CHAR =  'KSC'
  CHAR_DENSITY =  397
  WALL_POINTS  =  30
  BACKING      =  'INSULATED/'
&RAMP ID = 'KS', T = 20., F = 0.185 /
&RAMP ID = 'KS', T = 500., F = 0.185 /
&RAMP ID = 'KSC', T = 20., F = 0.08 /
&RAMP ID = 'KSC', T = 900., F = 0.08 /
&RAMP ID = 'CPV', T = 20., F = 1.162 /
&RAMP ID = 'CPV', T = 500., F = 1.162 /
&RAMP ID = 'CPC', T = 20., F = 0.337 /
&RAMP ID = 'CPC', T = 400., F = 0.337 /
&RAMP ID = 'CPC', T = 900., F = 0.337 /

```

Pynefloor

```

&SURF ID      =      'Pynefloor1'
  FYI         =  'Thermoplastic material'
  RGB         =  0.5,0.2,0.1
  MOISTURE_FRACTION =  0.10
  DELTA       =  0.020
  MASS_FLUX_CRITICAL =  0.075
  HEAT_OF_VAPORIZATION = 1400.
  TMPIGN      =  425
  TMPWAL0     =  321
  DENSITY     =  651.
  KS =  0.2313
  C_P =  1.919
  WALL_POINTS =  30
  BACKING     =  'INSULATED/'

```

Char Pynefloor

```

&SURF ID      =      'Pynefloor1'
  FYI         =  'Charring material'
  RGB         =  0.5,0.2,0.1
  PHASE       =  'CHAR'
  MOISTURE_FRACTION =  0.10
  DELTA       =  0.020
  TMPIGN      =  425
  HEAT_OF_VAPORIZATION = 500.
  DENSITY     =  651.
  TMPWAL0     =  321
  RAMP_KS     =  'KS'
  RAMP_C_P    =  'CPV'
  RAMP_C_P_CHAR =  'CPC'
  RAMP_KS_CHAR =  'KSC'
  CHAR_DENSITY = 584
  WALL_POINTS =  30
  BACKING     =  'INSULATED/'
&RAMP ID = 'KS', T = 20., F = 0.232 /
&RAMP ID = 'KS', T = 500., F = 0.232 /
&RAMP ID = 'KSC', T = 20., F = 0.102 /
&RAMP ID = 'KSC', T = 900., F = 0.102 /
&RAMP ID = 'CPV', T = 20., F = 1.919 /
&RAMP ID = 'CPV', T = 500., F = 1.919 /
&RAMP ID = 'CPC', T = 20., F = 0.487 /
&RAMP ID = 'CPC', T = 400., F = 0.487 /
&RAMP ID = 'CPC', T = 900., F = 0.487 /

```

Rimu

```

&SURF ID      =      'Rimu1'
  FYI          =  'Thermoplastic material'
  RGB          =  0.5,0.2,0.1
  MOISTURE_FRACTION =  0.10
  DELTA        =  0.021
  MASS_FLUX_CRITICAL =  0.075
  HEAT_OF_VAPORIZATION = 1400.
  TMPIGN       =  422
  TMPWAL0      =  353
  DENSITY      =  650.
  KS           =  0.2237
  C_P          =  1.155
  WALL_POINTS  =  30
  BACKING      =  'INSULATED/'

```

Char Rimu

```

&SURF ID      =      'Rimu1'
  FYI          =  'Charring material'
  RGB          =  0.5,0.2,0.1
  PHASE        =  'CHAR'
  MOISTURE_FRACTION =  0.10
  DELTA        =  0.021
  TMPIGN       =  422
  HEAT_OF_VAPORIZATION = 500.
  DENSITY      =  650.
  TMPWAL0      =  353
  RAMP_KS      =  'KS'
  RAMP_C_P     =  'CPV'
  RAMP_C_P_CHAR =  'CPC'
  RAMP_KS_CHAR =  'KSC'
  CHAR_DENSITY =  398
  WALL_POINTS  =  30
  BACKING      =  'INSULATED/'
&RAMP ID = 'KS', T = 20., F = 0.224 /
&RAMP ID = 'KS', T = 500., F = 0.224 /
&RAMP ID = 'KSC', T = 20., F = 0.103 /
&RAMP ID = 'KSC', T = 900., F = 0.103 /
&RAMP ID = 'CPV', T = 20., F = 1.155 /
&RAMP ID = 'CPV', T = 500., F = 1.155 /
&RAMP ID = 'CPC', T = 20., F = 0.433 /
&RAMP ID = 'CPC', T = 400., F = 0.433 /
&RAMP ID = 'CPC', T = 900., F = 0.433 /

```

Appendix H – Flame spread test calculations

Appendix H 1: Beech $\varepsilon=0.6$

Position of the flame front (mm)	Arrival time + 25s	Flame Front Arrival Time, t (s)	Actual Time (s)	t.x	$\Sigma(t.x)$	$\Sigma(t)$	$(\Sigma t)^2$	$\Sigma(x)$	t^2	$\Sigma(t^2)$	Flame Front Velocity, V (running 3 point less square fit)	m/s	$V^{-1/2}$	$q''e(x)$	F(t)	$q''e(x).F(t)$
0																
25																
50																
75																
100	26	1	396	39608.3	89243.62	793.17	629111	300	156882	314556.246	0.032	0.000		23.280	1.000	23.280
125	27	2	397	49635.3	148956	1191.2	1419072	375	157675	473026.117	0.000	0.025	6.325	22.715	1.000	22.715
150	28	3	398	59712.4	179187.2	1194.2	1426229	450	158470	475411.614	0.000	0.025	6.325	22.151	1.000	22.151
175	29	4	399	69839.5	209768.4	1198.2	1435799	525	159267	478604.276	0.000	0.016	7.888	21.210	1.000	21.210
200	31	6	401	80216.5	241199.6	1205.2	1452623	600	160867	484226.434	0.000	0.008	11.155	20.270	1.000	20.270
225	35	10	405	91143.6	273880.9	1216.2	1479260	675	164092	493127.255	0.000	0.006	13.444	19.024	1.000	19.024
250	40	15	410	102521	309737.1	1237.2	1530783	750	168168	510413.730	0.001	0.003	18.953	17.777	1.000	17.777
275	52	27	422	116073	350018.3	1270.2	1613531	825	178154	538238.191	0.001	0.002	23.745	16.155	1.000	16.155
300	68	43	438	131425	401574.5	1334.2	1780218	900	191916	594824.782	0.002	0.001	33.035	14.532	1.000	14.532
325	104	79	474	154077	471380.7	1443.2	2082965	975	224754	698719.821	0.003	0.001	43.493	12.886	1.000	12.886
350	161	136	531	185879	577736.9	1639.2	2687135	1050	282049	908864.256	0.005	0.000	57.343	11.240	1.000	11.240
375	264	239	634	237781	801693.1	2110.2	4453148	1125	402061	1577291.201	0.008	0.000	94.745	9.900	1.000	9.900
400	575	550	945	378033	1045880	2633.2	6933996	1183	893181	2406332.752	0.004	0.000	112.529	8.559	1.000	8.559
408	684	659	1054	430066					1111090					7.384	1.000	7.384

Appendix H 2: Beech $\epsilon=0.7$

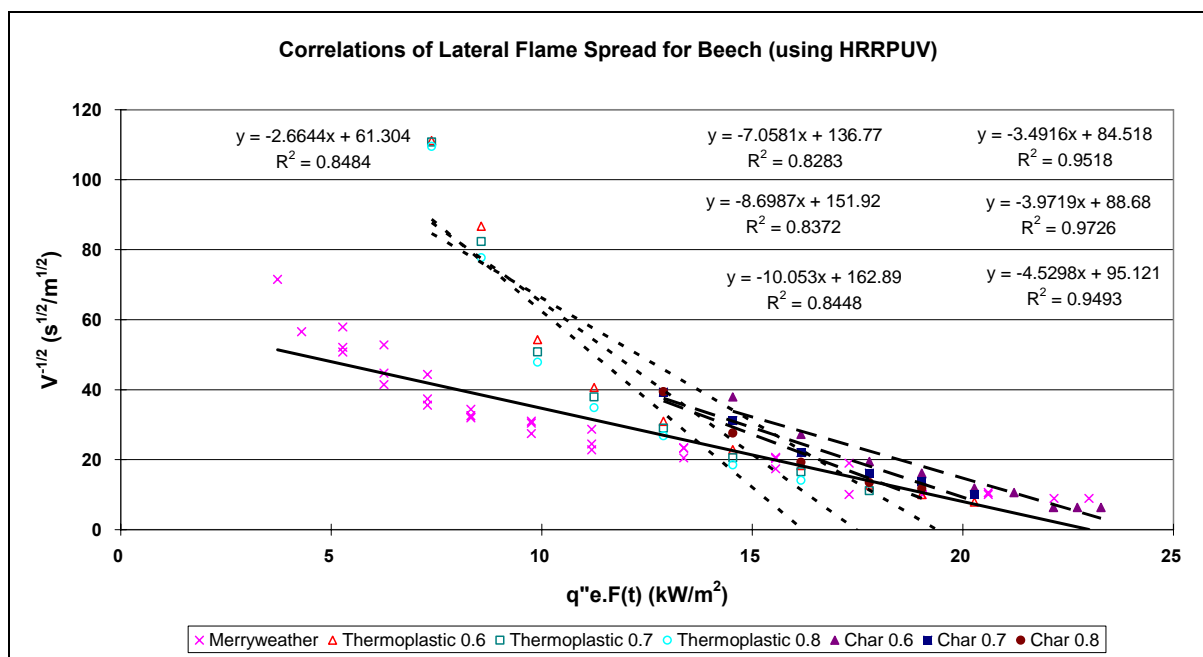
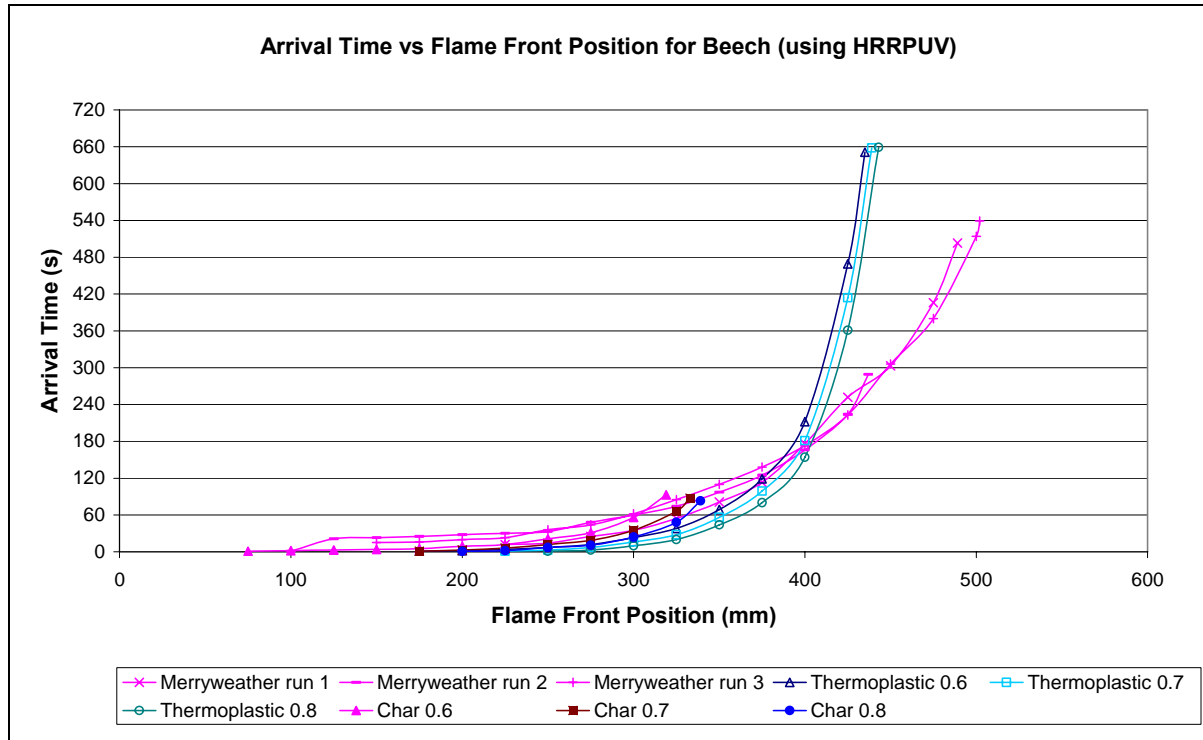
Position of the flame front (mm)	Arrival time + 25s	Flame Front Arrival Time, t (s)	Actual Time (s)	t.x	$\sum(t.x)$	$\sum(t)$	$(\sum t)^2$	$\sum(x)$	t^2	$\sum(t^2)$	Flame Front Velocity, V (running 3 point less square fit)	m/s	$V^{-1/2}$	$q''e(x)$	F(t)	$q''e(x).F(t)$
0																
25																
50																
75																
100																
125																
150	26	1	396	59412.4	128901.9	793.17	629111	450	156882	314556.246	0.032	0.000		22.151	1.000	22.151
175	27	2	397	69489.5	208518.4	1191.2	1419072	525	157675	473026.117	0.000	0.025	6.325	21.210	1.000	21.210
200	28	3	398	79616.5	239349.6	1196.2	1431010	600	158470	477011.945	0.000	0.012	9.309	20.270	1.000	20.270
225	31	6	401	90243.6	270880.9	1203.2	1447806	675	160867	482620.103	0.000	0.008	10.954	19.024	1.000	19.024
250	34	9	404	101021	304587.1	1217.2	1481693	750	163283	493962.420	0.001	0.004	15.335	17.777	1.000	17.777
275	42	17	412	113323	342468.3	1243.2	1545666	825	169812	515494.723	0.001	0.002	21.776	16.155	1.000	16.155
300	57	32	427	128125	390649.5	1298.2	1685448	900	182400	562968.825	0.002	0.001	31.321	14.532	1.000	14.532
325	89	64	459	149202	454805.7	1393.2	1941141	975	210757	650289.546	0.003	0.001	40.266	12.886	1.000	12.886
350	137	112	507	177479	550586.9	1563.2	2443745	1050	257133	824397.679	0.004	0.000	53.341	11.240	1.000	11.240
375	227	202	597	223906	744218.1	1961.2	3846495	1125	356508	1348231.544	0.008	0.000	86.893	9.900	1.000	9.900
400	487	462	857	342833	1000609	2507.2	6286294	1187	734591	2200081.900	0.005	0.000	110.475	8.559	1.000	8.559
412	683	658	1053	433870					1108983					7.384	1.000	7.384

Appendix H 3: Beech $\epsilon=0.8$

Position of the flame front (mm)	Arrival time + 25s	Flame Front Arrival Time, t (s)	Actual Time (s)	t.x	$\Sigma(t.x)$	$\Sigma(t)$	$(\Sigma t)^2$	$\Sigma(x)$	t^2	$\Sigma(t^2)$	Flame Front Velocity, V (running 3 point less square fit)	m/s	$V^{-1/2}$	$q''e(x)$	F(t)	$q''e(x).F(t)$
0																
25																
50																
75																
100																
125																
150																
175																
200	26	1	396	79216.5	168785.2	794.17	630699	600	156882	315351.412	0.032	0.000		20.270	1.000	20.270
225	28	3	398	89568.6	268805.9	1194.2	1426229	675	158470	475417.614	0.000	0.012	8.944	19.024	1.000	19.024
250	30	5	400	100021	302087.1	1207.2	1457448	750	160066	485884.765	0.001	0.004	15.802	17.777	1.000	17.777
275	39	14	409	112498	337943.3	1227.2	1506138	825	167349	502208.075	0.001	0.003	18.974	16.155	1.000	16.155
300	48	23	418	125425	381599.5	1269.2	1610991	900	174793	537579.026	0.002	0.001	26.560	14.532	1.000	14.532
325	72	47	442	143677	439930.7	1348.2	1817773	975	195437	608455.099	0.003	0.001	38.028	12.886	1.000	12.886
350	118	93	488	170829	529786.9	1504.2	2262763	1050	238225	763232.915	0.005	0.000	52.161	11.240	1.000	11.240
375	204	179	574	215281	704543.1	1858.2	3453086	1125	329571	1201543.498	0.007	0.000	80.996	9.900	1.000	9.900
400	426	401	796	318433	962028.5	2402.2	5770797	1190	633748	2028513.524	0.006	0.000	107.158	8.559	1.000	8.559
415	662	637	1032	428314					1065195					7.384	1.000	7.384

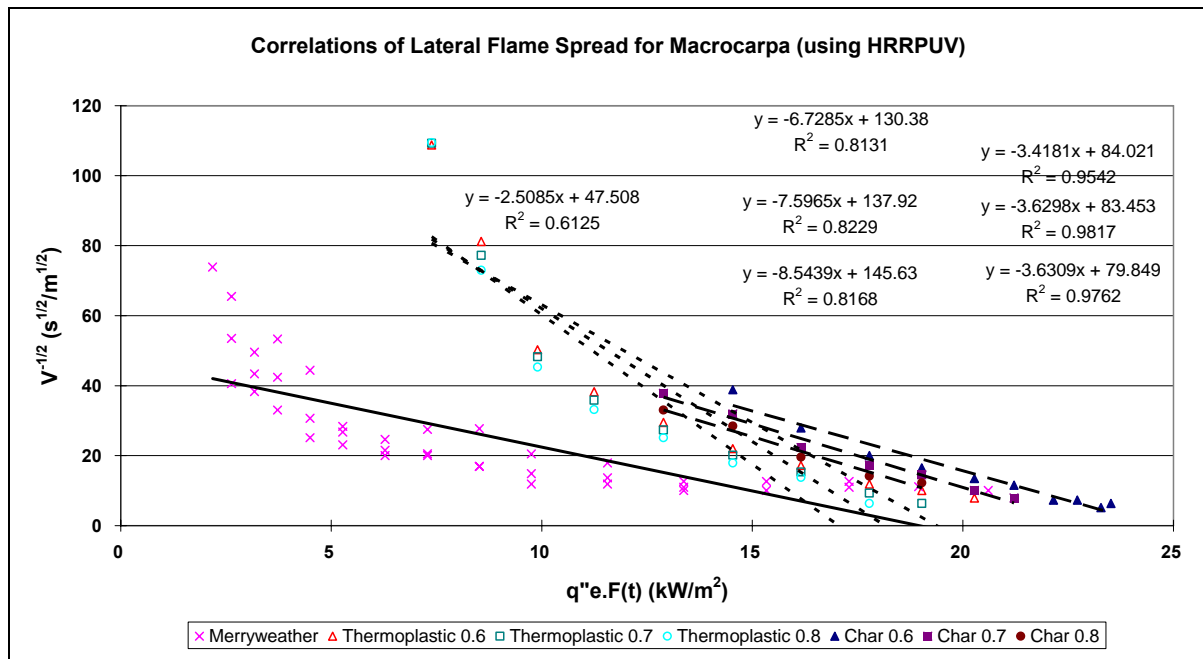
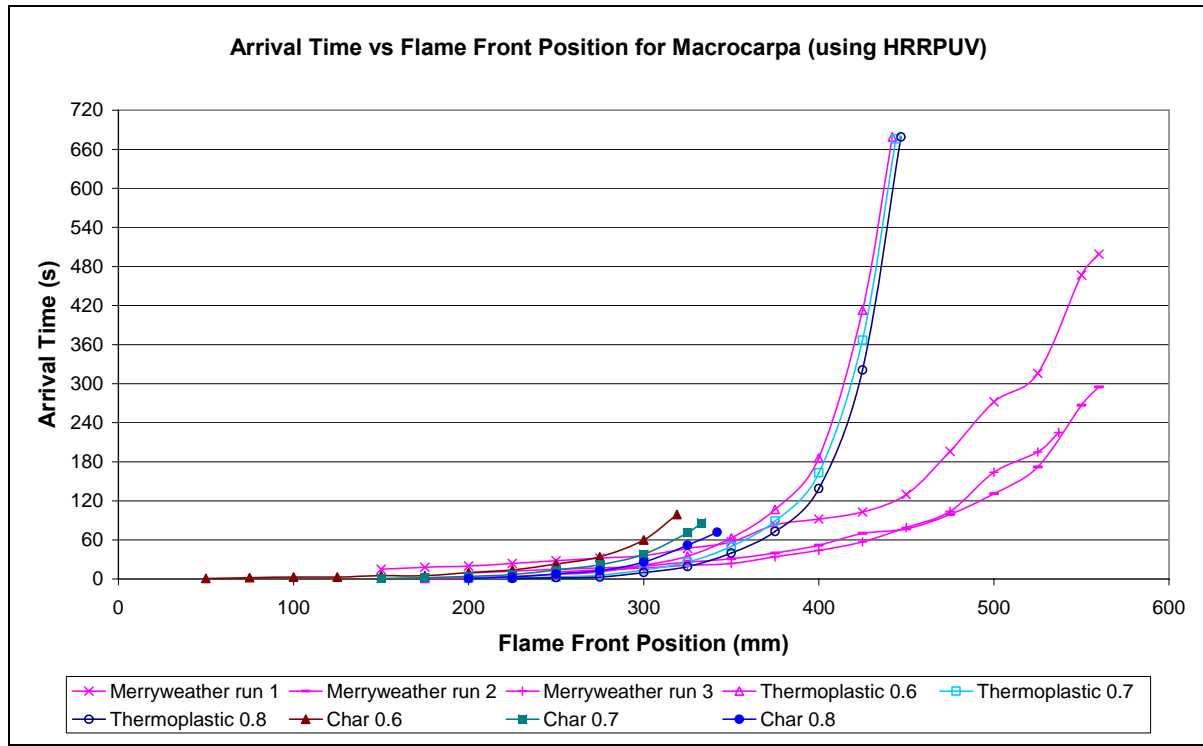
Appendix I – Flame spread results using HRRPUV

Beech



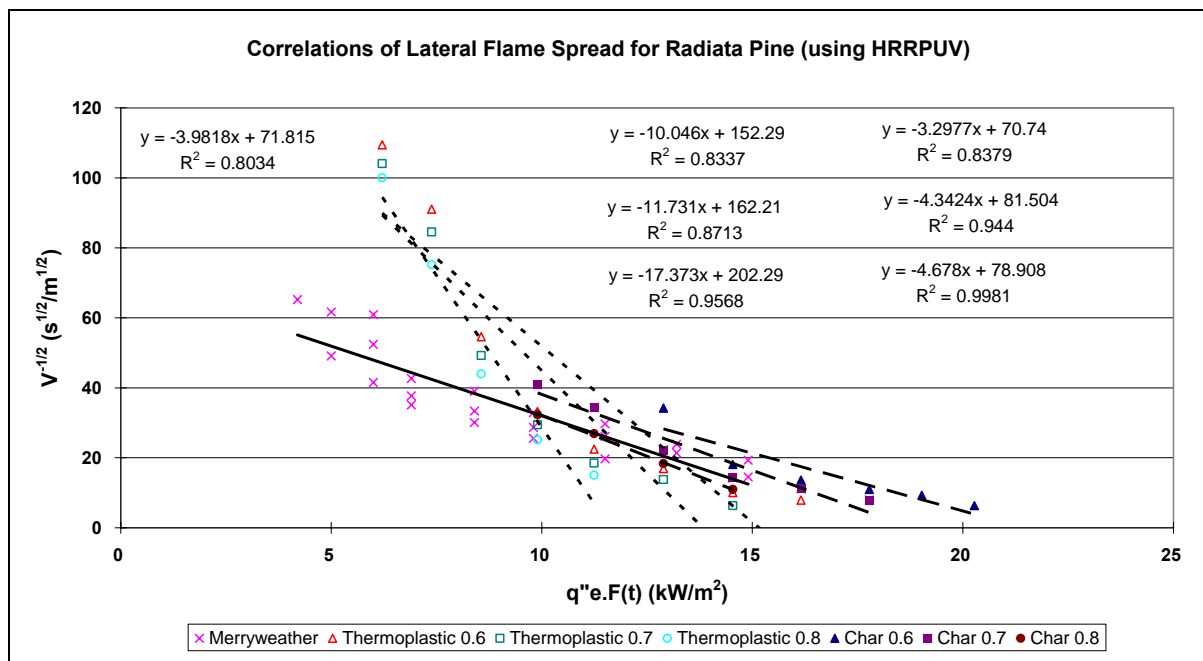
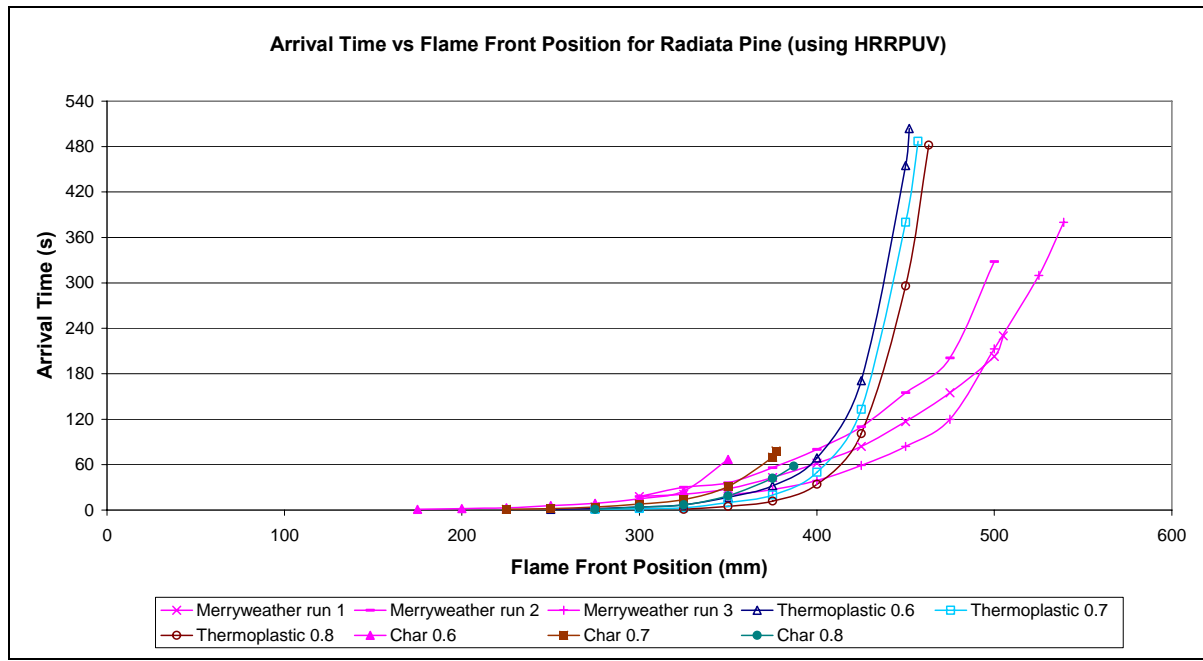
Appendix I – Flame spread results using HRRPUV

Macrocarpa



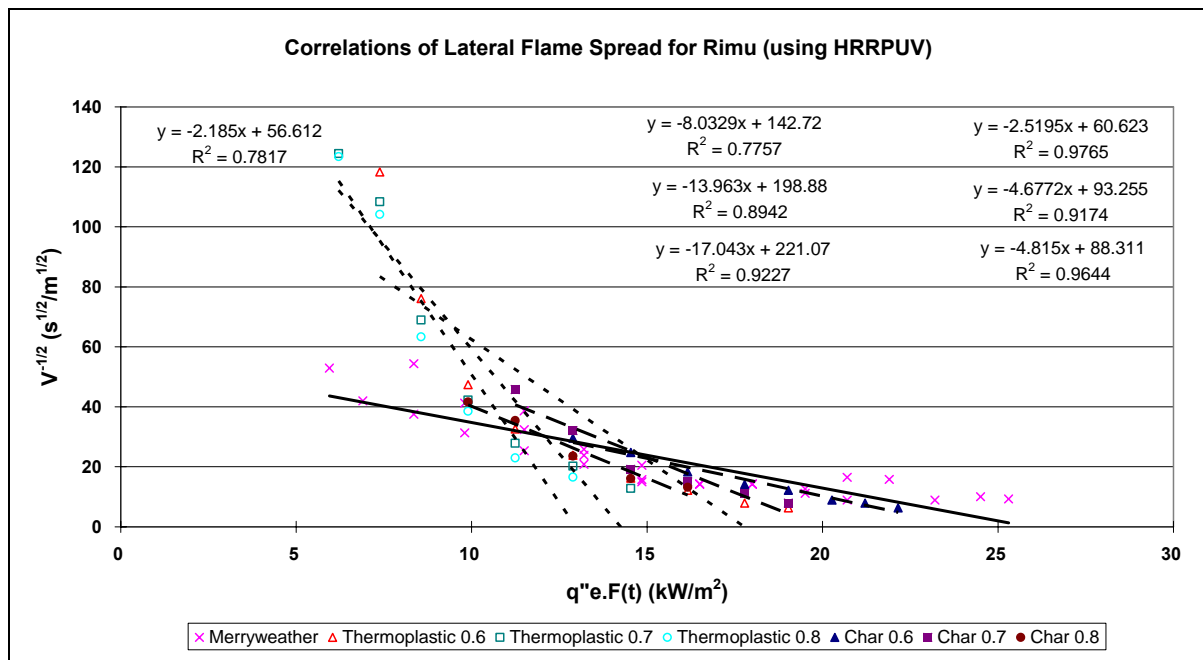
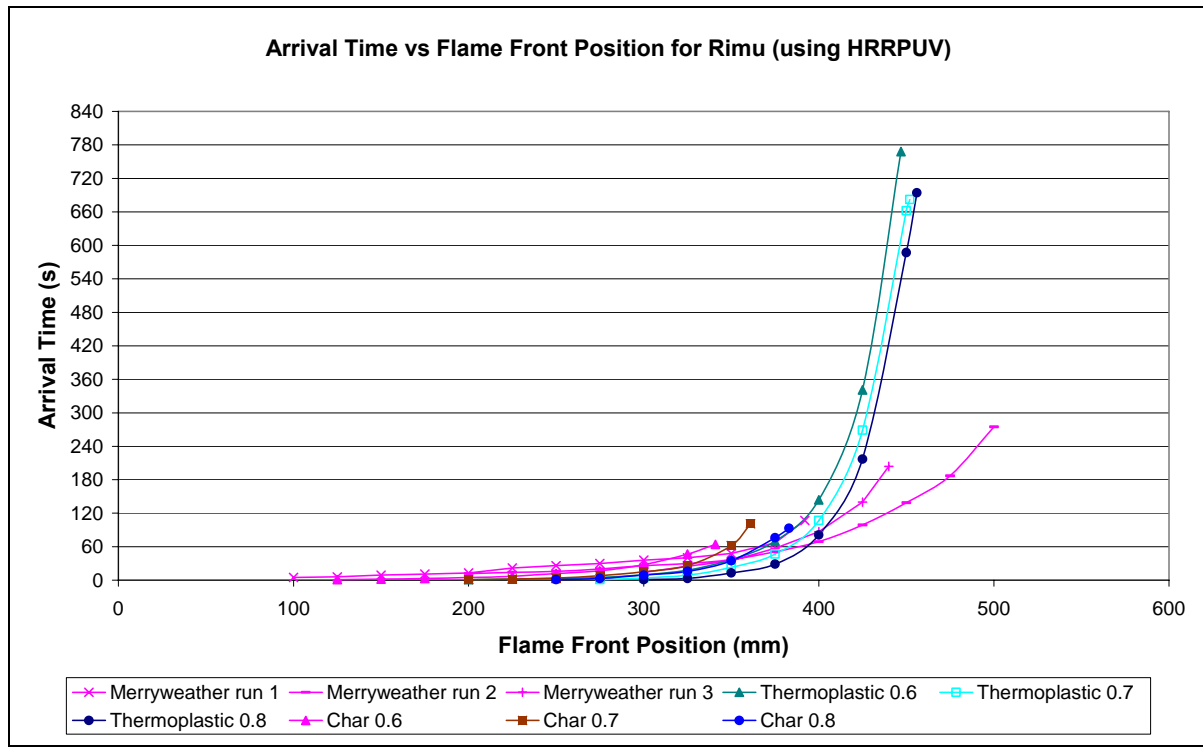
Appendix I – Flame spread results using HRRPUV

Radiata Pine



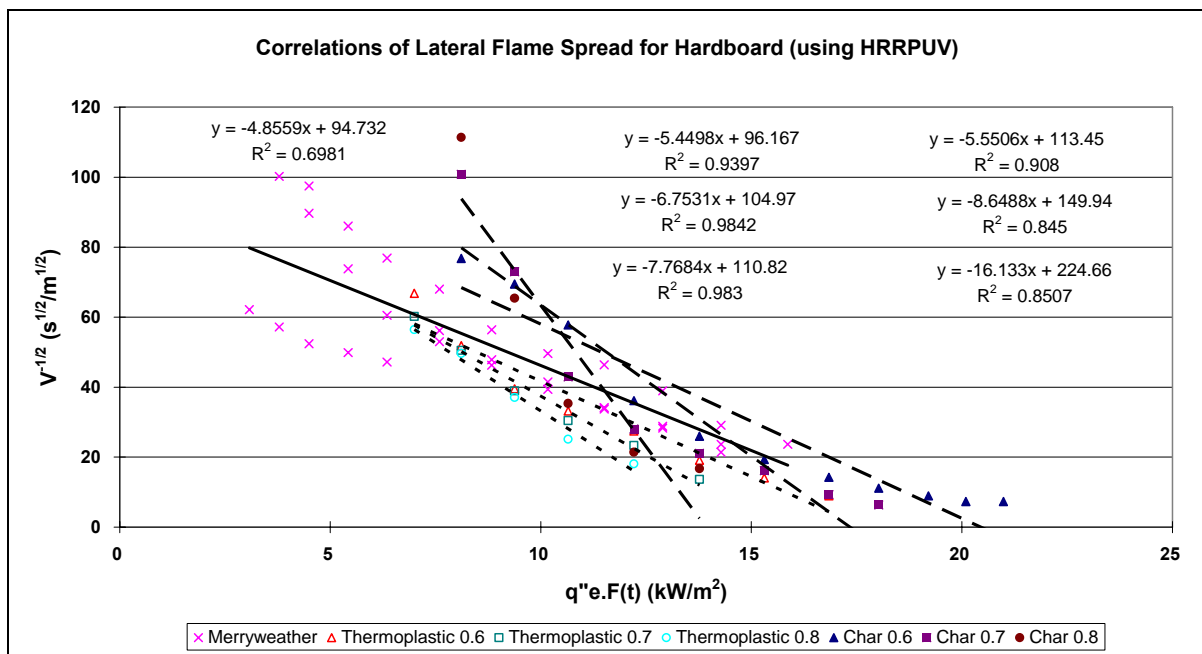
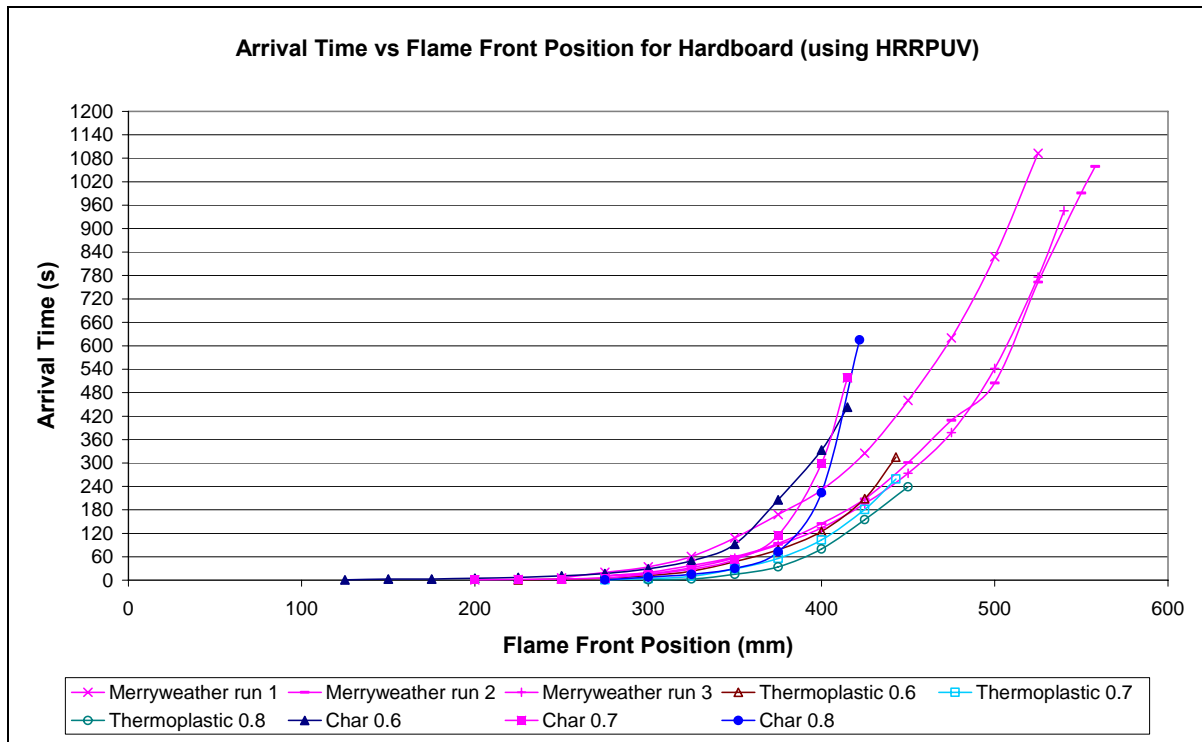
Appendix I – Flame spread results using HRRPUV

Rimu



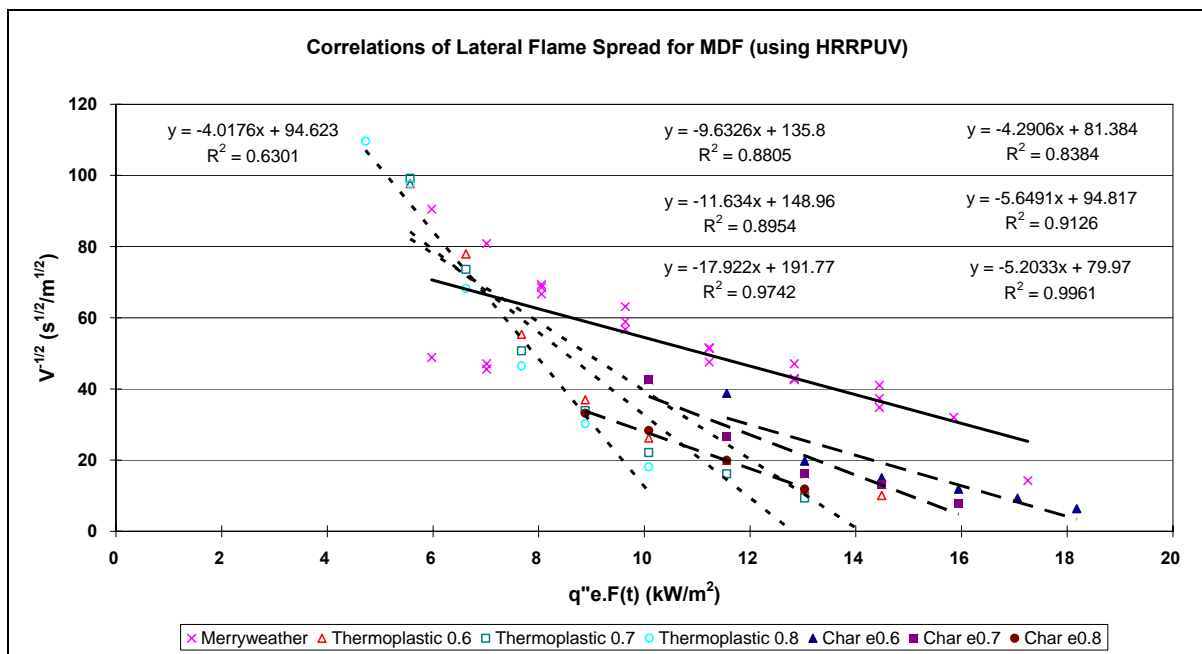
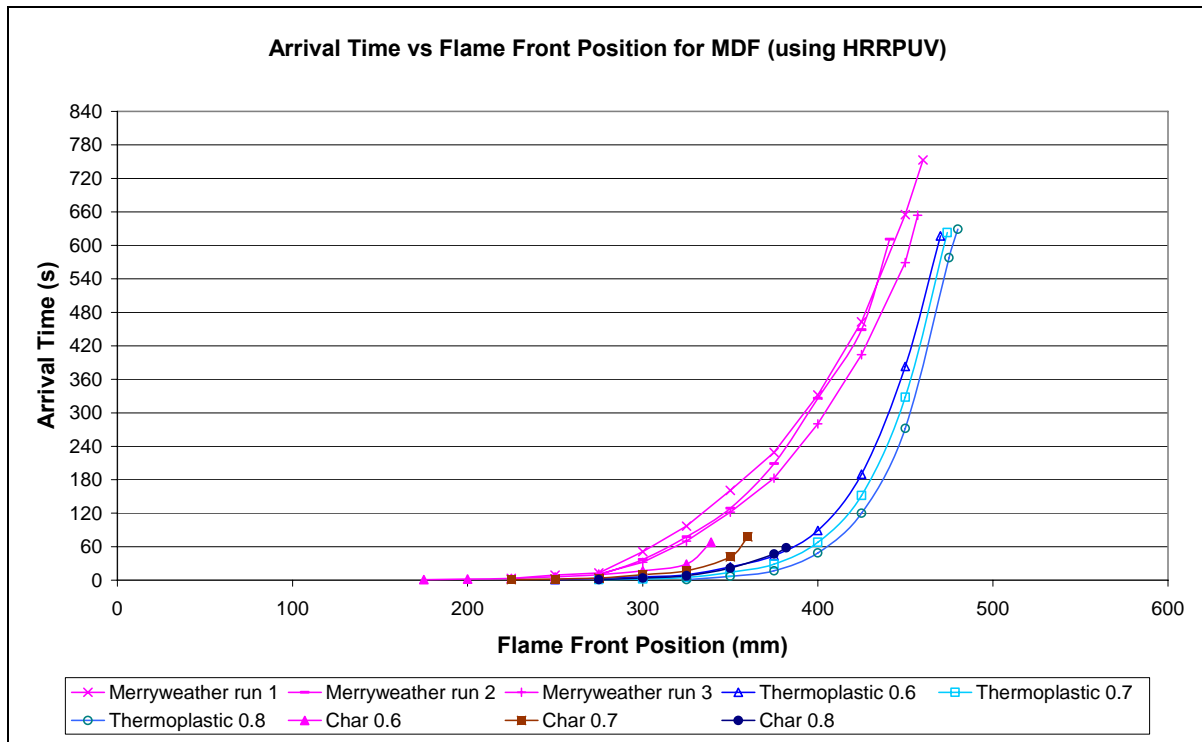
Appendix I – Flame spread results using HRRPUV

Hardboard



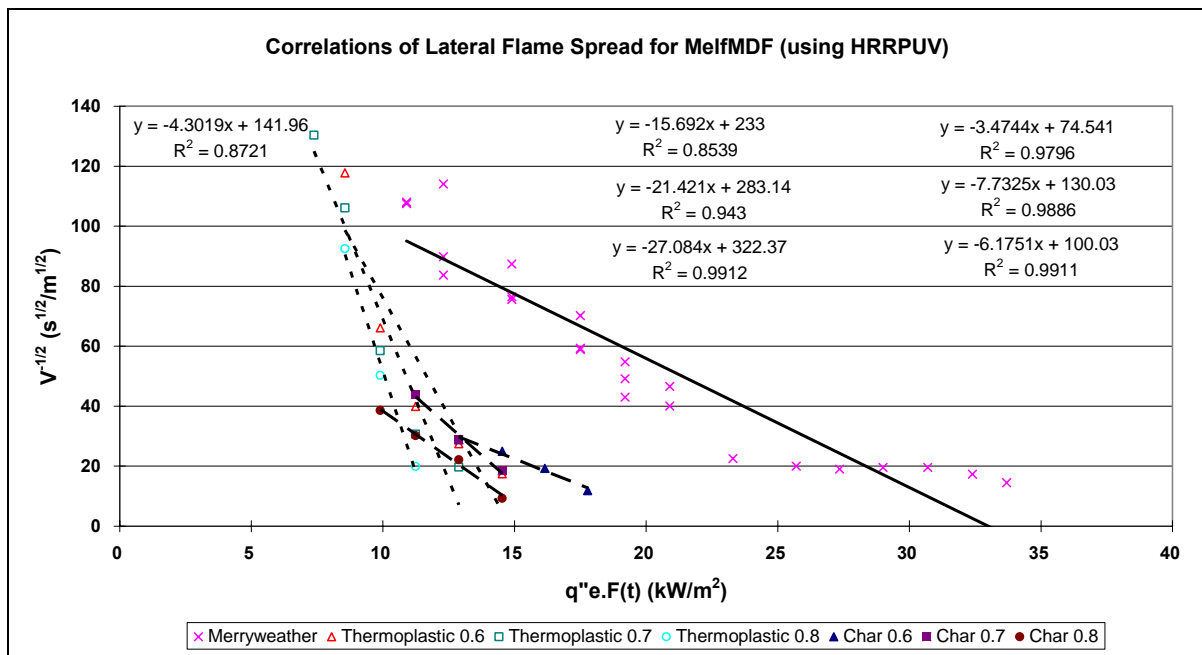
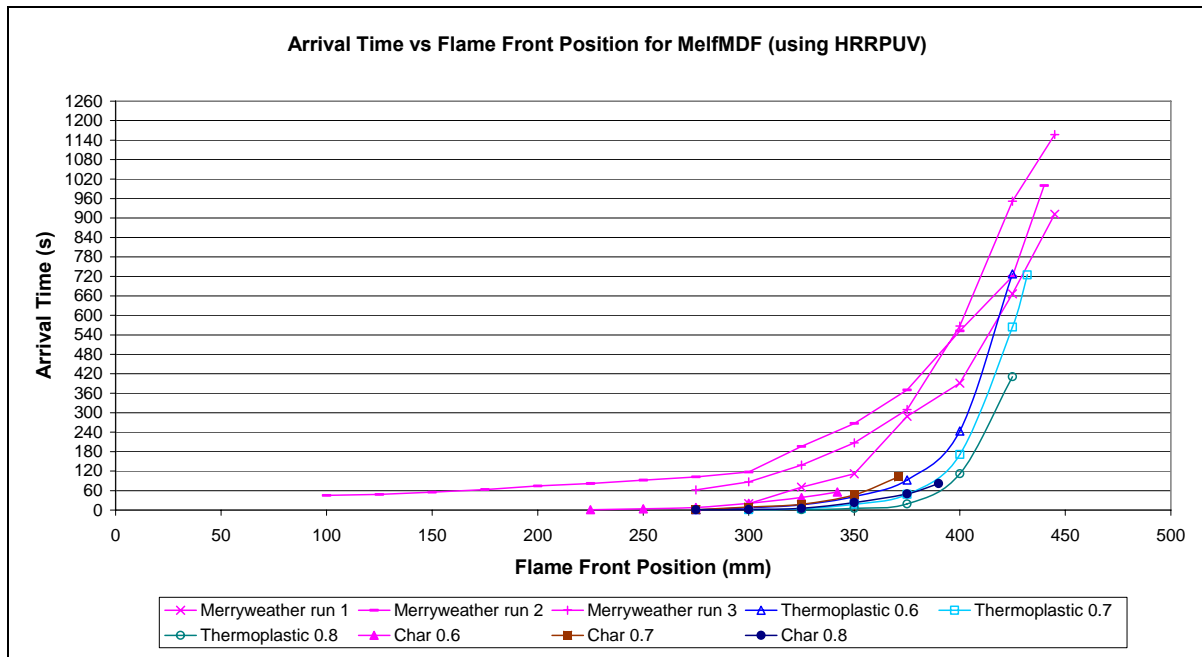
Appendix I – Flame spread results using HRRPUV

MDF



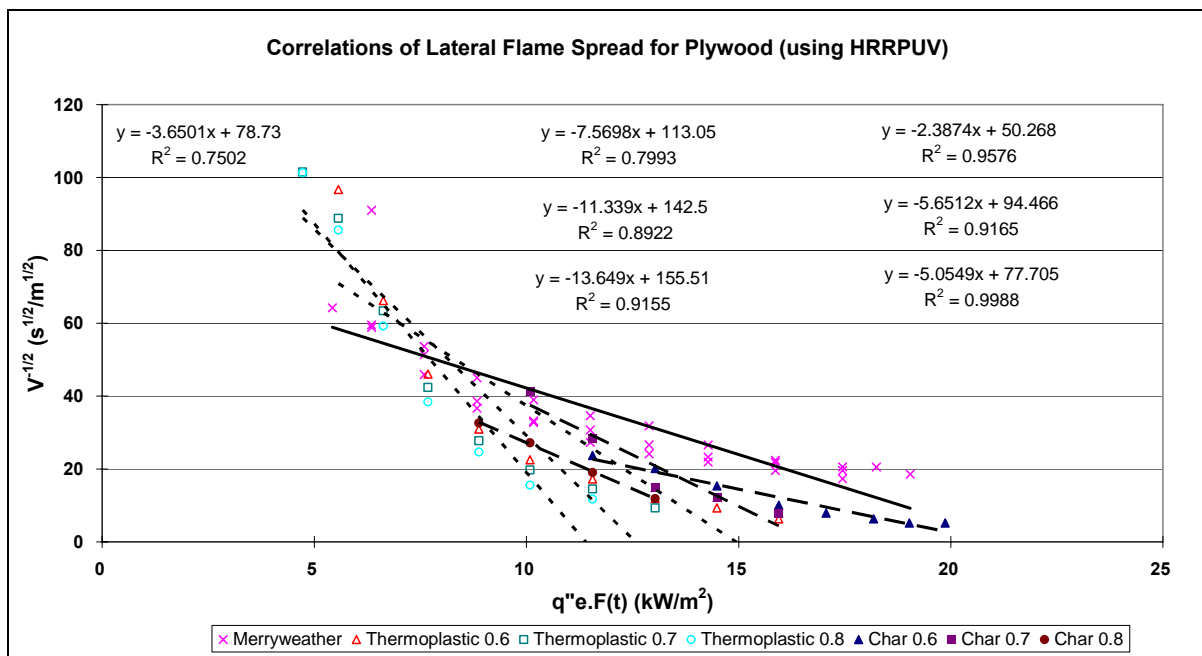
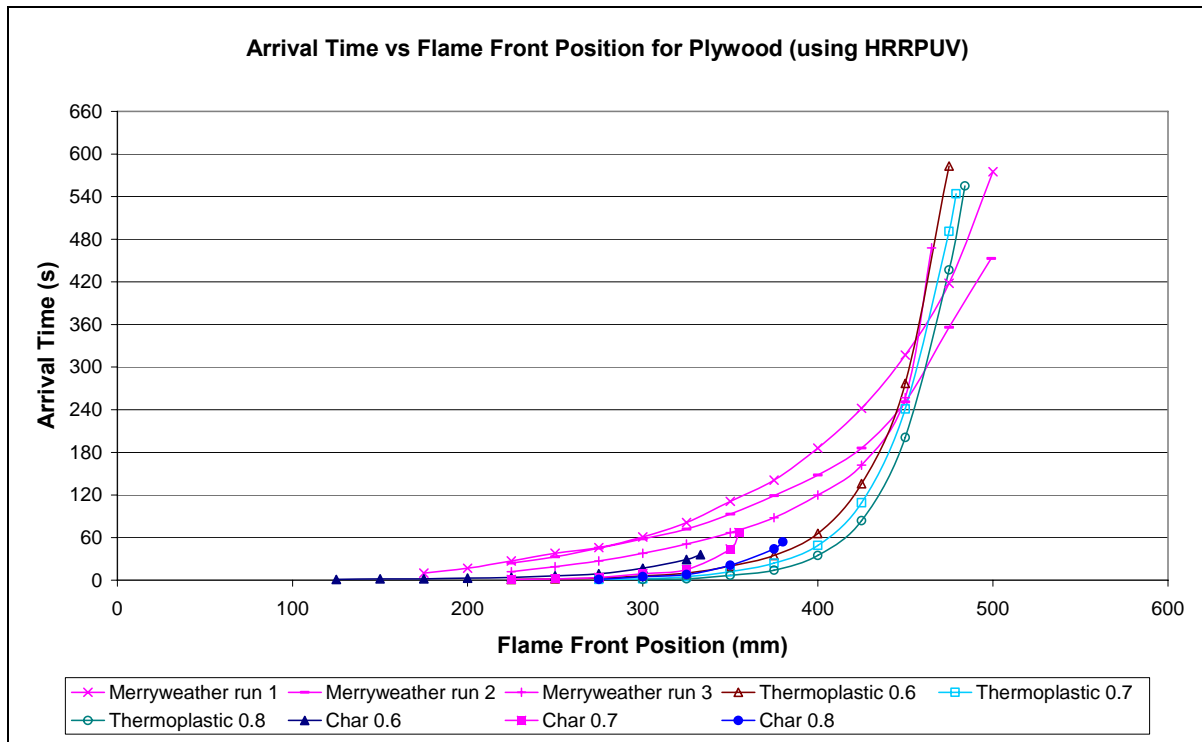
Appendix I – Flame spread results using HRRPUV

Melteca faced MDF



Appendix I – Flame spread results using HRRPUV

Plywood



Appendix I – Flame spread results using HRRPUV

Pynefloor

